Spring 5-7-2016

Inflammation- and Cancer-Associated Neurolymphatic Remodeling and Cachexia in Pancreatic Ductal Adenocarcinoma

Darci M. Fink
University of Nebraska Medical Center

INFLAMMATION- AND CANCER-ASSOCIATED NEUROLYMPHATIC REMODELING AND CACHEXIA IN PANCREATIC DUCTAL ADENOCARCINOMA

by

Darci M. Fink

A DISSERTATION

Presented to the Faculty of

the University of Nebraska Graduate College

in Partial Fulfillment of the Requirements

for the Degree of Doctor of Philosophy

Cancer Research Graduate Program

Under the Supervision of Professor Michael A. Hollingsworth

University of Nebraska Medical Center

Omaha, Nebraska

April, 2016

Supervisory Committee:

Vimla Band, Ph.D. Robert Lewis, Ph.D.

Richard MacDonald, Ph.D. Angie Rizzino, Ph.D.

INFLAMMATION- AND CANCER-ASSOCIATED NEUROLYMPHATIC REMODELING AND CACHEXIA IN PANCREATIC DUCTAL ADENOCARCINOMA

Darci M. Fink, Ph.D.

University of Nebraska, 2016

Supervisor: Michael A. Hollingsworth, Ph.D.

This work addresses two understudied elements of inflammation and malignancy—namely, (1) neurolymphatic remodeling during transitions in microenvironmental inflammatory status and (2) the systemic paraneoplastic inflammatory syndrome cancer-associated cachexia in the context of pancreatic adenocarcinoma (PDAC). Lymphatic vessels undergo dramatic phenotypic changes in initial inflammation, wound recovery, and recurrent inflammation. We identified complementary novel neuroremodeling behaviors under these conditions and hypothesized that both nerve and lymphatic remodeling were directed by a tissue remodeling factor with overlapping functions. We found that nerve growth factor (NGF) influenced not only nerves but also lymphatics. NGF stimulated lymphangiogenesis, inhibited lymphatic vessel regression during wound recovery, and increased nociception. NGF induced VEGF-C protein expression, and ablation of VEGFR-2/3 signaling abrogated NGF-mediated lymphangiogenesis, supporting a hierarchical model of NGF-VEGF signaling with NGF functioning upstream of the VEGF family. We next studied neurolymphatic remodeling in the context of malignancy using a novel murine live imaging platform. Lyve1CreERT2^{tdT} mice inducibly express tdTomato fluorescent protein in Lyve-1^{+} cells. We implanted fluorescently-labeled tumor cells into cornea and pinna and identified tumor-specific neurolymphatic architecture signatures that are distinct from those associated with nonmalignant inflammation, including disorganized hypersprouting nascent lymphatic vessels and a shift in nerve morphology to a phenotype previously associated only with wound recovery. We also found that manipulating the timing of establishment of

inflammation affected tumor cell persistence in tissue. In the final portion of this work, we studied cancer-associated inflammation in a broader context—*i.e.* the paraneoplastic syndrome cancer-associated cachexia. We sought to address discrepancies in the literature regarding cachexia gene expression with a unique set of PDAC skeletal muscle samples harvested at rapid autopsy and stratified based on severity of cachexia. We found differential expression of a number of candidate targets in PDAC samples compared to cancer-free controls including FAP-α, CAMKIIβ, FBXO32, TIE-1, and TRIM63 and challenged some previous findings. In summary, we defined a novel role for NGF signaling in lymphatics, identified microenvironment-specific neurolymphatic architecture signatures, and highlighted the complexity of cancer-associated cachexia while providing new data about this syndrome in the context of PDAC.

TABLE OF CONTENTS

List of Figures

List of Tables

Abbreviations

4-OHT	4-hydroxytamoxifen
AKT/PKB	Protein kinase B
ANG-1, -2	Angiopoietin 1, 2
ArmHms	Armenian hamster
BDNF	Brain-derived neurotrophic factor
BMI	Body mass index
BRCA2	Breast cancer type 2 susceptibility protein
BSA	Bovine serum albumin
CAF	Cancer-associated fibroblast
CAMK2B	Calcium/calmodulin-dependent protein kinase type II subunit beta
Cas9	CRISPR-associated protein 9
CCL21	Chemokine (C-C motif) ligand 21
CCR7	Chemokine (C-C motif) receptor 7
CD133	Prominin 1
CD4	Cluster of differentiation 4
CD8	Cluster of differentiation 8
Cdk5	Cyclin-dependent kinase 5
cDNA	Complementary DNA
CFSE	Carboxyfluorescein diacetate, succinimidyl ester
CLARITY	Hydrogel-tissue fusion and electrophoretic-clearing technology
cm	Centimeters
Cox2	Cyclooxygenase 2
CP	Chronic pancreatitis
CR	Case report
CRISPR	Clustered regularly-interspersed short palindromic repeats
Ct	Threshold cycle
CT	Computed tomography
CX3CL1	(Fractalkine); Chemokine (C-X3-C motif) ligand 1
CX3CR1	Chemokine (C-X3-C motif) receptor 1
CXCL12	Chemokine (C-X-C motif) ligand 12; Stromal cell-derived factor 1 (SDF-1)

CXCR4	C-X-C motif chemokine receptor 4
DC	Dendritic cell
ddH2O	Double-distilled water
DFS	Disease-free survival
Dky	Donkey
DNA	Deoxyribonucleic acid
DPC4	Deleted in pancreatic cancer locus 4; (SMAD4)
DRG	Dorsal root ganglion
e-/sLE	Extended- or standard lymphadenectomy
ECM	Extracellular matrix
Efnb2	Ephrin B2
EGF	Epidermal growth factor
ELISA	Enzyme-linked immunosorbent assay
EphB4	Ephrin type-B receptor 4
Erk-1, -2	Mitogen-activated protein kinase 3, 1
E-selectin	(CD62E: CD62 antigen-like family member E, ELAM-1: endothelial-leukocyte adhesion molecule 1, LECAM-2: leukocyte-endothelial cell adhesion molecule 2)
EUS	Endoscopic ultrasound
Exp	Expert consensus statement
FAP-α	Fibroblast activation protein alpha
FBG	Fasting blood glucose
FBXO32	F-box protein 32
Fc	Fragment, crystallizable
FDG-PET	Fluorodeoxyglucose-positron emission tomography
FGF2	Fibroblast growth factor 2
FGFR	Fibroblast growth factor receptor
FITC	Fluorescein isothiocyanate
FST	Follistatin
GAP43	Growth associated protein 43
GDNF	Glial cell derived neurotrophic factor
GFP	Green fluorescent protein
GFRα-1, -3	GDNF family receptor alpha 1, 3

GLUT1, 4	Glucose transporter 1, 4
GPCR	G-protein coupled receptor
Gt	Goat
H-, K-, N-Ras	Harvey-, Kirsten-, Neuroblastoma- rat sarcoma viral oncogene homolog
Her2/Neu	Erb-B2 receptor tyrosine kinase 2/Human epidermal growth factor receptor 2
IB	Immunoblot
ICAM-1	Intercellular adhesion molecule 1
IGF-1, -2	Insulin-like growth factor 1, 2
IL-1α, β	Interleukin 1 alpha, beta
KPC	LSL-$Kras^{G12D/+}$;LSL-$Trp53^{R172H/+}$;Pdx-1-Cre transgenic mouse model of spontaneous PDAC
KPCT	KPC mice crossed with ROSA-LSL-tdTomato reporter strain B6.Cg-$Gt(ROSA)26Sortm9^{(CAG-tdTomato)Hze}$/J
LEC	Lymphatic endothelial cell
LN	Lymph node
LNB	Lymph node burden
LND	Lymph node disease
LNR	Lymph node ratio
LVD	Lymphatic vessel density
LVI	Lymphatic vessel invasion
LYVE-1	Lymphatic vessel endothelial hyaluronan receptor 1
MAFbx	Muscle atrophy F-box; (Same as Atrogin-1 and FBXO32)
MAPK	Mitogen-activated protein kinase
mg	Milligrams
MHC	Major histocompatibility complex
mL	Milliliters
mm	Millimeters
MMP-2, -9, -10	Matrix metalloproteinase 2, 9, 10
mMs	Monoclonal mouse antibody
MP	Myenteric plexus
MRI	Magnetic resonance imaging
mRNA	Messenger RNA
mRt	Monoclonal rat antibody
MuRF-1	Muscle RING-finger protein 1; (Same as TRIM63)
NCAM	Neural cell adhesion molecule
NFDM	Non-fat dehydrated milk
NFκB	Nuclear factor kappa B
ng	Nanograms
NGF	Nerve growth factor
NN	Cachexia subcategory; No, normal or overweight BMI

NOB	Cachexia subcategory; No, obese
Notch1	Neurogenic locus notch homolog protein 1
Nrp-1, -2	Neuropilin 1, 2
Ntf3	Neurotrophin 3
Ntn-1, -4	Netrin 1, 4
NWL	Cachexia subcategory; No, weight loss
p	Phosphorylated
P	Prospective study
p16	(CDKN2A) Cyclin-dependent kinase inhibitor 2A
p53	(TP53) Cellular tumor protein p53
$p75^{NTR}$	p75 neurotrophin receptor
PALN	Para-aortic lymph node
PanIN	Pancreatic intraepithelial neoplasia
PBS	Phosphate-buffered saline
PCR	Polymerase chain reaction
PD	Pancreat(ic)oduodenectomy
PDAC	Pancreatic ductal adenocarcinoma
PDGF, -BB, -R	Platelet-derived growth factor, BB, receptor
PFA	Paraformaldehyde
pg	Picograms
pHH3	Phosphorylated histone H3
PKCY	Pdx1-Cre;$Kras^{G12D}$;$p53^{fl/+}$;$Rosa26^{YFP}$ mouse (spontaneous PDAC with YFP reporter)
Plxnd1	Plexin D1
PNI	Perineural invasion
pRb	Polyclonal rabbit antibody
Prox-1	Prospero-related homeobox 1
qRT-PCR	Quantitative real-time reverse transcription polymerase chain reaction
R	Retrospective study
RAP	Rapid autopsy program for pancreatic cancer
RCC	Renal cell carcinoma
RET	Proto-oncogene tyrosine protein kinase receptor Ret
Rip1Tag2	Sv40, large T tumor antigen in endocrine beta cells of mouse pancreas cause neuroendocrine tumors
RIPA	Radioimmunoprecipitation assay buffer
RNA	Ribonucleic acid
Robo 1, 4	Roundabout homolog 1, 4
RTKI	Receptor tyrosine kinase inhibitor
Rv	Review
S	Cachexia subcategory; yes, severe cachexia
SDS	Sodium dodecyl sulfate

Sema3E, A	Semaphorin 3E, A
Shh	Sonic hedgehog
Slit2	Slit homolog 2
TALA	Tumor-associated lymphangiogenesis
TAM	Tumor-associated macrophage
TBP	TATA box binding protein
TBS	Tris-buffered saline
TGF-β	Transforming growth factor beta
Tie-1, -2	Tyrosine kinase with immunoglobulin-like and EGF-like domains 1, 2
TNF-α	Tumor necrosis factor alpha
TNM	Tumor, node, metastasis system of cancer staging
TR	Texas red
T_{reg}	Regulatory T cell
TRIM63	Tripartite motif containing 63, E3 ubiquitin protein ligase
TRITC	Tetramethylrhodamine
TrkA	(NTRK1); Neurotrophic tyrosine kinase receptor type 1
Unc5b	Netrin receptor UNC-5 homolog B
uPA	Plasmin/urokinase plasminogen activator
VE-cadherin	Vascular endothelial cadherin
VEGF-A, -C, -D	Vascular endothelial growth factor A, C, D
VEGFR-1, -2, -3	Vascular endothelial growth factor receptor 1, 2, 3
YN	Cachexia subcategory; yes, normal or overweight BMI
YWL	Cachexia subcategory; yes, weight loss
µg	Micrograms
µL	Microliters
µm	Micrometers

Acknowledgements

I have been abundantly blessed with wonderful colleagues, mentors, friends, and family members. First to my mentors—Dr. Tony Hollingsworth and Dr. Rick Tempero—thank you. Thank you for listening to and helping to develop my ideas, for sound scientific discussion, for critical review of my written work, and for continually reinforcing the bigger "whys and hows" of collective scientific effort. Thank you for seeing something in me that I was unsure of myself and for serving as excellent examples of what it means to be a passionate scientist. To Tony specifically—I will always be grateful for the collaborative and networking opportunities you often went out of your way to provide for me and other graduate students in your lab. Thank you also for the environment of scientific freedom that you have created for your team. Your excitement about scientific advancement and translating discoveries to the clinic is palpable and infectious. And to Rick—I am grateful for your enthusiasm, your patience and effort in teaching me the fine surgical techniques that were so vital to this work, and your unflappable positive outlook. Thank you also for teaching me to distill complicated ideas into simple testable hypotheses.

To my committee members—Dr. Vimla Band, Dr. Robert Lewis, Dr. Richard MacDonald, and Dr. Angie Rizzino—thank you for helping me to grow professionally. Thank you for supporting me and my family, for building my confidence, and for your insight and lending your breadth of knowledge to my projects.

Next to my labmates—I have learned so much from you guys! Paul, Jim, Ryan, Seiya, and Roger—I'm quite certain I will never have the privilege of sharing *just exactly* such an office environment again☺. Maria, Ashley, and Neeley—thank you for your excellent technical and personal advice through this journey. Maria especially was instrumental in several of the

experiments included in this work—the *in vitro* LEC studies in Ch. I—and was a fantastic co-first author on the PDAC and lymphatics review (Maria M. Steele) that makes up portions of the introduction and discussion here; I couldn't have done it without you! Prathamesh adapted the CLARITY protocol to pancreas and other mouse organs, and Figure 33 could not have been generated without his ingenuity and persistence (Prathamesh Patil); thanks also for your friendship and constant willingness to drop whatever you're working on to lend a hand! All of the other lab members—Tom, Prakash, Kamiya, Kelly, Edwin, AJ, Winni, Steph, Judy, Rimma, and John—you have been wonderful colleagues, and working with you was a pleasure. This work would not have been possible without the excellent help of Phil Kelley and Alicia Connor at Boys Town National Research Hospital. Thank you for great discussions, technical assistance with my crazy huge experiments, and for just being great people! Thank you also to Marisa Zallocchi at Boys Town for the use of her stereoscope and nano-injector. Other friends along the way who kept me sane and just "got it"—Maria, Erin, Caroline, Catherine, and Courtney—thanks!

Next to technical support— I thank Janice A. Taylor and James R. Talaska of the Confocal Laser Scanning Microscope Core Facility at the University of Nebraska Medical Center for providing assistance with confocal microscopy and the Nebraska Research Initiative and the Eppley Cancer Center for their support of the Core Facility. I also thank Dr. James Eudy, Lisa Bough, and Xiaoyang Feng of the University of Nebraska Medical Center Microarray Core Facility for their assistance with the Quantibody Cytokine Array. I also thank Skip Kennedy of Boys Town National Research Hospital for his assistance in preparing figures in Ch. I for publication. Thank you also to the wonderful comparative medicine staff at UNMC and Boys Town.

To my family—I was unbelievably fortunate to grow up in an environment in which learning, critical thinking, creativity, and fun were our way of life. Though I took this for granted

at the time, I now realize just how rare the support and positivity of our home were—and I can't imagine how lucky I am to have gotten my start in such a place. Mom, Dad, and Drew—thanks for the conversations, the goofiness, for doing what was necessary to instill in me a good work ethic, and for the freedom to make my own mistakes, land in my own messes, and learn from them.

And to my husband—I've started writing this part about ten times now, and each set of phrases struggles more than the last to articulate my gratitude and love for you. Andrew, you are the smartest person I have ever met. You bring laughter and happiness into my life each day, and you make me a better person. I respect you, your character, your integrity, and your accomplishments more than I can say. Thank you for your sacrifices, your patience, and your sawdusty-shoulder through this chapter. I can't wait to see what the future holds for us and our Tiny Boy.

Finally, thanks be to the Lord! My Rock and my Redeemer, my Savior and Shepherd, Alleluia! Thank you for the amazing intricacies of this world you have created—as if I needed any more assurance in my life; this is all far too magnificent to have been a happy accident.

Oh Lord, my God, when I in awesome wonder
Consider all the worlds Thy hands have made
I see the stars, I hear the rolling thunder
Thy power throughout the universe displayed
Then sings my soul, my Savior, God, to Thee
How great Thou art, How great Thou art!

Lutheran Service Book #801
Carl Gustaf Boberg (tl. Stuart W. K. Hine)

Dedication

This dissertation is dedicated to the memory of my grandfather Harold L. Borkowski—Grandpa B.

We all watched in frustrated futility as cancer stole the man we loved.

Slowly. Painfully. Quietly.

He did not survive.

I dedicate this effort to his memory in the hopes that others like him and other families like mine may one day be spared the long and bitter grief that is an incurable cancer diagnosis.

INTRODUCTION[1]

[1] Portions of the material presented in this chapter have been previously published under the following reference: (Fink et al., 2015a)

Pancreatic Ductal Adenocarcinoma

Statistics and Progression

Pancreatic ductal adenocarcinoma (PDAC) is the fourth-leading cause of cancer-related death in both men and women in the United States (Siegel et al., 2016). Worldwide, PDAC results in over 330,000 deaths annually (Torre et al., 2015). Unlike the stable or decreasing trends of incidence and death rate achieved for other cancers in recent decades, the incidence of PDAC continues to rise (Siegel et al., 2016). These sobering statistics underscore the critical need for basic research examining the biology of this disease to drive development of new and effective therapies. PDAC progresses through several histologically-defined classifications of pre-malignant lesions, known as pancreatic intraepithelial neoplasias (PanINs), before manifesting as infiltrating adenocarcinoma and metastasizing to distant sites. PanINs do not show invasion into lymphatic or blood vessels or nerves (Maitra et al., 2005), but mice bearing these lesions had increased levels of neurotrophic factors, sensory innervation, and pain (Stopczynski et al., 2014). Progression through each PanIN stage has been linked to acquisition of a specific mutation or set of mutations with *HER2*/*NEU* and *KRAS* associated with PanIN-1A and -1B, *P16*/*CDKN2A* associated with PanIN-1B and -2, and *TP53*, *SMAD4*/*DPC4*, and *BRCA2* associated with PanIN-3 lesions (Hruban and Adsay, 2009; Wilentz et al., 2000). The presence of an inflammatory pancreatic microenvironment, such as that characteristic of pancreatitis, can exacerbate K-Ras oncogene-induced development of PanIN lesions and progression to PDAC by facilitating escape from senescence (Guerra et al., 2011) or through pancreatitis-mediated acinar to ductal cell metaplasia (Guerra et al., 2007). Despite our knowledge of this progression from normal parenchyma to aggressive malignancy, early detection of these histologic and genetic deviations in patients remains challenging. Most PDAC cases are diagnosed when the primary pancreas tumor has already metastasized to regional and distant locations (Siegel et al.,

2015). Five-year survival decreases dramatically as stage at diagnosis increases, with PDAC localized to the pancreas at diagnosis yielding a modest five-year survival rate of 27% compared to just 11% on presentation with regional metastases and a devastating 2% when distant metastases are present at diagnosis (Siegel et al., 2016). The presence of metastasis eliminates the only therapeutic strategy with proven curative potential—surgery—and leaves patients with debilitating rounds of chemotherapy and radiation as their only recourse to extend life a few precious months.

This work focuses on two microenvironment-responsive tissue networks important in cancer progression and metastasis: lymphatic vessels and nerves. Both of these systems are intimately associated with the pancreas and their functions are markedly altered in both inflammation and malignancy—although much remains poorly understood in these regards. In the following sections, we will outline normal lymphatic and nerve biology generally and as it relates to the pancreas, explore inflammation-mediated changes on these networks, and summarize what is known about their respective roles in the pancreatic tumor microenvironment with special emphasis on clinical diagnostic/prognostic metrics, imaging techniques, and therapies. We will also introduce the systemic paraneoplastic inflammatory syndrome cancer-associated cachexia in the context of pancreatic ductal adenocarcinoma.

The Lymphatic System: Normal Biology and Importance in PDAC

The lymphatic vasculature offers the most direct route from the primary tumor to the frequently-invaded draining lymph nodes during PDAC progression. Cancer metastasis into and through the lymphatic vasculature and lymph nodes occurs frequently in PDAC patients (DiMagno et al., 1999; Hezel et al., 2006; Katz et al., 2008) and is strongly correlated with poor prognosis (Benassai et al., 1999; Delcore et al., 1996; Kedra et al., 2001; Robinson et al., 2012).

The lymphatic system is responsible for maintenance of tissue fluid homeostasis, absorption of dietary fat, and leukocyte and antigen transport from tissues to lymph nodes for the initiation of immune responses (Maby-El Hajjami and Petrova, 2008; Stacker et al., 2014; Tammela and Alitalo, 2010). Originating in nearly all vascularized tissues, blind-ended lymphatic capillaries, or initial lymphatics, are specialized for the uptake of interstitial fluids, macromolecules, and leukocytes. They are composed of a single layer of endothelial cells with discontinuous intercellular junctions and lack a basement membrane (Baluk et al., 2007; Pflicke and Sixt, 2009). The endothelial membrane of the initial lymphatics is attached to the extracellular matrix (ECM) *via* anchoring filaments, which facilitate the opening of the lymphatic lumen during increased interstitial fluid pressure (Gerli et al., 2000; Solito et al., 1997). Upon entry into the lymphatic capillaries, lymph and its macromolecular and cellular contents are transported to larger pre-collecting lymphatic vessels and then to collecting vessels, composed of not just the endothelial layer but also smooth muscles to facilitate flow and bi-leaflet valves to prevent backflow (Bazigou et al., 2014; Leak and Burke, 1966; von der Weid and Zawieja, 2004). The afferent collecting lymphatics enter the lymph nodes where the lymph is filtered, and upon exiting the lymph nodes through the efferent collecting vessels, lymph passes through the major trunks of the lymphatic system, the thoracic duct and the right lymphatic trunk, and is then returned to the circulatory system (Alitalo and Detmar, 2012; Tammela and Alitalo, 2010).

The network of lymphatic vasculature and lymph nodes responsible for draining the pancreas is quite complex. In the normal pancreas, lymphatic vessels are typically located near blood vessels and are often found in the interlobular spaces of the pancreas (O'Morchoe, 1997). Classification of pancreatic nodes has not been uniformly standardized, although pancreatic lymph nodes are generally divided into regions based upon their location around the pancreas and the areas of drainage of the pancreas: head/neck, body/tail, left side, or right side

(reviewed in (Cesmebasi et al., 2015; Isaji et al., 2004)). Studies correlating primary tumor location and lymph node involvement following resection have helped to identify the regional patterns and probabilities of lymph node metastasis, but more analysis is needed for consistent accurate prediction of lymph node involvement (Fujita et al., 2010; Kanda et al., 2011; Nagakawa et al., 1994; Sun et al., 2010).

Although clinicians and researchers understand the importance of lymphatic invasion and lymph node involvement for pancreatic cancer patient prognosis and therapy selection, the biological processes that govern lymphatic invasion and metastasis remain understudied. For example, there is currently disagreement within the field as to whether lymphatic vessel expansion at the primary tumor site and draining lymph node is necessary for lymph node metastasis. Also, it has not been conclusively determined whether metastasis to the lymph nodes is a sequential step in distant organ spread or a final destination for tumor cells to promote immunosuppression. The potential role of lymphatics supporting immune suppression has led to questions of how normal and tumor-associated lymphatic endothelia may contribute to immune modulation within the tumor microenvironment and invaded lymph nodes either through trafficking functions or direct interactions with immune cells. These and many more questions have yet to be fully explained: how does the lymphatic endothelium regulate the entry of tumor cells into vessels; how do tumor cells evade immune cell recognition within lymphatic vessels and lymph nodes; what are the therapeutic implications of targeting lymphangiogenesis or other lymphatic-directed functions in patients with PDAC?

Lymphangiogenesis

Signaling and Regulation

While clearly akin to angiogenesis in many regards, progress to define the process of lymphangiogenesis has revealed distinct molecular mechanisms that direct its inception, regulation, and roles in inflammatory disease and malignancy. Like angiogenesis, new lymphatic vessel growth can be directed by many growth factors and regulated by intra- and extracellular signaling mechanisms. Primary growth factors associated with lymphangiogenesis include vascular endothelial growth factor-A (VEGF-A), -C, and -D signaling *via* vascular endothelial growth factor receptor-2 (VEGFR-2) and -3 and neuropilin-2 (NRP-2) (Achen et al., 1998; Bjorndahl et al., 2005b; Favier et al., 2006; Joukov et al., 1996; Oh et al., 1997a; Veikkola et al., 2001), and angiopoietin-1 (ANG-1) and -2 signaling through receptor TIE-2 (tyrosine kinase with immunoglobulin-like and EGF-like domains 2) (Morisada et al., 2005; Yan et al., 2012). Recent evidence shows that in addition to the VEGFs and angiopoietins, several other chemical messengers are also capable of directly or indirectly inducing lymphangiogenesis *in vitro* and/or *in vivo* in experimental model systems. Such mediators include growth factors fibroblast growth factor-2 (FGF-2) (Kubo et al., 2002), platelet-derived growth factor-BB (PDGF-BB) (Cao et al., 2004a; Miyazaki et al., 2014), nerve growth factor (NGF) (Fink et al., 2014) (discussed in Chapter I), insulin-like growth factor-1 (IGF-1) and -2 (Bjorndahl et al., 2005a), and hepatocyte growth factor (HGF) (Cao et al., 2006); inflammatory cytokines interleukin-1β (IL-1β) (Peppicelli et al., 2014; Ristimaki et al., 1998) and tumor necrosis factor-α (TNF-α) (Du et al., 2014; Peppicelli et al., 2014; Ristimaki et al., 1998); and other non-traditional signaling molecules lipid sphingosine-1-phosphate (Huang et al., 2013), cyclooxygenase 2 (COX2), and surface protein EP3/4 (Hosono et al., 2011). A role for integrins in lymphangiogenesis has been revealed with evidence of binding of VEGF-A, -C, and -D to lymphatic endothelial-specific integrin-α9β1 (Oommen et al.,

2011; Vlahakis et al., 2005). While each of these factors does induce new lymphatic vessel growth, not all lymphangiogenesis is created equal; a study of corneal lymphangiogenesis in response to VEGF-A, VEGF-C, or FGF-2-loaded micropellets revealed differences in both structure and function of lymphatic vessels and the proportion of blood to lymphatic vessels induced by these growth factors (Cao et al., 2004b). In the case of indirect stimulation of lymphangiogenesis, paracrine signals such as IL-1β (Peppicelli et al., 2014; Ristimaki et al., 1998) and TNF-α (Du et al., 2014; Peppicelli et al., 2014; Ristimaki et al., 1998) can drive increased expression of the VEGFs, most notably VEGF-C. This likely occurs through activation of the nuclear factor kappa B (NFκB) promoter to induce VEGF-C expression (Du et al., 2014). Other indirect inducers of lymphangiogenesis include COX2 and EP3/4, which may increase expression of VEGF-C and -D to modulate cell growth during inflammation (Hosono et al., 2011), and NGF, which increased expression of VEGF-C, but not VEGF-A, in a mouse corneal model of lymphangiogenesis (Fink et al., 2014). Some studies have attributed the secondary production of VEGFs, specifically VEGF-C, to an infiltrating macrophage population during periods of inflammation and malignancy (Cursiefen et al., 2004; Huang et al., 2013; Murakami et al., 2008; Peppicelli et al., 2014). Huang, *et al.*, have also identified B cells and dendritic cells (DCs) as candidate immune cell populations that may secrete VEGF-A, -C, and -D to influence lymphatic vessel organization and growth (Huang et al., 2013). B cells have also been shown to modulate lymphangiogenesis within lymph nodes in the context of tissue inflammation following experimental immunization (Angeli et al., 2006). In addition to their role in secretion of lymphangiogenic growth factors, Hall, *et al.*, have shown that tissue macrophages may directly contribute to new lymphatic vessel growth by transdifferentiation into a lymphatic endothelial progenitor-like phenotype and incorporation into growing vessels (Hall et al., 2012). The roles

of tumor-associated macrophages (TAMs) in lymphangiogenesis in the tumor microenvironment are discussed in more detail below.

Lymphangiogenesis is further controlled by regulation of growth factor and cytokine receptors on the lymphatic endothelial surface. Gene expression of VEGFR-1, -2, and -3 and NRP-1, and -2 is regulated by transcription factors GATA-binding protein 2 (GATA2) and LIM domain only 2 (LMO2) to influence both angiogenesis and lymphangiogenesis (Coma et al., 2013). Another transcription factor, COUP transcription factor 2 (COUP-TFII), increases expression of Nrp-2 to augment VEGF-C signaling (Lin et al., 2010). VEGFR-2 and -3 signaling is further modulated by bone marrow kinase in X chromosome (BMX) following its upregulation upon VEGF-A stimulation of lymphatic endothelial cells (LECs) (Jones et al., 2010). H-, N-, and K-Ras can also regulate VEGFR-3 signaling by inducing the up- or downregulation of that receptor (Ichise et al., 2010). Another mechanism of VEGFR-3 pathway signaling regulation in LECs is the IL-1β-dependent induction of microRNA-1236 (Jones et al., 2012) and the molecular scaffolding protein apoptosis signal-regulating kinase interacting protein-1 (AIP-1) (Zhou et al., 2014). The SLIT2-ROBO4 (Slit homolog 2-Roundabout homolog 4) signaling axis has been shown to regulate surrogate lymphangiogenesis behaviors in lung LECs in culture by modulating VEGF-C/VEGFR-3 pathway signaling (Yu et al., 2014). NFκB pathway signaling has been shown to further modulate inflammatory lymphangiogenesis by upregulating prospero-related homeobox-1 (Prox-1) and VEGFR-3 in a mouse model of peritonitis (Huang et al., 2013).

Tumor-Associated Lymphangiogenesis

The discussion above has primarily focused on the regulation of inflammatory lymphangiogenesis typical of an injury or infection. A related, but in many ways physiologically distinct process, is that of tumor-associated lymphangiogenesis (TALA). Factors elaborated by

tumor cells and other supporting cell types of the tumor microenvironment, such as cancer-associated fibroblasts (CAFs), TAMs, and DCs, interact with cognate receptors on the lymphatic endothelium both locally and in lymph nodes to influence lymphangiogenesis, lymph node metastasis, and tumor progression. Studies of human pancreatic cancer tissues have identified a role for TALA in lymph node metastasis and patient outcomes. Kurahara, *et al.*, found that high lymphatic vessel density (LVD) in PDAC head tumors predicted increased lymph node metastasis and decreased survival; they also showed increased LVD within metastatic lymph nodes (Kurahara et al., 2010). Wang, *et al.*, found that increased peritumoral LVD in human pancreatic carcinoma tissues correlated with unfavorable tumor differentiation status, increased lymphatic vessel invasion (LVI), and more lymph node metastasis, while this was not the case for intratumoral LVD (Wang et al., 2012). These data highlight the importance of peripancreatic lymphatics in the progression and metastasis of pancreatic cancer and their potential utility as both a predictor of patient outcomes and a possible therapeutic target.

As in inflammatory lymphangiogenesis, the VEGF-C/D signaling pathways appear to play an important role in TALA, although the exact mechanisms of their activity remain somewhat less clear. Kurahara, *et al.,* found increased VEGF-C and -D expression in patient PDAC tumor margins compared to the tumor interior and reported that high VEGF-C and -D expression in tumor margins correlated with increased LVI (VEGF-C) and lymph node metastasis (VEGF-C/D) and decreased five-year survival; expression levels of these proteins did not correlate with either hematogenous invasion or distant metastasis (Kurahara et al., 2004). A similar study of patient samples also showed increased VEGF-C and -D immunostaining at PDAC tumor margins that correlated with increased LVD, lymphatic and blood vessel invasion, lymph node metastasis, and overall survival (Zhang et al., 2007). Von Marschall, *et al.,* corroborated these findings with their evidence of increased VEGF-D and VEGFR-3 expression in human PDAC tissue

and of increased LVI, presence of intra- and peritumoral lymphatics, and lymph node metastasis (Von Marschall et al., 2005). Deletion of VEGF-D in mice resulted in impaired peritumoral lymphangiogenesis and decreased lymph node metastasis while having no effect on lymphatic development or inflammatory lymphangiogenesis suggesting a tumor microenvironment-specific role for VEGF-D signaling (Koch et al., 2009). In a Rip1Tag2 model of pancreatic β-cell carcinogenesis, Kopfstein, *et al.*, showed that VEGF-D expression in these tumors induced peritumoral lymphangiogenesis and lymph node and lung metastases (Kopfstein et al., 2007); a very similar study examining the role of VEGF-C in this context found increased lymphangiogenesis and lymph node metastasis but not distant metastases (Mandriota et al., 2001). In an orthotopic PDAC model, treatment with anti-VEGF-C short hairpin RNA decreased tumoral LVD and inhibited tumor growth (Shi et al., 2013). A role for microRNAs may also exist in the regulation of pancreatic TALA. Keklikoglou, *et al.,* recently described a mechanism of regulation of VEGF-C production in PDAC cells by miR-206. They showed that, in addition to regulating *KRAS* and annexin-A2 gene expression, restoration of miR-206 expression blocked tumor-associated angiogenesis and lymphangiogenesis, and its overexpression in pancreatic cancer cell lines disrupted the cell cycle restricting proliferation, impaired migration and invasion *in vitro*, and delayed tumor xenograft growth *in vivo* (Keklikoglou et al., 2014). While the role of hypoxia in lymphangiogenesis remains unclear, hypoxia-inducible factor 1 alpha (HIF-1α) expression has been shown to correlate with VEGF-C expression in PDAC of the pancreatic head and may be responsible for increased lymphangiogenesis and lymph node (LN) metastasis (Tao et al., 2006). Contrary to these studies, Sipos, *et al.*, examined the expression levels of lymphangiogenic factors, LVD, and effects on lymph node metastasis in human PDAC and orthotopic PDAC mouse models and found that VEGF-C and -D were not overexpressed in tumor tissues and that LVD within tumors was decreased while peritumoral LVD was increased. They

found no correlation between LVD or expression of VEGF-C or -D and rate of lymph node metastasis or patient outcomes and concluded that PDAC metastasis is independent of lymphangiogenesis (Sipos et al., 2005).

In vitro experiments have examined the effects of tumor-secreted VEGF-C on LEC surrogate lymphangiogenesis behaviors. Supernatant from a high VEGF-C-secreting cell line, MiaPaCa-2, increased LEC migration, and MiaPaCa-2 co-culture with LECs increased LEC tubulogenesis (Ochi et al., 2007). These effects may be dependent on kangai-1 (KAI-1; CD82) regulation as overexpression of that gene in MiaPaCa-2 resulted in decreased VEGF-C secretion, lymphangiogenesis, and lymph node metastasis (Liu et al., 2014a). Re-expression of tumor suppressor p16 in a MiaPaCa-2 orthotopic model had no effect on levels of VEGF-C or -D, but nevertheless resulted in decreased lymphangiogenesis, LVD, and lymph node metastasis suggesting an alternate mechanism of regulation (Schulz et al., 2008).

Overall, many studies examining the relationships among VEGF-C/D expression and lymphatic-related phenotypes have found that high VEGF-C/D levels correlate with increased lymphangiogenesis, lymphatic vessel invasion, and lymph node metastasis (or their surrogate *in vitro* counterpart behaviors). Whether a direct pathway can be drawn from tumor-associated lymphangiogenesis, to tumor cell invasion into lymphatic vessels, to tumor cell trafficking to lymph nodes, to establishment of lymph node metastases, to tumor cell exit of the lymph node by blood or lymphatic vessels and seeding of metastases at distant sites, to direct effects on patient outcomes is still unclear. Some of the studies we have discussed have supported portions of this pathway from lymphangiogenesis to distant metastases, but other data suggest that disease progression does not necessarily follow this linear sequence—*i.e.* the concept that lymphangiogenesis may not be required for lymphatic vessel invasion due to entry into pre-

existing lymphatics, or the possibility of trafficking of tumor cells to lymph nodes through blood vessels, or the results from Sipos, *et al.*, showing that lymph node metastasis and patient prognosis are *not* linked to VEGF-C/D levels (Sipos et al., 2005). Also complicating this discussion is the fact that tumor cells may themselves respond to VEGF-C/D signals in an autocrine manner further influencing their metastatic behaviors. Additional studies to systematically dissect each of the biological components of this proposed metastatic pathway are needed to concretely define their connections and contributions to disease progression.

Traditional neural signaling molecules also act to influence lymphatic vessel biology in the tumor microenvironment. Suppression of neural cell adhesion molecule (NCAM) induced VEGF-C and -D expression resulting in increased lymphangiogenesis and lymph node metastasis in the Rip1Tag2 mouse model (Crnic et al., 2004), while the presence of NCAM expression in pancreatic cancer tissues from patients correlated with better prognosis (Tezel et al., 2001). In another example derived from the Rip1Tag2 model, Slit2 induced Robo1 in LECs to increase lymphangiogenesis and lymph node metastasis (Yang et al., 2010). As previously mentioned, signaling of Slit2 through another receptor, Robo4, may also influence lymphangiogenesis behaviors such as growth, migration, and tubulogenesis, by modulating VEGF-C/VEGFR-3 signaling (Yu et al., 2014). NRP-2, a classical semaphorin receptor and VEGF pathway co-receptor, has also been shown to be a key regulator of TALA. It is expressed on intra- and peritumoral lymphatic vessels and lymph nodes; blocking its function *in vivo* decreased TALA, impaired tumor-associated lymphatic vessel function, and reduced lymph node and distant metastases (Caunt et al., 2008). These effects may be the result of impaired lymphatic sprouting (Xu et al., 2010). NRP-1 and -2 are also expressed on pancreatic tumor cells themselves (Dallas et al., 2008; Fukahi et al., 2004). In a model of colorectal cancer, TALA was stimulated by upregulation of Nrp-2 in LECs, and LVD correlated with the level of Nrp-2 expression; this Nrp-2

induction was mediated by integrin-α9β1 signaling in a VEGF-C/VEGFR-3 pathway-independent manner (Ou et al., 2015).

Other signaling pathways have also been implicated in regulation of TALA. In a mouse model of pancreatic β-cell carcinoma, both Ang-1 and -2 induced peritumoral lymphangiogenesis, but this new lymphatic vessel growth did not result in increased metastasis to either local lymph nodes or distant sites (Fagiani et al., 2011). Ang-2 expression in orthotopic PDAC xenografts resulted in increased LVD and lymphatic metastasis, and high levels of ANG-2 in patient serum samples correlated with lymph node metastasis and decreased survival. In MiaPaCa-2 cells, ANG-2 altered message levels of cytoskeletal and motility pathway molecules as well as decreasing expression of tumor suppressor genes (Schulz et al., 2011). The transforming growth factor-β (TGF-β) pathway may also be involved in TALA as expression of endoglin on intra- and peritumoral blood and lymphatic vessels in PDAC correlated with poor patient prognosis (Yoshitomi et al., 2008).

PDAC Invasion of Lymphatic Vessels and Metastasis to Lymph Nodes

Background

Lymphatic vessel invasion and subsequent metastasis to the lymph nodes are early and significant events frequently observed during pancreatic cancer progression (DiMagno et al., 1999; Hezel et al., 2006). Although lymphatic invasion and metastasis to the lymph nodes does not directly contribute to PDAC morbidity in patients, these pathologies are important indicators of the metastatic potential of this disease. In the clinical setting, lymph node status is used to assess disease progression, to select appropriate therapies, and to predict survival (Kawada and Taketo, 2011; Nathanson et al., 2015). Nearly all studies concur that lymph node status correlates with poor prognosis for pancreatic cancer patients (Benassai et al., 1999; Delcore et

al., 1996; Liu et al., 2015b; Robinson et al., 2012). Studies also agree that invasion of lymph nodes by PDAC occurs most frequently through the lymphatic vasculature rather than through direct/contiguous extension of the primary tumor to the lymph node (Buc et al., 2014; Konstantinidis et al., 2010; Pai et al., 2011), although direct extension to lymph nodes through nerves is often a feature of perineural invasion. The prognostic value of mode of lymph node invasion is still debated: some studies report poorer overall survival in patients with lymphatic vessel-directed metastasis as compared to direct invasion (Pai et al., 2011), while other reports show no survival difference between the two modes of lymph node invasion (Buc et al., 2014; Konstantinidis et al., 2010). Although lymph node invasion by PDAC occurs most frequently through the lymphatic vasculature, the LVD at the tumor site has not been conclusively correlated with either lymph node metastasis or prognosis due to conflicting study results (Sipos et al., 2005; Von Marschall et al., 2005; Wang et al., 2012; Zorgetto et al., 2013). This is also true for studies examining the expression of pro-lymphangiogenic factors such as VEGF-C and -D (Schneider et al., 2006; Sipos et al., 2005; Tang et al., 2001) (and in pancreatic endocrine tumors (Rubbia-Brandt et al., 2004)). The lack of standardized protocols for quantifying LVD in patients makes comparative analysis among collected data sets difficult. Some studies enumerate only intratumoral lymphatics in whole tumor sections, while others examine tumor margins for peritumoral lymphatics, and still others examine the sum of lymphatic vessels in both regions. In the continued absence of a standardized method, LVD has limited value as a metric for assessing pancreatic cancer progression.

PDAC tumors are often hypovascular with only sporadic blood and lymphatic vessels found among the tumor cells (Feig et al., 2012). These intratumoral lymphatic vessels are typically collapsed and nonfunctional due to direct compression by the tumor cells and the high internal pressure of the PDAC tumor microenvironment (Olszewski et al., 2012; Padera et al.,

2002; Schneider et al., 2006). However, even in the absence of functioning intratumoral lymphatic vessels, tumor cells are still capable of disseminating to lymph nodes, although identification of reliable sentinel lymph nodes remains challenging (Kanda et al., 2011). The lymphatic vessels located at the tumor margins are frequently described as enlarged with open lumens capable of being filled with tumor cells (Olszewski et al., 2012; Schneider et al., 2006), and drainage studies show that these peritumoral lymphatic vessels are, in fact, functional (Padera et al., 2002). Sipos and colleagues demonstrated that even in the absence of elevated LVD values and active lymphangiogenesis, PDAC patients still frequently presented with lymph node metastases (Sipos et al., 2005). This suggests that PDAC cells are capable of invading the pre-existing lymphatic vasculature, especially enlarged vessels at tumor margins.

Mechanisms/Players

Mechanisms regulating lymphatic invasion are not completely understood, but are gaining increasing research interest. Most of our knowledge of vascular invasion has come from studies of the blood vasculature that are now being extended to studies of lymphatic vessel properties and function. Initially, invasion of lymphatic vessels by tumor cells was considered to be a passive process with increased interstitial fluid pressure driving tumor cells into draining lymphatic vessels (Hartveit, 1990). Although increased interstitial pressure may contribute to tumor cell invasion, the concept of lymphatic-mediated tumor metastasis as a process that utilizes a “path of least resistance” is greatly oversimplified, and proteomics studies have identified distinctions between primary pancreatic tumors and their corresponding lymph node lesions (Naidoo et al., 2012). Comparisons of pancreas tumors with and without lymph node metastases revealed differences in protein expression intrinsic to these two pathological tumor presentations (Cui et al., 2009). In an effort to better understand the potential drivers of lymphatic metastasis, results of studies of leukocyte intravasation into lymphatic vessels are

now being examined for commonalities to tumor cell intravasation. Three key molecular players of invasion have emerged as likely candidates in the regulation of tumor-lymphatic interactions and metastasis: chemokine signaling, paired binding of adhesion protein partners, and alterations in lymphatic vessel barrier integrity.

Chemokines

Chemokines secreted by lymphatic endothelial cells contribute to inflammation and initiation of immune responses in part by regulating the chemotaxis of antigen presenting cells to the lymph nodes. These same molecules are also being studied for similar roles in tumor metastasis to lymph nodes. Two widely researched candidate chemokines are CCL21 (chemokine (C-C motif) ligand 21) and CXCL12 (chemokine (C-X-C motif) ligand 12) and their respective G-protein coupled receptors (GPCRs), CCR7 (chemokine (C-C motif) receptor 7) and CXCR4 (chemokine (C-X-C) motif receptor 4).

During normal immune responses, lymphatic endothelial cells secrete CCL21 to increase migration of $CCR7^{+}$ DCs toward the vessel and then to guide DCs to the lymph nodes (Tal et al., 2011; Vigl et al., 2011). Tumor cells, including those of pancreatic cancer, overexpress CCR7 and are capable of responding to CCL21 cues to facilitate their dissemination to the lymph nodes (Gunther et al., 2005; Hwang et al., 2012; Irino et al., 2014; Muller et al., 2001; Zhao et al., 2011). Guo, *et al.,* noted a correlation between CCR7 expression in tumor cells and frequency of lymph node metastasis in pancreatic cancer patients (Guo et al., 2013). Sperveslage, *et al.*, confirmed these results and also demonstrated that lymphatic vessels of PDAC patients had significantly higher expression of CCL21 compared to lymphatic vessels of the normal pancreas. Expression of CCL21 in lymphatic vessels correlated with increased lymphatic invasion and

lymph node metastasis in these patients, as did overexpression of CCR7 in pancreatic tumor cells *in vivo* (Sperveslage et al., 2012).

The expression of CCL21 in lymphatic endothelial cells is regulated by numerous inflammatory cytokines including TNF-α and IL-1β and is also influenced by increases in transmural flow (Miteva et al., 2010), both of which are often present in tumor microenvironments. *In vitro* co-culture work has demonstrated that CCR7-expressing tumor cells have increased chemotaxis toward CCL21-expressing lymphatic endothelial cells (Emmett et al., 2011; Issa et al., 2009; Shields et al., 2007). This chemotactic axis is used by tumor cells specifically for invasion into lymphatic vessels; tumor cell chemoattraction to blood endothelial cells does not use this mechanism (Issa et al., 2009; Pang et al., 2015). Blocking CCR7 or CCL21 expression and/or function inhibits lymphatic vessel invasion and metastasis to the lymph nodes *in vitro* and *in vivo* (Shields et al., 2007; Wiley et al., 2001; Yu et al., 2008b). This chemokine signaling axis appears to be regulated by and to work in concert with VEGF-C to synergistically promote lymphatic invasion of $CCR7^+$ and VEGFR-3^+ tumor cells (Issa et al., 2009).

Another chemokine axis that influences lymphatic metastasis is that of CXCL12-CXCR4. It has been widely documented that CXCR4-expressing tumor cells, including PDAC cells, home to organs with high CXCL12 expression, such as the lungs, bone marrow, and lymph nodes (Cardones et al., 2003; Cui et al., 2011; Kaifi et al., 2005; Muller et al., 2001). In PDAC patient tissues, high expression of CXCR4 was found in tumors, while lymph nodes expressed high levels of CXCL12 (Cui et al., 2011; Wehler et al., 2006). This expression pattern positively correlated with increased LVD values in the pancreas, lymph node metastasis frequency, and poor disease prognosis. Tumor-associated, but not normal uninflamed, LECs secrete ample amounts of CXCL12 in the tumor microenvironment and attract $CXCR4^+$ tumor cells to lymphatic vessels and

lymph nodes (Hirakawa et al., 2009; Kim et al., 2010b). Blocking the CXCR4-CXCL12 signaling axis has resulted in impaired lymph node metastasis in numerous tumor models (Chu et al., 2007; Liu et al., 2014b; Uchida et al., 2011). An *in vitro* breast cancer model demonstrated that CXCL12-treated LECs permitted greater transendothelial migration by breast cancer cells, and this permissiveness could be reversed by blocking CXCR4 in the LECs (Yagi et al., 2011). An *in vivo* model of melanoma demonstrated that stem-like, dual positive $CD133^{+}/CXCR4^{+}$ tumor cells were strongly associated with CXCL12-producing LECs and that these cells were resistant to chemotherapy (Kim et al., 2010b). Combinational treatment with a CXCR4 antagonist relieved this resistance and increased the efficacy of chemotherapy thereby reducing tumor growth and metastasis. This study suggested that CXCL12 secretion from lymphatic vessels supported a pro-metastatic and pro-survival niche for tumor cells. Further studies are required to elucidate whether or not these types of mechanisms are employed in PDAC and/or its tumor microenvironment.

Adhesion Proteins

Physical interactions between tumor cells and lymphatic endothelial cells may be another crucial regulator of tumor cell intravasation. Adhesion molecules such as E-selectin, intercellular adhesion molecule 1 (ICAM-1), and vascular adhesion molecule 1 (VCAM-1) are typically used by DCs to gain entry into inflamed lymphatic vessels during migration toward lymph nodes (Johnson et al., 2006; Miteva et al., 2010). Mounting evidence indicates that these same leukocyte adhesion molecules may also be important for controlling tumor cell entry into lymphatic vessels (Kawai et al., 2008; Viola et al., 2013; Yan et al., 2014). In a non-inflamed state, the lymphatic endothelium does not express or only very weakly expresses these adhesion molecules (Johnson et al., 2006; Sawa et al., 2007). Inflammatory conditions—such as those found during infection or tumor development—or a wound healing response quickly

increase the expression of these molecules on the lymphatic endothelium (Johnson et al., 2006; Miteva et al., 2010). Increased transmural flow, also characteristic of an inflamed microenvironment, upregulates ICAM-1 and E-selectin expression on an *in vitro* lymphatic endothelium resulting in increased DC binding (Miteva et al., 2010). A recent report shows that binding and transendothelial migration of breast cancer cells is also influenced by *in vitro* fluid flow, although the mechanisms governing these behaviors have not been elucidated (Pisano et al., 2015). When placed in co-culture with tumor cells, LECs display marked upregulation of adhesion molecules. Kawai, *et al.* (2008 and 2009), have demonstrated that invasive breast cancer cells, which express the αLβ2 ligand for ICAM-1, are capable of inducing the expression of E-selectin and ICAM-1 on lymphatic endothelial cells. They also demonstrated that blocking ICAM-1 impaired the ability of these tumor cells to bind to a lymphatic endothelium (Kawai et al., 2008; Kawai et al., 2009). Studies of the ability of adhesion proteins on lymphatic vessels to regulate tumor cell entry should be expanded to pancreatic cancer cell lines to determine if PDAC tumor cells can use similar mechanisms to bind and gain access to the lymphatic vasculature.

Lymphatic Vessel Barrier Integrity

The intrinsic cellular and molecular organizational characteristics of lymphatic vessels facilitate entry of immune cells and fluids from a collecting tissue bed—properties that may also allow these vessels to support tumor cell metastasis. The initial lymphatic capillaries within tissues are composed of only a single layer of endothelial cells with loose junctions between neighboring cells (Leak, 1976; Maby-El Hajjami and Petrova, 2008). Unlike the tightly-formed, continuously-arranged junctions between neighboring endothelial cells of the blood vasculature (Dejana et al., 2009), the junctional proteins—vascular endothelial cadherin (VE-cadherin), platelet/endothelial cell adhesion molecule-1 (PECAM-1), claudins, occludins, *etc*.—of initial

lymphatic vessels are discontinuously arranged, creating gaps between overlapping lymphatic endothelial cells (Baluk et al., 2007). These discontinuous junctions along with preformed openings in the basement membrane (Pflicke and Sixt, 2009) enable uptake of macromolecules, fluids, and cells by the initial lymphatic capillaries. As lymph and cells are transported up the lymphatic vasculature to the collecting lymphatic vessels, the discontinuous intercellular junctions become more constant and successive to prevent leakage prior to arrival at the lymph nodes (Baluk et al., 2007).

Data suggest that tumor cells are capable of modulating the barrier integrity of the lymphatic endothelium to further facilitate lymphatic vessel invasion (Kerjaschki et al., 2011). Lipoxygenase secretion by breast cancer cells has been shown to disrupt VE-cadherin junctions and induce endothelial cell repulsion, resulting in breaches in the lymphatic endothelium. Tumor-secreted VEGF-C also facilitates invasion by creating leaky lymphatic vasculature. VEGF-C induces the internalization of VE-cadherin, which, in turn, promotes tumor cell transendothelial migration (He et al., 2005; Tacconi et al., 2015). In a pancreatic tumor model, inhibiting Ang-2 signaling with a soluble Tie-2 receptor decreased lymphatic-directed metastasis to the lymph nodes (Schulz et al., 2011). This result may be explained by studies demonstrating that Ang-2 disrupts the barrier integrity of the lymphatic endothelium and increases lymphatic permeability through phosphorylation of VE-cadherin resulting in button-junction formation in the initial lymphatic capillaries (Zheng et al., 2014).

Comparative Tools and Models to Study Lymphatic Biology and Tumor-Lymphatic Interactions

The discoveries of lymphatic endothelium markers such as lymphatic vessel hyaluronan receptor-1 (Lyve-1) (Banerji et al., 1999), Prox-1 (Wigle and Oliver, 1999), VEGFR-3 (Kaipainen et al., 1995), and podoplanin (PDPN) (Breiteneder-Geleff et al., 1997; Schacht et al., 2003;

Wetterwald et al., 1996) have facilitated the development of new research methodologies and models with which to study lymphatic vessel biology under homeostasis and various disease pathologies as well as interactions between lymphatic endothelial cells, immune cells, and tumor cells *in vivo*. The mouse cornea and skin have emerged as two popular mammalian platforms for this type of work. Historically used for studies of angiogenesis, the murine corneal model system has proven equally informative for studies of lymphatic biology because of its unique characteristics. The normal healthy cornea harbors a single limbal lymphatic vessel ring at its periphery and is otherwise devoid of lymphatic vessels. Upon insult or injury, inflammatory lymphangiogenesis occurs resulting in extension of newly-synthesized lymphatic vessels from the limbal arcade toward the site of the stimulus. Corneal injury can be recapitulated experimentally by placement of sutures, mechanical debridement, or chemical burn. A refinement of this inflammatory model enabling more mechanistic dissection of lymphatic vessel behavior is the corneal micropocket assay in which a micropellet can be loaded with a protein or drug of interest and implanted into the cornea (Cao et al., 2011; Fink et al., 2014; Kenyon et al., 1996). Further modifications of traditional acute inflammatory protocols can induce wound recovery (Fink et al., 2014; Kelley et al., 2011a) and recurrent inflammation (Fink et al., 2014; Kelley et al., 2013a)—two additional distinct physiological microenvironments with implications for wound healing, chronic inflammatory disease, and tumor microenvironment research. Anatomical sites commonly used in skin imaging studies include murine dorsal surface, foot pad, and pinna. Unlike the cornea, the skin is vascularized with a dense network of lymphatic capillaries under steady state conditions. This presents an ideal system for studies of lymphatic vessel homeostasis and remodeling, local inflammatory lymphangiogenesis, and endothelium-immune/tumor interactions.

Both cornea and skin have also been employed in real time live-imaging and intravital microscopy studies (Kilarski et al., 2013; Li et al., 2012; Pflicke and Sixt, 2009; Steven et al., 2011). Early experiments of this type relied on injection and uptake of large fluorescent conjugate molecules such as FITC-dextran or explant immunostaining (Reviewed in (Tran Cao et al., 2011)) to label vasculature and other tissue antigens, but recently several genetically engineered mouse models (Bianchi et al., 2015; Choi et al., 2011; Connor et al., 2016; Hagerling et al., 2011; Martinez-Corral et al., 2012; Truman et al., 2012) have enabled more sophisticated lymphatic vessel-specific experimental designs. In these immunocompetent models, fluorescent protein expression is driven by lymphatic endothelium-specific promoters such as Prox-1, Lyve-1, or VEGFR-3 in either a constitutive or inducible manner. Inducible systems offer the advantages of titration and temporal control of fluorescence expression within the lymphatic endothelial compartment. Fluorescently labeled tumor or immune cells may be delivered to and tracked along with endogenously fluorescent lymphatic vessels providing insight into intravasation/extravasation behavior, cell trafficking and fate, and spread to draining lymph nodes. Translation of these techniques to studies of the pancreatic lymphatic vasculature specifically would provide insight into organ-specific lymphatic vessel biology and pancreatic tumor microenvironment contributions to lymphatic remodeling and lymphatic-mediated metastasis. We suggest combination of several existing technologies to examine these questions. First, crossing a spontaneous pancreatic ductal adenocarcinoma model containing a fluorescent reporter gene, such as the PKCY (Rhim et al., 2012) or KPCT mouse (Stopczynski et al., 2014), with one of the available lymphatic-specific reporter mice would facilitate visualization of cells of pancreatic origin and lymphatic vessels in two colors. Implantation of a pancreas window (Ritsma et al., 2013) in these animals could enable long term intravital microscopy studies of lymphatic vessel biology and tumor metastasis throughout the course of

disease progression, from PanIN formation through advanced metastatic disease. Finally, use of the CLARITY technique as previously described for brain (Chung and Deisseroth, 2013; Chung et al., 2013a) in concert with multiphoton microscopy and immunofluorescent staining would allow deep tissue visualization and reconstruction of full lymphatic vascular networks as well as detection of other important microenvironmental structures (such as nerve and blood vascular networks) and signaling molecules both peri- and intratumorally.

Other research and pre-clinical imaging models have further studied lymphatic vessel- and lymph node-related pathologies in cancer. High resolution magenetic resonance imaging (MRI) has proven an effective non-invasive strategy for mapping involved mouse lymph nodes in pancreatic ductal adenocarcinoma (Zhang et al., 2013). Multiphoton laser scanning microscopy work in a model of melanoma showed that functional lymphatic vessels are not present within the tumor proper and that functional peri-tumoral lymphatic vessels are sufficient to mediate metastasis (Padera et al., 2002). Other methods of lymph node and metastasis imaging (reviewed in (Tran Cao et al., 2011)) have included injection of dyes or radiotracers such as Lymphoseek for lymphoscintigraphy, injection and uptake of cancer-specific radio-labeled antibodies and their accumulation in affected lymph nodes, injection of fluorescent antibody conjugates against the lymphatic endothelium in combination with fluorescent reporter-expressing pancreatic cancer cells, and use of combinatorial bioluminescence and fluorescence resonance energy transfer (BRET-FRET) nanoparticles for mapping lymphovascular and node networks (Xiong et al., 2012). Fluorescence lifetime imaging microscopy (FLIM)-FRET (Nobis et al., 2013), optical coherence tomography (Huang et al., 1991), optical frequency domain imaging (Vakoc et al., 2009), photoacoustic tomography (Wang et al., 2003), higher-order harmonics generation (Wu et al., 2015), and Raman spectroscopy (Krafft and Popp, 2015) imaging technologies offer other options for reconstructive deep tissue imaging and analysis of single

cell signaling within an intact tumor microenvironment. Jeong and Jones, *et al.,* have also established a chronic lymph node window to facilitate long-term live imaging microscopy studies of lymph node biology, angiogenesis and lymphangiogenesis, and nodal deposition of metastatic tumor cells (Jeong et al., 2015). Application of CRISPR-Cas9 gene editing technology (Cong et al., 2013) may also prove useful in generating new pre-clinical models suitable for lymphatic vessel imaging in disease.

Clinical Imaging Techniques to Detect Pancreatic Cancer Lymph Node Metastasis

Despite research advances in comparative lymphatic vessel imaging, clinical imaging of pancreatic cancer patient lymphatic networks and lymph node status has remained challenging. Several groups have examined the utility of traditional clinical imaging platforms for detection of lymph node metastasis with limited success. Roche, *et al.*, have shown that examination of peripancreatic lymph nodes by computed tomography (CT) cannot accurately predict presence of metastatic deposits (Roche et al., 2003). Similarly, Imai, *et al.*, showed that CT, magnetic resonance imaging (MRI), and fluorodeoxyglucose-positron emission tomography (FDG-PET) were not consistently accurate in predicting pre-operative para-aortic lymph node involvement in pancreatic cancer patients (Imai et al., 2010). Conversely, another group had some success using endoscopic ultrasound (EUS) to differentiate benign and cancerous lymph nodes and to identify diseased pancreas; this technique has not been fully developed for widespread clinical use (Kumon et al., 2010). Cesmebasi, *et al.*, have recently reviewed other advances in clinical imaging techniques including EUS and lymphotropic nanoparticle-enhanced MRI, reporting that further refinement of these techniques may make them promising options to identify patterns of pancreatic cancer spread (Cesmebasi et al., 2015). Other groups have focused efforts on imaging routes of pancreatic drainage in attempts to identify sentinel lymph nodes for pancreatic tumors arising in various locations within the pancreas. Injection of indocyanine

green fluorescent dye into the pancreatic surface during pancreat(ic)oduodenectomy (PD) surgery allowed visualization of pancreatic lymphatic vessels intraoperatively and resulted in identification of seven routes of lymphatic drainage highlighting the complexity of the pancreatic lymphatic vascular network (Hirono et al., 2012). In a similar study methylene blue dye was injected peri- and intratumorally during pancreatic cancer resection, but the authors concluded that detection of patterns of pancreatic lymphatic drainage and sentinel lymph node identification were not feasible with this protocol (Kocher et al., 2007). Another group injected activated carbon particles or regular insulin colloid at resection and examined their patterns of spread to surgically-removed lymph nodes by histology. They documented uptake in several groups of lymph nodes and recommended new radical resection guidelines based on their findings (Nagakawa et al., 1994). Development and testing of additional lymphatic imaging technologies and their adaptation to pancreatic adenocarcinoma patients may make pre-operative identification of lymph node metastases a reality in the future (Karaman and Detmar, 2014; Nune et al., 2011; Sevick-Muraca et al., 2014).

Lymphatic Vessel-Nerve Interactions

Nerves and vasculature directly interact within the pancreatic microenvironment and can be influenced by overlapping signaling pathways in development and disease. Studies have shown that lymphatic vessels (Carlson et al., 1995; Mignini et al., 2012) and lymph nodes (Kayahara et al., 2007) are innervated, while dorsal root ganglia (DRGs) are known to be vascularized (Jimenez-Andrade et al., 2008). In the context of malignancy, these connections may represent an additional route of metastatic dissemination of tumor cells from either network to the other (Cheng et al., 2012; Ishikawa et al., 1988; Jimenez-Andrade et al., 2008; Kayahara et al., 2007). Tracts of continuous cancer cells with fingers projecting into perineural spaces and lymphatic vessels and lymph nodes have also been described (Kayahara et al., 2007; Suzuki et al., 1994). It

is well documented that vasculature and nerves can respond to the same molecular cues—termed neurovascular guidance molecules—for development and remodeling (Bouvree et al., 2012a; Caunt et al., 2008; Fink et al., 2014; Xu et al., 2010; Yang et al., 2010; Zhang et al., 2015), and many of these molecules, such as NRP-1 and -2, NGF, brain-derived neurotrophic factor (BDNF), FGF, IGF-2, netrin-1, semaphorin-3A, ephrin receptor B4, SLIT2, and ROBO1 may be differentially expressed or have altered signaling functions in the pancreatic tumor microenvironment, implicating them in cancer progression (Dallas et al., 2008; Fukahi et al., 2004; Gohrig et al., 2014; He et al., 2013a; Li and Zhao, 2013; Li et al., 2014; Mancino et al., 2011; Muller et al., 2007; Zhu et al., 1999a). As well, somatic alterations in axon guidance pathway genes are observed in a subset of pancreatic cancer genomes (Biankin et al., 2012). Remarkably, Chen, *et al.*, showed that in the absence of both perineural and lymphovascular invasion, the five-year survival rate for pancreatic adenocarcinoma patients was 71% (Chen et al., 2010). These studies underscore the importance of both lymphatics and nerves in the pancreatic tumor microenvironment and highlight the need for further mechanistic work interrogating the specific contributions of these tissue networks to disease progression and metastasis.

Pancreas-Associated Peripheral Nervous System: Normal Biology and Importance in PDAC

Nerve Microanatomy

Peripheral nerves are complex structures. The outer layer of a nerve is a tough matrix of collagen and elastin fibers known as the epineurium. The epineurium protects and houses several fascicles. Each fascicle is encased by a layer of endothelial cells called the perineurium and contains several bundles of nerve fibers, often myelinated, and their supporting glia (Schwann cells). The highly vascularized matrix within the perineurium and surrounding nerve fiber bundles is the endoneurium (Bapat et al., 2011a). Each bundle of nerve fibers contains

several axons projecting away from their parent cell body (residing in the brain, spinal cord, ganglion, etc.); efferent and afferent fibers and those of different branches of the nervous system (parasympathetic, sympathetic, sensory, etc.) may be contained within a single nerve.

Pancreatic Innervation

Nervous tissue surrounding the pancreas can be divided into six distinct regions detectable by MRI or CT: namely, the aortic, hepatic, splenic, and celiac plexuses, the superior mesenteric artery plexus, and the pancreatic head plexus (Zuo et al., 2012b). From this densely innervated peripancreatic region, sensory, sympathetic, and parasympathetic nerve fibers extend into the pancreas in nerves often closely associated with blood vessels (Bockman, 2007; Christians and Evans, 2009; Fernandez-Cruz et al., 1999). The two primary nerve systems innervating the pancreas are splanchnic and vagus; splanchnic nerves comprise efferent sympathetic fibers and afferent sensory fibers; vagal nerves comprise parasympathetic efferents and sensory afferents. Initial cell bodies of sympathetic neurons forming connections in the splanchnic system reside in the thoracic intermediolateral cell columns of the spinal cord; these fibers traverse sympathetic ganglia without synapse and eventually end in celiac plexus ganglia; postganglionic sympathetic fibers terminate near cells of intrapancreatic blood vessels, exocrine cells, or islets (Bockman, 2007). Neuronal cell bodies of parasympathetic fibers making up the vagus nerve reside in the brainstem; unlike their splanchnic counterparts, these do not terminate in the celiac plexus, but rather pass through it and terminate in intrapancreatic ganglia; postganglionic fibers then extend out to exocrine cells or islets (Bockman, 2007). The main function of pancreatic nerves is to control secretion of exocrine and endocrine products including digestive enzymes and hormones. Direct connections between gut and pancreas, termed the entero-pancreatic axis, also contribute to the intricacy of pancreatic innervation and modulate pancreatic secretions (Kirchgessner and Gershon, 1990). Indirect control of islets due

to regulation of blood flow by sympathetic innervation of vascular smooth muscle has also been described (Rodriguez-Diaz et al., 2011). While sensory fibers serve primarily as informers of pancreatic damage *via* transmission of pain signals, sensory responses to tastes and smells, as well as detection of glucose levels in blood or duodenum, can induce a change in pancreatic secretions (Bockman, 2007).

Perineural Invasion and Neuroremodeling in PDAC

Background

Perineural invasion (PNI) causes intense pain, often precludes curative resection, and may provide a mechanism of recurrence following otherwise successful surgery. A feature of several types of cancer, this devastating pathology complicates nearly all PDAC cases (Bapat et al., 2011b; Fernandez-Cruz et al., 1999; Sergeant et al., 2009) and contributes to decreased patient quality-of-life and reduced overall survival. As described above, the peripancreatic region is densely innervated and the pancreas parenchyma houses intrinsic ganglia. The term perineural invasion encompasses several specific nerve-tumor interactions including the following: presence of tumor immediately adjacent to intra- or extrapancreatic nerve, often applying pressure; infiltration of tumor cells into the nerve itself (may be into perineurium, epineurium, or endoneurium); or engulfment of peripancreatic nerve plexus or intrinsic ganglia by tumor-associated stroma (Farrow et al., 2008) or tumor proper. Nerves may also be recruited into the primary tumor as a result of neurotrophic factor release by tumor and stellate cells. Once inside a nerve, a tumor may extend within this space without invasion back out from nerve into adjacent tissue (Pour et al., 2003) or intraneural tumor may be linked to extraneural tumor at several places along an invaded nerve or continuous with tumor cells in lymphatics (Suzuki et al., 1994). Studies have characterized patterns of perineural spread from PDAC tumors arising in different parts of the pancreas. Pancreatic head tumors have been shown to

travel along the posterior hepatic plexus to the celiac plexus and ganglion, while tumors arising in the uncinate process may follow the innervation along the inferior pancreatoduodenal artery to the superior mesenteric artery (Yi et al., 2003). Another study classified tumors according to their origins in either dorsal or ventral pancreas based on embryologic pancreatic development; dorsal PDAC invaded the common hepatic artery plexus and plexus within the hepatoduodenal ligament while ventral carcinoma invaded pancreatic head plexus 1 and 2 and superior mesenteric artery plexus (Makino et al., 2008). Evidence suggests that PNI is an early event in the progression of PDAC. PNI was present in two very small PDAC tumors detected incidentally at autopsy (Case 1: 4 x 2 mm; Case 2: two separate lesions 2.6 x 0.7 mm and 1.2 x 0.5 mm) (Kimura et al., 1998) and has been found in samples comprising all stages of PDAC.

Players and Mechanisms

PDAC cells and nerves are often described in mutually supportive roles, with each cell type expressing receptors/ligands and elaborating factors into the microenvironment that support the proliferation, survival, and migration of the opposing cell type. *In vitro* work has demonstrated the reciprocal benefits of nerve and PDAC co-culture. T3M4 PDAC cells co-cultured with rat DRGs or neurons of the myenteric plexus (MP) displayed an elongated directional morphology targeted toward neurites prior to cell migration (Ceyhan et al., 2008), and MiaPaCa2/mouse DRG co-cultures showed larger PDAC colony size, increased neurite extension, enhanced proliferation, increased expression of survival genes MALT1 (mucosa-associated lymphoid tissue lymphoma translocation protein 1) and TRAF (TNF receptor associated factor), and decreased apoptosis (Dai et al., 2007). Similarly, MP and DRG neurons displayed increased neural density and hypertrophy when cultured in the presence of PDAC or chronic pancreatitis (CP) tissue extracts or PDAC cell line supernatant (Demir et al., 2010).

As with lymphatic-tumor interactions, adhesion proteins play a role in PDAC perineural invasion. Moesin and E-cadherin were significantly associated with PNI, and moesin expression in tumors also correlated with higher tumor grade, poor survival, and lymphovascular invasion (Torer et al., 2007). L1 cell adhesion molecule (L1-CAM) correlated with PNI, pain, lymph node metastasis, and vascular invasion, and was a negative prognostic factor (Ben et al., 2010). Schwann cells surround and support nerve fibers and are responsible for their myelination. Myelin-associated glycoprotein (MAG) is expressed by Schwann cells and has been shown to bind mucin 1 (MUC1), a mucin overexpressed and aberrantly glycosylated in PDAC (Swanson et al., 2007). Interestingly, the role of NCAM in PNI in PDAC and other cancers is less clear, with conflicting reports of its expression and correlation with nerve invasion (Fukuda et al., 2008; Kameda et al., 1999; Li et al., 2003; Solares et al., 2009). CD74 (HLA class II histocompatibility antigen gamma chain) has also been identified as a possible contributor to PNI as it is overexpressed in PDAC with PNI and in PDAC cell lines with a high propensity for PNI (Koide et al., 2006).

Several studies have demonstrated the importance of the chemokine (C-X3-C motif) receptor 1 (CX3CR1) and its sole ligand CX3CL1 (fractalkine) in PDAC PNI. CX3CR1 is present at high levels in PDAC cell lines and patient samples, and its expression is associated with intra- and extrapancreatic nerve invasion and tumor recurrence (Marchesi et al., 2008; Marchesi et al., 2010). CX3CL1 is present in neural tissue both as a membrane-bound ligand and in a secreted form; the secreted protein stimulated PDAC chemotaxis *in vitro* and PDAC-nerve interactions were mediated by the membrane-bound ligand binding its receptor (Marchesi et al., 2008). CX3CR1 is important for transendothelial migration of tumor cells (Marchesi et al., 2010) and DCs, and CX3CL1 is upregulated and secreted from lymphatics in inflammation, mediating DC transendothelial migration (Johnson and Jackson, 2013). CX3CL1/R1 are also overexpressed in

chronic pancreatitis, with highest expression in patients reporting severe pain; this signaling axis directs infiltration of inflammatory immune cells into the pancreas parenchyma and intrapancreatic nerves and activates supporting glia, implicating it in neuropathic pain (Ceyhan et al., 2009c).

Neurotrophic factors NGF and GDNF (glial cell-derived neurotrophic factor) have well-documented roles in promoting PDAC PNI and associated pain. NGF and its primary receptor TrkA (NTRK1; neurotrophic tyrosine kinase receptor type 1) are overexpressed in PDAC cells and are also present in pancreatic nerves. Significant differences in expression levels of these proteins were not detected among grades or stages of PDAC, but high NGF and TrkA were correlated with increased PNI and pain (Zhu et al., 1999b). NGF, GDNF family member artemin, and growth-associated protein 43 (GAP-43) expression levels were increased in PDAC and adjacent normal pancreas and associated with neural hypertrophy and density (Ceyhan et al., 2010). GAP-43 expression has also been linked to increased neural density and hypertrophy in CP as well as pain (Ceyhan et al., 2009a). Gene expression of the primary artemin receptor, GFRα3, also correlated with neural hypertrophy (Ceyhan et al., 2010); this study demonstrated a field effect in which NGF and artemin induced neural aberrations in areas of the pancreas without direct invasion of nerves by tumor. In addition to its expression in primary tumor, artemin has been shown to be overexpressed in metastases, nerves, and blood vessels and to promote PDAC invasion along with GFRα3/RET (Proto-oncogene tyrosine protein kinase receptor Ret) (Ceyhan et al., 2006). (GDNF family ligands bind GFRα family receptors; receptor-ligand complexes bind RET receptor tyrosine kinases to initiate downstream signal transduction (Airaksinen et al., 1999)). GDNF is also overexpressed in PDAC specimens and associated with intrapancreatic PNI and pain, while expression of RET has been shown to predict differentiation status, post-resection survival, and LVI (Zeng et al., 2008). In a study interrogating paracrine

regulation of PNI by peripheral nerves, GDNF, RET, and GFRα1 were overexpressed in PDAC with PNI; GDNF mediated longitudinal PDAC cell migration along nerve *in vitro;* PDAC cells demonstrated decreased nerve invasion to nerves derived from $GDNF^{+/-}$ mice; and RET inhibition with tyrosine kinase inhibitor pyrazolopyrimidine-1 blocked PNI *in vivo* (Gil et al., 2010).

Other factors implicated in PDAC PNI include the receptor ligand pair epidermal growth factor receptor (EGFR)-TNFα (Bockman et al., 1994), aberrant expression of microtubule-associated protein MAPRE2 in PDAC and its upregulation in PNI (Abiatari et al., 2009b), and upregulation of kinesin family member 14 (KIF14) and rho-GDP dissociation inhibitor beta (ARHGDIβ) (Abiatari et al., 2009a).

Pain

PDAC patients often suffer from severe pain. Pancreatic pain is thought to arise from two distinct processes—nociception and neuropathy—and may present as visceral pain or referred somatic pain. Sensory nerves transmit nociceptive signals upon activation by noxious stimuli within the microenvironment; tissue destruction, inflammatory factors elaborated from infiltrating immune cells, and molecules secreted from tumor cells can contribute to stimulation of nociception. Neuropathic pain is caused by damage to nerves themselves; desmoplastic stroma associated with PDAC is characterized by increased internal pressure that may damage nerves, as can direct invasion of nerves by tumor cells. Changes in the complement of nerve fibers present in nerves supplying the pancreas due to malignancy or inflammation may exacerbate pancreatic pain. One study showed that the number of sympathetic and cholinergic nerve fibers in pancreatic nerves, as measured by tyrosine hydroxylase and choline acetyltransferase staining, was lower in PDAC and CP, and this change was associated with increased patient pain; the authors suggested that a reciprocal increase in sensory nerve fibers

may coincide with depletion of sympathetic and cholinergic fibers, thus increasing nociceptive capacity (Ceyhan et al., 2009b). In addition to these intrinsic alterations in nerve fiber bundle composition, nerves in PDAC are often present at greater densities within the tissue and display hypertrophy, as described above. Other inflammatory diseases, such as inflammatory bowel disease (IBD) are characterized by neuropathic changes such as hypertrophy, hyperplasia, and axonal damage (Geboes and Collins, 1998), but these patients do not report the same caliber of pain as that experienced by PDAC patients, suggesting that neuroremodeling alone cannot explain the pathogenesis of PDAC-associated pain.

Treatment of PDAC pain has proven challenging. The location of the celiac plexus as a central hub within the pathway of pancreatic innervation has made it a target of pain relief techniques. Celiac plexus blockade (injection of alcohol to destroy nerve tissue) has had limited clinical success, likely due to referral of pain to other areas and involvement of nerves synapsing in other ganglia. Opioid pain relievers may offer some palliation, but patients often develop tolerance to these medications and become dependent upon ever-increasing doses of analgesics, which in turn carry their own sets of undesirable side effects (Inturrisi, 2003).

PNI and Clinical Outcomes

As with lymphatics, nerve-specific metrics can be used to predict outcomes in PDAC patients. A retrospective study of 153 resected PDAC patients found an inverse correlation between incidence of intrapancreatic PNI and disease-free survival (DFS); tumor stage did not predict presence of PNI (Shimada et al., 2011a). A prospective phase II clinical trial of 110 resected PDAC patients who received preoperative gemcitabine-based chemoradiation therapy identified PNI as the sole predictor of abdominal cavity recurrence, and positive lymph node status was the only predictor of distant recurrence; PNI and lymph node involvement were both

associated with decreased DFS (Takahashi et al., 2012). A study of 51 PDAC tumor samples found that NGF expression was positively associated with presence and degree (between epineurium and endoneurium vs. within endoneurium) of PNI, LN metastasis, and positive resection margins; degree of nerve infiltration was also identified as a negative prognostic factor and correlated with TrkA expression (Ma et al., 2008). Finally, a 500+ case study of pancreatic nerve alterations and pain found that only PDAC and CP displayed increased nerve density and hypertrophy among other pancreatic disease states including serous/mucinous cystadenomas, invasive/noninvasive intraductal papillary mucinous neoplasias, benign/malignant neuroendocrine tumors, ampullary cancer, and normal pancreas; this study also identified pain as a negative prognostic factor in PDAC (Ceyhan et al., 2009a). MRI and CT imaging have been used clinically to detect invaded extrapancreatic neural plexus in patients (Zuo et al., 2012a).

Perineural invasion has been implicated in local and distant recurrence after resection (Fernandez-Cruz et al., 1999; Kayahara et al., 1993; Masui et al., 2013; Shimada et al., 2011b). Micrometastatic deposits within nerves may foil an otherwise clean resection, and tumor cells may find sanctuary from chemotherapeutic agents in the relatively protected environment of a nerve. In an effort to decrease these effects, it has been suggested that extrapancreatic nerve tissue be removed as part of radical pancreatic resection procedures (Fernandez-Cruz et al., 1999; Kayahara et al., 1991; Kayahara et al., 1993; Masui et al., 2013; Meriggi et al., 2007; Samra et al., 2008)

Other Players in PDAC Microenvironment

The PDAC microenvironment is arguably one of the most complex of any tumor microenvironment, replete with CAFs, immunosuppressive leukocytes, tumor-associated blood/lymphatic endothelial networks, nerves, and a considerably dense ECM compartment.

Each of these components facilitates PDAC progression and dissemination and has the capacity to influence the normal lymphatic vasculature within the pancreas.

Figure 1. Pancreatic tumor microenvironment and lymph node metastasis. Cells of the tumor microenvironment are essential contributors to tumor growth, perineural invasion, lymphatic vessel invasion, and lymph node metastasis. CAFs and TAMs secrete pro-lymphangiogenic factors and proteases needed for lymphangiogenesis and metastasis. Lymphatic vessels act as conduits not only for tumor cell metastasis, but also for immunosuppressive cell and cytokine transport to lymph nodes. Mutual tropism between nerves and cancer cells through secreted cytokines and direct receptor-ligand interactions instigate perineural invasion, another route of pancreatic tumor metastasis. Vascularization of nerves and innervation of vessels may facilitate metastatic spread of tumor cells between these respective networks. (This figure was previously published in Fink et al., 2015a).

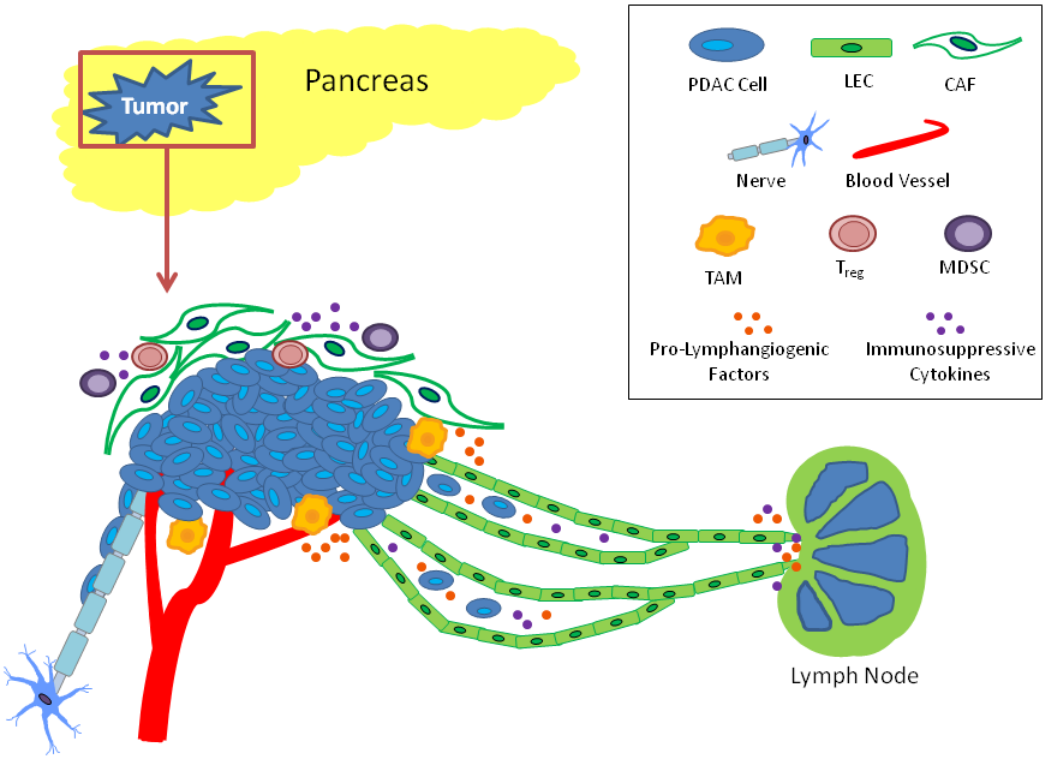
Tumor
Pancreas
PDAC Cell
LEC
CAF
Nerve
Blood Vessel
TAM
T_{reg}
MDSC
Pro-Lymphangiogenic Factors
Immunosuppressive Cytokines
Lymph Node

Figure 1

Cancer-Associated Fibroblasts

One of the most striking features of PDAC is the robust desmoplastic reaction seen within the primary tumor. Due to their abundance in the PDAC microenvironment, CAFs exert a strong influence over other microenvironmental cell types including the lymphatic endothelium (Hanahan and Coussens, 2012). One of the main protein regulators of desmoplasia in PDAC is sonic hedgehog (Shh) (Bailey et al., 2008; Tian et al., 2009). Bailey, *et al.* (2009), noted that Shh signaling in the CAFs of PDAC tumors led to the creation of a pro-angiogenic and pro-lymphangiogenic stromal compartment. When Shh signaling was inhibited in the CAFs, LVD decreased and lymph node metastasis was reduced. Data such as these suggest that CAFs primarily influence the lymphatic endothelium *via* secretion of various effector proteins. It has been demonstrated that CAFs of various tumor types, including PDAC, secrete a wide range of pro-lymphangiogenic factors such as VEGF-C, VEGF-D (Duong et al., 2012; Koyama et al., 2008), VEGF-A (Mace et al., 2013), epidermal growth factor (EGF) (Dadras, 2013), PDGF, and FGF (Feig et al., 2012). CAFs also secrete chemokines, including CXCL12, which has been shown to correlate with increased tumor aggressiveness, LVD values, and lymph node metastases in PDAC patient tissues (Cui et al., 2011; Feig et al., 2013). In addition to their direct action on lymphatic endothelia, many of these same secreted factors as well as pro-inflammatory cytokines allow CAFs to indirectly support lymphangiogenesis and lymphatic vessel invasion through the recruitment of pro-lymphangiogenic immune cells such as TAMs and DCs (Liao et al., 2009; Rasanen and Vaheri, 2010). Lastly, CAFs secrete matrix metalloproteinases (MMPs) and other proteases that remodel the ECM of tumors (Kessenbrock et al., 2010). This remodeling promotes tumor invasion of stroma and tumor vasculature and releases sequestered growth factors and cytokines from the ECM for tumor growth, angiogenesis, and lymphangiogenesis. A recent study by Shi, *et al.*, highlights an additional protease-related mechanism by which CAFs

may influence pancreatic cancer progression and lymphatic metastasis. Specific pancreatic stromal compartment deletion of protease-activated receptor-2 (PAR-2), a GPCR highly expressed in PDAC, resulted in decreased primary tumor size (due to anti-angiogenesis effects) but increased LVD and lymph node metastases (Shi et al., 2014).

Immune Cells and Immune Regulation

One of the main functions of lymphatic vessels is to transport leukocytes to lymph nodes for immune response initiation, uniquely positioning LECs to modulate immune responses in ways that may support tumor progression. As immune cell trafficking conduits, LECs are responsible for the transport of both antigens and antigen presenting cells, such as DCs, to the lymph nodes for immune response optimization (Tal et al., 2011). By regulating the expression and secretion of various chemokines in response to inflammation, injury, or tumor development, LECs can alter the recruitment of immune cells to the lymph nodes, and, as a result, influence the ensuing immune response (reviewed in (Aebischer et al., 2014; Liao and von der Weid, 2015)). Partially due to lymphatic-directed recruitment, tumor-draining lymph nodes demonstrate a more immunosuppressive environment as compared to normal lymph nodes with an increased presence of regulatory T cells (T_{regs}), myeloid-derived suppressor cells (MDSCs), immature and tolerogenic DCs, and immunosuppressive cytokines (Inman et al., 2014; Munn and Mellor, 2006; Podgrabinska et al., 2009; Shields et al., 2010). These immunosuppressive cells and cytokines accumulate in the lymph as a result of increased lymphatic drainage from the tumor site (Harrell et al., 2007). Within the lymph nodes TGF-β, a major driver of immune suppression, supports the differentiation and activation of T_{regs} as well as promoting tolerogenic and immature phenotypes of DCs (Ghiringhelli et al., 2005). As T_{regs} differentiate and accumulate, they secrete more TGF-β to further drive immune suppression. Interleukin-10 (IL-10) is another factor that supports the accumulation of immunosuppressive

cells in the lymph nodes by promoting T_{reg} activity (Seo et al., 2001b) and tolerogenic DC function (De Smedt et al., 1997; Seo et al., 2001b). Indoleamine 2,3-dioxygenase increases the generation of T_{regs} in the lymph nodes (Fallarino et al., 2006; Munn and Mellor, 2007), while concurrently inhibiting effector T cell activity (Munn et al., 2005). Other factors implicated in the accumulation of immunosuppressive cells in lymph nodes include interleukin-4 (IL-4), VEGF-A, and prostaglandin E_2 (Kim et al., 2006).

In addition to cellular and cytokine transport, LECs also transport tissue antigens (and in the case of cancer, tumor antigens) from peripheral tissues to lymph nodes. Studies have demonstrated that LECs, particularly those in the lymph nodes, are capable of scavenging these tissue and tumor antigens and cross-presenting them on major histocompatibility complex-I (MHC-I) (Hirosue et al., 2014; Lund et al., 2012). This can lead to immune tolerance through deletion of naive $CD8^+$ T cells as LECs lack co-stimulatory molecules needed to activate the T cells and instead express programmed death-ligand 1 (PD-L1), an inhibitory signal for T cells (Tewalt et al., 2012). LECs can also present scavenged exogenous tissue/tumor antigens on MHC-II molecules and likely induce immune tolerance through interactions with the inhibitory lymphocyte activation gene-3 (LAG-3) protein on $CD8^+$ T cells (Rouhani et al., 2015). These studies shed light on the phenomenon that when tumor cells are denied lymphatic vessel experience, such as through direct implantation into lymph nodes, tumor immunity is impaired through a robust $CD8^+$ T cell response (Preynat-Seauve et al., 2007). LECs also modulate immune responses by inhibiting DC maturation (Podgrabinska et al., 2009). Binding of DCs to the lymphatic endothelium *via* macrophage-1 antigen (Mac-1) and ICAM-1-mediated interactions during transendothelial migration can reduce the expression of co-stimulatory molecules on DCs needed for T cell activation. Studies such as these inspire new ideas regarding increased lymphangiogenesis at the tumor periphery and draining lymph nodes, suggesting that

it may influence tumor progression in two ways: 1) increasing metastatic routes for dissemination and 2) immune suppression through increased antigen scavenging and decreased DC maturation leading to T cell inhibition and immune tolerance (Swartz, 2014). Further investigation is needed to substantiate the immunosuppressive properties of the lymphatic endothelium and its specific contribution to disease progression as a component of the tumor microenvironment.

A reciprocal concept in relation to the capacity of LECs to affect immunity is that of immune cells inducing effects on LECs. One such tumor infiltrating immune cell type, TAMs, can be found in many tumor microenvironments, including PDAC (Condeelis and Pollard, 2006; Kurahara et al., 2013; Leek and Harris, 2002; Schoppmann et al., 2002), and their presence often correlates with poor patient prognosis (Jung et al., 2015; Kurahara et al., 2011; Sugimura et al., 2015; Yuan et al., 2014). TAMs promote tumor lymphangiogenesis through two mechanisms: paracrine secretion of pro-lymphangiogenic factors and transdifferentiation into LEC-like progenitor cells. TAMs secrete high levels of VEGF-C and -D, which, in turn, increases LVD in and around tumors (Kurahara et al., 2013; Schoppmann et al., 2002; Schoppmann et al., 2006; Wu et al., 2012). Indeed, TAM density has been shown to significantly correlate with increased LVD, lymphatic vessel invasion, and lymph node metastasis in many cancers (Ding et al., 2012; Kurahara et al., 2013; Schoppmann et al., 2006; Storr et al., 2012; Zhang et al., 2011). Inhibition or depletion of TAMs from tumor microenvironments significantly reduced LVD values and decreased the incidence of lymph node metastases compared to tumors with TAMs present (Fischer et al., 2007; Yang et al., 2011b; Zumsteg et al., 2009). However, depletion of TAMs did not completely inhibit lymph node metastasis as tumor cells were still able to invade pre-existing lymphatic vessels. These macrophages also secrete proteases such as MMP-2, MMP-9, and plasmin/urokinase plasminogen activator (uPA) that remodel the extracellular

microenvironment and release sequestered growth factors for lymphangiogenesis (Marconi et al., 2008; Ran and Montgomery, 2012). The plasmin/uPA system is also important for the proteolytic maturation of VEGF-C and -D increasing their affinity for VEGFR-3 (McColl et al., 2003). It has yet to be determined if TAMs secrete any of the other factors known to promote lymphangiogenesis. The second way TAMs contribute to lymphangiogenesis is by transdifferentiating into LEC-like progenitors both in inflammatory and tumor settings (Hall et al., 2012; Hunter et al., 2014; Schledzewski et al., 2006; Zumsteg et al., 2009). Transdifferentiated macrophages undergo genetic reprogramming (Hall et al., 2012) with increased expression of lymphatic markers Lyve-1, Prox-1, podoplanin, and VEGFR-3 (Hall et al., 2012; Lee et al., 2010; Maruyama et al., 2005; Zumsteg et al., 2009). Expression of LEC markers enables TAMs to physically incorporate into the newly developing lymphatic vasculature. The percentage of transdifferentiated TAMs within these newly formed lymphatic vessels is often less than 10% (Lee et al., 2010; Zumsteg et al., 2009) suggesting the main mechanism by which TAMs promote tumor-associated lymphangiogenesis is through secretion of pro-lymphangiogenic factors.

Another Inflammation-Associated Paraneoplastic Effect of PDAC: Cancer-Associated Cachexia

Considerations of cancer often focus on the direct effects of primary tumor and metastatic deposits on involved organs. However, cancer often results in systemic consequences beyond those directly attributable to compromised organ function. One such paraneoplastic syndrome is cancer-associated cachexia. Cancer cachexia negatively affects patient quality-of-life, decreases the efficacy of anti-tumor therapies either directly or by reducing patient tolerance for taxing treatment regimens, and may be responsible for shortened survival. Cachexia has been assigned both causal and complicating roles in its status as a cancer comorbidity (Muscaritoli et al., 2015). An international expert panel recently released a

consensus definition of cancer cachexia stating, “Cancer cachexia [is] a multifactorial syndrome defined by an ongoing loss of skeletal muscle mass (with or without loss of fat mass) that cannot be fully reversed by conventional nutritional support and leads to progressive functional impairment” (Fearon et al., 2011). The nature of cachexia as a progressive disease, beginning with understated and possibly reversible pre-cachexia symptoms and gradually advancing to a severe refractive state requiring specialized individual patient care is well recognized; although specific criteria for patient stratification differ among groups (Baracos, 2011; Fearon et al., 2011; Johns et al., 2014; Martin et al., 2015). Cachexia has also been described as a disorder of metabolic flux (Penet et al., 2011), with decreased appetite, anorexia, and early satiety contributing to decreased nutritional intake, while increased proteolysis, lipolysis, and altered carbohydrate metabolism promote an imbalance in anabolic and catabolic processes and increased resting energy expenditure (Argiles et al., 2014; Baracos, 2011); together these processes result in net weight loss, decreased skeletal muscle mass, weakness, fatigue, and overall decreased patient quality-of-life.

PDAC patients as a population are highly susceptible to cachexia. Cancer cachexia has been estimated to affect over 80% of pancreatic cancer patients and to directly contribute to 20% of cancer-related deaths (Argiles et al., 2014). PDAC patients with muscle loss after treatment displayed decreased survival compared to patients with stable muscle mass or muscle gain (Fogelman et al., 2014). Cachexia is also linked to disruption of the glucose-insulin axis often manifested in PDAC by the onset of type II diabetes mellitus. Glucose intolerance and insulin resistance may be implicated in loss of muscle mass in cancer-associated cachexia (Asp et al., 2010) (Reviewed in (Honors and Kinzig, 2012)). Treatment of C26 colon tumor-bearing mice with rosiglitazone ameliorated insulin resistance and began to reverse cachexia (Asp et al., 2010). Additionally, a large retrospective analysis of PDAC cases and controls has documented

an inverse relationship between fasting blood glucose (FBG) and body mass index (BMI) in the twelve months preceding PDAC diagnosis (Pannala et al., 2009) suggesting potential utility in early disease detection. Glucose neurotoxicity is also linked to repeated or persistent hyperglycemia, as is the case in diabetic neuropathy (Reviewed in (Tomlinson and Gardiner, 2008)). High FBG is also significantly associated with increased PNI, neural density, NGF and receptor $p75^{NTR}$ (p75 neurotrophin receptor) expression, and PDAC death rates (Li et al., 2011a).

Of special relevance to the present work are the contributions of perineural invasion and inflammation to cancer-associated cachexia. Inflammation is consistently ranked among the most important driving forces behind the development and progression of cancer cachexia (von Haehling and Anker, 2014) and has been placed with weight loss as one of the defining features of this syndrome (Argiles et al., 2014). Circulating factors secreted from tumor cells, supporting stromal cells, and activated immune cells in the tumor microenvironment contribute to the development of a systemic inflammatory profile. Serum from PDAC patients or tumor-bearing, but not tumor-resected, mice induced NFκB and downstream effector paired box 7 (Pax7) to promote muscle wasting (He et al., 2013b). Cachexia has been correlated with altered immune cell infiltrates in gastrointestinal tumors and increased levels of chemokines and inflammatory cytokines in tumor and adipose tissue compared to weight-stable cancer patients (de Matos-Neto et al., 2015). NGF has been implicated in driving this process as well. A unifying study by Ye and colleagues has suggested that NGF is a key regulator of tumor-associated inflammation and has shown that oral tumor progression, pain, and cachexia can all be ameliorated by NGF inhibition (Ye et al., 2011). Interest is rising in the possible connection between perineural invasion and PDAC-associated cachexia with a recent study of PDAC patients and in a mouse model of PDAC PNI showing that PNI drives astrocyte activation resulting in decreased BMI and cachexia (Imoto et al., 2012).

Diagnosis of cachexia—particularly that associated with cancer—remains clinically challenging, and new approaches are needed for its recognition and management (Muscaritoli et al., 2015). Rising obesity rates in the general populace and among cancer patients complicate detection. Loss of skeletal muscle mass may be masked by subcutaneous and visceral fat deposits, and establishing the etiology and threshold percentage of clinically significant involuntary weight loss may be difficult in overweight or obese patients (Martin et al., 2013a). A new use of routine abdominal CT scans originally ordered for PDAC diagnosis and staging is opening the door to objective determination of cachexia status. Lumbar skeletal muscle index can be derived from CT imaging and used to detect occult muscle wasting masked by obesity to determine cachexia status independently of BMI (Martin et al., 2013a; Tan et al., 2009).

Summary and Points Addressed

Nerves and lymphatic vessels are two tissue networks that both participate in and are influenced by changes in a microenvironmental tissue milieu. The specific phenotypic and functional alterations of these networks and their regulation in acute inflammation, wound recovery, recurrent inflammation, and tumor-associated inflammation are not well defined. We studied these changes in cornea and skin of mice under the described inflammatory states and in the context of melanoma or PDAC tumor microenvironments. The involvement of lymphatics and nerves in PDAC disease progression is well established; presence of lymph node metastasis or perineural invasion negatively affects prognosis. Another inflammation-related component of PDAC with negative implications for patient survival is the common co-morbidity cancer-associated cachexia. We aimed to address understudied areas of inflammation and PDAC biology, and the subsequent chapters detail our studies of the following points: (1) neurolymphatic remodeling during transitions between tissue microenvironmental states and a novel wound recovery-associated nerve phenotype, (2) connections between the lymphatic

vasculature and the peripheral nervous system and the regulation of neurolymphatic remodeling by the canonical nerve survival and patterning factor NGF, (3) distinctions in inflammation- and cancer-associated neurolymphatic remodeling identified through use of a novel live-imaging fluorescent mouse platform and implications of these neurolymphatic architecture signatures for PDAC detection and treatment, and (4) gene expression profiling of PDAC skeletal muscle samples stratified by cachexia severity vs. cancer-free controls.

CHAPTER I. Nerve Growth Factor Regulates Neurolymphatic Remodeling during Corneal Inflammation and Resolution[2]

[2] Portions of the material presented in this chapter have been previously published under the following reference: (Fink et al., 2014a)

Introduction

Acute inflammation commonly results in either wound recovery or the development of a chronic inflammatory reaction. The biologic mechanisms that direct these outcomes are not well understood, despite the negative clinical implications of chronic inflammation. The concept that wound recovery and the resolution of inflammation are passive processes has been challenged by evidence that active processes trigger a switch from pro- to anti-inflammatory mediators in the tissue microenvironment that in turn resolve inflammation (Serhan and Savill, 2005; Serhan et al., 2007; Serhan et al., 2008).

Networks of nerves, blood vasculature, and lymphatic endothelia are strikingly similar in their anatomical organization and location. Nerves and vasculature respond to overlapping or complementary environmental cues to direct their developmental patterning and maintenance (Adams and Eichmann, 2010; Bouvree et al., 2012b; Chauvet et al., 2013; Gelfand et al., 2009; Larrivee et al., 2009; Melani and Weinstein, 2010). Signals elaborated by cells of one network may influence the behavior of cells in an adjacent network (Mukouyama et al., 2002). There is evidence for shared neurovascular guidance pathways in conditions of tissue disruption, such as neurodegenerative disease or malignancy (Buchler et al., 2005; Entschladen et al., 2006; Entschladen et al., 2008; Quaegebeur et al., 2011).

We hypothesized that common mechanisms regulated neurolymphatic remodeling during inflammation and wound recovery. A corneal model of initial inflammation, wound recovery, and recurrent inflammation was developed to investigate mechanisms that regulate the structure and function of sensory nerves and lymphatic vessels, as these systems influence pain and swelling during the resolution of inflammation. Accessibility and the neurovascular features unique to the cornea make it an ideal system in which to examine neurolymphatic

architecture and function during an inflammatory episode and wound recovery. The cornea is densely innervated (Belmonte et al., 2004; McKenna and Lwigale, 2011; Muller et al., 2003; ZANDER and WEDDELL, 1951), primarily with sensory nerves derived from the ophthalmic branch of the trigeminal nerve (Marfurt et al., 1989). Sympathetic nerves, from the superior cervical ganglion (Marfurt et al., 1989), and parasympathetic nerves, from the main and accessory ciliary ganglia (Marfurt et al., 1998) are less common. During homeostasis, the corneal vasculature is limited to a peri-corneal limbal arcade. Angiogenesis and lymphangiogenesis from the limbus can be stimulated experimentally using suture-induced inflammation (Kelley et al., 2011b; Kelley et al., 2013b). In this work corneal sutures were used to induce initial inflammation; suture removal stimulated wound recovery; and replacement of corneal sutures induced recurrent inflammation.

Examination of several candidate neurovascular guidance molecules for mRNA expression during initial inflammation, wound recovery, and recurrent inflammation in the cornea revealed that NGF gene expression was tightly correlated with these distinct physiologic states. We therefore examined the contribution of NGF to alterations in lymphatic vasculature and neural structures during wound recovery. We also evaluated pain—a clinically-relevant physiological measurement.

These results reveal the capacity of NGF to inhibit neurolymphatic remodeling and the resolution of pain during wound recovery. We show for the first time that NGF can induce lymphangiogenesis as an upstream driver of a hierarchical signaling pathway in which VEGF family members are downstream effectors. These findings implicate NGF as a pathogenic factor that inhibits important aspects of wound recovery.

Materials and Methods

Mice

All experimental procedures were approved by the Institutional Animal Care and Use Committees of Boys Town National Research Hospital and the University of Nebraska Medical Center in accordance with NIH guidelines. Experiments were carried out in six- to ten-week-old female 129S2/SvPasCrl mice purchased from Charles River Laboratories (Wilmington, MA).

Corneal Surgical Procedures

Prior to all surgical procedures, mice were anesthetized by intraperitoneal administration of a mixture of ketamine (100 mg/kg) and xylazine (10 mg/kg). Mice were euthanized by ketamine/xylazine overdose or by CO_2 asphyxiation and cervical dislocation.

The corneal model of initial inflammation, wound recovery, and recurrent inflammation was described previously, as were the injection techniques for VEGFR-2/3 decoy receptors (Kelley et al., 2013b).

Administration of NGF during Wound Recovery

2.5S NGF (B.5017, Harlan Laboratories, Indianapolis, IN) was resuspended at 100 µg/mL in phosphate-buffered saline (PBS), pH 7.4. Approximately 10 µL of suspension was delivered per subconjunctival injection with a 33 gauge needle.

Micropellet Preparation and Micropocket Assay Procedures

A 4 mm^2 nylon mesh was used to mold a mixture of 12% (w/w) poly(2-hydroxyethyl methacrylate) (192066-10G, Sigma-Aldrich, St. Louis, MO) solution in 95% ethanol, sucrose octasulfate-aluminum complex (S0652-1G, Sigma-Aldrich), and cytokine into micropellets measuring approximately 305 µm x 305 µm x 460 µm. Experimental micropellets contained approximately 200 ng of carrier-free recombinant mouse β-NGF (1156-NG-100/CF, R&D

Systems), recombinant human VEGF-C, CF (2179-VC-025/CF, R&D Systems), or PBS only. A 20 or 27 gauge needle was used to create a pocket in the center of the cornea, and a fine forceps was used to place a pellet under the corneal flap.

Immunofluorescence Imaging of Whole Mount Corneas and Axial Sections and Data Collection

Dissection and Staining

Globes were enucleated and fixed in 1% paraformaldehyde (PFA) in PBS, pH 7.4, for one hour. Corneas were dissected out and either hemi-sectioned or slit at each quadrant with a small incision. Fixation was repeated for one hour. Corneas were blocked and permeabilized in a sterile-filtered PBS, pH 7.4, solution containing 5.2% BSA, 0.3% Triton X-100, and 0.2% NaN_3 (blocking solution) for one hour shaking at room temperature. Primary antibodies were diluted in blocking solution and applied to corneas overnight shaking at room temperature. Corneas were washed in a sterile-filtered PBS, pH 7.4, solution containing 0.2% BSA, 0.3% Triton X-100, and 0.2% NaN_3 (wash buffer) three times for one hour shaking at room temperature. Secondary antibodies were diluted in blocking solution and applied to the corneas overnight shaking at room temperature. After three one-hour washes in wash buffer, corneas were mounted on glass microscope slides with mounting medium containing DAPI and stored at 4°C. Primary antibodies: pRb α-Ms β-III tubulin (ab18207, Abcam, Cambridge, MA), mRt α-Ms Lyve-1 (sc-65647, Santa Cruz Biotechnology, Santa Cruz, CA), ArmHms α-Ms CD-31 (MAB1398Z, EMD Millipore, Billerica, MA), Rt α-Ms phospho-histone H3 (H9908, Sigma-Aldrich, St. Louis, MO). Secondary antibodies: 488 Dky α-Rb IgG (AlexaFluor A21206, Life Technologies, Carlsbad, CA), 488 Dky α-Rt IgG (AlexaFluor A21208, Life Technologies), 549 Dky α-Rt IgG (DyLight 712-505-150, Jackson ImmunoResearch Laboratories, West Grove, PA), 649 Gt α-ArmHms IgG (DyLight 127-495-160, Jackson ImmunoResearch Laboratories).

Whole Mount Imaging

Whole mount corneas were visualized on a Zeiss Axio A.1 epifluorescence microscope or a Leica stereoscope. 100X epifluorescence images were obtained using SPOT Advanced software (SPOT Imaging Solutions, Sterling Heights, MI). 32X stereofluorescence images were obtained using Leica Application Suite software (Leica Microsystems, Inc., Buffalo Grove, IL). 200X and 400X z-stacks were obtained using a Zeiss 510META confocal microscope (Carl Zeiss AG, Oberkochen, Germany). Images were compiled and analyzed using ZEN 2009, BioImageXD (Kankaanpaa et al., 2012) and ImageJ (Schneider et al., 2012) software packages.

Quantification of Corneal Nerve Density

Epifluorescence images were color-inverted and overlaid with a 25,000 pixels^2 grid with random offset using ImageJ. Portions of the grid lying outside of or overlapping the limbal arcade were excluded from the analysis. β-III tubulin$^+$ nerves intersecting grid line segments were manually counted in the X and Y directions. To derive density from counted intersections, raw data were normalized to the number of grid squares counted in each image. Both intact and hemisected whole mount corneas were included in the analysis.

Corneal wound bed nerve density was derived by using ImageJ to superimpose a grid over β-III tubulin immunofluorescence photomicrographs. A line was drawn around each wound bed and the area measured using ImageJ. Nerves intersecting gridlines within the wound bed area were quantified and counts normalized to wound bed area.

Quantification of Corneal Nerve Clusters

Corneal nerve clusters were defined as tortuous nerve endings organized in a clustered pattern originating from a single larger nerve and extending in three dimensions. Clusters were

identified and counted manually from epifluorescence images of intact and hemisected corneal whole mounts.

Quantification of Nerve Density at Micropellet

Epifluorescence or confocal images were overlaid with a 3,000 pixels^2 grid with random offset using ImageJ. Portions of the grid lying outside of the pellet were excluded from the analysis. β-III tubulin$^+$ nerves intersecting grid line segments were manually counted. To derive density from counted intersections, raw data were normalized to the number of grid squares counted in each image.

Quantification of Lymphatic Vessel Density and Length

Epi- or stereofluorescence micrographs were imported into ImageJ and overlaid with a 0.02 inches^2 grid with random offset. To determine lymphatic vessel density, grid squares displaying Lyve-1$^+$ fluorescent signal were quantified using the Cell Counter feature of the ImageJ software. Grid squares intersecting the limbal arcade were excluded from the quantification. To quantify lymphatic vessel length, the ImageJ Freehand Line tool was used to trace along the length from origin at the limbus to tip of every-other Lyve-1$^+$ lymphatic vessel in stereofluorescence micrographs and the length of each line measured using the ImageJ Measure feature.

Quantification of Lymphatic Vessel Fragments

A lymphatic vessel fragment was defined as a group of Lyve-1$^+$ lymphatic endothelial cells present in the cornea that was no longer continuous with vessels sprouted from the limbal lymphatic vessel. Following exogenous administration of NGF or PBS during wound recovery, Lyve-1 immunostained corneas were analyzed by epifluorescence microscopy. The number of lymphatic vessel fragments per cornea was counted manually.

Quantification of Average Remaining Wound Size

Light stereofluorescence micrographs were imported into ImageJ and the Freehand Line and Measure Area tools were used to trace around each of the four wound beds in each image and to quantify the areas. The area of each wound bed was treated as an individual *n* in further analyses.

Aesthesiometry

A Luneau Cochet-Bonnet aesthesiometer (Ophthalmic Instrument Co., Inc., Stoughton, MA) was used to measure corneal sensitivity. The nylon monofilament of the aesthesiometer was extended to its full length of 6.0 cm and touched to the corneal surface until first visible bending. Monofilament length was decreased by 0.5 cm increments and touched to the cornea again until a blink response was elicited from the animal. If an animal held its eye closed so as to prevent measurement, we assigned a reading of "7.0".

In Vitro and Biochemical Assays

RNA Isolation, cDNA Library Construction, and qRT-PCR Characterization of Expression of Neurovascular Guidance Genes and NGF Receptors Genes

Total RNA was isolated from mouse cornea, uninvolved human skeletal muscle obtained at rapid autopsy from pancreatic cancer patients, and adult human dermal lymphatic endothelial cells (Lonza, Walkersville, MD) by TRIzol (Life Technologies, Carlsbad, CA) or the RNeasy Mini Kit (Qiagen, Venlo, Netherlands) according to the manufacturers' instructions. 10 µL linear acrylamide (AM9520, 5 mg/mL, Life Technologies) was added to each corneal sample as a carrier prior to RNA isolation. cDNA libraries were prepared using the SuperScript III First-Strand Synthesis System (18080051, Life Technologies). Mouse qRT-PCR reactions were performed in triplicate and assayed on the Applied BioSystems StepOnePlus Real-Time PCR System (Life Technologies). Expression was normalized to GAPDH. Data was analyzed using the

$\Delta\Delta C_t$ method. Gene expression levels in unmanipulated samples were set at 1.0. Target gene expression levels in other tissue conditions are expressed as fold change relative to unmanipulated control levels.

TaqMan Gene Expression Assays used for mouse qRT-PCR experiments: GAPDH - 4352339E, NGF - Mm00443039_m1, MMP10 - Mm00444630_m1, IL1-α - Mm00439620_m1, BDNF - Mm04230607_s1, Ntf3 - Mm00435413_s1, Nrp1 - Mm00435379_m1, Nrp2 - Mm00803099_m1, Sema3e - Mm00441305_m1, Plxnd1 - Mm01184367_m1, Ntn1 - Mm00500896_m1, Ntn4 - Mm00480462_m1, Unc5b - Mm00504054_m1, Slit2 - Mm00662153_m1, Robo4 - Mm00452963_m1, Robo1 - Mm00803879_m1, Efnb2 - Mm01215897_m1, Ephb4 - Mm01201157_m1, Notch1 - Mm00435249_m1, Cdk5 - Mm00432447_g1, FGF2 – Mm00433287_m1, Vegfa - Mm01281449_m1, Vegfc - Mm00437310_m1, Vegfd - Mm00438963_m1 (Life Technologies, Carlsbad, CA).

Human qRT-PCR reactions were performed in triplicate and analyzed on a BioRad C1000 Thermal Cycler CFX96instrument (Bio-Rad Laboratories, Inc., Hercules, CA). TaqMan Gene Expression Assays used for human qRT-PCR experiments: TBP - Hs00427521_m1, NTRK1 - Hs01021011_m1, NGFR - Hs00609977_m1 (Life Technologies). Expression was normalized to TATA box binding protein (TBP). Data was analyzed using the $\Delta\Delta C_t$ method. Average skeletal muscle expression levels of NTRK1 and NGFR were set at 1.0. Average receptor gene expression levels in LEC samples were expressed as fold change relative to skeletal muscle levels. C_t values below the level of detection were designated as 40.0, the upper limit of cycles used in these reactions.

Lymphatic Endothelial Cell Culture

Adult human dermal lymphatic endothelial cells (LECs) were purchased from Lonza (Walkersville, MD) and cultured to the company's specifications. Media used to culture LECs was Endothelial Growth Media-2MV supplemented with recommended growth factors (EGM-2MV). For serum starvation Endothelial Basal Media-2 (EBM-2) was used.

NGF and LEC Migration Assays

Lower wells of 24-well (8.0 μm pore membrane) Boyden chambers (BD Biosciences, San Jose, CA) were loaded with 750 μL EGM-2MV media diluted 1:5 with serum-free EBM-2 and supplemented with increasing doses of recombinant mouse NGF (0, 0.5, 1.0, 5.0 μg/ml). 2.5 x 10^4 LECs diluted in EBM-2 were seeded into the upper inserts of the Boyden chamber and incubated for 24 hours. After 24 hour migration, membranes were washed with PBS and non-migratory cells were removed by mechanical force with a cotton-tipped applicator. Cells were then fixed and stained using Differential Quik Staining Kit (Polysciences, Inc., Warrington, PA). Membranes were removed from the inserts and mounted on slides. A Nikon Eclipse 90i microscope at 10X magnification was used to image four representative quadrants of the membrane and the number of migratory LECs was quantified.

Treatment of LECs with Cytokines

1.5 x 10^5 LECs were seeded into 60 x 15 mm tissue culture plates and allowed to adhere overnight. Cells were then starved for 16 hours in EBM-2. Following starvation, LECs were treated with either fresh EBM-2 or with EBM-2 containing either 4 μg/ml recombinant NGF or 0.5 μg/ml recombinant VEGF-C for 1, 5, 15, or 30 minutes. Cells were then washed twice with PBS and lysates collected with a radioimmunoprecipitation assay (RIPA) lysis buffer (150 mM sodium chloride, 1% IGEPAL, 0.5% sodium deoxycholate, 0.1% sodium dodecyl sulfate (SDS), 50

mM Tris buffer) containing a Roche mini PMSF tablet and phosphatase inhibitors sodium fluoride, sodium pyrophosphate, and sodium orthovanadate all at 1 mM.

Immunoblotting

Lysates were prepared in RIPA buffer or RayBiotech Cell Lysis Buffer (RayBiotech, Inc., Norcross, GA) and were incubated with 4X SDS sample buffer and 2-mercaptoethanol and run on NuPAGE 10% Bis-Tris gels at 150 V for 75 minutes using the XCell SureLock Mini Cell electrophoresis system (Life Technologies, Carlsbad, CA). Transfer was accomplished using the Mini Trans-Blot Electrophoretic Transfer Cell (BioRad Laboratories, Inc., Hercules, CA) at 100 V for 75 minutes onto Immobilon-FL or Immobilon-P polyvinylidene fluoride (PVDF) membranes (EMD Millipore, Billerica, MA). Blots were blocked overnight shaking at 4°C in 5% BSA in PBS with 1X Halt Protease & Phosphatase Inhibitor Cocktail and ethylenediaminetetraacetic acid (EDTA) (Thermo Scientific, Rockford, IL) or in 5% non-fat dehydrated milk (NFDM) in tris-buffered saline (TBS) containing 0.1% Tween-20 (TBS-T). Primary antibodies were incubated in 0.1% Tween in PBS (PBS-T) + 2.5% BSA or in TBS-T + 5% NFDM for 1 to 3.5 hours shaking at room temperature. Blots were washed three times for 15 minutes in PBS-T or TBS-T. Secondary antibodies were incubated in PBS-T + 2.5% BSA or TBS-T + 5% NFDM for 45 minutes to one hour shaking at room temperature. Blots were washed three times for 15 minutes in PBS-T + 0.01% SDS or in TBS-T followed by a one minute wash in ddH_2O. Blots were imaged using the LI-COR Odyssey fluorescence imaging system and software (Lincoln, NE) or were incubated with chemiluminescence reagents and x-ray film developed with a Kodak X-OMAT 2000 processor.

Tubulogenesis Assays

Wells of a 96-well plate were coated with Matrigel Basement Membrane Matrix (BD Biosciences, Bedford, MA) according to manufacturer's specifications for growth in a three

dimensional matrix. LECs were incubated with increasing doses of recombinant human NGF, VEGF-C, or a combination of NGF and VEGF-C diluted in EBM-2 as indicated for 30 minutes at 4°C and then added to Matrigel-coated wells (1.2 x 10^4 LECs/well). After four hours, LECs had formed tube-like networks and phase contrast images were collected. Tubulogenesis was quantified by counting the number of tubes per image. Each treatment was performed in triplicate.

NGF ELISA

Levels of NGF protein in unmanipulated and inflamed corneas were assayed by enzyme-linked immunosorbent assay (ELISA) using the Mouse NGF/β-NGF ELISA Kit (EK0470, Boster Biotechnology Co., Ltd., Pleasanton, CA) according to the manufacturer's instructions. Individual corneal lysates were prepared in RayBiotech Cell Lysis Buffer (RayBiotech, Inc., Norcross, GA), homogenized with a plastic pestle homogenizer, and cleared by centrifugation. Each sample was divided 90/10 into two wells of the ELISA plate and diluted accordingly with sample buffer. Right corneas from three animals made up each group. Optical density (OD) absorbance readings were measured in triplicate using a Titertek Multiskan PLUS plate reader.

VEGF-A Protein Quantification

Levels of VEGF-A protein were quantified in corneas bearing either a PBS or NGF pellet. We performed a corneal pocket assay and prepared lysates as described above. Lysates from two corneas were combined to make up each sample. Six corneas comprised each group. VEGF-A content was assayed using the Quantibody Mouse Cytokine Array 1 (RayBiotech, Inc., Norcross, GA). The array was scanned using the GenePix 4000B (Molecular Devices (Axon Instruments), Silicon Valley, CA) and data was collected using the GenePix Pro software at several PMT values ranging from 540 to 790 gain. The PMT gain 590 scan generated the best

VEGF-A standard curve and data from this scan was analyzed using the Q-Analyzer Software for QAM-CYT-1 (RayBiotech, Inc.).

Statistical Analysis

Data were analyzed with GraphPad Prism 5 software (GraphPad Software, Inc., La Jolla, CA) using Student's T-Test or One-Way ANOVA with Dunnett's Multiple Comparison Post-Test or Bonferroni Post-Test. An asterisk (*) denotes the control group. A bracket between the control and experimental groups indicates statistical significance with $p < 0.05$. In cases comparing two experimental groups, a bracket between these groups indicates statistical significance with $p < 0.05$.

Results

Characterization of Neural and Lymphatic Remodeling in a Corneal Model of Inflammation and Resolution

We characterized structural and architectural changes in corneal lymphatic vessels and nerves through four distinct physiological conditions: healthy unmanipulated cornea, initial inflammation, wound recovery, and recurrent inflammation (Figure 2A). In this model system, inflammation was induced by placement of a suture in each quadrant of the mouse cornea. Suture removal stimulated wound recovery. Recurrent inflammation was induced by placement of a second set of four sutures. DAPI-stained corneal axial sections demonstrated gross thickening of the visibly-wounded cornea during both initial and recurrent inflammation (Figure 3A). Wound-recovered cornea displayed an intact epithelium and decreased to normal thickness. Levels of interleukin-1α (IL-1α) and matrixmetalloproteinase-10 (MMP-10) messenger RNA by qRT-PCR were consistent with inflammation and wound recovery. IL-1α expression was approximately six-fold higher and MMP-10 eleven-fold higher during initial inflammation compared to unmanipulated controls. During wound recovery, levels of IL-1α and MMP-10 decreased, and levels increased about five-fold with recurrent inflammation (Figure 3B).

Figure 2. Corneal model of initial inflammation, wound recovery, and recurrent inflammation. *A*. Schematic depicts timing of corneal suture placement and removal to induce four distinct tissue microenvironmental conditions: healthy unmanipulated, initial inflammation, wound recovery, and recurrent inflammation. *B*. Schematics illustrate two corneal mounting styles: hemisected whole mount and whole mount. Images are 100X epifluorescence photomicrographs of corneas immunostained for Lyve-1 (orange) and β-III tubulin (green) and harvested at the indicated time points. Top panel shows Lyve-1^{+} lymphatic vessels. Bottom panel shows β-III $tubulin^{+}$ corneal nerves. Scale bars are 100 μm. *C*. Lymphatic vessel density was quantified from images like those shown in (*B*). *D*. Nerve density was quantified from images like those shown in (*B*). *E*. Corneal nerve clusters were quantified in wound-recovered tissue. *F*. A Cochet-Bonnet corneal aesthesiometer was used to measure corneal sensitivity. (This figure was previously published in Fink et al., 2014a).

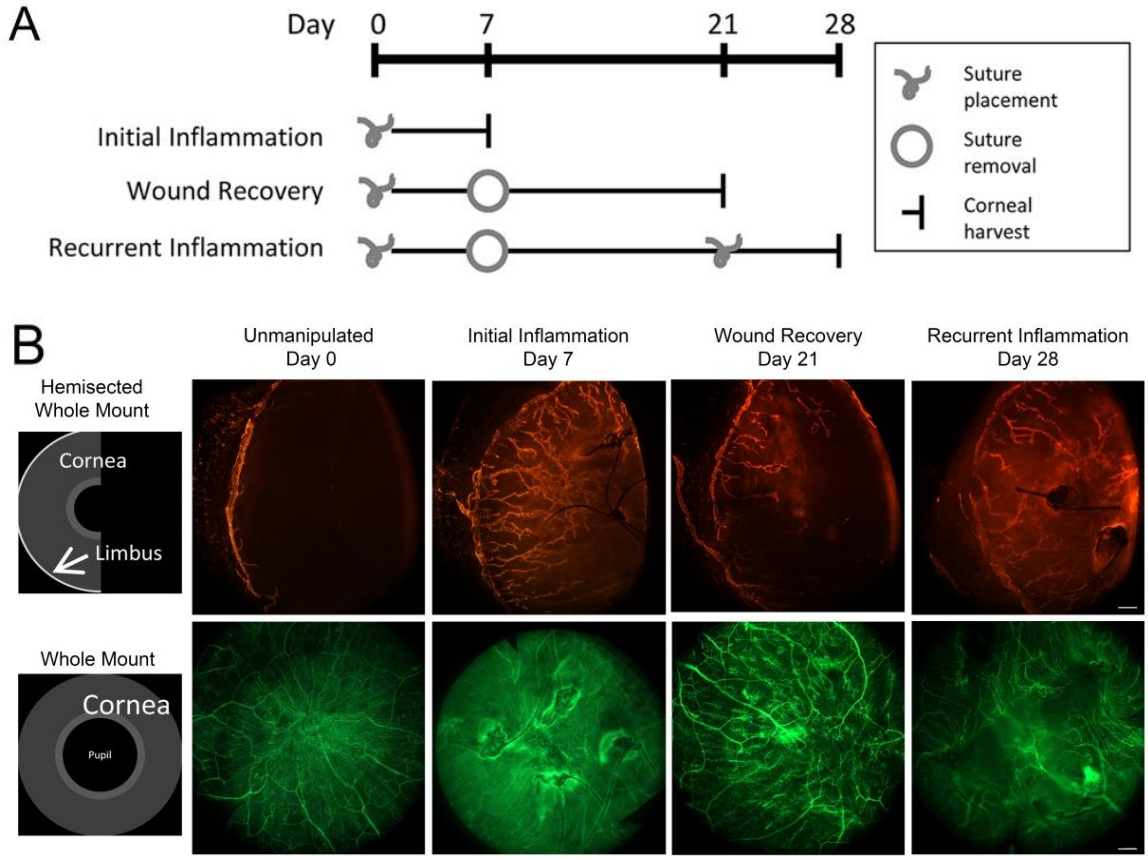
A
Day
0
7
21
28
Initial Inflammation
Wound Recovery
Recurrent Inflammation
Suture placement
Suture removal
Corneal harvest
B
Unmanipulated Day 0
Initial Inflammation Day 7
Wound Recovery Day 21
Recurrent Inflammation Day 28
Hemisected Whole Mount
Cornea
Limbus
Whole Mount
Cornea
Pupil

Figure 2A, B

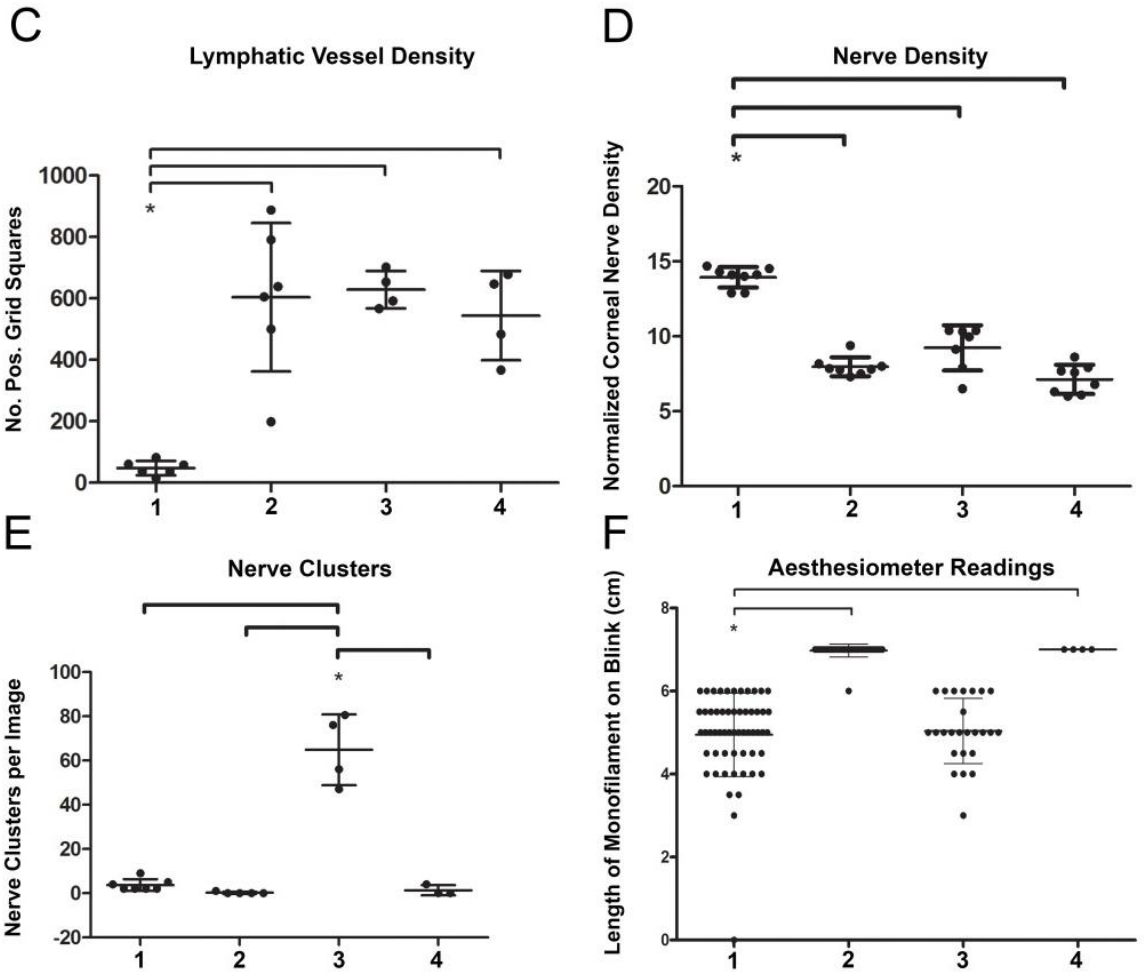

1: Unmanipulated
2: Initial Inflammation
3: Wound Recovery
4: Recurrent Inflammation

Figure 2C - F

Figure 3. Induction of inflammation, wound recovery, and recurrent inflammation in the mouse cornea. Corneal surgeries were performed as described in Figure 1A to induce initial inflammation, wound recovery, and recurrent inflammation. Corneas were harvested and stained with DAPI for epifluorescence microscopy analysis or RNA was extracted for gene expression analysis. *A.* Schematic depicts mount style of frozen corneal axial sections. 200X DAPI-stained corneal axial section epifluorescence micrographs. Scale bar = 100 µm. *B.* qRT-PCR results showing levels of gene expression of inflammatory cytokines MMP10 (*left panel*) and IL1-α (*right panel*). (This figure was previously published in Fink et al., 2014a).

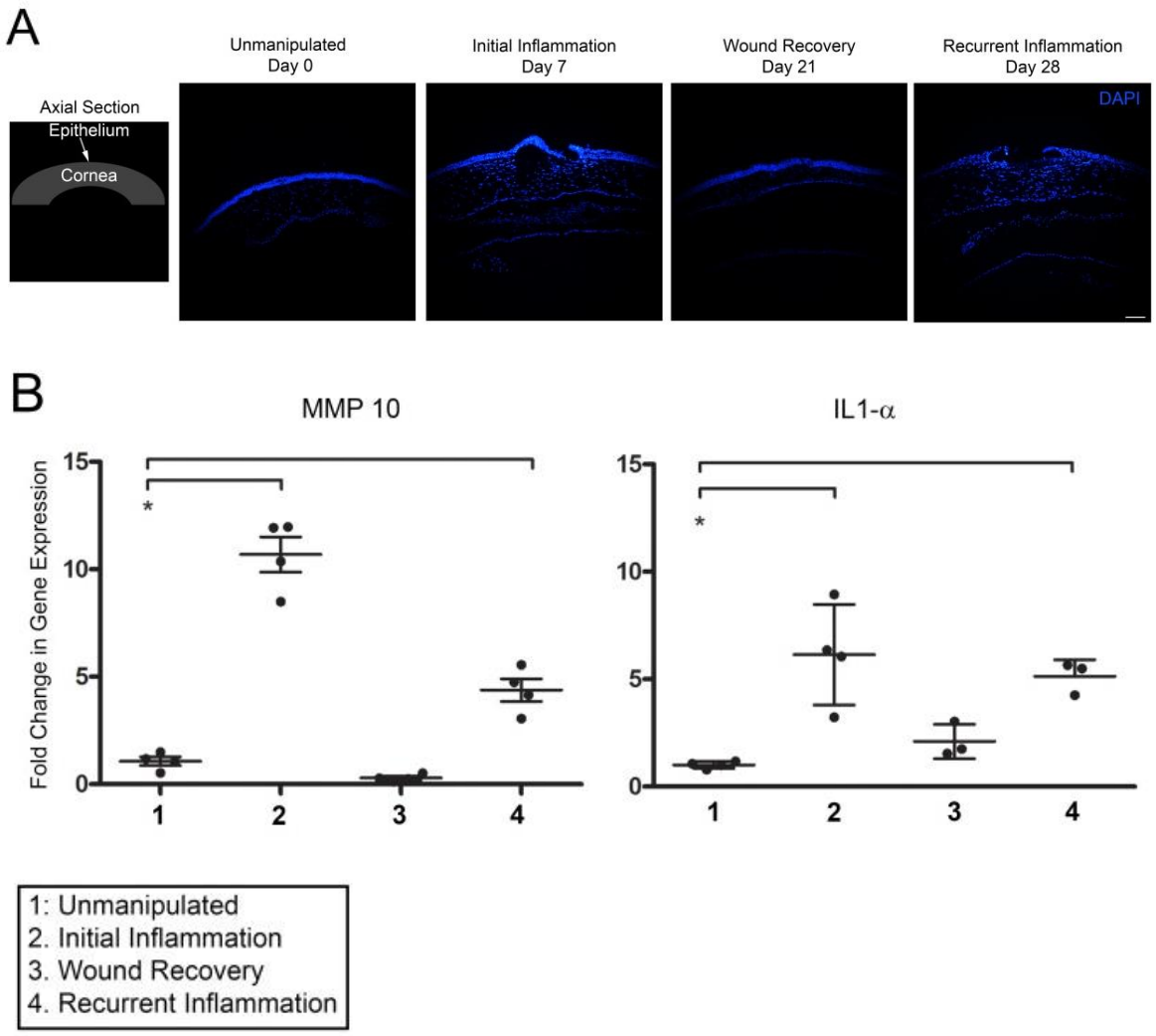
A
Unmanipulated
Day 0
Initial Inflammation
Day 7
Wound Recovery
Day 21
Recurrent Inflammation
Day 28
Axial Section
Epithelium
Cornea
DAPI
B
MMP 10
IL1-α
Fold Change in Gene Expression
15
10
5
0
*
1
2
3
4
1: Unmanipulated
2. Initial Inflammation
3. Wound Recovery
4. Recurrent Inflammation

Figure 3

The lymphatic vessel remodeling that occurs in this system has been previously described (Kelley et al., 2013b). We detected inflammatory lymphangiogenesis associated with initial inflammation, lymphatic vessel regression associated with wound recovery, and an accelerated lymphatic vessel response termed lymphatic vessel memory associated with recurrent inflammation (Figure 2B, C).

We uncovered novel neuroremodeling events as we characterized the distinct tissue microenvironments generated in this model system. Detection of nerves by β-III tubulin immunofluorescence revealed three distinct neural phenotypes corresponding to unmanipulated, inflamed, and wound-recovered tissue states, respectively (Figure 2B). Unmanipulated control corneas exhibited a very dense plexus of fine nerves organized in a regular swirled distribution present just below the epithelium. These sub-epithelial nerves stemmed from thicker branched nerves lying deep within the corneal stroma and terminated in the epithelium. During initial inflammation, the regular swirled pattern of sub-epithelial nerves was disrupted. These nerves appeared grossly thickened and were present at a relatively low density. Nerves tracked toward sites of injury, often exhibiting 90 degree bends and growing around and through suture knots. Contrary to what we anticipated, nerves in wound-recovered tissue did not re-adopt their pre-morbid swirled morphology. Instead, nerves displayed a novel phenotype characterized by their termination in tight tortuous groups, which we have termed clusters. Quantification of these clusters showed their near-exclusive presence in wound-recovered cornea (Figure 2E). Recurrent inflammation resulted in a nerve phenotype very similar to that of initial inflammation with low nerve density and thickened nerves turning toward and knotting around sutures (Figure 2B, D).

Given the different nerve morphologies observed, we investigated the possibility that sensory nerve function was consequentially altered. A Cochet-Bonnet aesthesiometer was used to quantify corneal sensitivity and revealed that inflamed corneas were significantly more sensitive than unmanipulated or wound-recovered corneas (Figure 2F). This result suggested a connection between pain and the specific neuroremodeling events that accompany inflammation—both initial and recurrent. Although the morphology of nerves in wound-recovered tissue was greatly altered compared to normal cornea, nerves in wound-recovered tissue transmitted sensitivity signals at the same level as normal healthy nerves; only inflamed tissue was more sensitive.

Expression Profiling of NGF and Other Neurovascular Guidance Family Members

The dramatic changes in neurolymphatic anatomy during inflammation and wound recovery led us to profile expression of several families of neurovascular guidance genes. RNA was extracted from corneas in the following conditions: unmanipulated, initial inflammation, wound recovery, and one-, three-, and seven-day recurrent inflammation. We sampled the recurrent inflammation condition at three time points in order to better understand the kinetics of a second inflammatory response. Of all of the molecules studied, we observed the most dynamic changes in the expression of NGF (Figure 4A). NGF mRNA levels increased with inflammation about six-fold over control and decreased during wound recovery. In recurrent inflammation, NGF levels were increased about seven-fold over control at days one and three, with a more modest increase of approximately four-fold observed at day seven. The robust and rapid increase in NGF mRNA suggested that its expression was correlated with inflammation and wound recovery. We examined the expression of several other neurovascular guidance molecules including two other members of the neurotrophin family: brain-derived neurotrophic factor (*Bdnf*) and neurotrophin-3 (*Ntf3*); four members of the semaphorin/plexin-neuropilin

signaling pathway: neuropilin-1 (*Nrp1*), neuropilin-2 (*Nrp2*), semaphorin 3e (*Sema3e*), and plexin-d1 (*Plxnd1*); three members of the netrin/unc family: netrin-1 (*Ntn1*), netrin-4 (*Ntn4*), and unc-5 homolog B (*Unc5b*); three members of the slit/robo family: slit-2 (*Slit2*), roundabout-4 (*Robo4*), and roundabout-1 (*Robo1*); two members of the ephrin/eph family: ephrin-b2 (*Efnb2*), and Eph receptor B4 (*Ephb4*); as well as neurogenic locus notch homolog 1 (*Notch1*), cyclin-dependent kinase 5 (*Cdk5*), and fibroblast growth factor 2 (*Fgf2*) (Figure 5). Among these, members of the Netrin/Unc and Ephrin/Eph signaling axes were consistently downregulated during inflammation. We did not detect consistent patterns of changes in expression of other neurovascular guidance gene families.

We performed an ELISA for NGF in unmanipulated and initial inflammation corneal lysates to determine if NGF protein levels were upregulated during initial inflammation. The results showed that NGF protein levels did not change with inflammation (Figure 4B). These dramatic differences in transcriptional and translational regulation of NGF expression led us to further characterize the role of NGF in neurolymphatic remodeling during inflammation and wound recovery.

Figure 4. NGF mRNA and protein expression during inflammation and wound recovery. *A.* NGF expression (mRNA) in corneas was evaluated by qRT-PCR in healthy unmanipulated cornea and during initial inflammation, wound recovery, and days one, three, and seven of recurrent inflammation. *B.* NGF protein expression in corneal lysates was evaluated by ELISA. (This figure was previously published in Fink et al., 2014a).

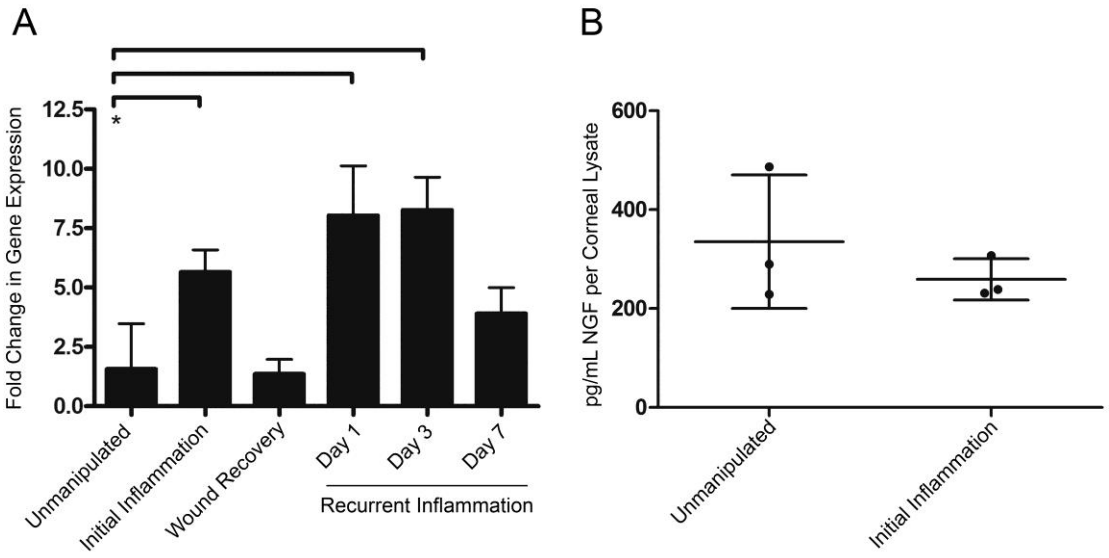
A
Fold Change in Gene Expression
12.5
10.0
7.5
5.0
2.5
0.0
*
Unmanipulated
Initial Inflammation
Wound Recovery
Day 1
Day 3
Day 7
Recurrent Inflammation
B
pg/mL NGF per Corneal Lysate
600
400
200
0
Unmanipulated
Initial Inflammation

Figure 4

Figure 5. Changes in neurovascular guidance molecule gene expression during initial inflammation, wound recovery, and recurrent inflammation time course. Corneal surgeries were performed as described to induce initial inflammation, wound recovery, and a recurrent inflammation time course. RNA was extracted for qRT-PCR analysis of genes representing neurovascular guidance families. (This figure was previously published in Fink et al., 2014a).

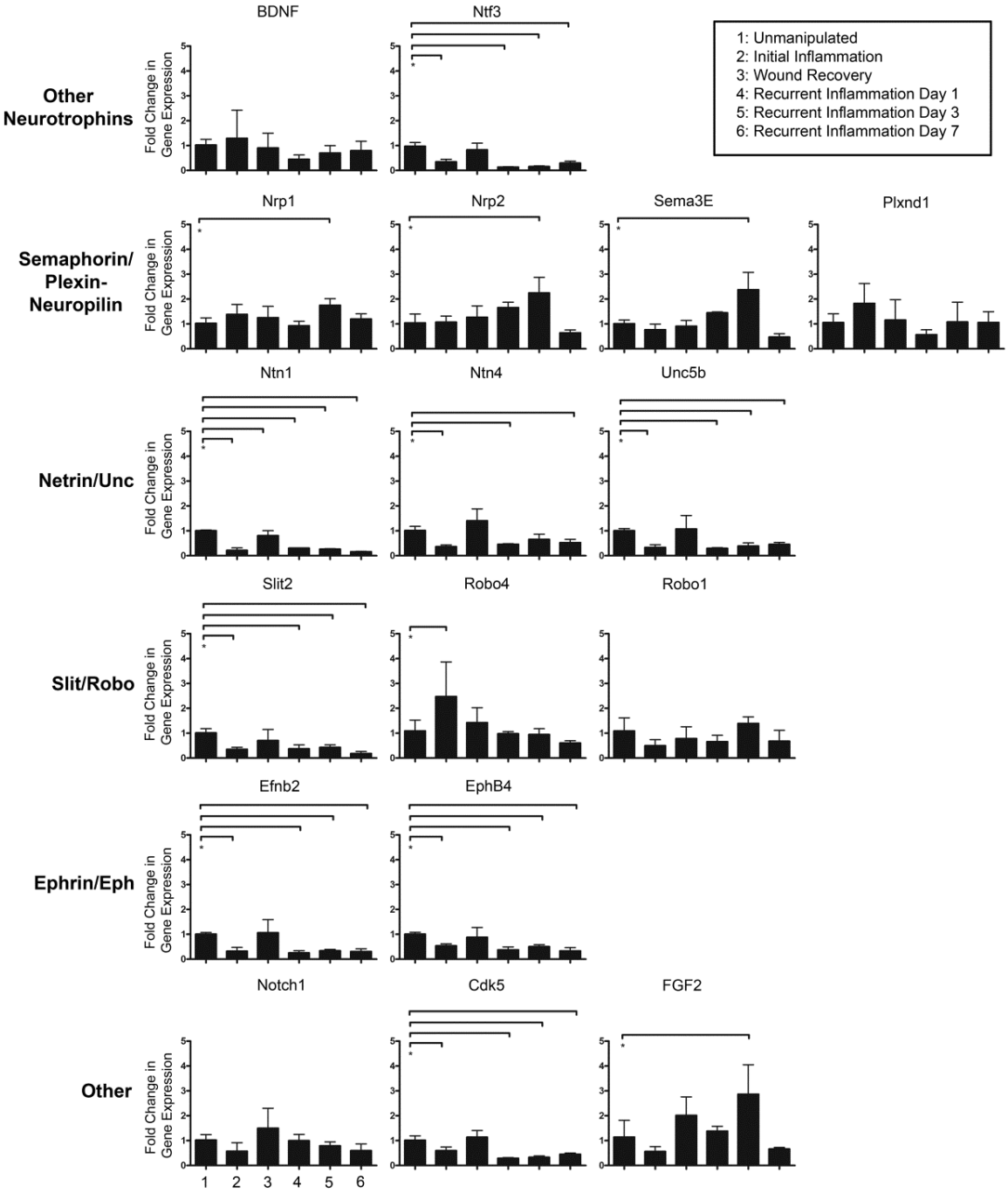
1: Unmanipulated
2: Initial Inflammation
3: Wound Recovery
4: Recurrent Inflammation Day 1
5: Recurrent Inflammation Day 3
6: Recurrent Inflammation Day 7
Other Neurotrophins
Semaphorin/ Plexin- Neuropilin
Netrin/Unc
Slit/Robo
Ephrin/Eph
Other
BDNF
Ntf3
Nrp1
Nrp2
Sema3E
Plxnd1
Ntn1
Ntn4
Unc5b
Slit2
Robo4
Robo1
Efnb2
EphB4
Notch1
Cdk5
FGF2
Fold Change in Gene Expression
1 2 3 4 5 6

Figure 5

Effects of Adding Exogenous NGF through Wound Recovery

We sought to investigate the effect of adding exogenous NGF during wound recovery. It was necessary to first establish the baseline kinetics of neural and lymphatic remodeling during wound recovery, a process that involves the resolution of inflammation. A wound recovery time course experiment was performed in which sutures were removed and corneas were harvested at several time points throughout the course of an extended 21-day wound recovery (Figure 6A). Concomitantly, corneal sensitivity was evaluated by aesthesiometry as inflammation resolved. We found that lymphatic vessel density decreased gradually throughout the wound recovery period, while nerve density remained at a constant and relatively low level as compared to controls from previous experiments (Figure 6B). Nerve distribution and morphology showed changes throughout the time course. Nerves in early wound recovery (days one through four) displayed features similar to those observed in initial inflammation, *i.e.* tracking toward sites of injury, low density, and overall thickening. Nerves at these time points were also very densely associated with healing wound beds. By day seven of wound recovery, nerves no longer tracked toward wound beds, but rather appeared as loose clusters or individually following tortuous paths. Nerve thickness decreased, approaching that seen in the normal condition. By day ten, the dense networks at wound beds were no longer evident, and clusters were the predominant nerve phenotype visible within the corneal tissue. These clusters persisted through day twenty-one. Assessment of corneal sensitivity by aesthesiometry revealed a steady decrease in the corneal hypersensitivity created by inflammation with a return to normal levels by day seven of wound recovery (Figure 6C).

Figure 6. Wound recovery time course. Wound recovery was stimulated by suture removal and corneas were harvested at the indicated time points, immunostained for Lyve-1 and β-III tubulin, and analyzed by epifluorescence microscopy. *A.* 100X immunofluorescence micrographs of Lyve-1^{+} lymphatic vessels (*top panel*) and β-III tubulin^{+} nerves (*bottom panel*). Scale bars = 100 μm. *B*. Quantification of corneal nerve density from images like those in (*A*). *C*. Measurements of corneal sensitivity through extended wound recovery time course. (This figure was previously published in Fink et al., 2014a).

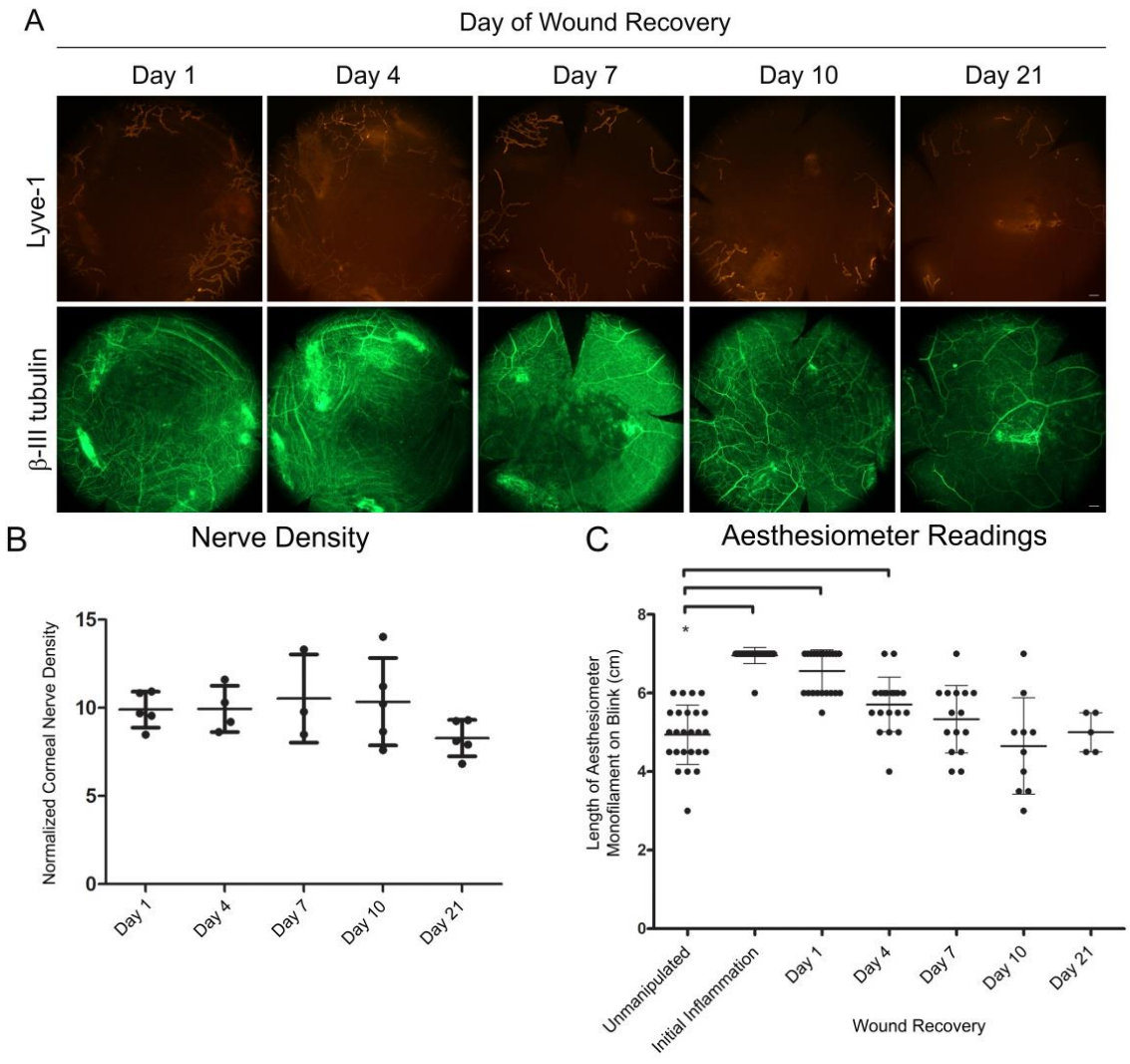
A
Day of Wound Recovery
Day 1
Day 4
Day 7
Day 10
Day 21
Lyve-1
β-III tubulin
B
Nerve Density
Normalized Corneal Nerve Density
15
10
5
0
Day 1
Day 4
Day 7
Day 10
Day 21
C
Aesthesiometer Readings
Length of Aesthesiometer Monofilament on Blink (cm)
8
6
4
2
0
*
Unmanipulated
Initial Inflammation
Day 1
Day 4
Day 7
Day 10
Day 21
Wound Recovery

Figure 6

This better understanding of the dynamic anatomical and physiological events that accompany a period of wound recovery allowed us to test the effects of NGF administration on specific features of wound recovery. Following suture removal to induce wound recovery, mouse β-NGF or PBS control was administered subconjunctivally every other day for fourteen days with commensurate aesthesiometer readings. Lymphatic vessel density remained significantly higher in mice treated with NGF (Figure 7A, B), and there was a significant reduction in lymphatic vessel fragmentation (Figure 7A, E), a hallmark of normal lymphatic regression during wound recovery (Figure 7H). We measured remaining corneal ulcers from control and NGF-treated corneas and found no difference in average remaining wound size with NGF administration (Figure 7A, C). While nerves did form clusters under both treatment conditions (Figure 7A, F), mice treated with NGF showed nerves organized in dense mesh-like networks that encompassed the wound bed (Figure 7A, D). NGF-treated corneas were significantly more sensitive than PBS controls at days two through fourteen of wound recovery (Figure 7G).

Figure 7. Effects of NGF administration during wound recovery on lymphatic vessel regression, nerve density at corneal wounds, and corneal sensitivity. After removing sutures to stimulate wound recovery, mouse β-NGF or PBS control was injected subconjunctivally every other day for two weeks. Corneas were harvested, immunostained for Lyve-1 and β-III tubulin, and analyzed by whole mount microscopy. *A*. Epifluorescence images of Lyve-1$^+$ lymphatic vessels (*left panel,* scale bar = 100 µm, 100X), bright field images showing remaining wound beds at sites of suture placement (*center panel,* scale bar = 200 µm, 32X), epifluorescence images of β-III tubulin$^+$ nerves (*right panel,* scale bar = 200 µm, 32X). Expanded detail shows confocal analysis of β-III tubulin$^+$ nerves at wound beds (*offset panel far right,* scale bar = 100 µm, 200X). *B*. Analysis of effects of exogenous NGF administration on corneal lymphatic vessel density during wound recovery from images like those in (*A*). *C*. Quantification of average remaining wound size following administration of NGF or PBS. *D*. Nerve density at remaining wound beds quantified from confocal immunofluorescence images. *E.* Quantification of lymphatic vessel fragments discontinuous with limbal lymphatic vessel. *F.* Quantification of nerve clusters in wound-recovered cornea following administration of NGF or PBS. *G*. Measurements of corneal sensitivity throughout wound recovery period with administration of NGF or PBS. *H*. 200X confocal immunofluorescence micrograph showing lymphatic vessel fragments (*arrowheads*). Scale bar = 100 µm. (This figure was previously published in Fink et al., 2014a).

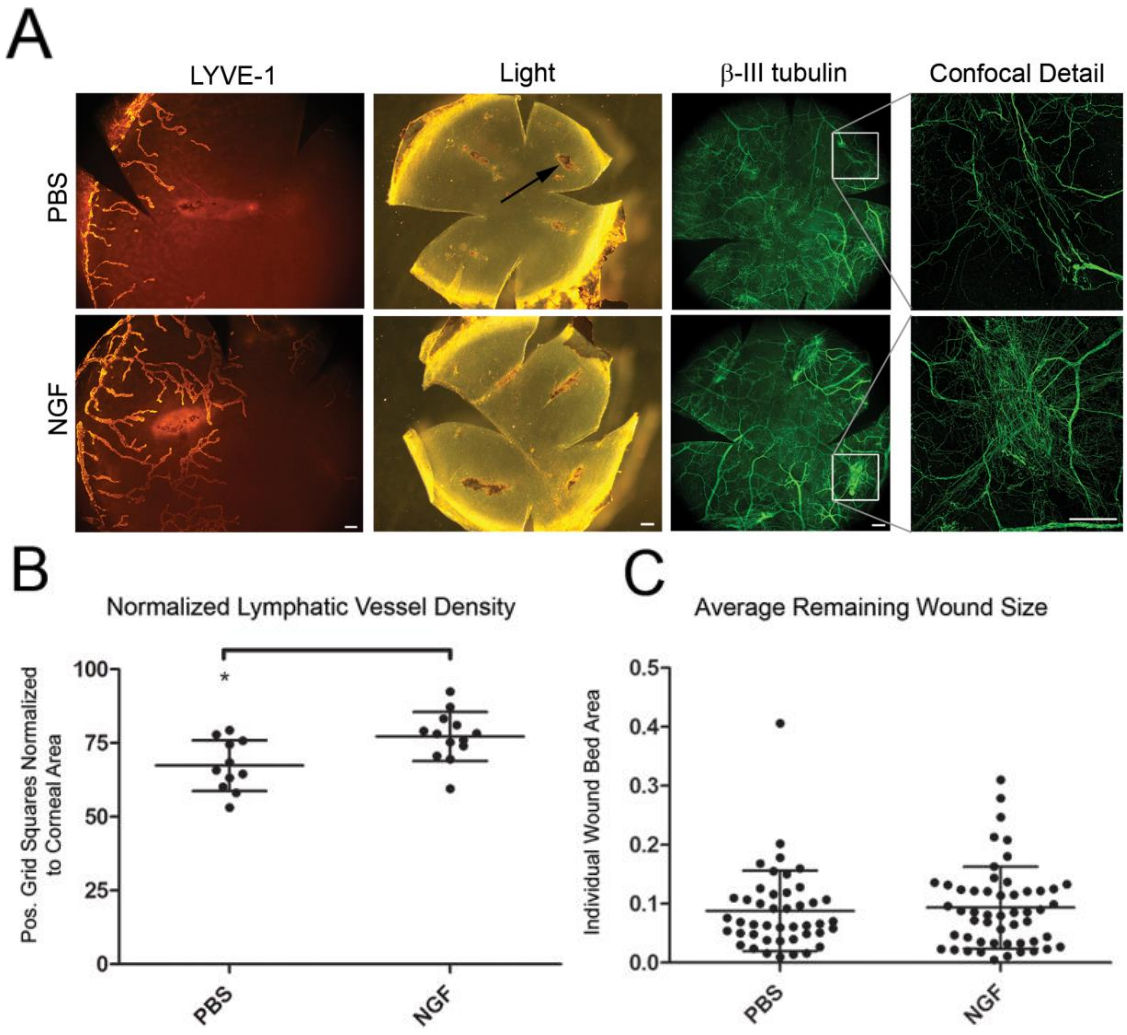
A
LYVE-1
Light
β-III tubulin
Confocal Detail
PBS
NGF
B
Normalized Lymphatic Vessel Density
Pos. Grid Squares Normalized to Corneal Area
100
75
50
25
0
*
PBS
NGF
C
Average Remaining Wound Size
Individual Wound Bed Area
0.5
0.4
0.3
0.2
0.1
0.0
PBS
NGF

Figure 7A - C

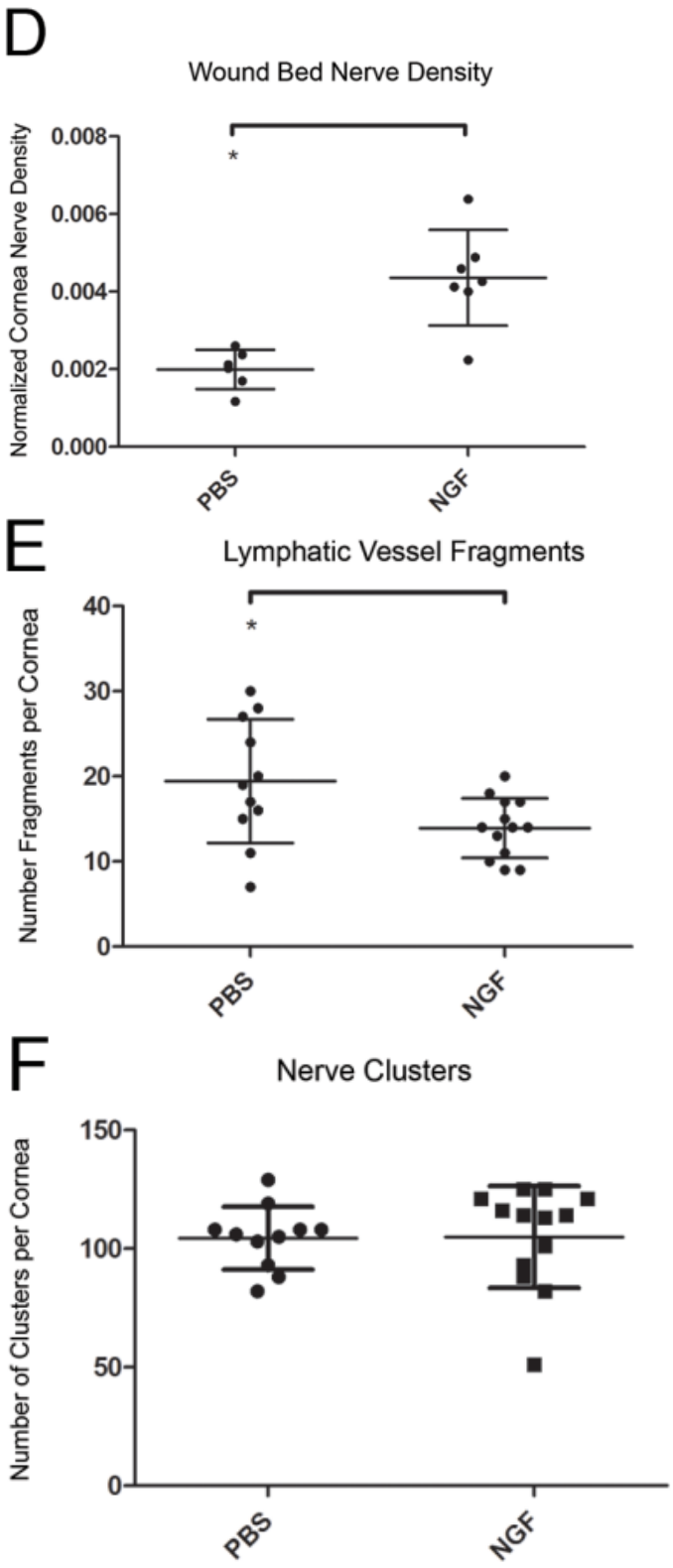
D
Wound Bed Nerve Density
Normalized Cornea Nerve Density
0.008
0.006
0.004
0.002
0.000
*
PBS
NGF
E
Lymphatic Vessel Fragments
Number Fragments per Cornea
40
30
20
10
0
*
PBS
NGF
F
Nerve Clusters
Number of Clusters per Cornea
150
100
50
0
PBS
NGF

Figure 7D - F

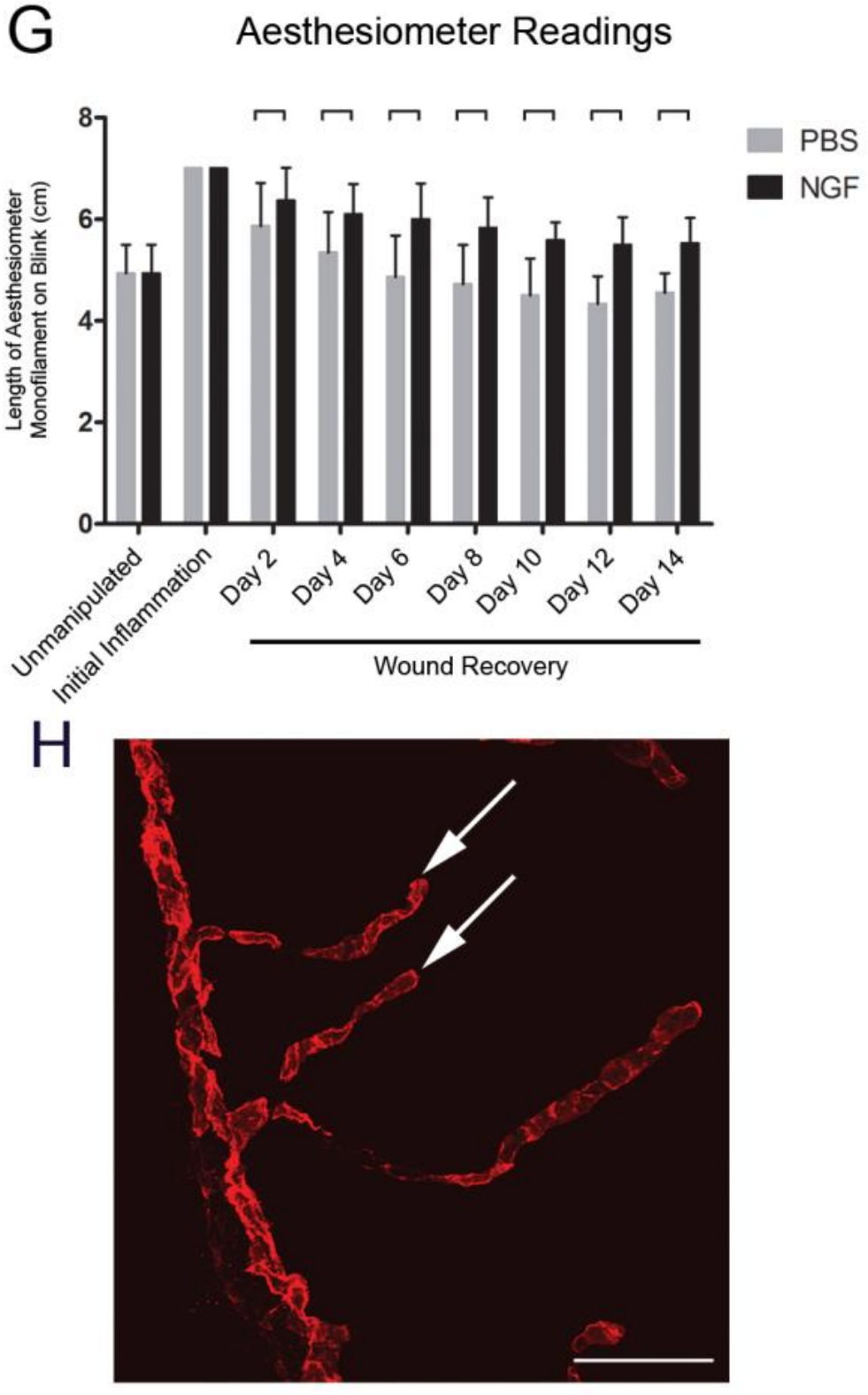
G
Aesthesiometer Readings
Length of Aesthesiometer Monofilament on Blink (cm)
8
6
4
2
0
PBS
NGF
Unmanipulated
Initial Inflammation
Day 2
Day 4
Day 6
Day 8
Day 10
Day 12
Day 14
Wound Recovery
H

Figure 7G, H

NGF Stimulates Lymphangiogenesis

Given the inhibition of lymphatic vessel regression by NGF, we sought to determine if NGF was capable of inducing lymphangiogenesis in the cornea. A corneal micropocket assay was used to test this hypothesis. Micropellets loaded with PBS control, VEGF-C, or NGF were placed in a corneal micropocket for seven days, after which corneas were harvested and analyzed using immunofluorescence microscopy (Figure 8A). β-III tubulin staining showed corneal nerves tracking toward pellets in all three conditions. Nerve density did not change at pellets loaded with cytokine (Figure 8A, B). VEGF-C and NGF stimulated lymphangiogenesis (Figure 8A). Measurement of lymphatic vessel density (Figure 8C) and length (Figure 8D) confirmed that VEGF-C and NGF significantly increased lymphangiogenesis over PBS control. NGF-induced lymphatic vessels were significantly longer than those induced by VEGF-C (Figure 8D). Analysis of lymphatic endothelial cell proliferation in newly synthesized lymphatic vessels by quantification of phosphorylated histone H3 staining in Lyve-1^{+} cells showed an increased number of proliferation events in the presence of NGF and VEGF-C (Figure 8E).

Figure 8. NGF induces lymphangiogenesis. Micropellets loaded with PBS, VEGF-C, or NGF were positioned in a corneal micropocket. Corneas were harvested seven days after pellet implantation, immunostained for Lyve-1, β-III tubulin, and phosphorylated histone H3 and analyzed by whole mount and confocal microscopy. *A*. Epifluorescence images of β-III tubulin$^+$ corneal nerves (*top panel,* scale bar = 100 µm, 100X), confocal detail images of β-III tubulin$^+$ nerves at micropellets embedded in cornea (*middle panel,* scale bar = 100 µm, 100X), epifluorescence images of Lyve-1$^+$ lymphatic vessels (*bottom panel,* scale bar = 100 µm, 100X), and confocal detail images of Lyve-1$^+$ lymphatic vessel tip cells (*bottom panel, inset,* scale bar = 100 µm, 200X). *B.* Quantification of corneal nerve density at micropellets loaded with PBS, VEGF-C, or NGF from confocal images like those shown in (*A*). *C*. Quantification of lymphatic vessel density in response to cytokine micropellets from images such as those shown in *(A). D.* Quantification of length of lymphatic vessel outgrowth from limbus. *E*. Proliferation of Lyve-1$^+$ lymphatic endothelial cells as quantified by positive staining for phosphorylated histone H3. (This figure was previously published in Fink et al., 2014a).

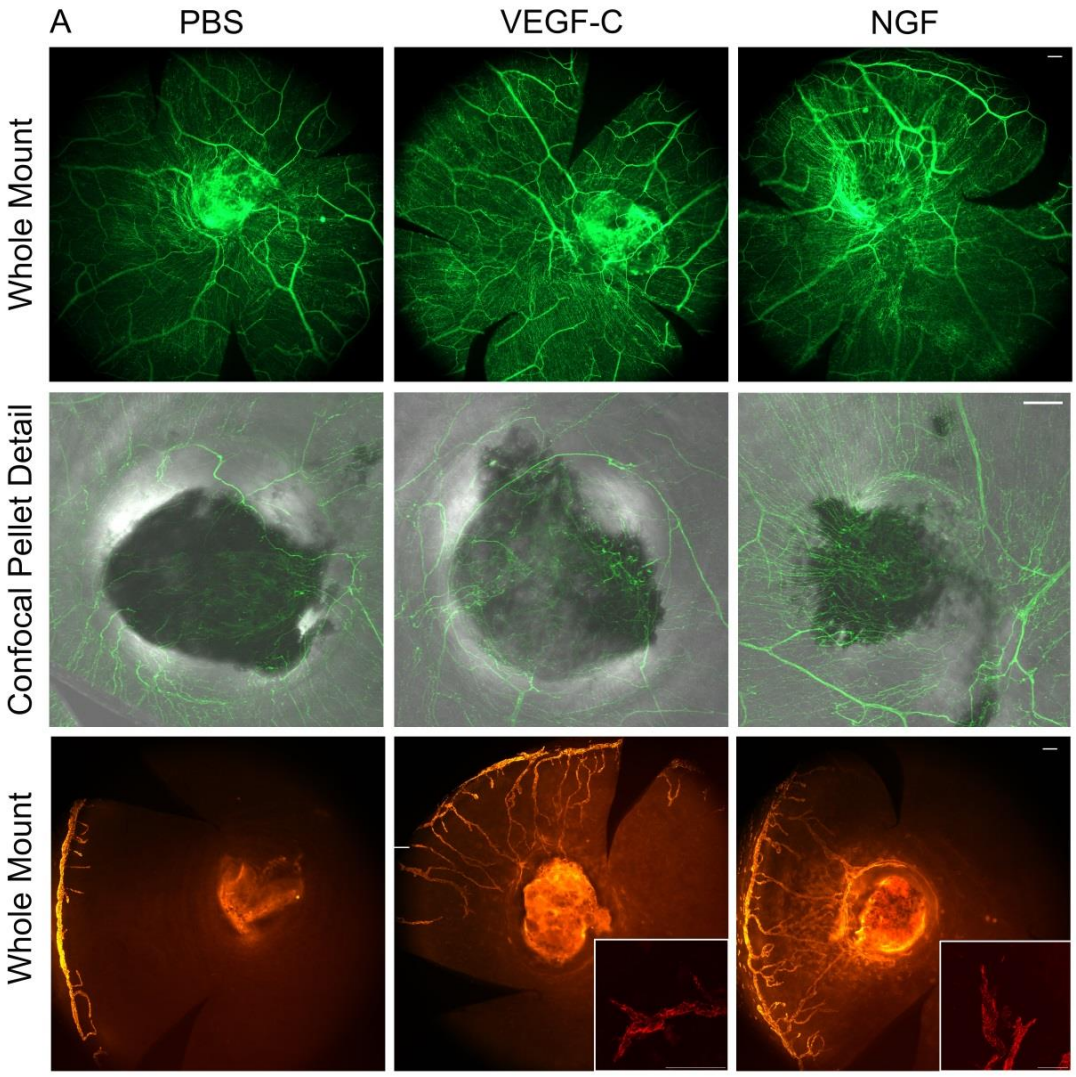
A
PBS
VEGF-C
NGF
Whole Mount
Confocal Pellet Detail
Whole Mount

Figure 8A

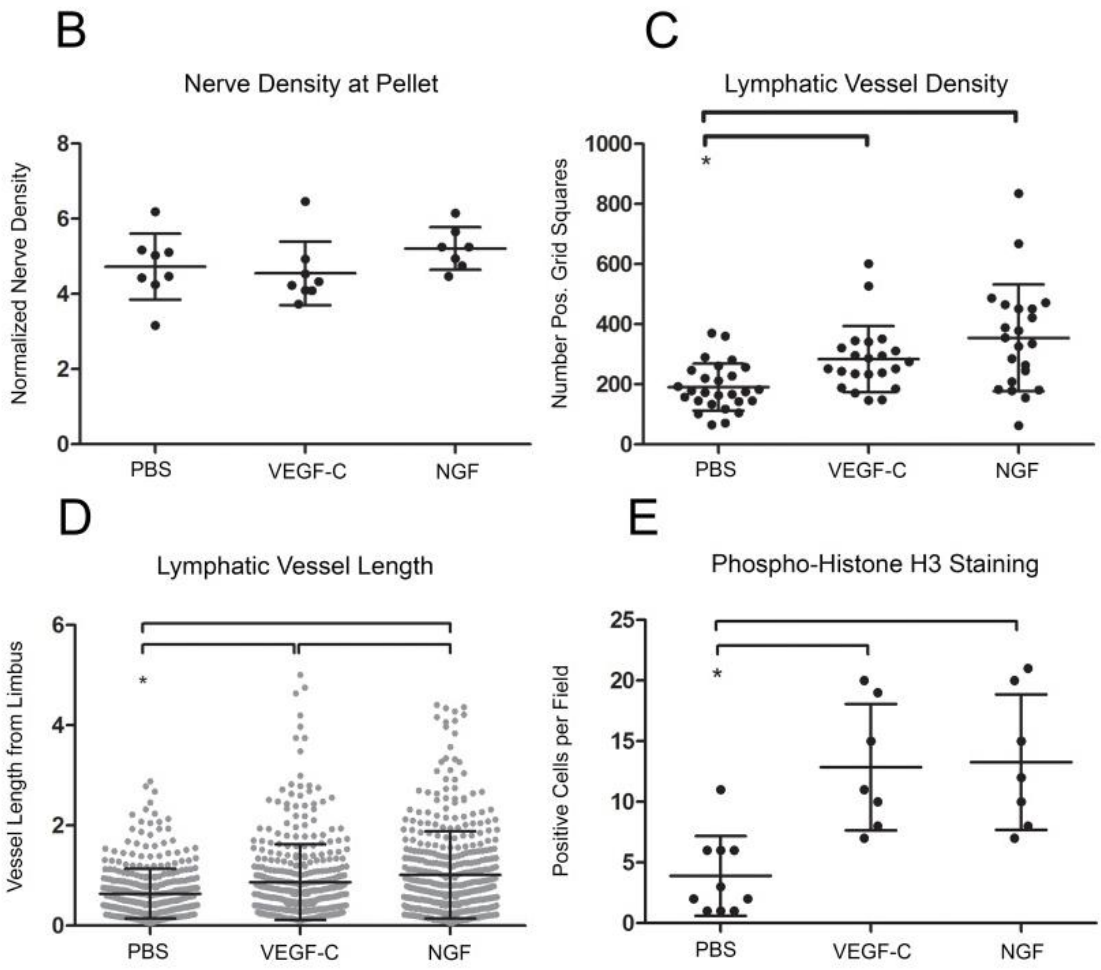
B
Nerve Density at Pellet
Normalized Nerve Density
0
2
4
6
8
PBS
VEGF-C
NGF
C
Lymphatic Vessel Density
Number Pos. Grid Squares
0
200
400
600
800
1000
*
PBS
VEGF-C
NGF
D
Lymphatic Vessel Length
Vessel Length from Limbus
0
2
4
6
*
PBS
VEGF-C
NGF
E
Phospho-Histone H3 Staining
Positive Cells per Field
0
5
10
15
20
25
*
PBS
VEGF-C
NGF

Figure 8B - E

We also examined the gene expression of NGF and known lymphangiogenic cytokines VEGF-A, -C, and -D in corneas with a PBS or NGF pocket as well as in the unmanipulated and initial inflammation conditions. NGF gene expression increased during initial inflammation and did not change with PBS or NGF pellet placement (Figure 9A). VEGF-A gene expression displayed the same pattern as NGF with an increase in initial inflammation and no change in the presence of a PBS or NGF pellet (Figure 9B). VEGF-C gene expression trended toward an increase during initial inflammation and was significantly higher than the unmanipulated condition in the presence of an NGF pellet (Figure 9C). VEGF-D gene expression remained unchanged in all conditions (Figure 9D). We also assayed VEGF-A and -C protein levels in corneas with a PBS or NGF pellet. Quantification of VEGF-A protein levels by cytokine microarray showed no change with an NGF pellet (Figure 9E). Western blotting detected an increase in three isoforms of VEGF-C in the presence of an NGF pellet (Figure 9F). These results show an increase in both VEGF-C mRNA and protein in the presence of an NGF pellet, but not VEGF-A or -D, and suggest that NGF may induce expression of VEGF-C, the canonical lymphangiogenic cytokine, in the cornea.

Figure 9. mRNA and protein expression profiling of lymphangiogenic cytokines. Conditions of initial inflammation, PBS pellet, or NGF pellet were created by placement of sutures or appropriate pellet as described. *A.* NGF gene expression from corneal RNA from unmanipulated, initial inflammation, PBS pellet, and NGF pellet conditions. *B*. VEGF-A gene expression. *C*. VEGF-C gene expression. *D*. VEGF-D gene expression. *E.* VEGF-A protein quantification from cytokine array from corneas with PBS pellet or NGF pellet. *F*. VEGF-C protein quantification by western blot from corneas with PBS pellet or NGF pellet. β-actin was included as a loading control. (This figure was previously published in Fink et al., 2014a).

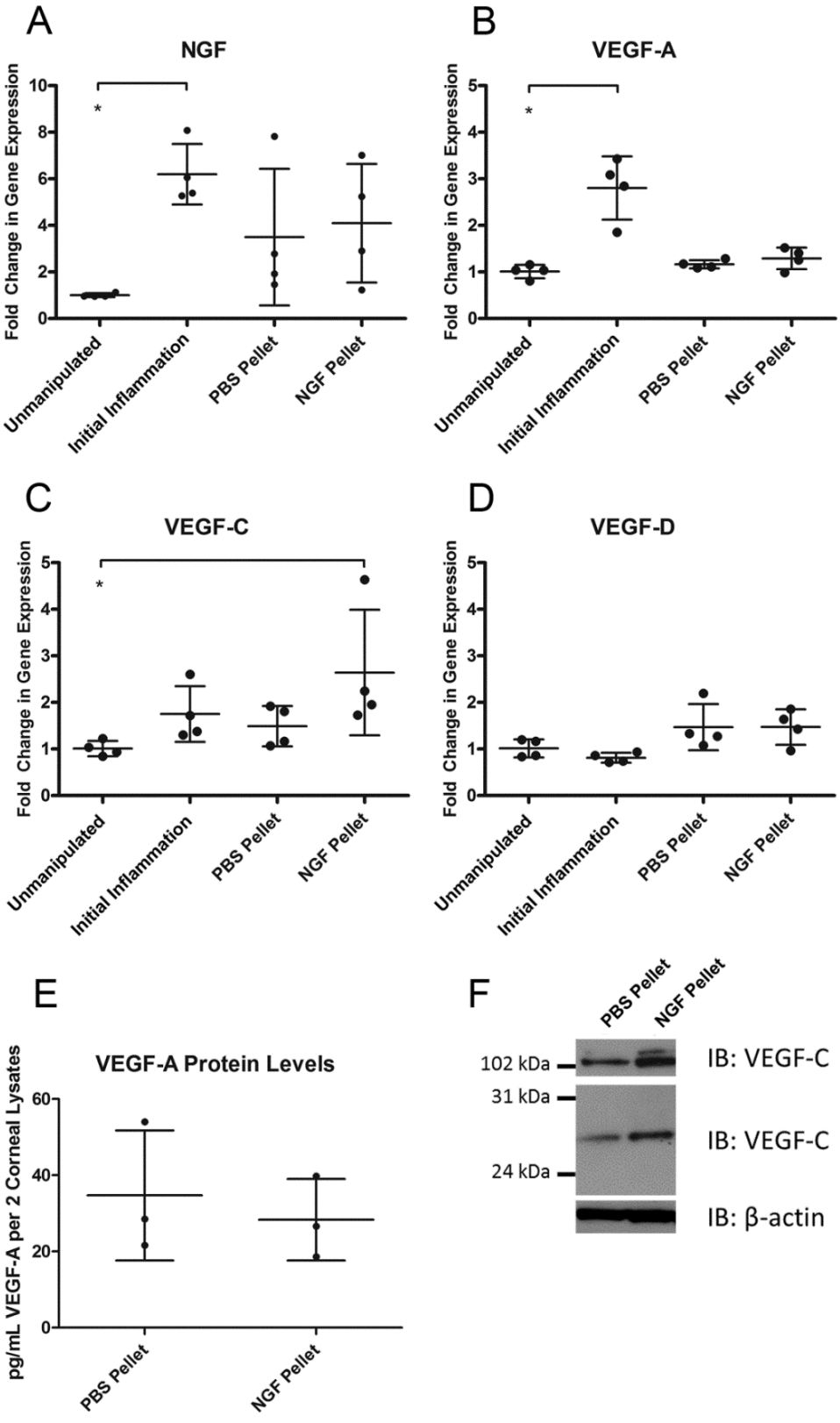
A
NGF
Fold Change in Gene Expression
10
8
6
4
2
0
*
Unmanipulated
Initial Inflammation
PBS Pellet
NGF Pellet
B
VEGF-A
Fold Change in Gene Expression
5
4
3
2
1
0
*
Unmanipulated
Initial Inflammation
PBS Pellet
NGF Pellet
C
VEGF-C
Fold Change in Gene Expression
5
4
3
2
1
0
*
Unmanipulated
Initial Inflammation
PBS Pellet
NGF Pellet
D
VEGF-D
Fold Change in Gene Expression
5
4
3
2
1
0
Unmanipulated
Initial Inflammation
PBS Pellet
NGF Pellet
E
VEGF-A Protein Levels
pg/mL VEGF-A per 2 Corneal Lysates
60
40
20
0
PBS Pellet
NGF Pellet
F
PBS Pellet
NGF Pellet
102 kDa
31 kDa
24 kDa
IB: VEGF-C
IB: VEGF-C
IB: β-actin

Figure 9

***In Vitro* Interrogation of NGF Activity on Adult Human Dermal Lymphatic Endothelial Cells**

Considering that NGF stimulated corneal lymphatic vessels and VEGF-C mRNA and protein expression *in vivo*, we investigated whether NGF acted directly on lymphatic endothelial cells (LECs). We examined the potential of NGF as a chemoattractant in Boyden-chamber migration assays. NGF induced a modest but statistically significant increase in migration of LECs (Figure 10A). Because of the low numbers of migratory cells in these assays, we postulated that NGF might have activity only on a subpopulation of cells or that VEGF-C might be required for robust migration. We also examined the potential of NGF to stimulate tube formation in LECs. Two concentrations of NGF, positive control VEGF-C, and the two cytokines in combination were equally capable of increasing tubulogenesis in LECs cultured in Matrigel at four hours (Figure 10B).

LECs were evaluated for expression of mRNA for canonical NGF receptors TrkA and $p75^{NTR}$ by qRT-PCR. Human skeletal muscle was used as a positive control for expression of these receptors. Gene expression of TrkA was 11.2-fold lower in LECs than in skeletal muscle (Figure 10C). Expression of $p75^{NTR}$ was 317.1-fold lower in LECs than in skeletal muscle (Figure 10D). These results suggested that these receptors were not expressed on these cells.

We studied the expression of signaling phosphoproteins downstream of receptor tyrosine kinases that are known to induce LEC proliferation and migration. Levels of phosphorylated mitogen-activated protein kinase 3/1 (pERK1/2) and phosphorylated AKT (pAKT) were examined in LEC lysates treated with NGF or positive-control VEGF-C for 1, 5, 15, or 30 minutes. As expected, VEGF-C induced phosphorylation of pERK1/2 and pAKT at 15 and 30 minutes. NGF treatment did not induce phosphorylation of these downstream effectors (Figure 10E).

Figure 10. In vitro experiments examining the effects of NGF on LECs. *A.* Adult human dermal lymphatic endothelial cells (LECs) were seeded in the upper inserts of Boyden chamber migration plates. NGF was added to the lower wells at the indicated concentrations. Migratory cells were quantified. *B.* Matrigel was placed in tissue culture plate wells. LECs were incubated with the indicated cytokines and then added to wells. Tubes were quantified at four hours. *C.* RNA was extracted from LECs or positive control adult human skeletal muscle and cDNA was synthesized. Gene expression levels of NGF receptor TrkA were quantified by qRT-PCR. *D.* Gene expression levels of $p75^{NTR}$ in human skeletal muscle and LECs. *E.* RIPA lysates were made from LECs treated with the indicated cytokines for 1, 5, 15, or 30 minutes. Western blot analysis was performed for the indicated proteins using β-actin as a loading control. (This figure was previously published in Fink et al., 2014a).

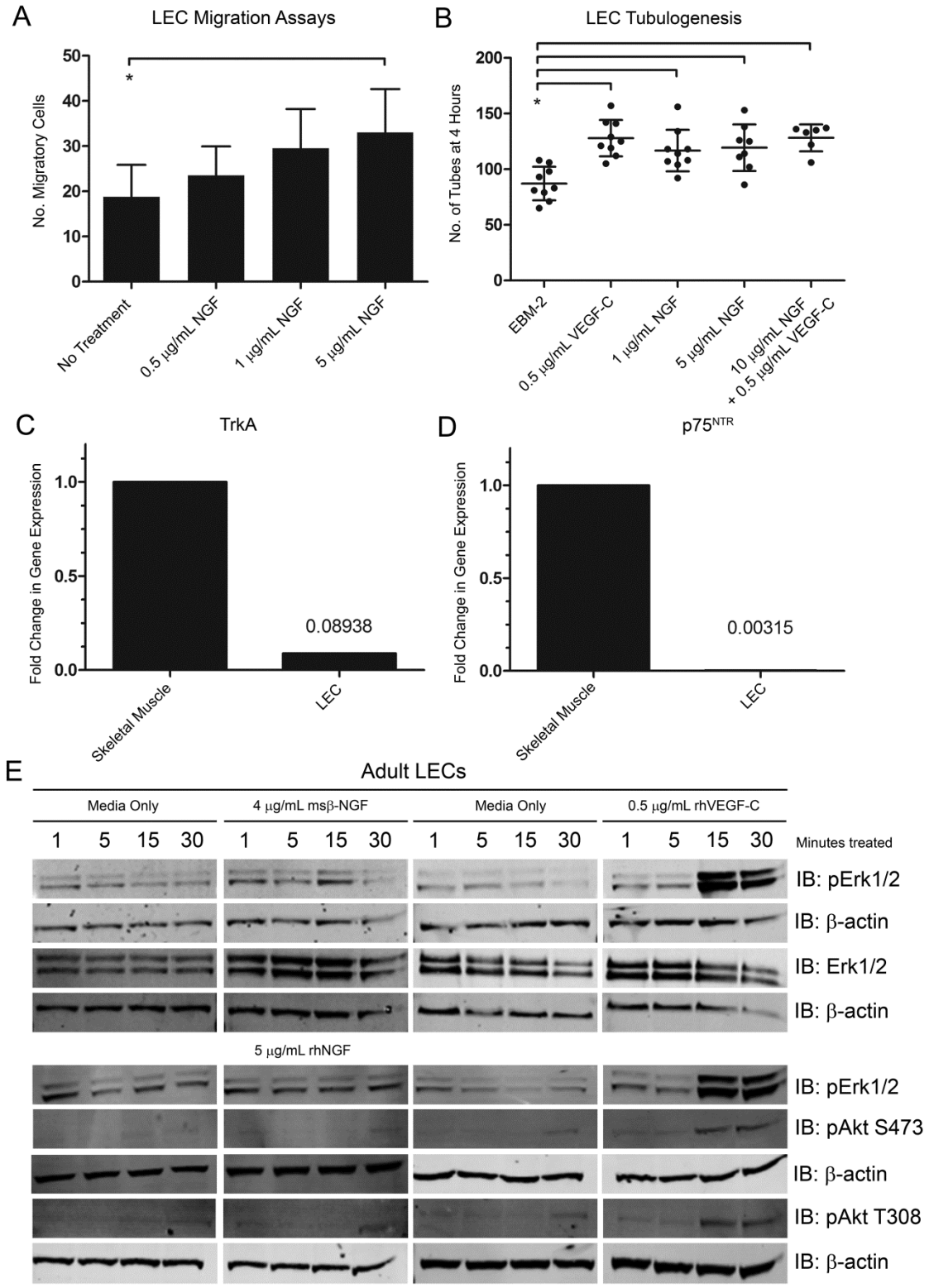
A
LEC Migration Assays
No. Migratory Cells
No Treatment
0.5 μg/mL NGF
1 μg/mL NGF
5 μg/mL NGF
B
LEC Tubulogenesis
No. of Tubes at 4 Hours
EBM-2
0.5 μg/mL VEGF-C
1 μg/mL NGF
5 μg/mL NGF
10 μg/mL NGF + 0.5 μg/mL VEGF-C
C
TrkA
Fold Change in Gene Expression
0.08938
Skeletal Muscle
LEC
D
p75NTR
Fold Change in Gene Expression
0.00315
Skeletal Muscle
LEC
E
Adult LECs
Media Only
4 μg/mL msβ-NGF
Media Only
0.5 μg/mL rhVEGF-C
1 5 15 30
Minutes treated
IB: pErk1/2
IB: β-actin
IB: Erk1/2
IB: β-actin
5 μg/mL rhNGF
IB: pErk1/2
IB: pAkt S473
IB: β-actin
IB: pAkt T308
IB: β-actin

Figure 10

Taken together, these results suggest that NGF does not act through its canonical receptors or through typical receptor tyrosine kinase signaling pathways on populations of LECs in culture.

VEGFR-2/3 Decoy Receptors Block NGF Pellet-Mediated Corneal Lymphangiogenesis

A combinatorial experimental approach was taken to investigate the hierarchical nature of NGF/VEGF-C signaling *in vivo.* An initial set of experiments showed that subconjunctival injection of VEGFR-2/3 decoy receptors during initial inflammation blocked suture-mediated lymphangiogenesis while having no effect on overall corneal nerve density (Figure 11A, B). This result confirmed the efficacy of ablating VEGFR-2/3 signaling on inflammatory lymphangiogenesis and suggested that blocking this signaling mechanism does not affect inflammatory neuroremodeling.

Figure 11. VEGFR-2/3 decoy receptor treatment ablates suture-mediated lymphangiogenesis and does not affect neural remodeling. Corneas were inflamed with four sutures on experimental day zero. Fc control or a solution of VEGFR-2/3 decoy receptors was administered subconjunctivally on days zero, two, and four. Corneas were harvested on day seven, immunostained for Lyve-1 and β-III tubulin, and analyzed by whole mount epifluorescence microscopy. *A.* 100X immunofluorescence micrographs of Lyve-1^+ lymphatic vessels (*top panel*) and β-III $tubulin^+$ nerves (*bottom panel*). Scale bar = 100 μm. *B*. Quantification of corneal nerve density from images like those in (*A*). (This figure was previously published in Fink et al., 2014a).

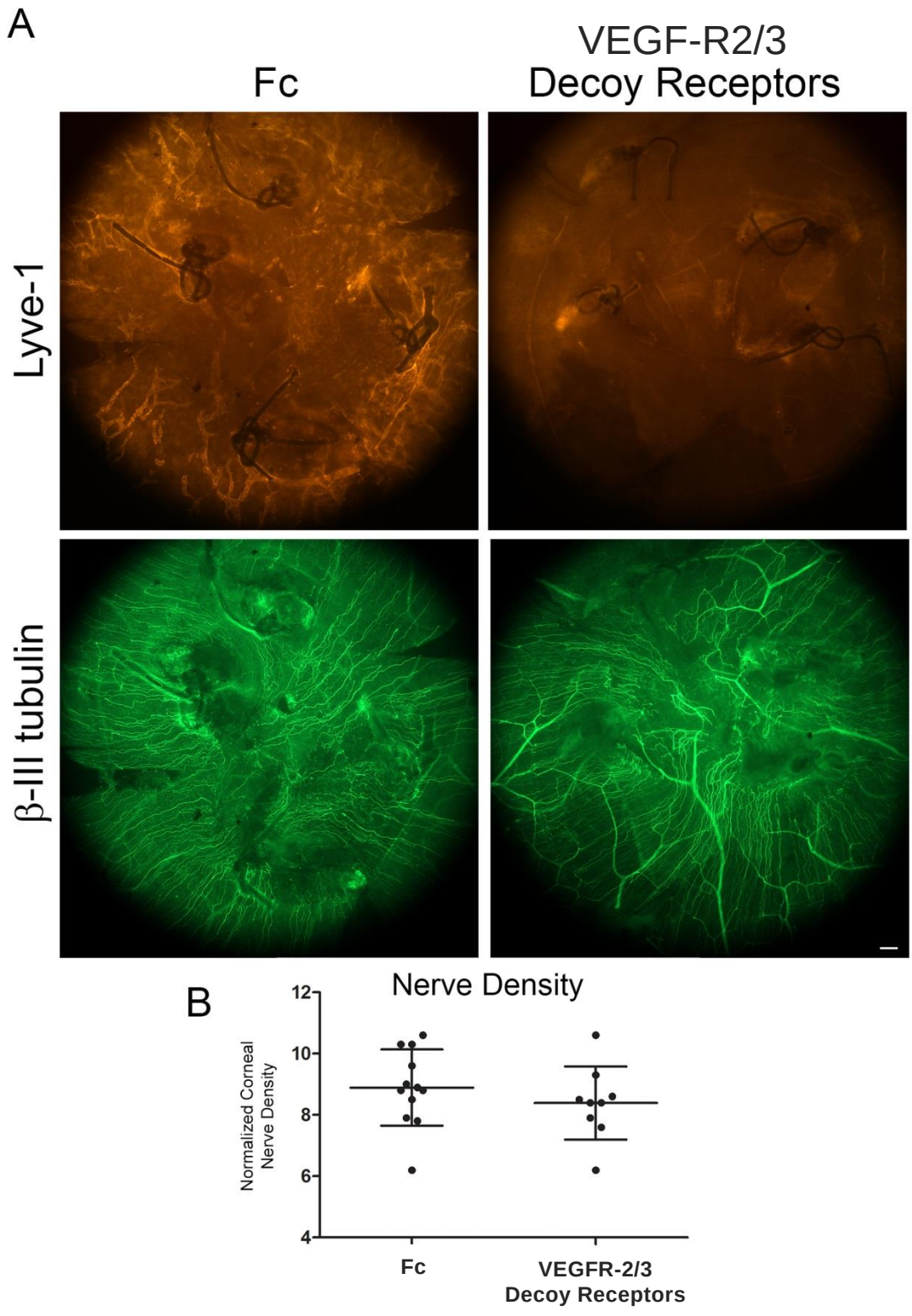
A
Fc
VEGF-R2/3
Decoy Receptors
Lyve-1
β-III tubulin
B
Nerve Density
Normalized Corneal Nerve Density
12
10
8
6
4
Fc
VEGFR-2/3
Decoy Receptors

Figure 11

We investigated the effects of VEGFR-2/3 signaling blockade on NGF-mediated lymphangiogenesis. Micropellets loaded with PBS or NGF were placed in the cornea to induce lymphangiogenesis followed by subconjunctival injection of VEGFR-2/3 decoy receptors or Fc control (Figure 12A). PBS control pellet paired with Fc control subconjunctival injection stimulated minimal lymphangiogenesis. NGF-laden pellet and Fc control injection induced robust lymphangiogenesis. NGF-laden pellet coupled with blockade of VEGFR-2/3 signaling by decoy receptor injection ablated lymphangiogenesis. Lymphatic vessel density was significantly higher in the NGF pellet and Fc injection condition, while the addition of VEGFR-2/3 decoy receptors to the system significantly reduced lymphatic vessel density and length (Figure 12B). These results suggest that the capacity of NGF to induce lymphangiogenesis in the cornea is largely mediated through indirect effects (stimulation of production of VEGF-C) on cell types other than lymphatic endothelial cells.

Figure 12. VEGFR-2/3 decoy receptors ablate NGF pellet-mediated corneal lymphangiogenesis. Micropellets loaded with PBS or NGF were positioned in a corneal micropocket on experimental day zero. Fc control or a solution of VEGFR-2/3 decoy receptors was administered subconjunctivally on days zero, two, and four. Corneas were harvested on day seven, immunostained for Lyve-1 and β-III tubulin, and analyzed by whole mount microscopy. *A*. 100X epifluorescence images of β-III tubulin^{+} corneal nerves (*top panel*) and Lyve-1^{+} lymphatic vessels (*bottom panel*). Scale bars = 100 µm. *B*. Quantification of lymphatic vessel density (*left panel*) and length of outgrowth from limbus (*right panel*). (This figure was previously published in Fink et al., 2014a).

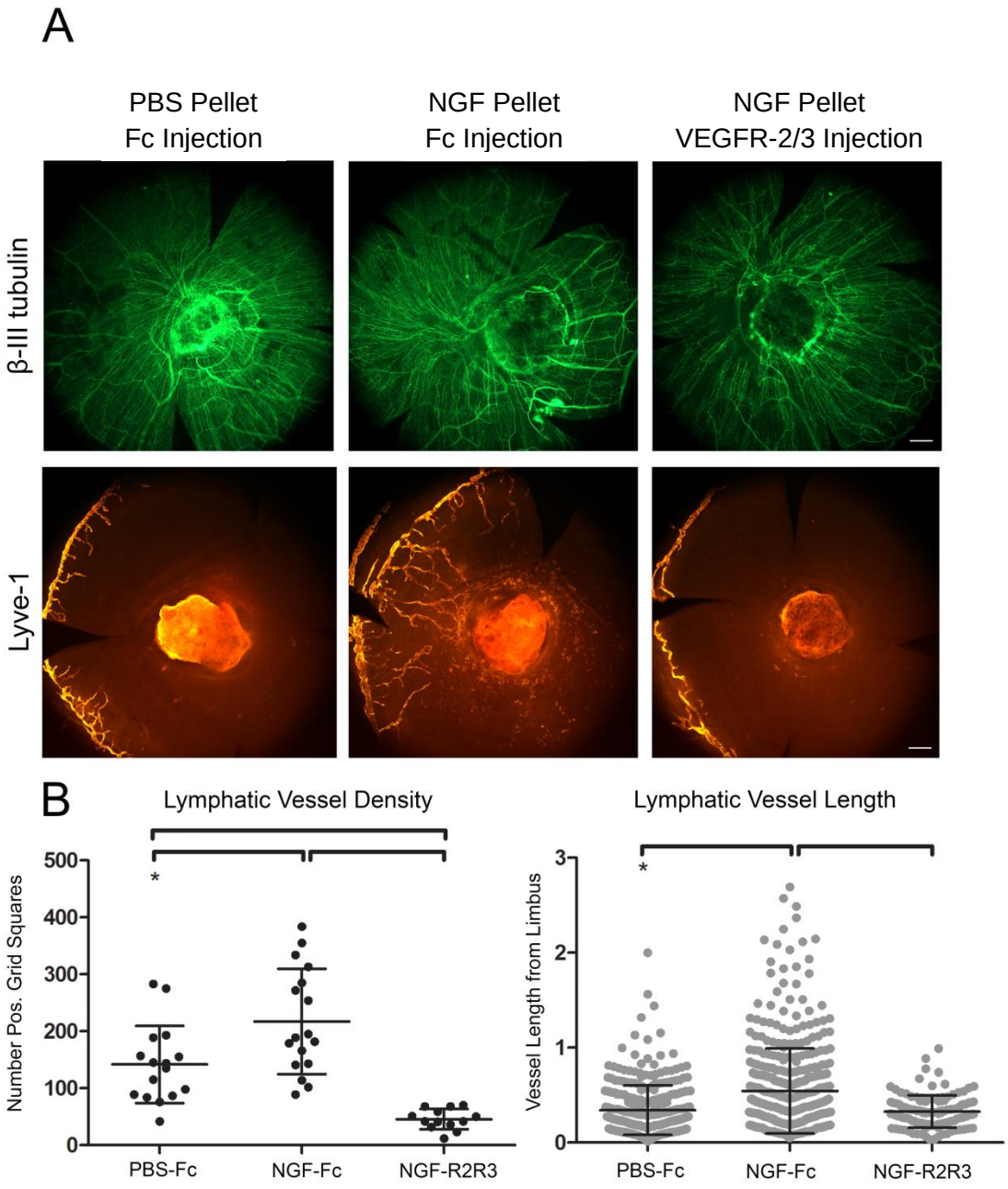
A
PBS Pellet
Fc Injection
NGF Pellet
Fc Injection
NGF Pellet
VEGFR-2/3 Injection
β-III tubulin
Lyve-1
B
Lymphatic Vessel Density
Number Pos. Grid Squares
500
400
300
200
100
0
*
PBS-Fc
NGF-Fc
NGF-R2R3
Lymphatic Vessel Length
Vessel Length from Limbus
3
2
1
0
*
PBS-Fc
NGF-Fc
NGF-R2R3

Figure 12

Discussion

Our studies investigated the mechanistic basis for the resolution of two of the cardinal features of inflammation—pain and tissue edema—during wound recovery. We characterized the behavior of two classes of tissue microenvironmental structures in the cornea, the nerves and the lymphatic vessels, during episodes of inflammation and wound healing. We show synchronized neurolymphatic remodeling during inflammation and wound recovery that is regulated by NGF and its downstream effectors, including VEGF-C. These studies demonstrate that NGF stimulates lymphangiogenesis and increases pain, and they implicate NGF as a pathogenic factor that inhibits the neural and lymphatic vascular remodeling processes associated with wound recovery.

Neurolymphatic Remodeling and Wound Recovery

A corneal model of initial inflammation, wound recovery, and recurrent inflammation was used to explore mechanisms that coordinately regulate neurolymphatic remodeling. This study features experimental results from wound recovery and recurrent inflammation conditions, two understudied physiologic states with significant clinical relevance. Histological and biochemical results supported our conclusion that this model represents these physiologic states.

We and others have previously shown that sutures induce lymphangiogenesis from the corneal limbus and that suture removal stimulates wound recovery and lymphatic vessel regression (Kelley et al., 2011b). Suture placement may transect or induce neuropraxia in a subset of corneal nerves. However, the data presented here reveal new aspects of neural and lymphatic responses to inflammation and injury, processes similar to severe clinical corneal infection or direct trauma.

During initial inflammation, we observed synthesis of new Lyve-1^{+} lymphatic vessels and remodeling of β-III tubulin^{+} neural structures to wound-centric tracking with sharp directional turns. Nerves also displayed thickening and a decrease in density, similar to previous observations (Donaghy, 2003; Ferrari et al., 2013). We visualized regressed Lyve-1^{+} lymphatic vessels and β-III tubulin^{+} neural clusters during wound recovery. Recurrent inflammation accelerated the development of a lymphatic vessel network (Kelley et al., 2013b) and induced neural remodeling, changing nerve clusters to a wound-centric organization. We also detected marked changes in corneal sensitivity that represented a physiological consequence of neural remodeling events. Among several classes of neurovascular guidance molecules, we identified NGF mRNA to have increased expression during inflammation compared to unmanipulated control and wound recovery conditions. Surprisingly, NGF protein levels were similar in control compared to conditions of initial corneal inflammation. Expression of immature or alternately processed biologically active forms of NGF, such as proNGF or other cleavage or post-translationally modified products, may not have been detected by the ELISA we performed.

It is well known that several cell types present in the cornea including epithelium, endothelium, keratocytes, and nerves express NGF and/or the NGF receptors TrkA and p75^{NTR} (Blanco-Mezquita et al., 2013; Lambiase et al., 1998a; Lambiase et al., 2000b; Sornelli et al., 2010; Woo et al., 2005; You et al., 2000). Here we show that NGF inhibited the normal processes of wound recovery by inhibiting lymphatic vessel regression, maintaining high nerve density in wounds, and increasing pain. Interestingly, NGF did not appear to affect epithelial wound closure. Previous studies have described conflicting results related to the effects of manipulating the NGF pathway. Administration of NGF to the cornea has been shown to increase presence of corneal nerves and increase rates of epithelial proliferation (Blanco-Mezquita et al., 2013; Esquenazi et al., 2005; You et al., 2000), improve corneal healing after

capsaicin administration and epithelial scraping (Lambiase et al., 2012), and increase wound closure (Lambiase et al., 2000b). Other studies have shown that NGF has no effect on wound closure (Woo et al., 2005). Administration of an NGF blocking antibody has been shown either to slow epithelial wound healing (Lambiase et al., 2000b) or to have no effect (Woo et al., 2005). These different observations may reflect model-to-model variability and possibly the pan-regulatory functions of NGF.

NGF Induced Lymphangiogenesis

In our studies with micropellets loaded with NGF, we documented the unexpected finding of stimulating new lymphatic vessel growth. We considered the possibility that NGF acted directly on LECs that expressed the canonical receptors for NGF, TrkA and $p75^{NTR}$, or a non-canonical receptor tyrosine kinase. The data did not support this hypothesis, as we did not detect TrkA and $p75^{NTR}$ expression or phosphorylation of two known downstream signaling mediators, Erk and Akt, in LECs treated with NGF. The results of LEC migration and tubulogenesis assays were intriguing and suggested that NGF may bind to a non-canonical receptor and transduce migratory signals *via* effectors other than Erk or Akt. We explored an alternative but non-exclusive hypothesis that NGF stimulated LECs indirectly through effects on other cell types.

Members of the VEGF family have been shown to induce lymphangiogenesis directly by interacting with VEGF receptors expressed by LECs (Cao et al., 2004c; Jeltsch et al., 1997; Oh et al., 1997b; Sweat et al., 2014). We explored this *in vivo* and showed that NGF-laden pellets stimulated expression of VEGF-C mRNA and protein and that lymphangiogenesis stimulated by NGF pellets was dependent upon the VEGF-A and -C signaling axes.

This is the first report describing that NGF stimulates lymphangiogenesis, indirectly *via* VEGF family members. Blocking VEGF-A and -C signaling with decoy receptors ablated both VEGF-C- and NGF-induced lymphangiogenesis and did not affect neural remodeling. NGF pellets have also been shown to induce angiogenesis in rat corneas (Seo et al., 2001a), and other studies have defined a relationship between the VEGF and NGF signaling axes. Production of VEGF-A has been documented in several models of neural development, disease, or injury and has been shown to be stimulated by NGF administration under certain conditions, presenting the possibility that corneal nerves are the source of one or more VEGF family members (Calza et al., 2001; Li et al., 2013; Mukouyama et al., 2005; Nakamura et al., 2011; Samii et al., 1999; Saygili et al., 2011). Studies with bevacizumab, which binds VEGF-A (Bock et al., 2007; Bock et al., 2009), provide further support for crosstalk between these two signaling pathways including changes in NGF levels (Jee and Lee, 2012; Kim et al., 2010a; Rossi et al., 2012) and nerve activity (Bock et al., 2009; Li et al., 2011b; Yu et al., 2008a). The results of the *in vivo* studies presented here support a similar model of NGF and VEGF-C cross regulation to coordinately regulate neural structures and lymphatic vessel growth. These findings are consistent with a model in which NGF functions as an overarching regulatory molecule with primary neural targets and downstream secondary targets regulating lymphangiogenesis *via* VEGF family members.

Facilitating Wound Recovery

The resolution of inflammation and wound recovery are universally important biological processes. Here we investigated these processes in two basic physiologic systems, the lymphatic vasculature and the nervous system in the cornea. The distribution, density, and functions of the lymphatic vessels and nerves vary considerably from organ to organ presumably to meet the unique physiologic and pathologic challenges presented in specific

microenvironments. Whether the operational mechanisms that we have defined in the cornea can be generalized to other organs systems is unclear.

Other preclinical and clinical studies have investigated the contribution of NGF to corneal disease. Consistent with the findings reported here, $TrkA^{-/-}$ mice display decreased innervation of corneal stroma and epithelium and decreased corneal sensitivity (de Castro et al., 1998), and clinical studies have shown that topical NGF treatment generally increased corneal sensitivity (Joo et al., 2004; Lambiase et al., 2000a). In other clinical studies, topical administration of NGF eye drops has been perceived as generally favorable by observations of decreased healing time and increased epithelial closure in refractive disease (Bonini et al., 2000; Cellini et al., 2006; Lambiase et al., 1998b; Lambiase et al., 2003; Lambiase et al., 2011; Mauro et al., 2007; Tan et al., 2006), presumably by stimulating epithelial migration (You et al., 2000). The findings presented here suggest that NGF serves as part of a signaling hierarchy that regulates neurolymphatic remodeling in the cornea, and that clinical strategies to block NGF function may facilitate wound recovery by modulating these processes.

CHAPTER II. Defining Tumor-Induced Alterations to Microenvironmental Neurolymphatic Networks by Live Imaging[3]

[3] Portions of the material presented in this chapter have been previously published under the following references: (Fink et al., 2014b, Fink et al., 2015b)

Introduction

We previously used a corneal model to characterize neurolymphatic remodeling events during inflammation, wound recovery, and recurrent inflammation and identified common regulatory mechanisms shared by both tissue networks. Here, we extended these studies to investigate neurolymphatic remodeling dynamics and tumor-lymphatic interactions in nonmalignant and tumor-associated inflammatory microenvironments in real time with a novel live imaging platform.

During acute inflammation, new lymphatic vessels sprout from the existing lymphatic vasculature in the direction of the inflammatory stimulus. This process is directed by lymphangiogenic cytokines and requires extensive coordination as the cells migrate through the tissue and form new lymphatic capillaries. These newly-synthesized lymphatic vessels are functional and can traffic inflammatory immune cells such as macrophages to and from an inflamed area. Tissue nerve networks also undergo structural and functional changes in the presence of inflammation. Nerves track toward and engulf stimuli and display altered nociceptive properties.

Lymphatic vessels and nerves are two types of tissue microenvironmental networks often invaded by tumor cells during metastatic spread. Despite the clinical importance of lymphatic vessel invasion, lymph node status, and perineural invasion in cancer staging, treatment decisions, and patient outcomes, neurolymphatic remodeling in malignancy remains an understudied biological process. Little is known about how structural changes to these networks may be associated with the earliest events of metastasis or exploited to facilitate early detection of malignancy.

We used real-time live imaging microscopy to study lymphatic vessel remodeling and tumor-lymphatic dynamics in a novel transgenic murine model and used immunostaining to extend our studies to nerve networks. In the Lyve1CreERT2^{tdT} mouse, tamoxifen-inducible tdTomato fluorescent protein is expressed in Lyve-1^{+} cells—lymphatic, but not blood vascular, endothelia and a subset of macrophages. This approach, coupled with the development of customized fluorescent stereomicroscopy techniques, allowed us to visualize tdTomato-expressing lymphatic vasculature in remarkable detail in live mice. We focused our studies on two tissues: pinna and cornea. The respective anatomical features of the pinna and cornea made them ideal platforms for live imaging microscopy studies of nascent and steady-state lymphatic vessels, surgical manipulations, and delivery of tumor cells. Two-color imaging allowed us to simultaneously track tumor cells at single-cell resolution and morphologic changes in lymphatic vessels. We clearly visualized and documented several key behaviors of metastasizing tumor cells including tumor-lymphatic interactions, presence of tumor cells in vessels, clearing from vessels, and the accumulation of tumor cells in draining lymph nodes.

We also found differences in nerve and lymphatic architectures in suture- and tumor-associated inflammatory microenvironments. Local nerve and lymphatic remodeling behaviors unique to malignant inflammation were induced in the vicinity of both minimal and large tumor burdens and tracked over time; field effects extended beyond sites of tumor residence to alter structures in adjacent regions. Tumor- and suture-associated remodeling signatures could be induced simultaneously in either pinna or cornea at the positions of tumor cells and sutures. These characteristic neurolymphatic architecture signatures generated in the presence of a very small number of tumor cells and distinct from those associated with acute nonmalignant inflammation could represent a target for early detection of malignancy.

Materials and Methods

Lyve1CreERT2^{tdT} Mouse Model

All experimental procedures were approved by the Institutional Animal Care and Use Committees of Boys Town National Research Hospital or the University of Nebraska Medical Center in accordance with NIH guidelines. Representative Images are presented; in general, observations were confirmed three times. The generation of this transgenic mouse model, validation of fluorescent protein expression in the appropriate cell type, and back-crossing to C57BL/6 has been previously described (Connor et al., 2016). In short, administration of 4-hydroxytamoxifen (4-OHT) drives expression of tdTomato fluorescent protein in Lyve-1^{+} cells, including the lymphatic endothelium and a subset of macrophages. Conversion of nearly all Lyve-1^{+} cells is possible with high-dose 4-OHT administration, while immunofluorescence co-staining for Lyve-1 shows that conversion penetrance can be titrated down to minor populations of cells by modifications of 4-OHT dose and schedule. Fluorescent protein is most concentrated in the nuclei of cells with diffuse cytoplasmic expression. We have shown tdTomato fluorescent protein expression in the lymphatic vasculature present in and around several organs including cornea, pinna, lymph node, spleen, pancreas, stomach, and intestine by live imaging and stereofluorescence microscopy of 4-OHT-treated mice at necropsy (Figure 13).

Figure 13. Lyve1CreERT2^{tdT} transgenic mouse model displays tdTomato fluorescent protein expression in lymphatic endothelium. Administration of 4-hydroxytamoxifen as described induces tdTomato fluorescent protein expression in cells expressing the Lyve-1 promoter. Bright field and Texas Red (TR) stereofluorescence microscopy live imaging (*A, B*) or imaging at necropsy (*C*-*G*) shows tdTomato expression in lymphatic vessels in several tissues and organs. *A*. Newly synthesized corneal lymphatic vessels growing out from limbal arcade in response to sutures are tdTomato^{+}. *B*. Lymphatic vessel networks present in mouse pinna under steady state conditions express tdTomato. *C*. Lymph nodes (here, submandibular; magnification greater in *right* panel) express tdTomator. *D.* Lyve-1^{+} cells of spleen express tdTomato. *E*-*G*. Lymphatic tissue associated with digestive organs including pancreas, stomach, and intestine are tdTomato^{+}. *H*. Whole mount pinna. Endogenous tdTomato protein is present in nucleus, cytoplasm, and cellular projections of lymphatic endothelial cells and survives paraformaldehyde fixation for confocal microscopy.

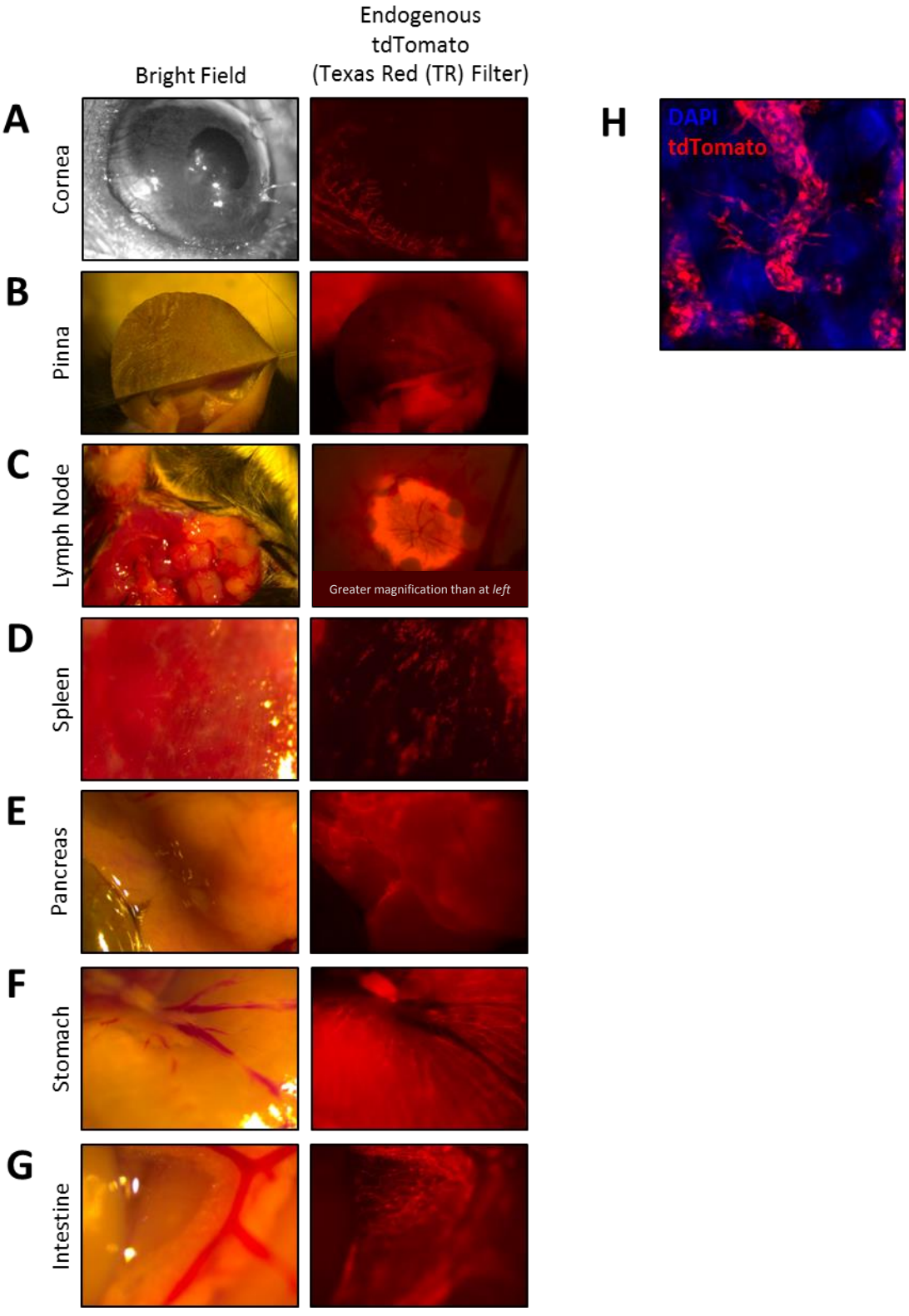
Bright Field
Endogenous tdTomato (Texas Red (TR) Filter)
A
Cornea
B
Pinna
C
Lymph Node
Greater magnification than at *left*
D
Spleen
E
Pancreas
F
Stomach
G
Intestine
H
DAPI
tdTomato

Figure 13

Induction of Fluorescence with 4-hydroxytamoxifen

Expression of tdTomato protein in Lyve-1^{+} cells of the Lyve1CreERT2^{tdT} mouse model was induced by administration of 4-hydroxytamoxifen (4-OHT) suspended in sunflower oil. As described above, this transgenic mouse was engineered to allow titration of tdTomato expression by varying the level of 4-OHT administered to each individual animal. For all of the experiments described in this work, expression of tdTomato fluorescent protein in all cells expressing Lyve-1 was desired. To achieve this high level of expression, 1 mg of 4-OHT was injected intraperitoneally each day for three days with a fourth booster dose administered as needed.

Cell Lines

The Lyve1CreERT2^{tdT} mouse has been back-crossed to the C57BL/6 genetic background, enabling tumor studies with syngeneic cell lines. We used the following cell lines: B16 melanoma, KPC pancreatic adenocarcinoma, and E0771 medullary breast carcinoma. The B16 melanoma cell line was a kind gift from Dr. James E. Talmadge at the University of Nebraska Medical Center, Omaha, NE. The KPC cell line used in these experiments was derived in our laboratory from a KPC mouse tumor (mouse #WT6012). KPC mice (LSL-Kras$^{G12D/+}$;LSL-Trp53$^{R172H/+}$;Pdx-1-Cre) are genetically engineered to develop spontaneous pancreatic adenocarcinoma (Hingorani et al., 2005). E0771 is an aggressive estrogen receptor^{+} (ER) medullary breast cancer cell line (Ewens et al., 2005); it was a kind gift from Dr. Rakesh Singh at the University of Nebraska Medical Center, Omaha, NE.

Surgical Procedures: Cornea

Surgeries were performed on the right eye of each animal. Prior to all surgical procedures, mice were deeply anesthetized by intraperitoneal administration of a mixture of

ketamine (100 mg/kg) and xylazine (10 mg/kg). Topical anesthetic proparacaine was applied to the corneal surface before surgery. Mice were euthanized by ketamine/xylazine overdose or by CO_2 asphyxiation and death ensured by cervical dislocation.

Establishment of Inflammatory and Wound Recovered Corneal Microenvironments

The corneal model of initial inflammation, wound recovery, and recurrent inflammation was described in detail in Chapter I. Briefly, to establish initial inflammation a 10-0 nylon monofilament suture was placed in each quadrant of the mouse cornea and left in residence for seven days. In experiments comparing pre-sutured, simultaneously-sutured, and unsutured environments, the pre-sutured condition was defined as placement of sutures three days prior to tumor pellet implantation. The simultaneously-sutured condition consisted of sutures placed immediately prior to pellet placement on the same day. For the unsutured condition, pellets were placed in previously unmanipulated corneas.

Micropellet Preparation, Tumor Loading, and Corneal Implantation

Micropellet preparation was described in detail in Chapter I. Briefly, nylon mesh was used to mold a mixture of 12% (w/w) poly(2-hydroxyethyl methacrylate) solution in 95% ethanol and a sucrose octasulfate-aluminum complex into micropellets. Tumor cells were labeled with CFSE (carboxyfluorescein diacetate, succinimidyl ester, Vybrant CFDA SE Cell Tracer Kit, Invitrogen) or CMRA (CellTracker Orange CMRA, ThermoFisher) live cell tracker dye according to the manufacturers' instructions and loaded in suspension onto a micropellet *ex vivo*. A tumor-bearing pellet was placed into a micropocket in the cornea by making a slit with a 20 or 27 gauge needle and using fine forceps to tuck the pellet under the corneal flap. Presence of CFSE-labeled cells in the cornea was confirmed immediately following implantation *via* live imaging fluorescence microscopy.

Tumor Cell Injection

Labeled tumor cells were delivered to the cornea by either: injection with a 33 gauge needle into a micropocket made with a 20 or 27 gauge needle or by pulling a 10-0 nylon monofilament suture through a suspension of tumor cells on the surface of the cornea.

Immunofluorescence Imaging of Whole Mount Corneas

Dissection and Staining

These procedures were described in detail in Chapter I. Briefly, corneas were dissected out of PFA-fixed globes, fixed a second time, blocked, and permeabilized. Primary antibodies were diluted in BSA blocking solution and applied to corneas overnight shaking at room temperature. Corneas were washed three times. Secondary antibodies were diluted in blocking solution and applied to the corneas overnight shaking at room temperature. After three washes, corneas were mounted and stored at 4°C. Primary antibodies: pRb α-Ms β-III tubulin (ab18207, Abcam, Cambridge, MA), mRt α-Ms Lyve-1 (sc-65647, Santa Cruz Biotechnology, Santa Cruz, CA). Secondary antibodies: 488 Dky α-Rb IgG (AlexaFluor A21206, Life Technologies, Carlsbad, CA), 488 Dky α-Rt IgG (AlexaFluor A21208, Life Technologies), 549 Dky α-Rt IgG (DyLight 712-505-150, Jackson ImmunoResearch Laboratories, West Grove, PA).

Whole Mount Imaging

Whole mount corneas were visualized on a Zeiss Axio A.1 epifluorescence microscope or a Leica stereoscope. 100X epifluorescence images were obtained using SPOT Advanced software (SPOT Imaging Solutions, Sterling Heights, MI). 32X stereofluorescence images were obtained using Leica Application Suite software (Leica Microsystems, Inc., Buffalo Grove, IL). 200X and 400X z-stacks were obtained using a Zeiss 510META confocal microscope (Carl Zeiss

AG, Oberkochen, Germany). Images were compiled and analyzed using ZEN 2009, BioImageXD (Kankaanpaa et al., 2012) and ImageJ (Schneider et al., 2012) software packages.

Surgical Procedures: Pinna

Prior to all surgical procedures, mice were deeply anesthetized by intraperitoneal administration of a mixture of ketamine (100 mg/kg) and xylazine (10 mg/kg). Pinna was depilated by application of Nair Hair Removal Lotion (Church and Dwight Co, Inc., Ewing, NJ) according to the manufacturer's instructions. Mice were euthanized by ketamine/xylazine overdose or by CO_2 asphyxiation and death ensured by cervical dislocation.

Establishment of Local Inflammatory Microenvironment

Dissolvable (5-0 chromic gut) or nylon monofilament (10-0) sutures were placed in the pinna. Sutures passed through both layers of ear skin. Duration of residence, number, and location of sutures varied depending on experimental conditions and are described below as is appropriate.

Tumor Cell Delivery

CFSE- or CMRA-labeled tumor cells were delivered to the pinna by either: end-on injection of a large or small bolus dose of cells into and between the two layers of ear skin with a 33 gauge needle or injection at a specific location with a 33 gauge needle or pulled glass pipette attached to a compressed gas-powered microinjector (Model PLI-100A Basic Pico-Injector 64-1735, Warner Instruments, Hamden, CT).

Immunofluorescence Imaging of Whole Mount Pinnae

Dissection and Staining

Intact pinnae were removed and fixed in 1% paraformaldehyde in PBS, pH 7.4, shaking at room temperature. Sections were washed in PBS and then blocked and permeabilized in a

sterile-filtered PBS, pH 7.4, solution containing 5.2% BSA, 0.3% Triton X-100, and 0.2% NaN_3 (blocking solution) for two days at 4°C. Primary antibodies were diluted in blocking solution and applied to pinnae overnight shaking at room temperature. Tissue was washed in a sterile-filtered PBS, pH 7.4, solution containing 0.2% BSA, 0.3% Triton X-100, and 0.2% NaN_3 (wash buffer) three times for one hour shaking at room temperature. Secondary antibodies were diluted in blocking solution and applied overnight shaking at room temperature. After three one hour washes, tissue was mounted for imaging and stored at 4°C.

Whole Mount Imaging

Whole mount pinnae were visualized on a Zeiss Axio A.1 epifluorescence microscope or a Leica stereoscope. 100X epifluorescence images were obtained using SPOT Advanced software (SPOT Imaging Solutions, Sterling Heights, MI). 32X stereofluorescence images were obtained using Leica Application Suite software (Leica Microsystems, Inc., Buffalo Grove, IL). 200X and 400X z-stacks were obtained using a Zeiss 510META confocal microscope (Carl Zeiss AG, Oberkochen, Germany). Images were compiled and analyzed using ZEN 2009, BioImageXD (Kankaanpaa et al., 2012) and ImageJ (Schneider et al., 2012) software packages.

Live Imaging Microscopy: Mouse Cornea and Pinna

Mice were deeply anesthetized as described above. Imaging was performed using GFP (Green Fluorescent Protein) and TR (Texas Red) filter sets on a Leica MZ10F modular stereo microscope for fluorescent imaging with a Fluo III rapid filter changer, a Leica Planap × 1.0 objective, and a Leica DFC310FX camera using the Leica Application Suite software version 4.0.0.8777 (Leica Microsystems, Inc., (Buffalo Grove, IL). Imaging was performed using FITC (fluorescein isothiocyanate) and TRITC (tetramethylrhodamine) filter sets on a Zeiss Axio Zoom.V16 fluorescence stereo zoom microscope with a Zeiss Plan-NeofluarZ 1.0 × 0.25 NA

objective and a Zeiss AxioCam MRm camera using ZEN 2012 Blue Edition software version 1.1.1.0 (Carl Zeiss AG, Oberkochen, Germany).

Cornea was imaged by using fine forceps to position and stabilize the globe; focus on either limbal vasculature or central cornea was achieved in this way. Extraneous vibration from respiratory motions was minimized by gently stabilizing the head with a large forceps.

Pinna was immobilized and mounted for imaging for up to one hour by loosely securing it in a customized mounting apparatus consisting of small glass plates and adjustable clamps. Positioning the pinna on this platform effectively brought the tissue into one plane and decreased movement due to respiration. Lymphatic vessel landmarks within the tissue allowed us to return to the same field during several imaging sessions.

Results

Sutures Induce Inflammatory Neurolymphatic Remodeling in Mouse Pinna

We studied alterations in lymphatic vessel and nerve morphology in mouse pinna in response to placement of sutures in live animals over several days. Lymphatic vessels are normally present in the homeostatic mouse pinna in two plexuses within the tissue. These plexuses are defined by uniform distribution of blind-ended lymphatic capillaries throughout the pinna in stochastic conformations and with frequent anastomoses. We placed dissolvable (Figure 14A, B *lower panel*) or nylon (Figure 14B *upper panel*) sutures through the pinna of Lyve1CreERT2^{tdT} mice in which tdTomato fluorescence had been induced by administration of 4-OHT. Changes in tdTomato^{+} lymphatic vessel architecture were characterized over several days following suture placement. With either suture type, we observed a local decrease in lymphatic vessel density at the site of suture placement. Development of a "zone-of-clearing" in which no tdTomato^{+} lymphatic endothelial cells were present resulted at every suture site individually, while normal lymphatic vessel architecture as seen in homeostasis was maintained in areas away from and between sutures (Figure 14B *right panel*). Several days after suture placement we observed local lymphangiogenic sprouting into the site of wounds (Figure 14C). Single tdTomato^{+} cells infiltrated areas previously devoid of lymphatic vessels around sutures. Newly synthesized lymphatic vessel sprouts branched off of existing lymphatic vessels into wounded regions.

Figure 14. Sutures induce local pinna lymphatic vessel remodeling. *A.* Live imaging. Dissolvable or nylon sutures were placed through the depilated Lyve1CreERT2^{tdT} mouse pinna. *B*. Live imaging. Suture placement resulted in local decrease in lymphatic vessel density and formation of "zone-of-clearing" (*dashed lines*) around suture sites (*). *C*. Live-imaging of mounted ear several days after suture placement (*left panel,* Texas Red filter; *right panel,* bright field); Local sprouting into previous suture site zone-of-clearing (*dashed lines higher magnification box*).

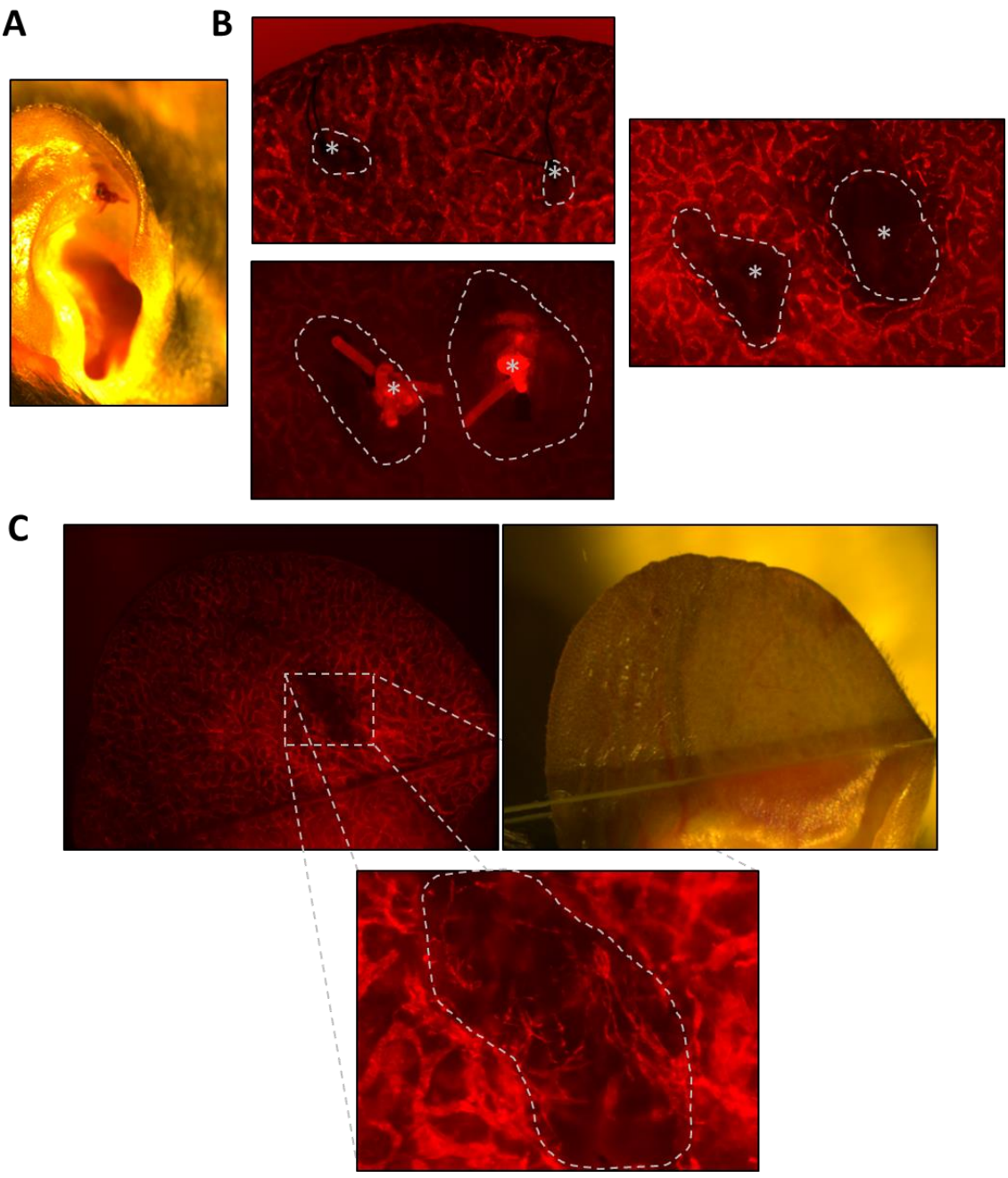

Figure 14

We also studied the behavior of nerves in response to suture placement in the mouse pinna (Figure 15). As with vascular supply, each layer of ear skin is independently innervated. In homeostasis, large nerve trunks enter the base of the pinna and fan out toward the edges with extensive branching and anastomoses forming dense plexuses. Upon stimulation with a suture, neuroremodeling in the pinna was similar to that observed in the cornea. A dramatic increase in nerve density was observed at the margins of wounds. Nerve bundles tracked in an organized manner toward the site of injury, encircled and penetrated it forming a dense net-like structure. Sprouting lymphatic vessel tips maintained distance from the injury, while nerves were present at greater density in this region.

Figure 15. Sutures induce local pinna neuroremodeling. Two 5-0 chromic gut sutures were placed through the depilated Lyve1CreERT2^{tdT} mouse pinna. Maximum intensity projections of 100X confocal micrographs are shown. Size bars = 100 µm. Pinna nerves (β-III tubulin-immunolabeling, *green*) and lymphatic vessels (endogenous tdTomato^{+}, *red*). *A.* Networks of nerves and lymphatic vessels in homeostasis in a region away from sutures. *B.* Local increase in nerve density and altered morphology in immediate vicinity of suture (*). Lymphatic vessels are positioned away from suture site and display sprouting tips (*arrows*).

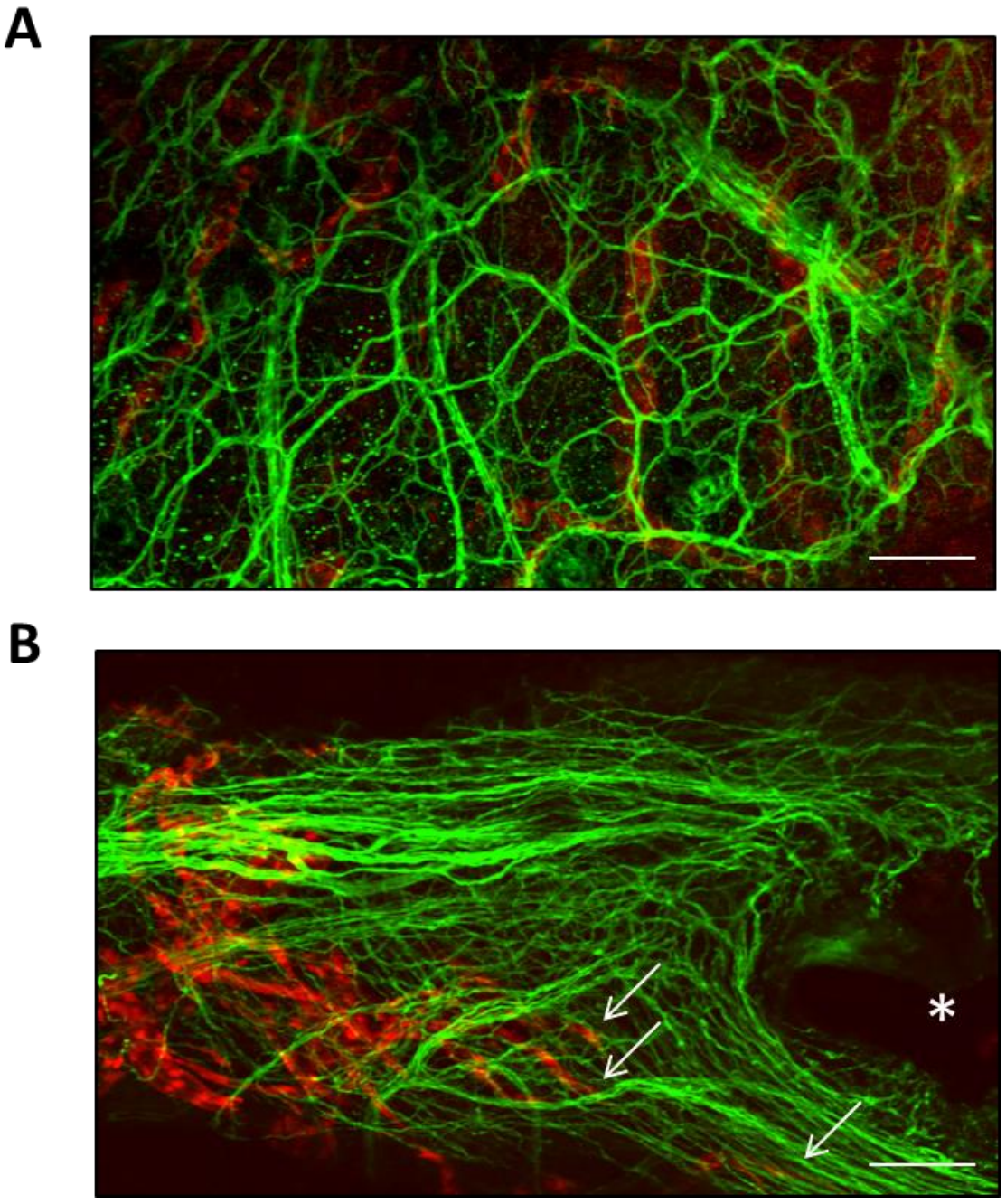

Figure 15

Very Small Tumor Burden Induces Lymphatic Vessel Remodeling and Is Cleared from Tissue

We studied tumor behavior and lymphatic vessel response to presence of tumor cells in the mouse pinna. We delivered varied loads of tumor cells, ranging from less than a hundred cells to more than a million, to the pinna with and without sutures. We used live imaging microscopy to investigate tumor-associated lymphatic vessel remodeling, to track tumor cells through pinna tissue, and to evaluate lymph node status at necropsy.

We found that the presence of a very small tumor burden was sufficient to induce localized lymphatic vessel remodeling (Figure 16). Lymphatic vessels in the immediate vicinity of a group of tumor cells displayed stochastic sprouting at the site of tumor residence after seven days. Tips of growing lymphatic vessels were often multi-sprouted, and anastomosis occurred to form lymphatic vessel ring structures. Vessels farther away from tumor cells did not display any alterations in morphology, likely demonstrating the localized effects of lymphangiogenic cytokines secreted from these very small groups of cells.

We found that tumor cells disappeared from sites of residence in the tissue. By day seven, no tumor cells were visible at their previous locations. This could indicate clearance by activated immune cells, intravasation into blood or lymphatic vessels and transport away, or cell death and clearance of remaining fluorescent cell debris.

Figure 16. Tumor cells induce local unsutured pinna lymphatic vessel remodeling and are cleared from tissue. *A-F.* CFSE-labeled B16 melanoma cells were injected into the Lyve1CreERT2^{tdT} unsutured depilated mouse pinna. Live stereofluorescence microscopy was used to track CFSE-labeled tumor cells (*green*) and tdTomato-expressing lymphatic endothelial cells (*red*) over seven days. Lymphatics are visible with both the Texas Red (TR) and Green Fluorescent Protein (GFP) filter sets due to the brightness and broad fluorescence emission spectrum of tdTomato protein. *A, D*. Site of CFSE-labeled B16 tumor cell residence in pinna (*arrow*) on imaging day 1. *B, E*. Return to site of tumor cell residence on imaging day 7. Tumor cells are no longer present. Local lymphangiogenic sprouting and anastomosis can be visualized. *C, F.* Higher magnification view of lymphatic endothelial sprouts and ring anastomosis.

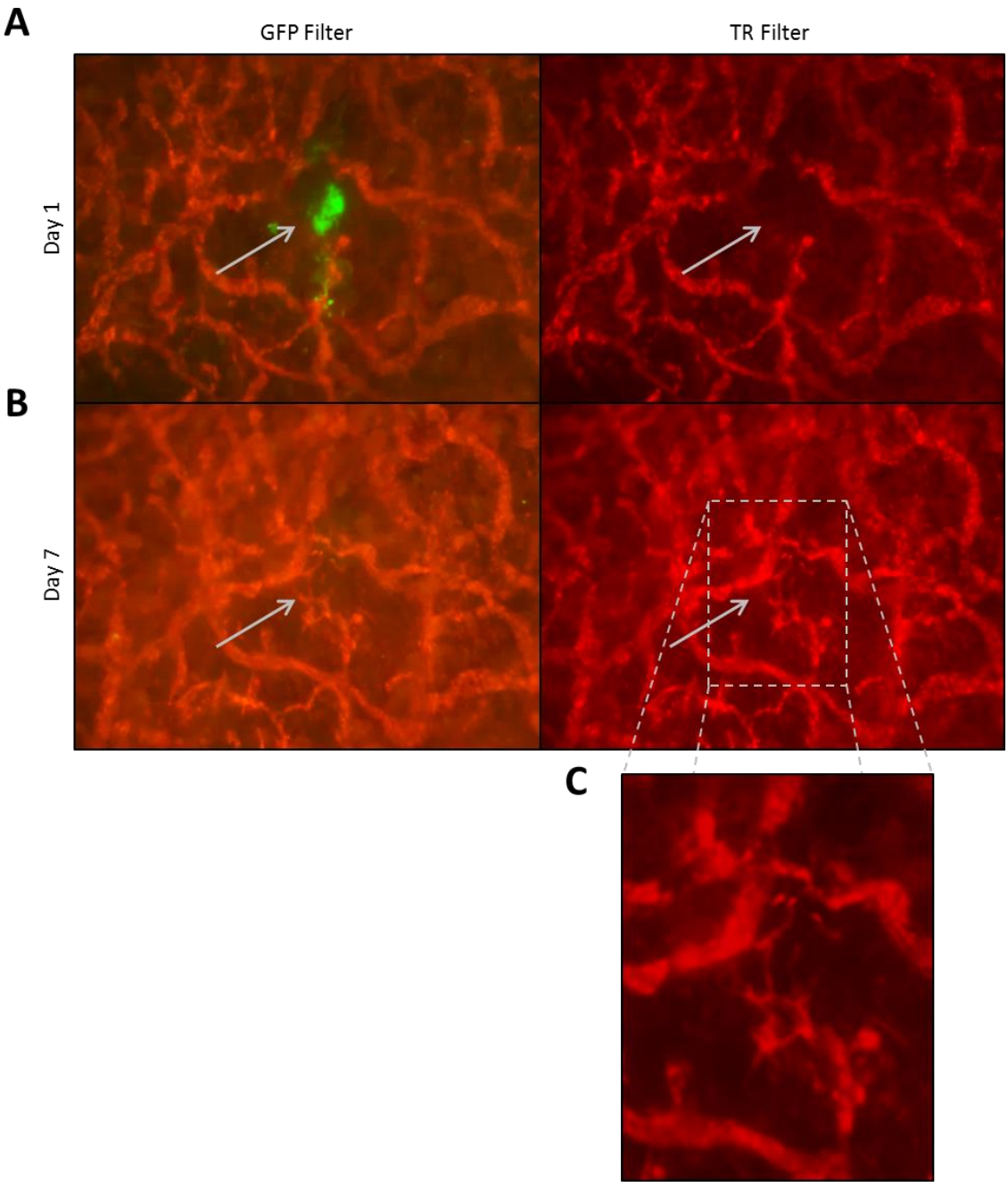

Figure 16A-C

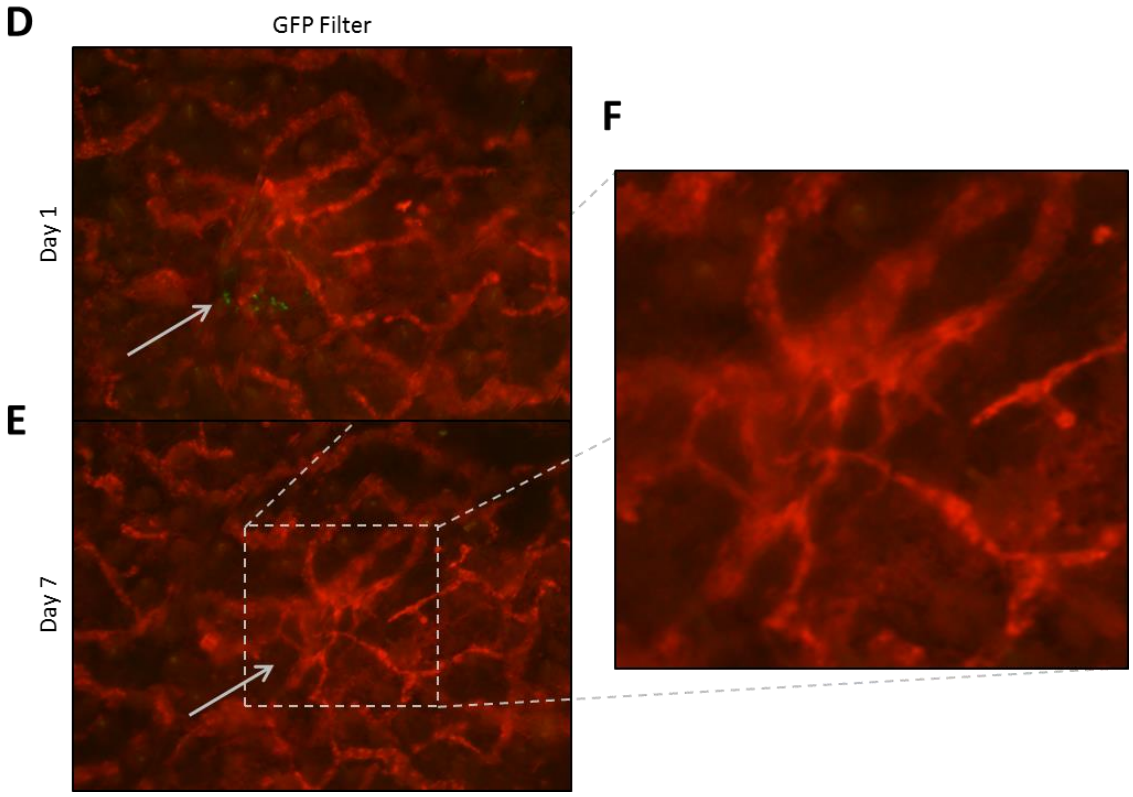

Figure 16D-F

Tumor Cells Enter Lymphatic Vessels and Traffic to Lymph Nodes

We designed experiments to investigate possible trafficking of tumor cells through lymphatic vessels. This would represent a mechanism of clearance from tissue and mimic metastasis to lymph nodes. We injected a large bolus dose of CFSE-labeled B16 melanoma cells into the edge of the Lyve1CreERT2^{tdT} pinna. One day after injection, lymphatic vessels half the distance of the pinna away from the injection site and distinct from the circular region of injected cell suspension harbored CFSE^{+} tumor cells. Both groups of cells and single cells could be visualized in the lumen of lymphatic vessels (Figure 17A, *top panel*). Cells resident in the extravascular pinna tissue could also be visualized in these regions, suggesting possible intravasation/extravasation activity at these sites, although we did not directly observe these behaviors.

The relatively stable nature of the pinna lymphatic vasculature architecture facilitated returning to landmark vessel structures in the tissue for sequential imaging over time. We returned to the areas of tumor-bearing lymphatic vessels on day two after injection, or 24 hours after first observing this phenomenon. We detected no CFSE signal in the vessels that had housed tumor cells the previous day and did not find similar groups of cells in vessels within the neighboring tissue (Figure 17A, *bottom panel*). This suggested that the tumor cells had been cleared from the pinna lymphatic vasculature and transported to the lymph nodes.

At necropsy on day seven, we examined lymph nodes for the presence of CFSE^{+} cells (Figure 17B). Across experiments we found tumor cells in lymph nodes in several locations including submandibular, axial, and inguinal nodes.

Figure 17. Tumor cells enter unsutured pinna lymphatic vessels, are cleared from vessels, and are present in lymph nodes at necropsy. CFSE-labeled B16 melanoma cells (*green*) were injected into the periphery of the depilated Lyve-1CreERT2^{tdT} mouse pinna. Tumor cells and tdTomato^{+} lymphatic vessels (*orange*) were followed by live imaging stereofluorescence microscopy. *A*. Tumor cells are visible in groups in lymphatic vessels on imaging day 1 (*arrows, top panel*). Identification of landmark lymphatic vessel structures facilitated imaging of the same regions 24 hours later. Tumor cells are no longer present at their previous locations within lymphatic vessels (*arrows, bottom panel*). *B*. CFSE^{+} cells are present in draining lymph nodes at necropsy.

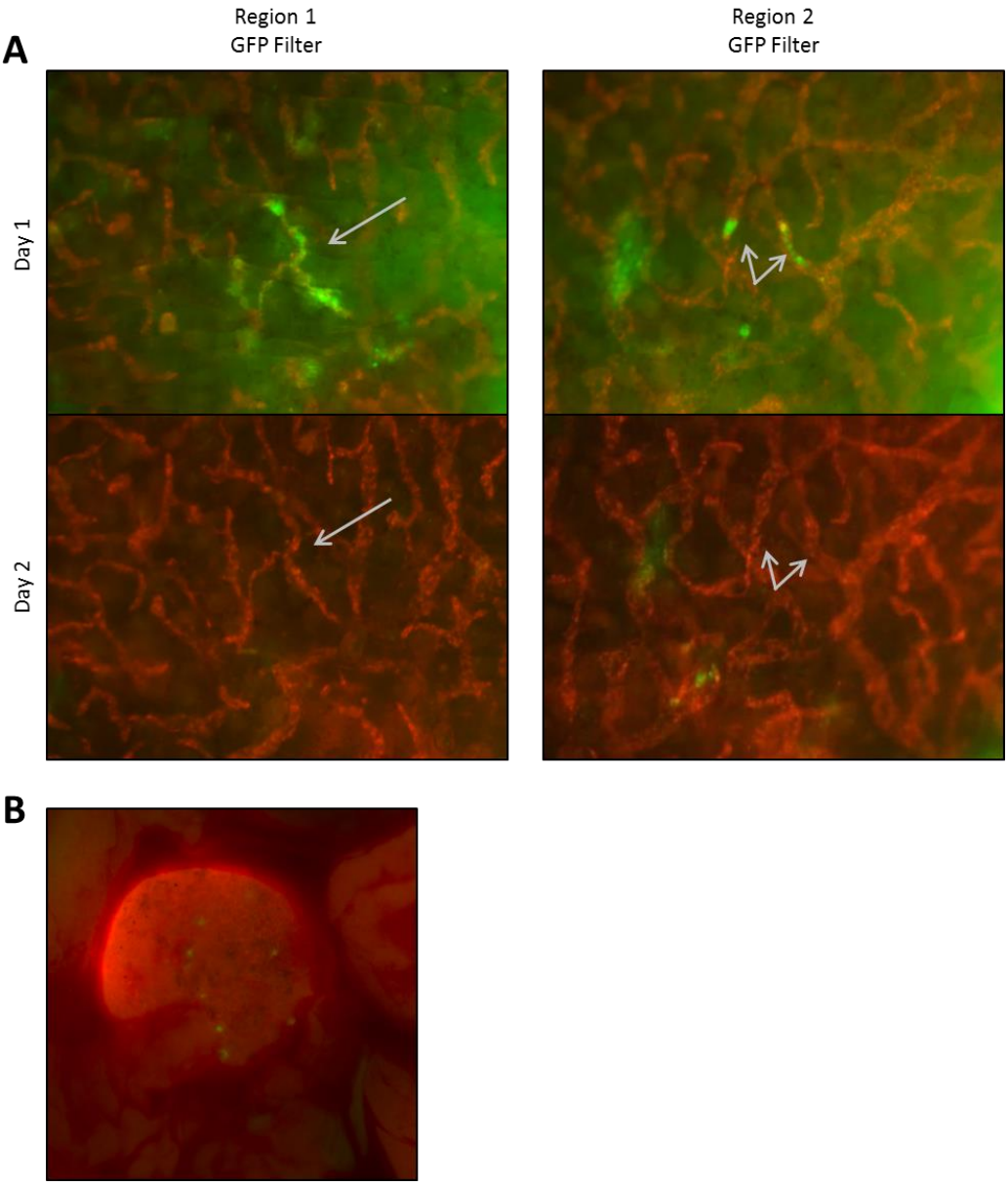

Figure 17

Spatially Localized Suture- and Tumor-Associated Lymphatic Vessel Remodeling

We established that placement of a suture or delivery of a minimal tumor burden results in two distinct patterns of skin lymphatic remodeling. We next studied these remodeling behaviors in different contexts: first, we investigated lymphatic remodeling in the presence of a much larger tumor burden, and second, we created distinct suture- or tumor-associated microenvironments within the same pinna.

We first established local zones of nonmalignant inflammation with the placement of chromic gut sutures in the Lyve1CreERT2^{tdT} mouse pinna; one suture was placed in the center of the pinna and another in the upper quadrant, leaving a large area free of inflammatory stimuli (Figure 18A). After three days, a medium dose of CFSE-labeled B16 melanoma cells was injected into the margin of the pinna opposite the sutures. Sutured locations displayed the characteristic loss of lymphatic capillaries immediately adjacent to stimuli with some sprouting into wounded area (Figure 18A, E). Lymphatic vessels in the area of tumor challenge appeared grossly enlarged; closer examination at necropsy on day seven revealed dramatic hypersprouting morphology in the tumor-associated microenvironment (Figure 18A-C). Single sprouts budded off existing vessels in all directions; single cells not incorporated into the vascular network infiltrated spaced between vessels; single and elongated cells lined up in thin extended chains among larger lymphatic capillaries (Figure 18C).

Tumor cells were in close association with lymphatic vessels of both ear skin layers as revealed by dissection at necropsy (Figure 18B). Single and groups of cells were present at various distances from the bolus injection site within the tissue (Figure 18A-C). Lymph nodes at necropsy were positive for tumor metastases (Figure 18D).

Figure 18. Establishment of wound- and tumor-associated inflammatory microenvironments in separate regions of the mouse pinna results in distinct patterns of lymphatic remodeling. Sutures were placed in the depilated Lyve1CreERT2^{tdT} mouse pinna. Three days later, a large bolus dose of CFSE-labeled B16 melanoma cells in suspension was injected into the margin of the pinna. Tumor cells and lymphatic vessels were tracked for seven days by live imaging. At necropsy on day seven, the two layers of ear skin were separated to reveal the intact lymphatic vessel plexuses, and the draining lymph nodes were examined for the presence of CFSE^{+} cells. *A*. Intact pinna shows CFSE signal at site of tumor cell injection and sites of suture placement (*). *B*. Two layers of ear skin are separated at necropsy. Tumor cells have moved through tissue away from injection site. *C*. Higher magnification of designated area from *B*. Lymphatic vessels display hypersprouting morphology in immediate vicinity of tumor cells. In the *right panel*, three images taken at different focal depths were stitched together to form this micrograph. *Black lines* indicated by *arrows* demarcate transitions between the images. *D*. CFSE^{+} cells are present in draining lymph node. *E*. Higher magnification images of sites of suture placement. Characteristic “zone-of-clearing” is present around wound. Some sprouting is present at lower edge of *right panel*.

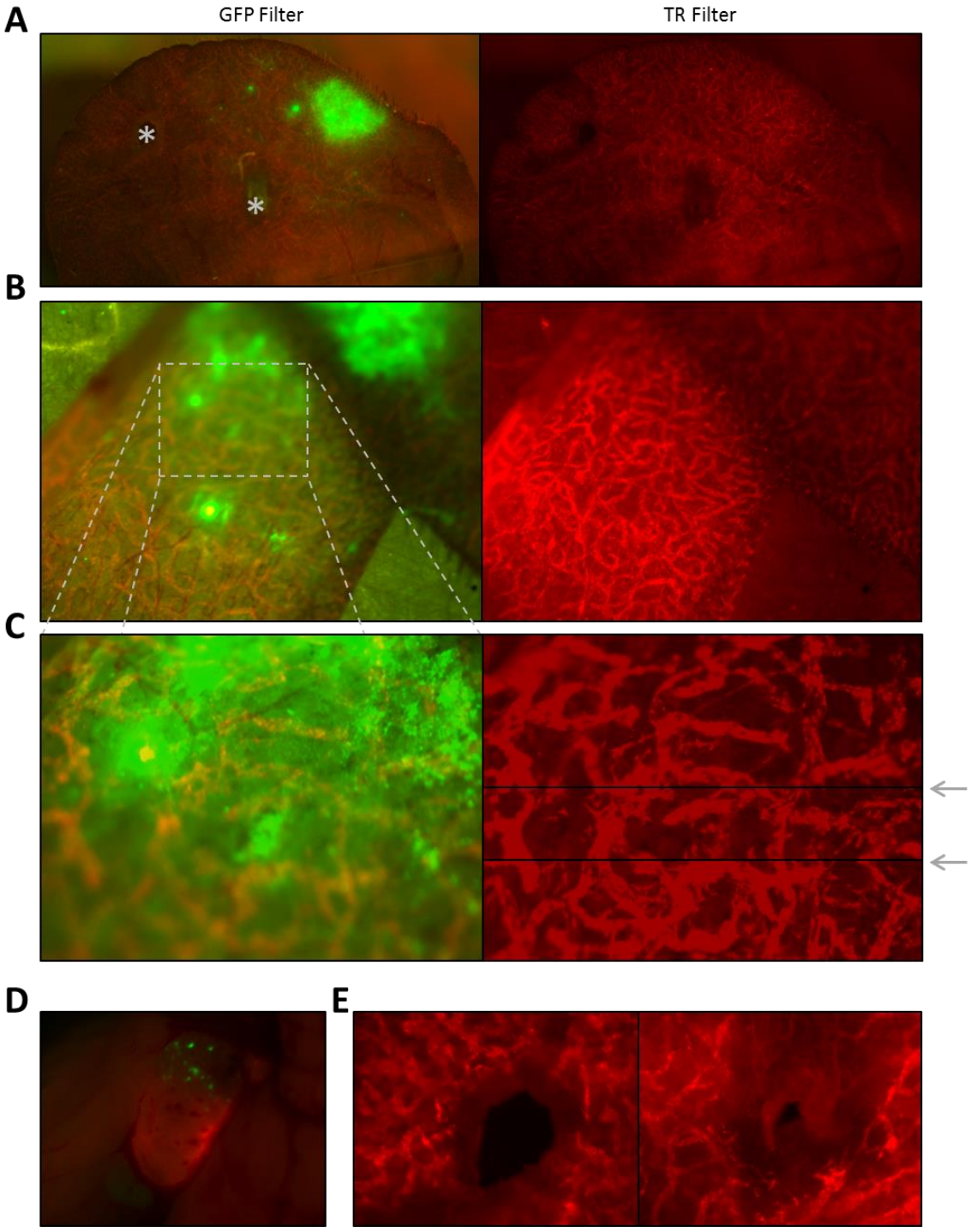

Figure 18

Delivery of Tumor Cells to Cornea is Feasible and Cells Are Viable

To this point, all of our work had been done in the context of an orthotopic model of melanoma, *i.e.* study of B16 melanoma cells in the syngeneic murine skin. To better address tumor-associated neuroremodeling and to track inflammatory new lymphatic vessel synthesis in a setting normally devoid of lymphatic vessels, we transitioned our studies to a corneal live imaging platform. Our previous work had established the utility of micropellet implantation as a means to administer cytokine to the cornea, and we now tested this method for tumor cell delivery. As there was some uncertainty about whether or not the corneal microenvironment would be hospitable to tumor cells, we also tested tumor cell viability after implantation.

Several methods of loading tumor cells onto micropellets were tested, and allowing tumor cells in high cell numbers in suspension to adhere to the pellet matrix was suitable (Figure 19A). Pellets were implanted into a pocket made by a small incision as described for cytokine pellets, and we determined that pocket placement either in the center of the cornea or at the midpoint between the corneal apex and temporal limbal arcade was feasible and facilitated the desired experiments. Pellets could be placed in tissue with or without sutures without excessive disruption of ocular globe integrity (Figure 19B, C). We also tested direct injection of tumor cell suspension into a corneal pocket and found this to be a reasonable alternative delivery method (Figure 19D). The most notable difference in the two techniques was the dissemination of tumor cells from the injection site.

To ascertain tumor cell viability following injection we observed cell morphology by live imaging and followed $CFSE^{+}$ cells in culture derived from harvested corneal explants previously injected with tumor cells. Injected tumor cells often displayed spindle shaped morphology and cell-cell interactions visible by live imaging microscopy. CFSE-labeled cells grew out of corneal

explants and could be subcultured and grown on coverslips for confocal microscopy (Figure 19E). CFSE signal was clearly present in cells; cells displayed expected morphology; nuclei were intact. Variations in signal intensity indicate that rates of cell division varied among clones.

Figure 19. Tumor cells are viable after corneal implantation. *A.* CFSE-labeled B16 melanoma (shown here), E0771 breast cancer, or KPC pancreatic cancer cells were loaded onto a micropellet *ex vivo*. *B.* Sutured mouse cornea before tumor administration. Size bar = 250 µm. *C.* A tumor-bearing pellet was placed into a micropocket in the center of the cornea. Presence of tumor cells was confirmed by live imaging immediately following pellet implantation. Size bar = 250 µm. *D.* CFSE-labeled B16 melanoma cells (*green*) in suspension were directly injected into the Lyve1CreERT2^{tdT} cornea and visualized by live imaging (endogenous tdTomato fluorescence, *red*). Size bar = 250 µm. *E*. Five days after administration of tumor cells, corneal explants were placed in tissue culture. CFSE^{+} cells grew out of explants onto coverslips and were imaged by confocal microscopy. 400X maximum intensity projection shown (CFSE, *green*; DAPI, *blue*). Size bar = 50 µm.

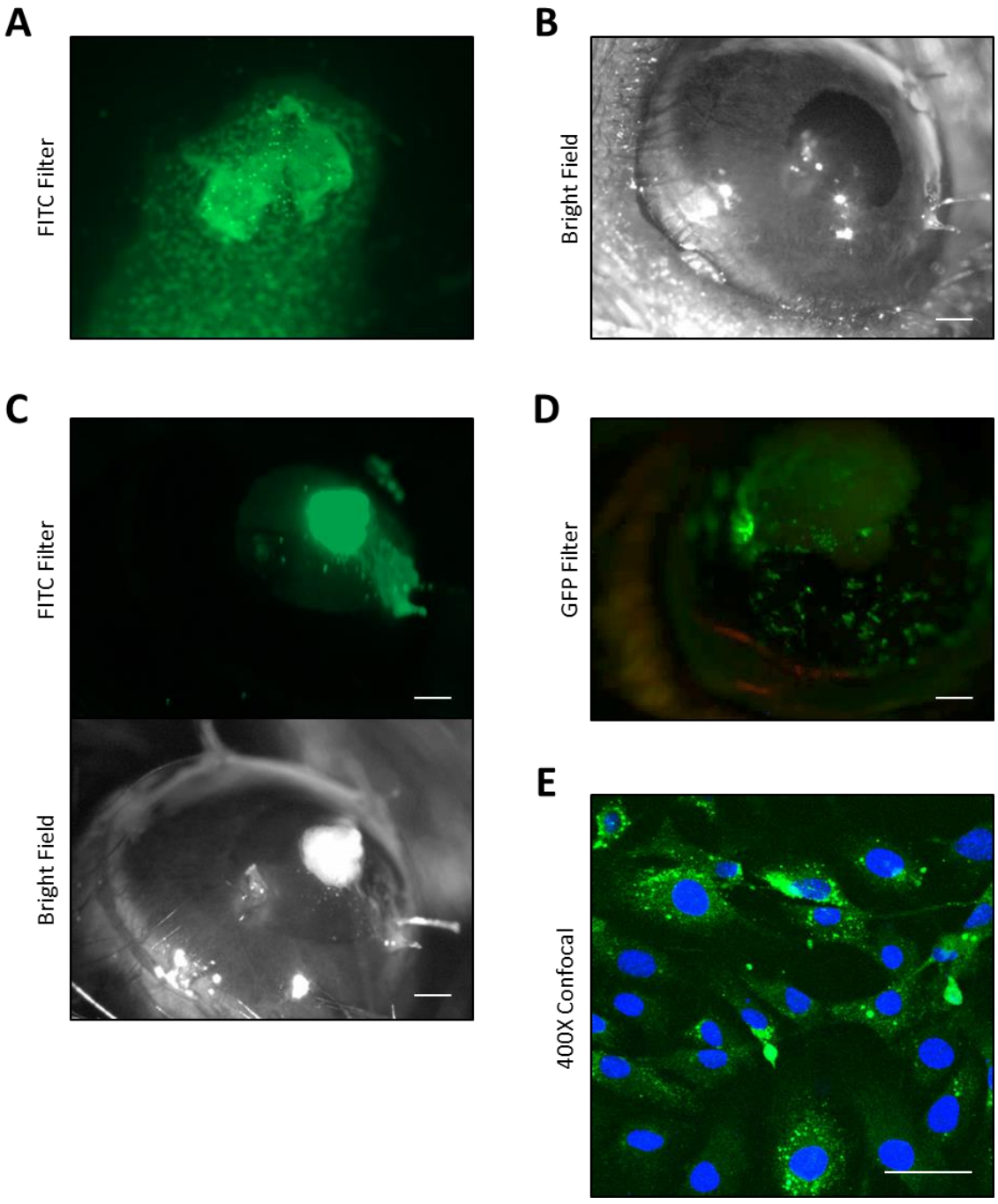
A
FITC Filter
B
Bright Field
C
FITC Filter
Bright Field
D
GFP Filter
E
400X Confocal

Figure 19

Tumor Cells Induce Local Corneal Neuroremodeling

Presence of tumor cells in the cornea had both local and field effects on nerve architecture. In the presence or absence of sutures, delivery of a modest dose of tumor cells resulted in localized decreases in nerve density in the immediate vicinity of tumor cells (Figure 20A, B). This local effect was seen regardless of tumor position within the tissue. Nerve density was decreased around cells located in the center or periphery of the cornea; proximity of tumor cells to sutures also did not affect this remodeling. All classes of corneal nerves were affected, including large stromal trunks, subepithelial leashes, and epithelial nerve endings. Local neuroremodeling was accompanied by broader effects. In cases in which only a few tumor cells remained resident in the cornea after injection, we saw local nerve cluster formation and transition of the surrounding tissue to a more wound recovery-like phenotype. Nerves displayed a more tortuous morphology and often terminated in small clusters (Figure 20C-E).

Addition of tumor cells to an inflammatory microenvironment attenuated typical inflammatory neuroremodeling. As characterized in Chapter I, in suture-mediated nonmalignant inflammation thickened nerves drive toward stimuli and are present at extremely high density at suture sites, often engulfing the foreign body (Figure 20F). Here, nerve morphology was more variable and included nerves terminating in clusters typically only seen in wound recovery (Figure 2E), though large diameter sprouting lymphatic vessels confirmed that the sutured tissue was inflamed (Figure 20E).

Figure 20. Tumor cells induce local neuroremodeling in the presence or absence of sutures. *A, D.* B16 melanoma cells were labeled with CMRA Orange CellTracker dye and injected into the uninflamed cornea. Size bar = 250 µm. *A.* Tumor cells are resident at several locations within the tissue (*arrows*). Corneas were harvested on day three and nerves stained for β-III tubulin. Size bar = 250 µm. *B.* Corneas were sutured and CMRA-labeled B16 melanoma cells were injected the same day. *Arrows* indicate positions of tumor residence. Tissue was harvested and stained as in *A*. Size bar = 250 µm. *C.* CFSE-labeled B16 melanoma cells were injected into the cornea; tissue was harvested on day nine. Size bar = 250 µm. *E.* Confocal micrograph of Lyve-1-stained lymphatic vessels and β-III tubulin-stained nerves in the sutured cornea in the presence of injected CFSE-labeled B16 melanoma cells (*arrows*). Size bar = 100 µm. *F.* Confocal micrograph of suture in corneal tissue without the addition of tumor cells. Size bar = 100 µm.

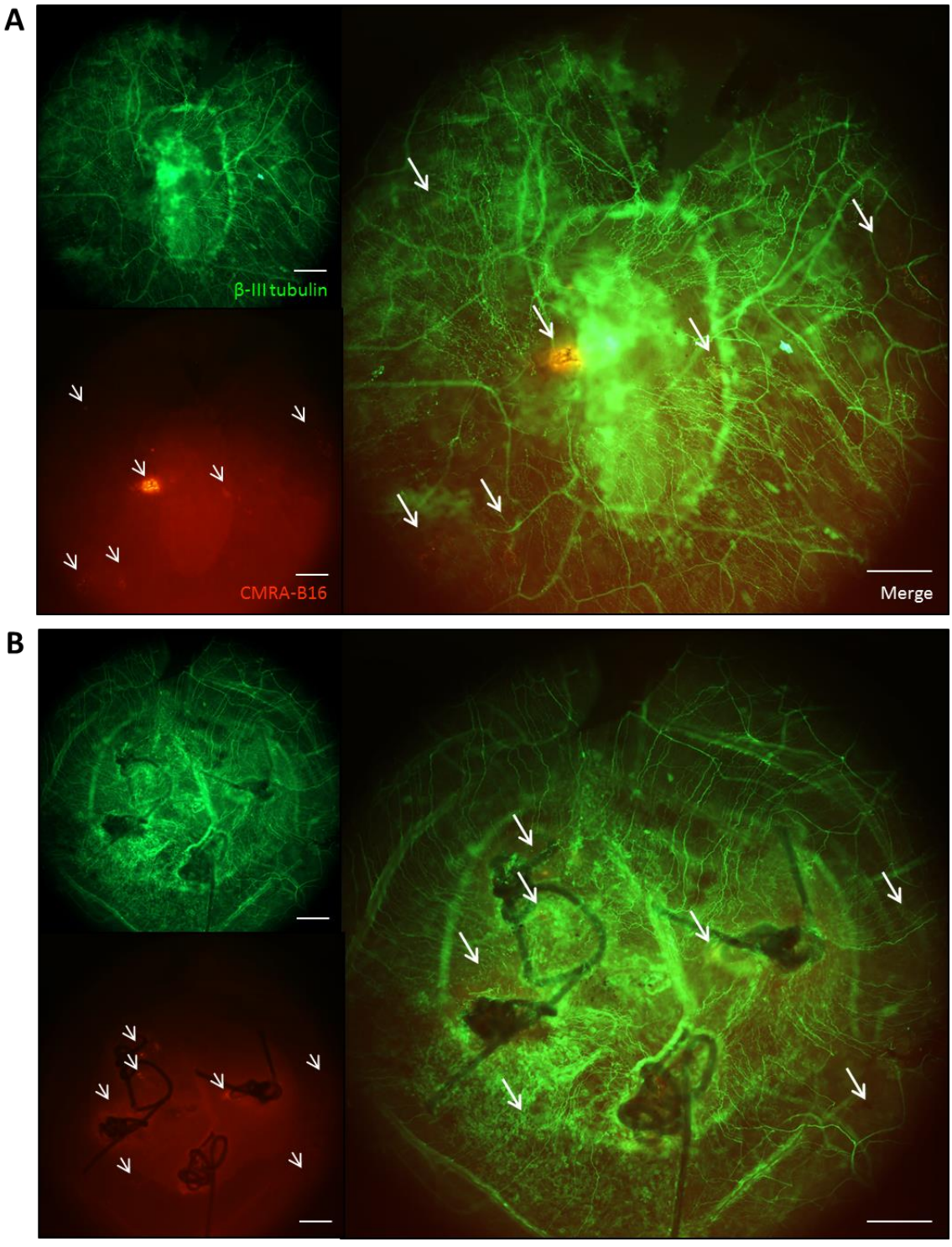

Figure 20A, B

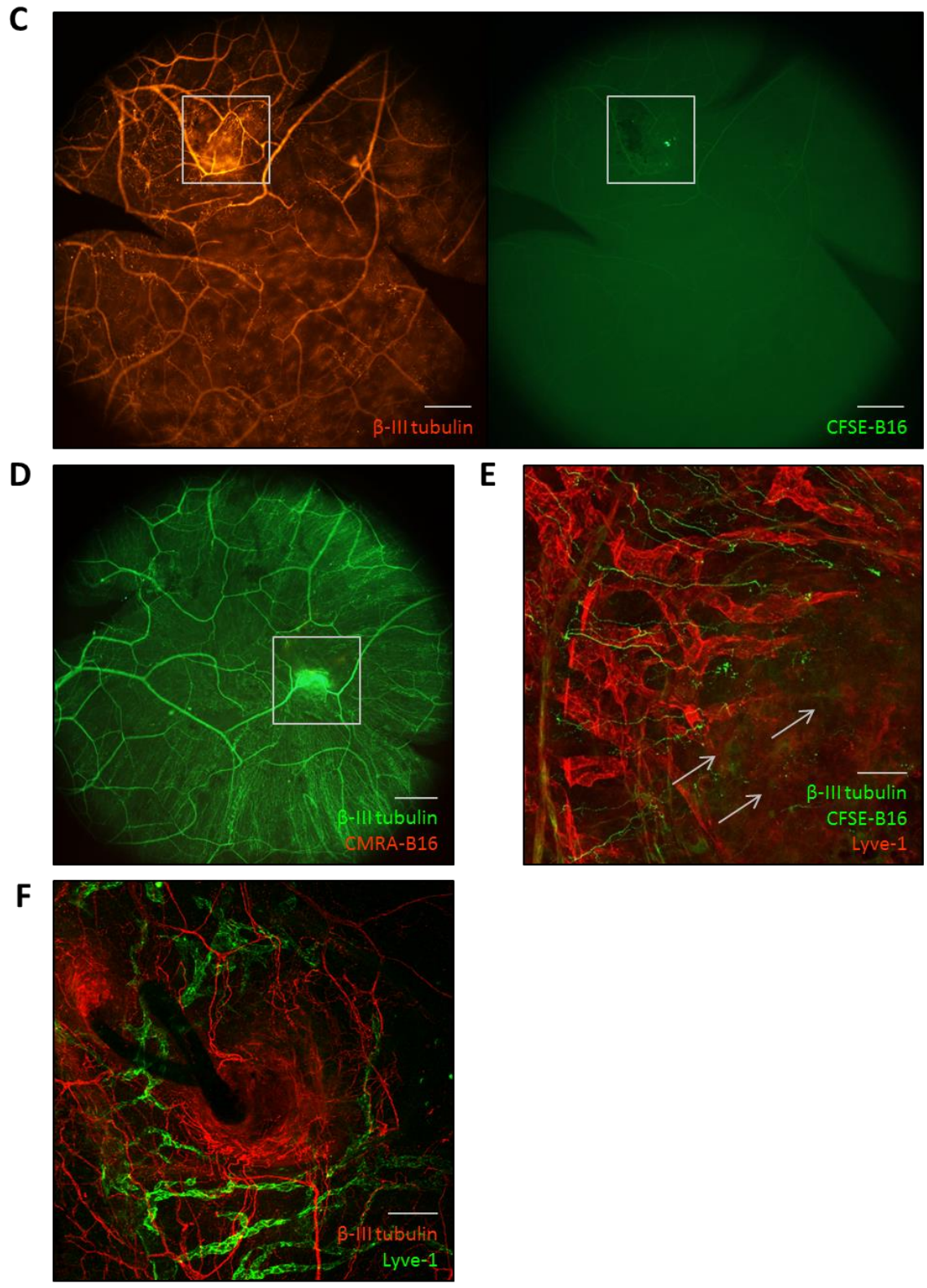
C
β-III tubulin
CFSE-B16
D
β-III tubulin
CMRA-B16
E
β-III tubulin
CFSE-B16
Lyve-1
F
β-III tubulin
Lyve-1

Figure 20C-E

Tumor Cells Induce Lymphangiogenesis

Our studies in the pinna were limited by the nature of that tissue's lymphatic vasculature. The dense regularly distributed lymphatic vessels present in homeostasis were capable of only minor localized remodeling events after suture placement or tumor challenge. We used the corneal platform to investigate tumor-directed new lymphatic vessel synthesis; this was facilitated by the lack of vascularization under steady state conditions.

We injected tumor cells into micropockets in unsutured corneas. By day two (Figure 21A, *upper panel*), some tumor cells had migrated away from the micropocket and spread through the corneal tissue. Many of these cells had moved to the limbal region, where nerve, lymphatic, and blood vessel arcades are located. The majority of injected cells remained at the injection site. By day six (Figure 21A, *middle panel*), new lymphatic vessels had sprouted from the limbal vessels and were growing toward the tumor cells. Most of the cells that had migrated away from the injection site were no longer visible in the tissue. Marked lymphangiogenesis occurred by day eight (Figure 21A, *lower panel*). New lymphatic vessel growth was more pronounced from limbal locations nearer the tumor cells, but sprouting occurred from limbal lymphatic vessels in each corneal quadrant (Figure 21B). Single tdTomato^{+} cells also migrated through the tissue toward the tumor burden. These results support the hypothesis that there is a secreted chemotactic factor gradient emanating from tumor cells that directs lymphatic vessel sprouting and lymphatic endothelial cell or macrophage migration toward the source of chemoattractant.

Figure 21. Tumor cells alone stimulate new lymphatic vessel growth. CFSE-labeled B16 melanoma cells were injected into a Lyve1CreERT2^{tdT} mouse corneal micropocket placed near the temporal limbus. *A.* Tumor cells and lymphatic vessels were monitored by fluorescence live imaging microscopy for eight days at 32X, 50X, and 80X. Size bar = 100 µm. *B.* Each quadrant of harvested tissue was imaged at 100X by epifluorescence microscopy and images were compiled to form composite images shown. Tumor injection site is bright focus in *bottom right* image of composite. Size bar = 250 µm.

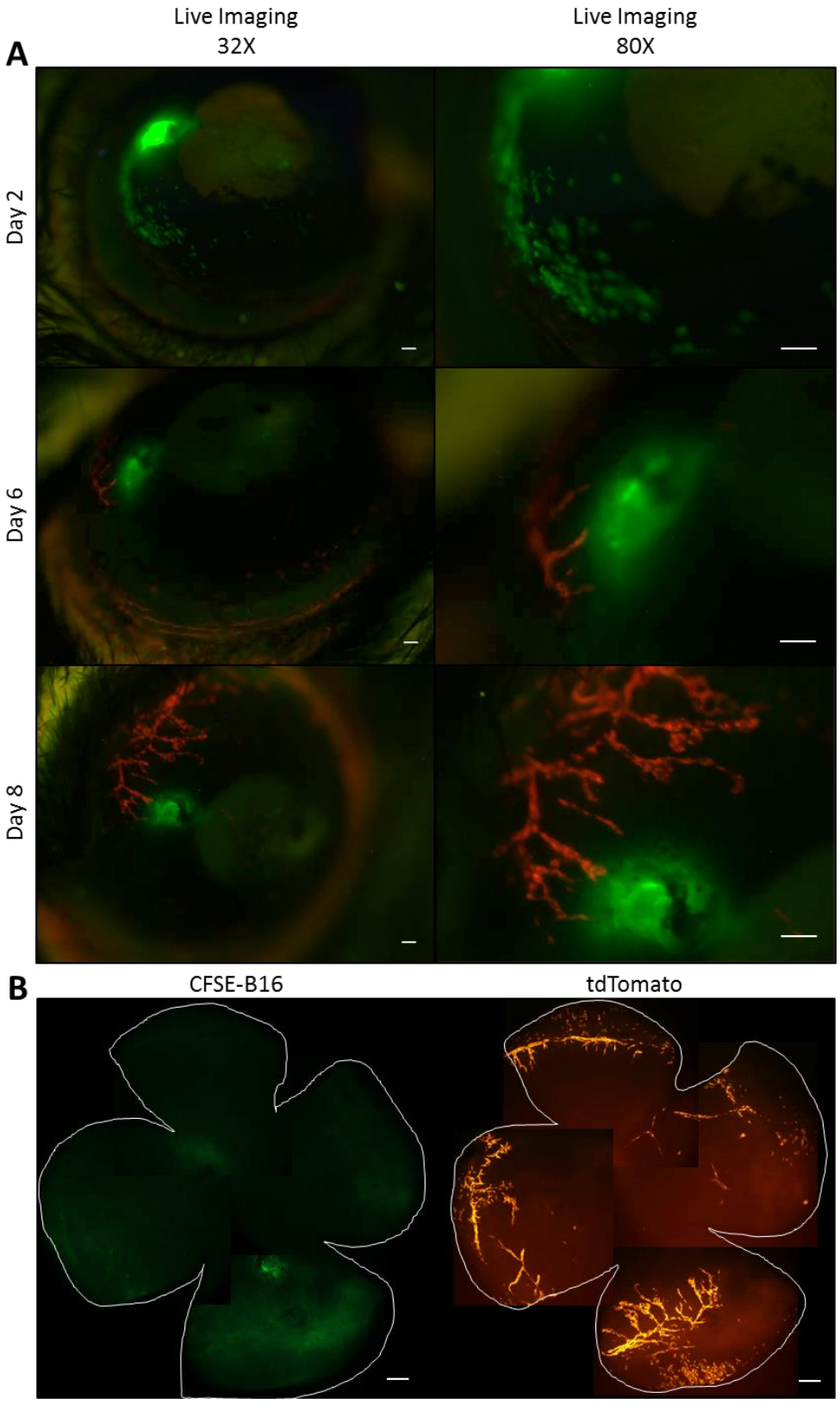
A
Live Imaging
32X
Live Imaging
80X
Day 2
Day 6
Day 8
B
CFSE-B16
tdTomato

Figure 21

Unique Lymphatic Structures Arise in Inflammatory Lymphangiogenesis in the Presence of Tumor Cells

We identified several types of unique lymphatic vessel behavior and architecture in tissues bearing both sutures and tumor cells (Figure 22, Figure 23, Figure 24). We previously established that in corneal tissue inflamed by sutures alone, lymphatic vessels adopted a chalice-like morphology as they neared the location of a suture and did not penetrate within the immediate vicinity of the suture (Figure 2B, Figure 20F). This did not change in the presence of a tumor pellet in the center of the cornea with sutures in each quadrant (Figure 22A). Conversely however, hypertrophic lymphatic vessels with activated multi-sprouted tips approached and invaded tumor pellets from all directions, completely taking them over in some cases (Figure 22A, B, Figure 24A). Tumor cells interacted with newly synthesized lymphatic vessels (Figure 22C), and single tdTomato-expressing cells could be seen in close contact with tumor cells as well near tumor pellets (Figure 22D). Although blood vessels do not express Lyve-1 and do not, therefore, express tdTomato fluorescent protein in the Lyve1CreERT2^{tdT} mouse model, we were able to visualize the contrast of dark blood flowing in these vessels against the autofluorescence of the eye lens. Angiogenesis also occurred in these corneas, and sprouting blood capillaries invaded tumor pellets along with lymphatics (Figure 22B, Figure 24A).

We also identified disorganized lymphatic vessels sprouting from the corneal limbus in response to both a large injected tumor burden and tumor bearing pellets (Figure 24) in sutured tissue. Highly irregular lymphatic endothelial sprouts with no discernable organized vascular architecture grew out of the limbus near tumor pocket placement (Figure 23). This occurred in tissue that was sutured the same day as tumor injection. In tissue that was pre-sutured six days before tumor pellet placement, two types of lymphatic vessels were present (Figure 24C). Large, well-organized vessels with both sprouting and bulbous termini typical of suture-

mediated lymphangiogenesis were present alongside thin, disorganized, discontinuous structures that appeared to be immature or incompletely synthesized. Many single cells were present in these regions, many of which were elongated. Live imaging of these structures over time with the aid of tissue landmarks highlighted their disorganized nature and suggested that some of the larger, more typical lymphatics in these regions were well-established prior to tumor implantation and had originally been stimulated by suturing, while the more disorganized structures emerged in the presence of tumor burden (Figure 24B).

Figure 22. Lymphatic vessels respond differently to suture and tumor stimuli. CFSE-labeled B16 melanoma cells were loaded onto micropellets and placed in pockets in the center of Lyve1CreERT2^{tdT} corneas that had been sutured with four 10-0 nylon sutures six days earlier. Tumor cells (*green*) and tdTomato^{+} lymphatic vessels (*red*) were tracked by live imaging microscopy for several days. *A.* Sutures are indicated by asterisks (*). Pellets are outlined with *dashed lines*. Size bar = 100 µm. *B*. Blood vessels are visible as dark structures against lens autofluorescence alongside lymphatic vessels and tumor cells. Size bar = 100 µm. *C.* Tumor cell interactions with newly-synthesized lymphatic vessels (*arrows*). Size bar = 100 µm. *D.* Single tdTomato^{+} cells interacting with tumor cells at margins of pellet (*arrows*). Size bar = 100 µm.

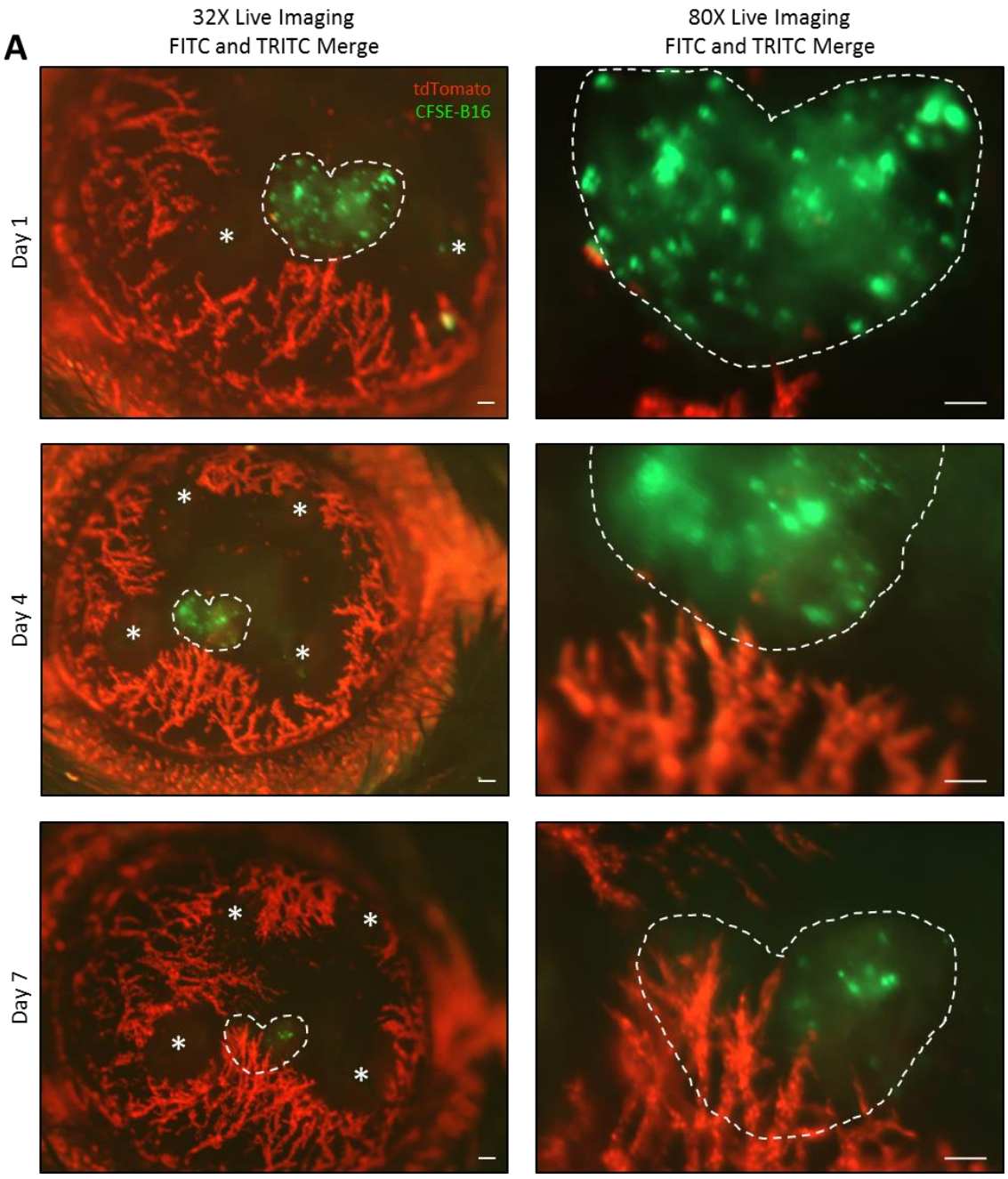
A
32X Live Imaging
FITC and TRITC Merge
80X Live Imaging
FITC and TRITC Merge
tdTomato
CFSE-B16
Day 1
Day 4
Day 7

Figure 22A

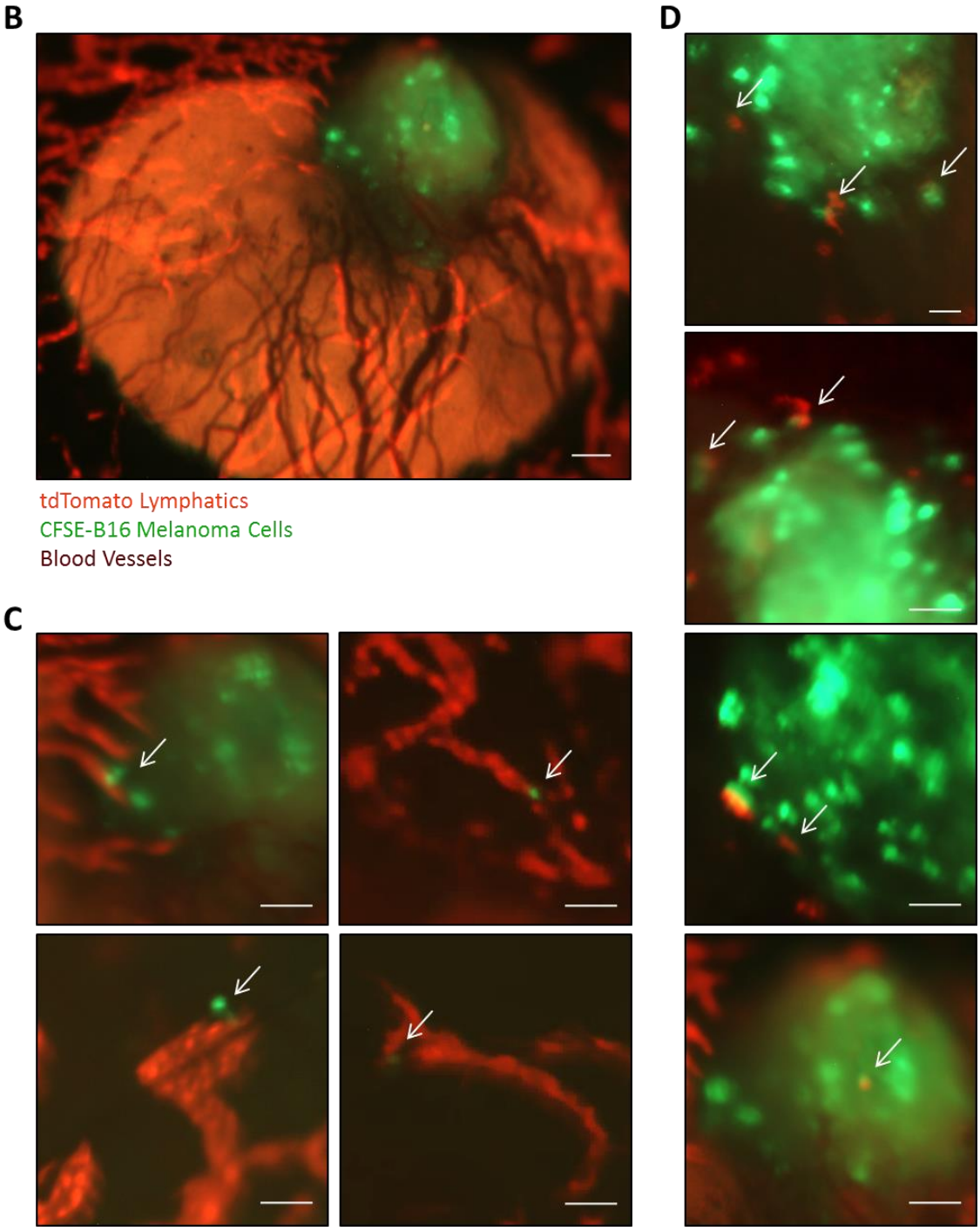
B
D
tdTomato Lymphatics
CFSE-B16 Melanoma Cells
Blood Vessels
C

Figure 22B

Figure 23. New lymphatic vessels growing in the presence of sutures and large tumor burden are disorganized. Lyve1CreERT2^{tdT} corneas were sutured with four 10-0 nylon sutures and injected with a large dose of CFSE-labeled B16 melanoma cells on the same day. *A.* Tumor cells (*green*) and lymphatic vessels (*red*) were tracked for eight days by live imaging microscopy. *Dashed line* indicates limbus. Size bar = 100 µm. *B.* 100X epifluorescence micrograph of endogenous tdTomato signal in lymphatic vessels sprouting from limbus (*dashed line*) in fixed tissue after harvest on day eight. Size bar = 100 µm.

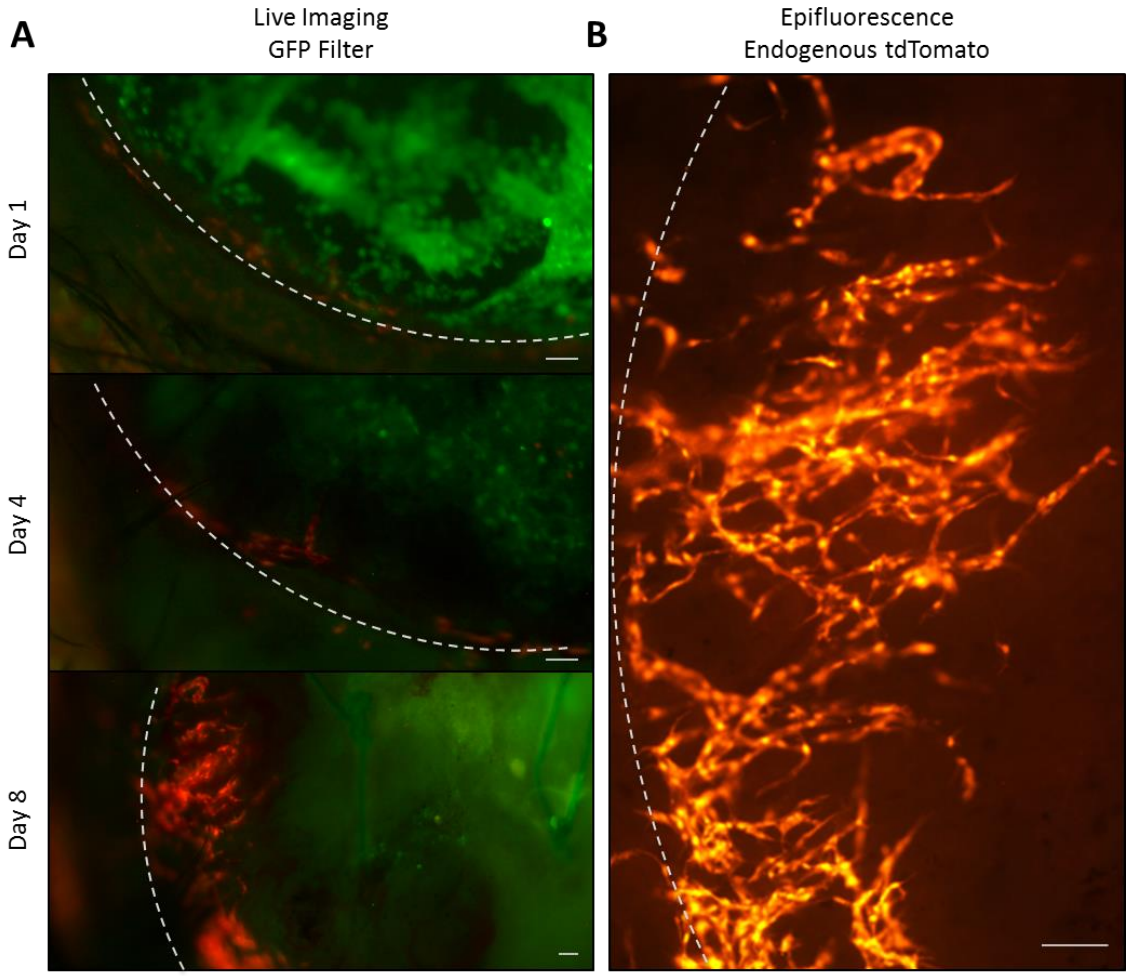
A
Live Imaging
GFP Filter
B
Epifluorescence
Endogenous tdTomato
Day 1
Day 4
Day 8

Figure 23

Figure 24. Presence of lymphatic vessels of two distinct morphologies in corneas bearing sutures and tumor cells. CFSE-labeled B16 melanoma cells were loaded onto micropellets and placed in pockets in the center of Lyve1CreERT2^{tdT} corneas that had been sutured with four 10-0 nylon sutures six days earlier. *A, B.* Tumor cells and tdTomato^{+} lymphatic vessels were tracked by live imaging microscopy for several days. A region of interest was identified for closer monitoring over time with landmarks (*A, Day 6, dashed box*). *Blue dot* indicates suture landmark. *Yellow star* indicates hooked lymphatic vessel landmark. Time course of images of this region make up *B*. Size bar = 100 µm. *C*. 100X epifluorescence micrograph of tdTomato^{+} lymphatic vessels co-immunostained for Lyve-1 with a 549 nm emission wavelength (overlaps tdTomato emission spectrum) secondary antibody. Size bar = 100 µm.

A

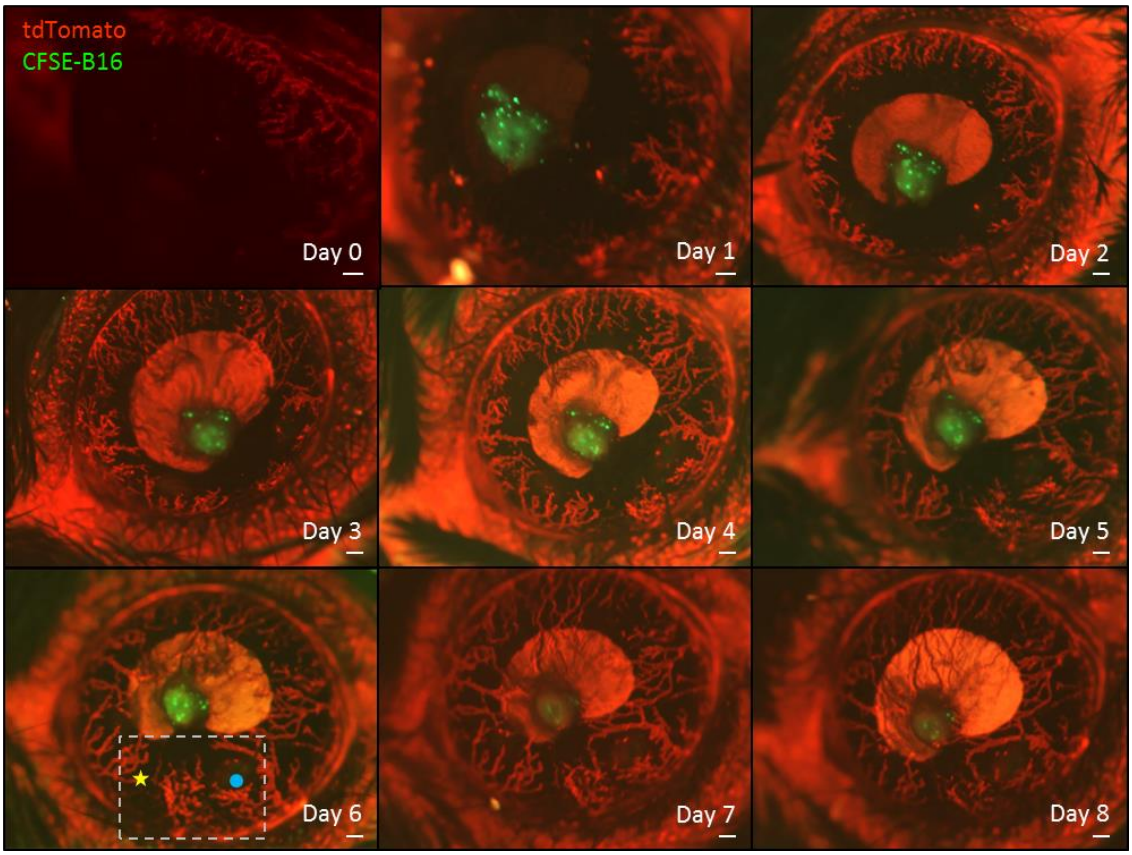
tdTomato
CFSE-B16
Day 0
Day 1
Day 2
Day 3
Day 4
Day 5
Day 6
Day 7
Day 8

Figure 24A

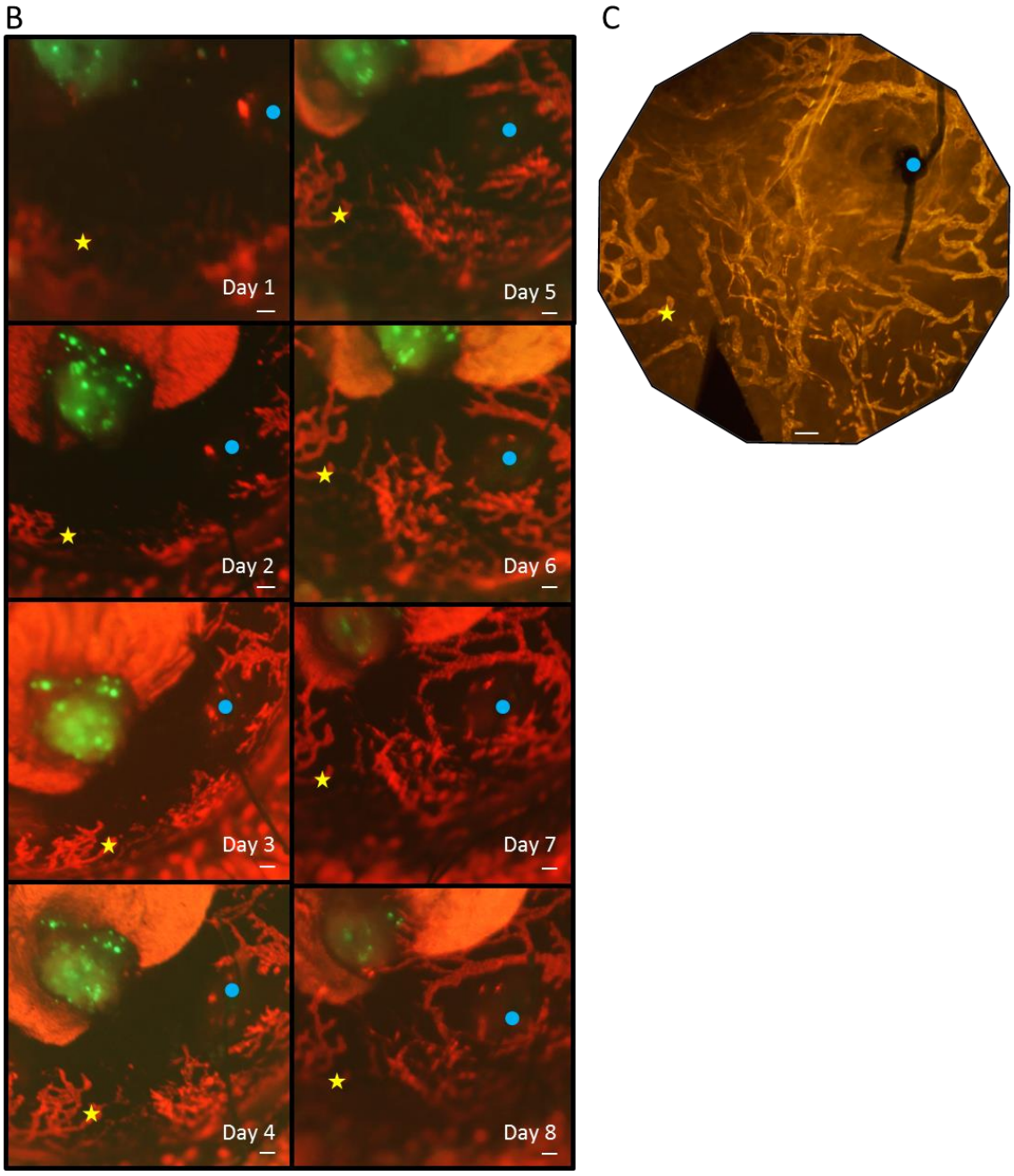

Figure 24B, C

Simultaneous Establishment of an Inflammatory Microenvironment Prolongs Tumor Residency in Cornea

In several of our previous experiments, we noted an effect of the inflammatory status of corneal tissue on success of prolonged tumor imaging after tumor delivery. To further study this effect, we established three microenvironmental conditions in the cornea prior to tumor cell injection by placing sutures at different time points and following tumor cell signal over time by live imaging. Corneas were unsutured, sutured three days before injection of tumor cells (pre-sutured), or sutured immediately prior to tumor injection on the same day. We performed these experiments with two different cell lines syngeneic to C57BL/6 mice: E0771 estrogen receptor^{+} medullary breast carcinoma cells and KPC pancreatic adenocarcinoma cells. Similar results were seen with both cell lines. By day two after injection, cells were distributed throughout the cornea in all conditions. By day four, the groups had separated. Unsutured corneas had only a few cells remaining; these were concentrated at the injection site and near the limbal vascular arcade. The few cells remaining in the pre-sutured corneas were resident at the injection site and near sutures. By contrast, corneas that had been sutured the same day as tumor injection had tumor cells distributed throughout—at the injection site, sites of sutures, near the limbus, and in the corneal parenchyma away from any of these structures. These results suggested that aspects of the earliest events in the establishment of a suture-mediated inflammatory response in the cornea (before day three) affected tumor biology such that cells remained resident at the site of this inflammatory response.

Figure 25. Timing of inflammatory microenvironment establishment influences tumor cell behavior in tissue. E0771 breast cancer or KPC pancreatic cancer cells were labeled with CFSE (*green*) and injected into a micropocket of a C57BL/6 mouse cornea in one of the following conditions: unsutured, sutured three days prior to tumor injection, or sutured the same day as tumor cell administration. Live imaging was performed on days two and four post tumor injection and corneas were harvested on day four. Harvested tissue was fixed and lymphatic vessels were immunostained for Lyve-1 (*orange*). Live imaging: 32X. Epifluorescence: 100X. Size bar = 200 μm.

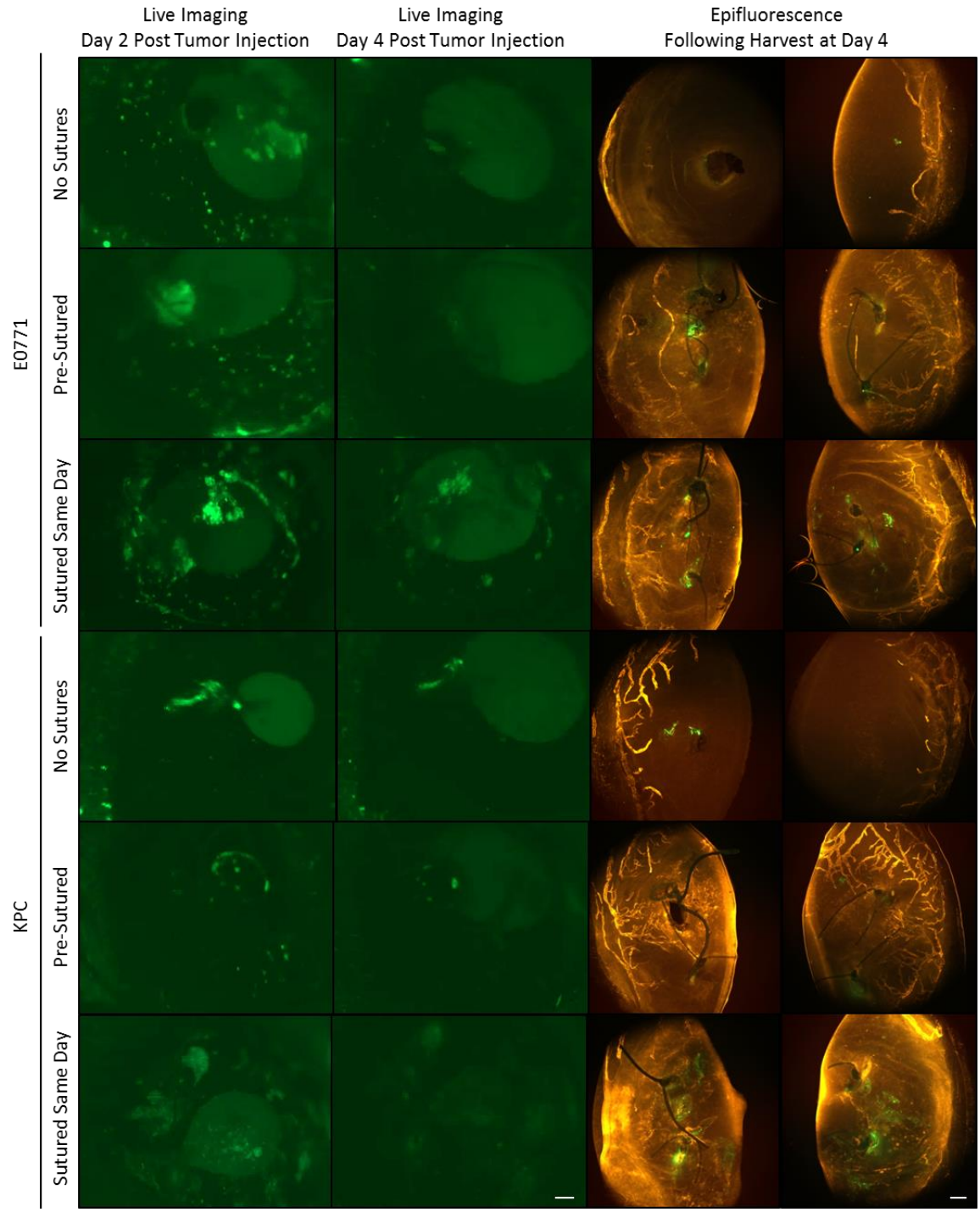
Live Imaging
Day 2 Post Tumor Injection
Live Imaging
Day 4 Post Tumor Injection
Epifluorescence
Following Harvest at Day 4
E0771
KPC
No Sutures
Pre-Sutured
Sutured Same Day
No Sutures
Pre-Sutured
Sutured Same Day

Figure 25

Discussion

Distinct Stimulus-Dependent Neurolymphatic Remodeling Signatures and Mini-Microenvironments

We used live imaging microscopy to visualize kinetics and dynamics of lymphatic vessel remodeling in physiologically distinct microenvironmental conditions induced by physical injury or tumor burden. Sutures caused directional lymphangiogenic sprouting from existing vessels, but nascent lymphatics did not enter a "zone-of-clearing" immediately surrounding each suture. Tumor-associated lymphangiogenesis was quite different. The presence of a very small number of tumor cells resulted in a disorganized multi-directional hypersprouting lymphangiogenic phenotype. This effect was even more pronounced in the presence of a larger tumor burden. Lymphatic vessels were not inhibited from entering the tissue immediately adjacent to tumor cells; sprouting lymphatics contacted and invaded tumor-bearing pellets and interacted directly with tumor cells. These two distinct stimulus-dependent modes of new lymphatic vessel growth were not mutually exclusive. Placing sutures and tumor cells in the same pinna or cornea resulted in localized lymphangiogenesis responses commensurate with stimulus type. This intra-tissue variability, even in a region as small as one quadrant of the mouse cornea, demonstrated the true *micro* nature of a microenvironment. Regardless of inflammatory status or presence of malignancy, "tissue microenvironments" are inherently hypervariable and plastic and are composed of an infinite number of stochastically shifting mini-microenvironments responding to changes in local complements of cytokines, resident cell types, tissue pressure, metabolite flux, *etc*.

We also found stimulus-dependent differences in neuroremodeling. Similar to the effect on lymphatic vessels, placement of a suture resulted in a directional shift in nerve organization, with nerves bending to track toward the stimulus. Nerves grew into and around

suture knots at very high density. Addition of tumor cells to a sutured environment resulted in both local and broader neuroremodeling effects. Tumor cell presence in an inflamed tissue caused local decreases in density of nervous structures of all sizes; this was in contrast to the effect seen upon tumor placement in unsutured tissue in which tumor cells caused local nerve cluster formation. A transition toward a more tortuous phenotype and the presence of small nerve clusters was also broadly seen in sutured tissue with tumor cells. The appearance of nerve clusters in these two tissue states—unsutured + tumor and sutured + tumor—was striking given our previous characterization of this phenotype as a feature restricted to wound-recovered tissue (sutures placed to induce inflammation, then removed to stimulate healing).

Simultaneous Inflammation Prolongs Tumor Residency

We unexpectedly found that placement of tumor cells and sutures in the cornea on the same day prolonged tumor residency. This was an incidental finding of several preliminary experiments with B16 melanoma cells and was confirmed using both the E0771 medullary breast carcinoma cell line and a KPC pancreatic adenocarcinoma cell line. The majority of tumor cells injected into the unsutured mouse cornea were no longer visible by live imaging or epifluorescence microscopy of fixed tissue after several days. Pre-inflammation of tissue by placement of sutures three days before tumor injection resulted in a similar loss of tumor signal, although some cells remained near sutures and at the injection site. In striking contrast to these two conditions, signal from tumor cells injected into the cornea on the same day as suturing was visible for several days by live imaging as well as in fixed whole mount corneas.

We considered the possibility that in the same-day sutured condition, lymphatic vessel sprouts (and sprouting blood vessels) would not have had sufficient time to extend and mature as may be required for tumor cell trafficking away from the injection site. In our live imaging

experiments we documented the simultaneous presence of “typical” large newly-synthesized lymphatic vessels and disorganized incomplete atypical lymphatic structures in pre-sutured tissue. The presence of larger suture-induced lymphatics in pre-sutured tissue may have provided a means of migration out of the cornea for tumor cells in the pre-sutured condition that was not yet available to tumor cells in the same-day sutured group. While this may be true, we also saw loss of tumor cell signal in the unsutured condition. We showed that injection of tumor cells is sufficient to induce lymphangiogenesis in unsutured tissue, but it seems that the low level of lymphangiogenic sprouting in response to tumor cells in the early days of implantation would not be sufficient to quickly clear a large injected tumor burden. If this were the case, it would also be reasonable to assume a similar tumor-lymphangiogenesis effect in same-day sutured tissue. Taken together, this suggested that another mechanism must explain the extended residency of cells in the same-day group.

We also considered attack of tumor cells by phagocytic immune cells as an explanation for loss of tumor signal. Again, however, the similarity in tumor behavior between the unsutured and pre-sutured conditions was confounding. Infiltrating immune cells would presumably travel through lymphatic and/or blood vasculature to reach the tumor site and enter the corneal parenchyma. This could explain the difference between the pre-sutured and same-day sutured conditions, but not the unsutured group. Relative immune privilege is a well-described characteristic of the unmanipulated cornea. Additionally, were phagocytic immune cells responsible for clearing of tumor cells, we would still expect to see CFSE signal in these cells.

While the answer to this question remains unclear, we suggest that aspects of the earliest events of inflammation predispose tumor cell residence in the cornea. These may, in

fact, be considered either positive or negative regulators of tumor cell behavior, depending on point of view. Inflammatory factors in the tissue may, for example, down regulate cell migration and proliferation causing them to stay resident at their point of injection with little diminishing of signal. Contrariwise, factors may promote cell survival in this condition while cells without the benefit of a new inflammatory reaction undergo cell death and signal diffuses away. It is also possible that two different mechanisms govern loss of cell signal in the unsutured and pre-sutured conditions. Dissecting these nuances will require more careful study, however, these results demonstrate the importance of inflammation in the establishment and progression of a tumor.

Additional Uses for Lyve1CreERT2^{tdT} Live Imaging Platform

The Lyve1CreERT2^{tdT} cornea and pinna live imaging platforms we have described here could be used in the future to study many other aspects of basic lymphatic biology and tumor-lymphatic interactions. Some key questions to be addressed might include: How does a tumor cell intravasate into a lymphatic vessel? Do specific features of lymphatic vessel architecture or physical properties of tumor cells affect this process? How do circulating tumor cells in lymphatic vessels pause, extravasate, and enter tissues to form metastases? Do these processes differ from mechanisms used by leukocytes? Might putative druggable targets be identified that regulate physical lymphatic remodeling? Do other characteristics of organ-specific microenvironments affect the biology of metastasis for tumor cells that arise there? Inflamed corneal lymphatic vessels may be activated to facilitate immune cell trafficking. Do these activation properties also equip lymphatic vessels to support tumor cell trafficking, or are they not required by tumor cells? What role do Lyve-1-expressing macrophages play in lymphatic vessel remodeling and interactions with tumor cells? Does “flipping the switch” from inflammation to wound recovery in the tumor microenvironment affect tumor cell proliferation

and metastasis? How does the presence of specific cytokines affect tumor-lymphatic interactions? What molecular features distinguish tumor- and suture-associated lymphatic vessels? Intravascular tumor cells from those that remain resident in tissue? Can these features be targeted for clinical imaging?

CHAPTER III. Pancreatic Cancer Cachexia in Rapid Autopsy Muscle Tissue Samples

Introduction

Pancreatic ductal adenocarcinoma patients are often plagued with the paraneoplastic syndrome cachexia. This progressive disease has been linked to low-grade systemic inflammation and as such has broad effects on several aspects of patient quality-of-life. Cachexia results in unintentional weight loss, loss of muscle mass, weakness, and increased frailty. Cancer-associated cachexia may cause reduced tolerance for chemotherapy and has been implicated in decreased overall survival. Despite the importance of this disease for outcomes and quality-of-life, little is known about the effects of cachexia on skeletal muscle of PDAC patients. The KPC mouse model of PDAC, designed to develop spontaneous pancreas tumors, does show a cachexia phenotype (Hingorani et al., 2005), but while animal models can provide some insight into human disease, these artificial systems often fall short in their attempts to mirror the intricacy of the human condition.

We studied PDAC-associated cachexia in skeletal muscle samples taken from patients within hours of death at rapid autopsy and normal control samples from cancer-free donors. We isolated total muscular RNA and examined the expression levels of six genes reported to be important in cachexia, involved in muscle atrophy or wasting, or activated in exercise. The genes we studied were: Fibroblast activation protein alpha (*FAP*), follistatin (*FST*), calcium/calmodulin-dependent protein kinase type II subunit beta (*CAMK2B*), tyrosine kinase with immunoglobulin-like and EGF-like domains 1 (*TIE1*), tripartite motif containing 63 (*TRIM63*), and F-box protein 32 (*FBXO32*).

FAP-α expression has been reported in cancer-associated fibroblasts (CAFs) and stromal cells of other tissues including skeletal muscle. Cachectic KPC mice displayed decreased skeletal muscle mass and reduced levels of *Fap* and *Fst* gene expression (Roberts et al., 2013). We

expected to find similar decreases in *FAP* and *FST* expression levels in our human cachexia samples. *CAMK2B* and *TIE1* were identified as possible biomarkers of cancer-associated cachexia in a study of upper gastrointestinal cancer (including pancreatic) patient muscle samples (Stephens et al., 2010). We expected to see increased expression of these exercise-activated genes in cachexia patients over non-cachectic or normal controls. TRIM63 and FBXO32 are E3 ubiquitin ligases important in the ubiquitin-proteasome pathway of protein degradation. Studies in rat models of muscle atrophy first described the importance of the E3 ubiquitin ligase family of proteins in muscle disease. Animal homologs of human TRIM63 and FBXO32 were consistently upregulated across models; loss of either of these enzymes resulted in resistance to muscle wasting (Bodine et al., 2001). We expected to detect increased levels of *TRIM63* and *FBXO32* in cachectic PDAC patients compared to non-cachectic patients or normal controls.

Materials and Methods

Rapid Autopsy Procedures

Local patients diagnosed with pancreatic cancer voluntarily enrolled in a Rapid Autopsy Pancreas (RAP) program. Trunk-only autopsies were performed within approximately three hours of death by a pathologist, pathology resident, and research volunteer sample collection team at the University of Nebraska Medical Center. All abdominal organs were removed and analyzed for presence of pancreatic adenocarcinoma grossly and by microscopic histology. Organs typically examined and collected included: pancreas, spleen, liver, stomach, gall bladder, adrenal gland, kidney, small bowel, large bowel, rectum, prostate, diaphragm, lung, heart apex, omentum, nerve, lymph node, and skeletal muscle. Organs were sliced into approximately 0.75" thick sections and each section was macrodissected and annotated with regard to disease presentation according to the following pathologic designations: primary tumor (pancreas only), metastatic lesion, margin of primary or metastatic tumor and uninvolved parenchyma, or uninvolved parenchyma. Dissected specimens were flash frozen in liquid nitrogen, transferred to dry ice, and stored long-term at -80°C. Skeletal muscle was customarily collected from psoas or pectoral muscle.

Skeletal Muscle Specimens from Normal Patients

Normal control human skeletal muscle samples were obtained from the Comparative Human Tissue Network or the National Disease Research Interchange. Only fresh frozen muscle from donors without a previous cancer diagnosis was accepted. Muscle samples were received after shipment on dry ice and stored at -80°C. Demographic information for PDAC patients and normal donors are listed in Table 1.

Patient Characteristics

Table 1. Muscle Donor Characteristics		
	PDAC Patients (n=58)	Normal Controls (n=15)
Mean Age	68.03	54.73
Sex (M/F)	38/20	14/1
Race		
White	57	14
Hispanic	0	1
Black	1	0

Designation of Cachexia Status

Cachexia status (Yes or No) was assigned at autopsy by a pathologist at the University of Nebraska Medical Center in Omaha, NE. These two groups were further stratified into the following categories based on weight loss, BMI, and other clinical or pathology notes: yes, severe cachexia (S); yes, weight loss (YWL); yes, normal or overweight BMI (YN); no, weight loss (NWL); no, normal or overweight BMI (NN); and no, obese (NOB). Patients included in group S were of normal or underweight BMI and presented with significant weight loss of greater than 14 kg, or were of normal or underweight BMI and had a specific pathology note such as "severe cachexia" or "emaciated; presented with extreme weakness". YWL inclusion criteria were normal or overweight BMI at autopsy and weight loss of greater than 3 kg. YN patients were of normal or overweight BMI and did not have weight loss. The NWL group was composed of patients who were not cachectic and had weight loss of greater than 3 kg. NN patients did not have cachexia and were of normal or overweight BMI. Patients in the NOB category were not cachectic and had a BMI in the obese range at autopsy.

Pancreatic Cancer Collaborative Registry

The Pancreatic Cancer Collaborative Registry is a database maintained by the University of Nebraska Medical Center in Omaha, NE. This database contains demographic data about pancreatic cancer patients as well as treatment histories, information about family members, and lifestyle data such as alcohol and tobacco use. We had access to data from the first 50 rapid autopsy patients, or 74% of the population included in our other analyses.

RNA Isolation Procedure, Reagents, and Quality Control

Total RNA was isolated from muscle specimens of approximately 0.3 g in mass according to our modified TRIzol extraction protocol optimized for skeletal muscle[4]. RNA concentration and presence of contaminants was tested using a NanoDrop 1000 spectrophotometer and ND 1000 V3.6.0 software (ThermoFisher Scientific). RNA quality was tested by Fragment Analyzer (Advanced Analytical Technologies, Inc., Ames, IA) or BioAnalyzer (Agilent Technologies, Inc., Santa Clara, CA). Data was analyzed using the ProSize 2 software (Advanced Analytical Technologies, Inc., Ames, IA) or 2100 Expert software (Agilent Technologies, Inc., Santa Clara, CA). RNA quality value of 6.0 was set as the minimum threshold for gene expression analysis. The average quality score for our normal control sample set was 6.8 and that of our experimental RAP sample set was 7.6.

cDNA Library Construction and qRT-PCR

cDNA libraries were constructed using the Verso cDNA kit (Cat. #AB1453A/B, ThermoFisher Scientific) according to the manufacturer's instructions. An additional digestion with RNase H (Cat. #18021071, ThermoFisher) to remove RNA-DNA duplexes was performed at 37°C for 20 minutes following cDNA synthesis. cDNA was stored at -20°C.

Gene expression was quantified by qRT-PCR using 20X TaqMan Gene Expression Assay hydrolysis probes (Applied Biosystems) as shown in Table 2 at 1X (900 nM) in each 20 µL reaction. Reactions were performed in triplicate using 2X Universal PCR Master Mix (Applied Biosystems) and analyzed on a BioRad C1000 Thermal Cycler CFX96 instrument (Bio-Rad Laboratories, Inc., Hercules, CA). Automated reaction conditions were as follows: Initial hold

[4] Full protocol provided in Appendix A.

50°C 2 minutes; Initial denaturation 95°C 10 minutes; 40 cycles of denaturation (95°C 15 seconds), annealing and extension (60°C 1 minute); Final hold 4°C.

Data Analysis and Statistics

Gene expression data were analyzed using the standard curve method. Plasmids containing genes of interest were purchased from Open Biosystems and DNA isolated by QIAprep Miniprep (Qiagen) according to the manufacturer's instructions. Standard curves were generated by serial ten-fold dilution of plasmid DNA and amplification by qRT-PCR using TaqMan Gene Expression Assays. R^2 values and amplification efficiencies were within accepted ranges. Standard curves were used to calculate experimental copies per reaction. These values were normalized to housekeeping gene *TBP* expression levels. Standard curve regression equations and other calculations are shown in Table 2.

Data were analyzed using statistical software GraphPad Prism 5 (GraphPad Software, Inc., La Jolla, CA). Groups were compared using 1 way ANOVA and Tukey's Multiple Comparison Test post-hoc. (* indicates $p < 0.05$. ** indicates $p < 0.01$. *** indicates $p < 0.001$.) Pearson correlation coefficient and associated *p* values were calculated for the Pancreatic Cancer Clinical Registry data correlative analysis using this software.

Table 2. TaqMan Gene Expression Assays and Plasmid Standard Curve Analyses

Gene Symbol	FAP	FST	CAMK2B	TBP	FBXO32	TRIM63	TIE1
Gene Name	Fibroblast activation protein alpha	Follistatin	Calcium/ calmodulin-dependent protein kinase type II subunit beta	TATA box binding protein	F-box protein 32	Tripartite motif containing 63, E3 ubiquitin protein ligase	Tyrosine kinase with immuno-globulin-like and EGF-like domains 1
TaqMan Gene Expression Assay	Hs00990806_m1	Hs00246256_m1	Hs00365799_m1	Hs00427621_m1	Hs01041408_m1	Hs00261590_m1	Hs00178500_m1
Vector	pDNR-LIB	pOTB7	pOTB7	pCMV-SPORT6	pBluescriptR	pINCY	pCMV-SPORT6
Open Biosystems Cat.#	MHS1011-7509787	MHS1011-60751	MHS4771-99610862	MHS1010-980516668	MHS1010-7295752	IHS1380-97433020	MHS1010-7508594
Plasmid Size (bp)	4161	1815	1815	4396	2990	4126	4396
Insert	BC026250	BC004107	BC019070	BC110341	BC024030	LIFESEQ 4042617	BC038239
Insert Size (bp)	2648	1326	1896	1887	1212	1664	3960
Mass of Plasmid + Insert (g/Copy)	7.46E-18	3.44E-18	4.07E-18	6.89E-18	4.61E-18	6.35E-18	9.16E-18
[Plasmid + Insert] (g/µL)	4.68E-08	2.95E-07	4.03E-07	2.76E-07	1.63E-07	4.19E-08	4.77E-07
Copies/µL	6.27E+09	8.56E+10	9.90E+10	4.00E+10	3.53E+10	6.60E+09	5.20E+10
Standard Curve Regression (10-Fold Dilutions)	y = -3.1370x + 39.764	y = -3.3203x + 40.540	y = -3.6087x + 42.277	y = -3.4411x + 40.908	y = -3.4374x + 41.074	y = -3.5086x + 42.166	y = -3.1577x + 34.928
R^2	0.999	0.989	0.993	0.994	0.999	0.999	0.996
Amplifi-cation Coefficient	2.08	2.00	1.89	1.95	1.95	1.93	2.07
% Efficiency	108.34	100.07	89.28	95.26	95.40	92.76	107.34

Results

Differences in Gene Expression in Pancreatic Cancer Patients vs. Normal Controls

We found significant differences in gene expression levels between PDAC patient skeletal muscle samples regardless of cachexia status and normal control skeletal muscle for all genes analyzed except *FST* (Figure 26). *FAP* expression was lower in cancer patients compared to normal controls. The same was true of *CAMK2B* expression. *TIE1* levels were also decreased in PDAC patients. *TRIM63* was expressed at a higher level in both cachectic and non-cachectic PDAC patients compared to normal controls. *FBXO32* gene expression was also higher in cancer patients than normal donors.

Differences in Gene Expression in Cachectic vs. Non-Cachectic Pancreatic Cancer Patients

There were no significant differences in the expression of any of the genes we analyzed in skeletal muscle samples of cachectic and non-cachectic PDAC patients based on the original Yes/No cachexia status designations. We decided to further stratify patients into subgroups based on additional clinical and pathology notes, weight loss history, and BMI at time of death. Cachectic and non-cachectic patients were reclassified into the following six subgroups: yes, severe cachexia (S); yes, weight loss (YWL); yes, normal or overweight BMI (YN); no, weight loss (NWL); no, normal or overweight BMI (NN); and no, obese (NOB). Specific inclusion criteria for each group are described above.

Subgroup Gene Expression Analysis

There were no significant differences in gene expression between PDAC patient subgroups for any of the genes analyzed. Gene expression in some subdivided groups was significantly different than normal controls. YWL and NWL groups had lower expression of *FAP* than controls, but the other subgroups were no longer significantly different (Figure 27). As

with the Yes/No analysis, no subgroups showed differential *FST* expression compared to normal controls (Figure 28). Expression levels of *CAMK2B* (Figure 29) and *TIE1* (Figure 30) were significantly lower in all subgroups compared to control levels. For *TRIM63*, subgroups S, YN, NN, and NOB displayed higher expression than controls (Figure 31). S, NWL, NN, and NOB samples had higher levels of *FBXO32* than normal control muscle samples (Figure 32).

PDAC Cachexia and Alcohol Use, Tobacco Use, and Diabetes Status

We analyzed Pancreatic Cancer Collaborative Registry data on alcohol use, tobacco use, and diabetes mellitus status of the majority of the PDAC patients included in this study (Table 3). We found no correlation between alcohol use, tobacco use, or diabetes status with cachexia status in our patient population. There was also no correlation of any of these variables with one another.

Figure 26. Cachexia gene expression normalized to TBP. Gene expression of putative cachexia-associated genes in skeletal muscle samples from cachectic and non-cachectic pancreatic ductal adenocarcinoma patients and normal donor controls that had no history of cancer. Data normalized to TBP. (** indicates $p < 0.01$. *** indicates $p < 0.001$.)

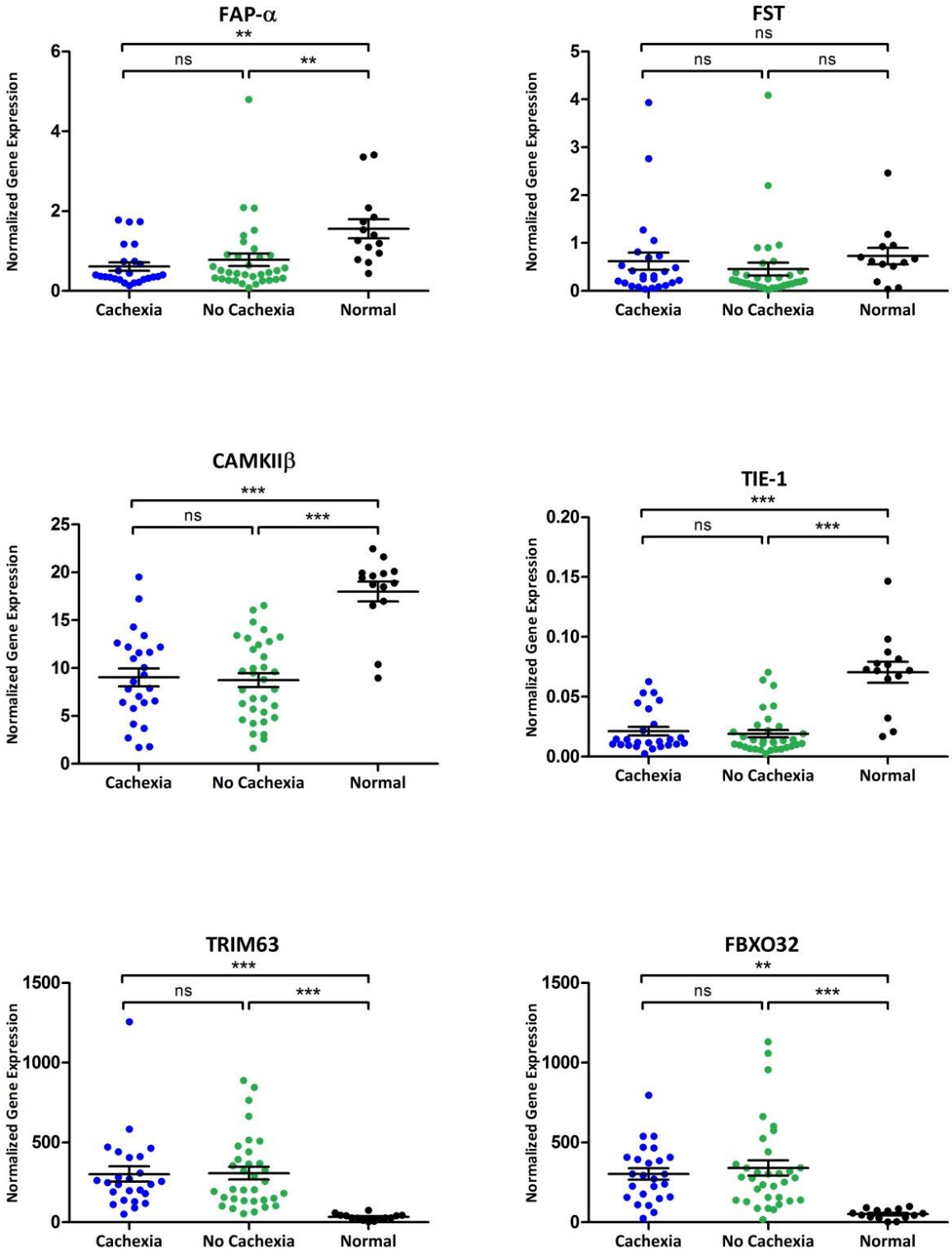
FAP-α
**
ns
**
Normalized Gene Expression
6
4
2
0
Cachexia
No Cachexia
Normal
FST
ns
ns
ns
Normalized Gene Expression
5
4
3
2
1
0
Cachexia
No Cachexia
Normal
CAMKIIβ
***
ns
***
Normalized Gene Expression
25
20
15
10
5
0
Cachexia
No Cachexia
Normal
TIE-1
***
ns
***
Normalized Gene Expression
0.20
0.15
0.10
0.05
0.00
Cachexia
No Cachexia
Normal
TRIM63
***
ns
***
Normalized Gene Expression
1500
1000
500
0
Cachexia
No Cachexia
Normal
FBXO32
**
ns
***
Normalized Gene Expression
1500
1000
500
0
Cachexia
No Cachexia
Normal

Figure 26

Figure 27. FAP-α gene expression based on modified cachexia status. Gene expression in skeletal muscle samples from cachectic and non-cachectic pancreatic ductal adenocarcinoma patients and normal donor controls that had no history of cancer. Data normalized to *TBP*.
(* indicates $p < 0.05$. ** indicates $p < 0.01$.)

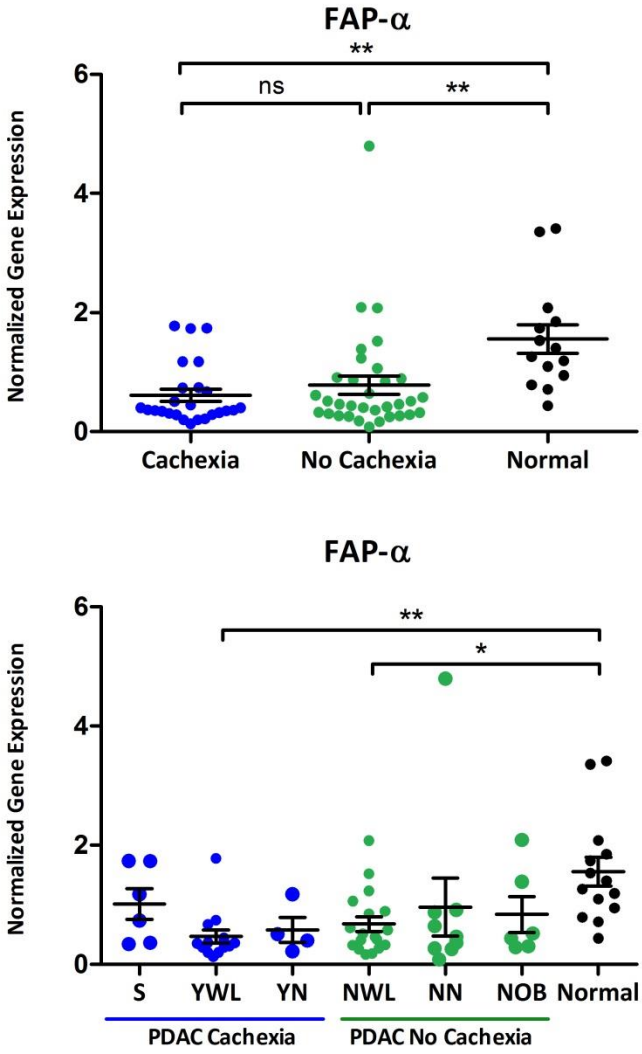
FAP-α
**
ns
**
Normalized Gene Expression
6
4
2
0
Cachexia
No Cachexia
Normal
FAP-α
**
*
Normalized Gene Expression
6
4
2
0
S
YWL
YN
NWL
NN
NOB
Normal
PDAC Cachexia
PDAC No Cachexia

Figure 27

Figure 28. FST gene expression based on modified cachexia status. Gene expression in skeletal muscle samples from cachectic and non-cachectic pancreatic ductal adenocarcinoma patients and normal donor controls that had no history of cancer. Data normalized to *TBP*. (Ns = not significant.) There was no significant difference between any of the groups in the *lower panel*.

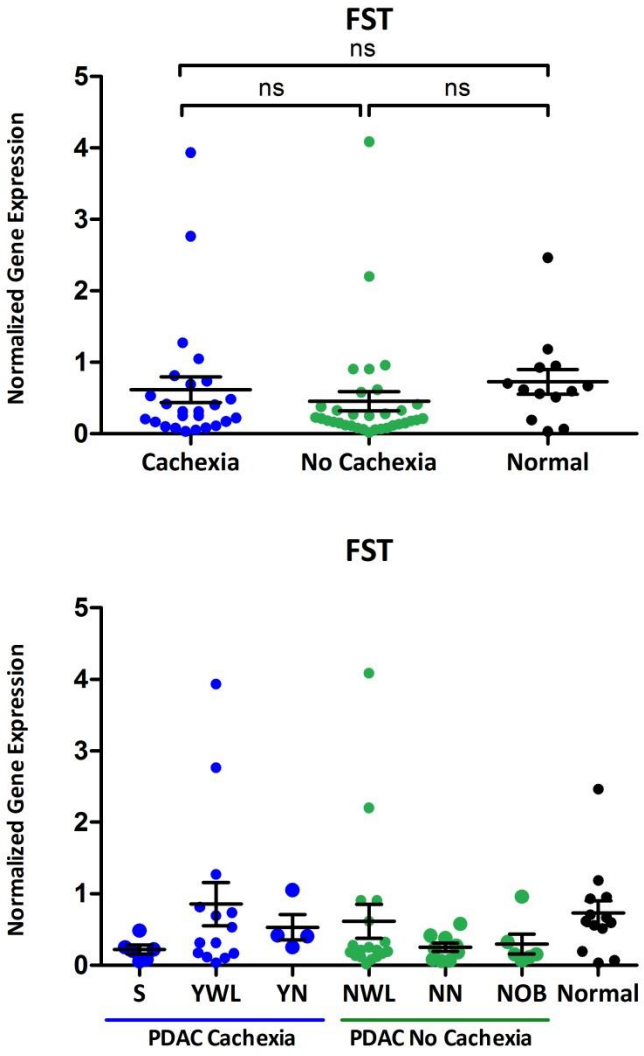
FST
ns
ns
ns
Normalized Gene Expression
5
4
3
2
1
0
Cachexia
No Cachexia
Normal
FST
Normalized Gene Expression
5
4
3
2
1
0
S
YWL
YN
NWL
NN
NOB
Normal
PDAC Cachexia
PDAC No Cachexia

Figure 28

Figure 29. CAMKIIβ gene expression based on modified cachexia status. Gene expression in skeletal muscle samples from cachectic and non-cachectic pancreatic ductal adenocarcinoma patients and normal donor controls that had no history of cancer. Data normalized to *TBP*.
(* indicates $p < 0.05$. ** indicates $p < 0.01$. *** indicates $p < 0.001$.)

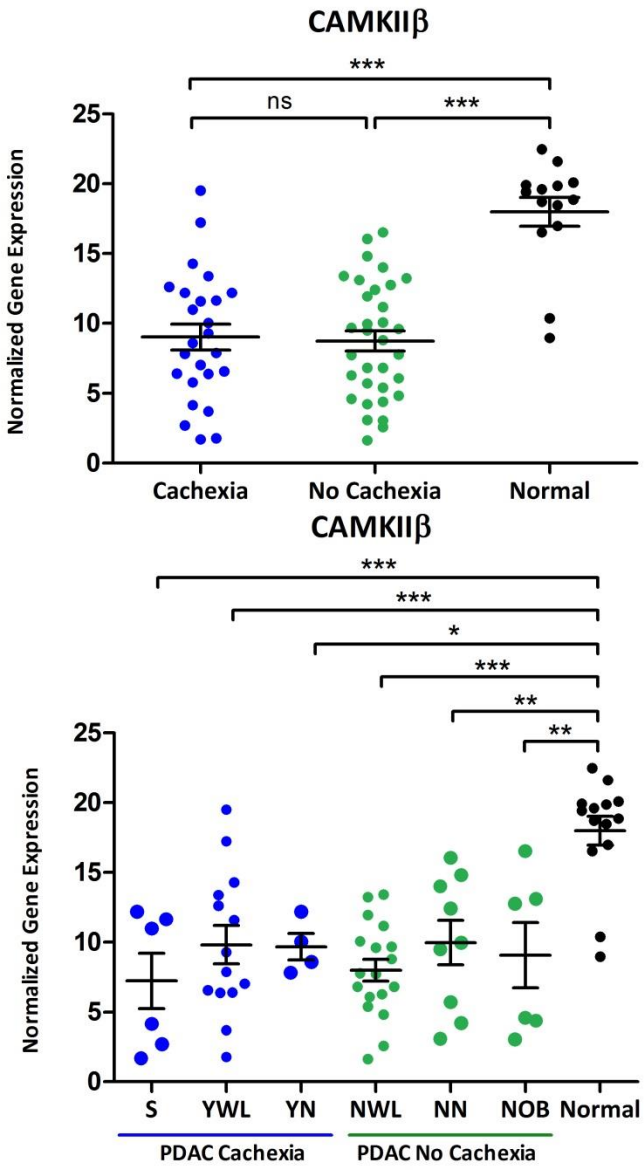
CAMKIIβ
***
ns
***
Normalized Gene Expression
25
20
15
10
5
0
Cachexia
No Cachexia
Normal
CAMKIIβ
***
***
*
***
**
**
Normalized Gene Expression
25
20
15
10
5
0
S
YWL
YN
NWL
NN
NOB
Normal
PDAC Cachexia
PDAC No Cachexia

Figure 29

Figure 30. TIE-1 gene expression based on modified cachexia status. Gene expression in skeletal muscle samples from cachectic and non-cachectic pancreatic ductal adenocarcinoma patients and normal donor controls that had no history of cancer. Data normalized to *TBP*.
(* indicates $p < 0.05$. *** indicates $p < 0.001$.)

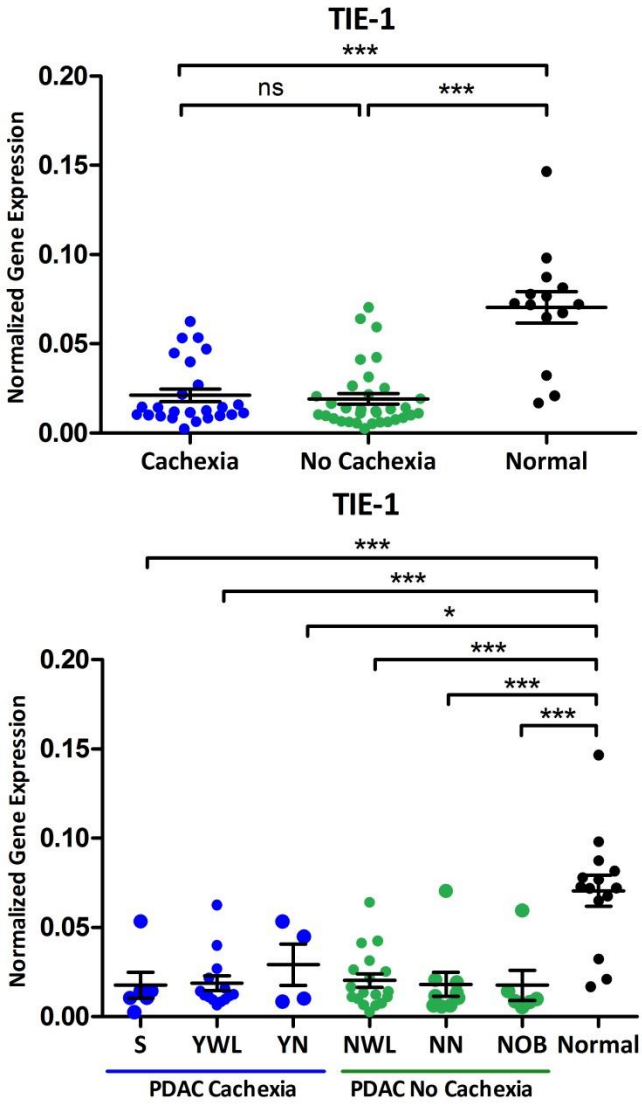
TIE-1
***
ns
***
0.20
0.15
0.10
0.05
0.00
Normalized Gene Expression
Cachexia
No Cachexia
Normal
TIE-1
***
***
*
***
***
***
0.20
0.15
0.10
0.05
0.00
Normalized Gene Expression
S
YWL
YN
NWL
NN
NOB
Normal
PDAC Cachexia
PDAC No Cachexia

Figure 30

Figure 31. TRIM63 gene expression based on modified cachexia status. Gene expression in skeletal muscle samples from cachectic and non-cachectic pancreatic ductal adenocarcinoma patients and normal donor controls that had no history of cancer. Data normalized to *TBP*.
(* indicates $p < 0.05$. ** indicates $p < 0.01$. *** indicates $p < 0.001$.)

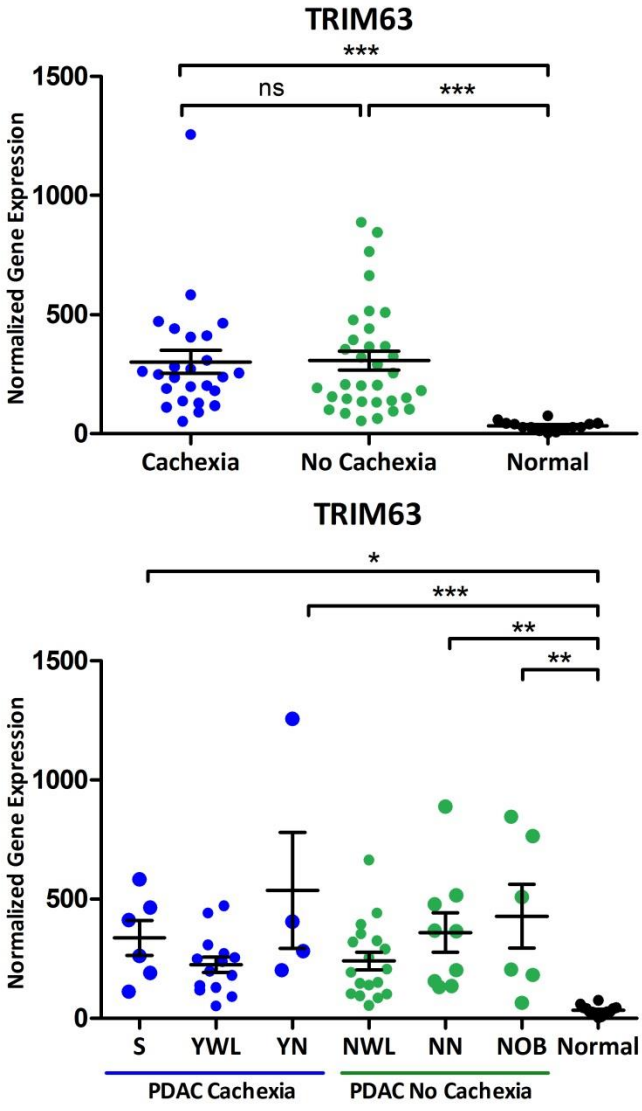
TRIM63
***
ns
***
1500
1000
500
0
Normalized Gene Expression
Cachexia
No Cachexia
Normal
TRIM63
*
***
**
**
1500
1000
500
0
Normalized Gene Expression
S
YWL
YN
NWL
NN
NOB
Normal
PDAC Cachexia
PDAC No Cachexia

Figure 31

Figure 32. FBXO32 gene expression based on modified cachexia status. Gene expression in skeletal muscle samples from cachectic and non-cachectic pancreatic ductal adenocarcinoma patients and normal donor controls that had no history of cancer. Data normalized to *TBP*.
(* indicates $p < 0.05$. ** indicates $p < 0.01$. *** indicates $p < 0.001$.)

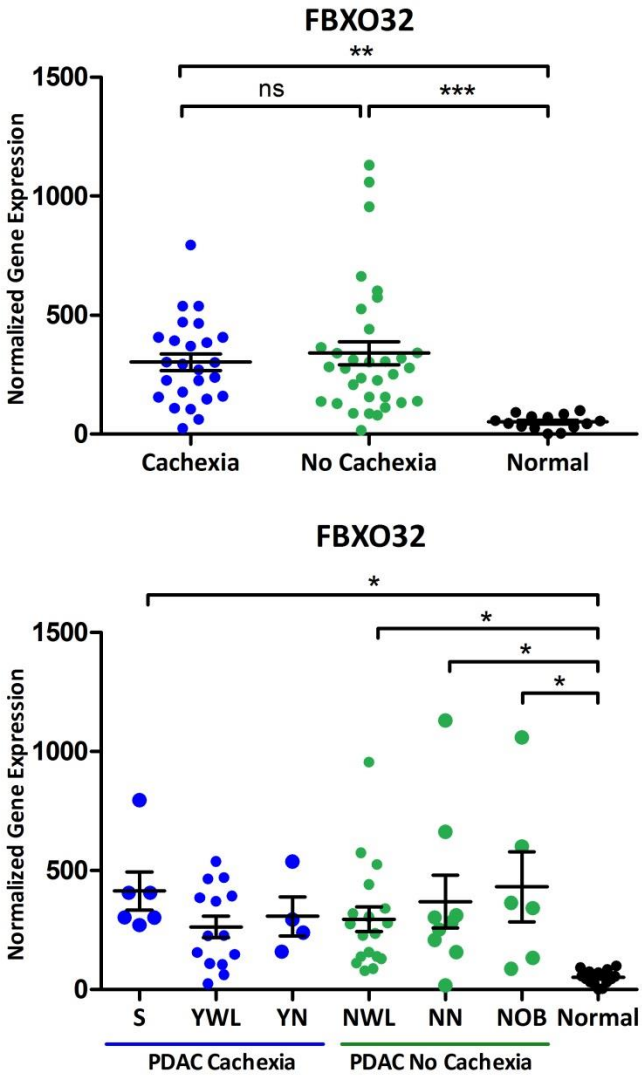
FBXO32
**
ns
***
1500
1000
500
0
Normalized Gene Expression
Cachexia
No Cachexia
Normal
FBXO32
*
*
*
*
1500
1000
500
0
Normalized Gene Expression
S
YWL
YN
NWL
NN
NOB
Normal
PDAC Cachexia
PDAC No Cachexia

Figure 32

Table 3. Cachexia Status Does Not Correlate with Alcohol or Tobacco Use or Diabetes Status				
Correlation Coefficient, *r*				
	Cachexia Status	**Alcohol Use**	**Tobacco Use**	**Diabetes Status**
Cachexia Status		0.340	0.181	-0.002
Alcohol Use			0.248	0.053
Tobacco Use				-0.015
Diabetes Status				
***P* values**				
	Cachexia Status	**Alcohol Use**	**Tobacco Use**	**Diabetes Status**
Cachexia Status		0.040	0.292	0.990
Alcohol Use			0.204	0.757
Tobacco Use				0.929
Diabetes Status				

Discussion

Previous Studies of Cachexia Gene Expression

We studied expression levels of genes previously reported to have a role in cachexia, muscle wasting, or exercise using skeletal muscle samples taken at rapid autopsy from pancreatic ductal adenocarcinoma patients and normal control muscle samples. We found upregulation of *FAP*, *TRIM63*, and *FBXO32* in PDAC samples irrespective of cachexia status compared to controls. We found no significant difference in *FST* expression in PDAC samples with and without cachexia and compared to normal controls. *CAMK2B* and *TIE1* were downregulated in cachectic and non-cachectic PDAC skeletal muscle compared to controls. We found no significant differences in gene expression between PDAC patients with and without cachexia. Cancer cachexia is a progressive disease; further stratification of PDAC patients according to severity of cachexia, however, did not reveal additional differences in gene expression among cachectic and non-cachectic subgroups.

Several studies have examined the role of FAP-α in cancer-associated cachexia and its relationship to FST, TRIM63, and FBXO32. Depletion of FAP^+ fibroblasts by genetic ablation or chimeric antigen receptor (CAR) T cell targeting caused muscle wasting and cachexia (Roberts et al., 2013; Tran et al., 2013). KPC mice bearing spontaneous PDAC and mice with C26 colon tumors developed cancer-associated cachexia and concomitant decreases in FAP-expressing fibroblasts (Roberts et al., 2013). These cells are the major source of FST, and their loss resulted in decreased FST levels. Decreased FST was accompanied by concomitant increases in atrogin1[5] and MuRF-1 (muscle RING finger protein-1) expression in cachectic mice only (Roberts et al.,

[5] As much of the previous work in cancer cachexia was done in mouse models, alternative nomenclature is often used in referring to genes. Atrogin-1 and MAFbx are alternative names for FBXO32. MuRF-1 is another name for TRIM63.

2013). Our findings of increased *FAP* expression and no change in *FST* levels in stand in contrast to these mouse data. We also found parallels in gene expression of PDAC patient skeletal muscle samples regardless of cachexia status compared to cancer-free controls, while in the KPC mouse study, littermates and non-cachectic KPC gene expression profiles were consistently similar while cachectic KPC samples displayed a different pattern of expression. A study of gastric cancer patients also found no change in *FST* expression across patient and control skeletal muscle samples. That group, however, did not find increased ubiquitin ligase pathway genes; they reported no significant difference in levels of MuRF1 and atrogin-1 between cancer patient samples and controls (D'Orlando et al., 2014). A study of several rat models of muscle atrophy reported increased expression of MuRF1 and muscle atrophy F-box (MAFbx) (Bodine et al., 2001). A study of human upper gastrointestinal cancers, including PDAC, found no increases in ubiquitin ligase pathway genes *TRIM63* and *FBXO32* or exercise-activated genes *CAMK2B* and *TIE1* expression, but these genes were upregulated in mouse models (Gallagher et al., 2012). Another study of human tissue found correlations between weight loss and the levels of *CAMK2B* and *TIE1*, but not MuRF1 or MAFbx (Stephens et al., 2010). These discrepancies illustrate the limitations of animal models in recapitulating human disease and heterogeneity among cancer types and in human patient populations.

Study Limitations

Our study had several limitations. First, we had a small sample size. Nearly all of our patients and controls were white, and the age and gender distributions of normal tissue donors were different than those in the PDAC population. Second, normal control samples in many cases were not derived from disease-free donors. Tissue was excluded in the event of patient history of cancer, but many of the samples were taken from diseased limbs. Co-morbidities associated with our control samples included gangrene, ischemia, vascular disease, and

osteomyelitis. Finally, we profiled only gene expression. Many levels of regulation lie between message levels and functional output of a specific protein.

The universal differences in gene expression between RAP PDAC skeletal muscle samples and normal control samples raise the question of whether a fundamental difference in sample sets (such as tissue handling conditions) could be responsible rather than a biological effect. There are several reasons why we do not believe that to be the case. We used standard nucleic acid spectrophotometry and fragmentation analysis procedures to confirm RNA quality of each sample. The average RNA quality score for the RAP cohort was 7.6, and that of the normal control group was 6.8, both of which were above the established lower threshold value of 6.0 for quantitative gene expression analysis. Samples for which minimum quality thresholds could not be achieved after two extraction attempts were excluded from our study. We also confirmed equal expression of housekeeping gene *TBP* across groups. The mean *TBP* threshold cycle in the RAP group was 26.27, and that of the normal control group was 27.28; two outliers in the normal group with threshold cycle values of 31.43 and 32.65, respectively, were responsible for this shift, and their exclusion resulted in a normal group average of 26.48. Additionally, the bidirectional nature of the differences in experimental gene expression did not support the notion that one sample set was universally of poorer quality than the other. Three of the genes studied were more highly expressed in normal control samples compared to RAP samples, one gene's expression was not significantly different between groups, and two genes were present at lower levels in normal samples. If the levels of all genes were lower in normal controls than RAP samples, we might conclude that the difference in RNA quality between the two cohorts (7.6 vs. 6.8) accounted for this difference, but that was not the case here.

Additional Studies with RAP Tissues Based on Cachexia Status

Despite the relatively small number of patients who have been studied in the PDAC rapid autopsy program (nearly 100), the tissue samples in our repository are some of the most comprehensive and well-annotated in the world. We routinely collect primary pancreas tumor, metastatic lesions from all involved organs, tumor margins, adjacent normal organ parenchyma, and other sites not directly infiltrated by carcinoma but that may nevertheless be affected by the systemic consequences of end-stage PDAC, such as skeletal muscle. Clinical records are also available for these patients. Future studies extending the work done here in pancreatic cancer cachexia could include evaluation of circulating inflammatory factors in patient serum samples, analysis of cardiac muscle for cachexia-associated pathology, studies of how the various pancreatic cancer treatment regimens affect cancer cachexia and vice versa, and examination of how cachexia impacts disease progression and overall survival. Patient CT scans routinely performed in PDAC diagnosis and staging could also be used to track development of cachexia over time as it relates to disease progression and to include a quantifiable metric (lumbar skeletal muscle index) in the process of assigning cachexia status (Martin et al., 2013b; Tan et al., 2009). Finally, although diabetes status did not correlate with cachexia in this analysis, evidence suggests a connection between diabetes mellitus and cachexia (Asp et al., 2010; Honors and Kinzig, 2012; Pannala et al., 2009). Further studies with these unique tissues could more carefully dissect the interplay of insulin resistance, glucose neurotoxicity, pancreatic tumor progression, cachexia, and perineural invasion.

DISCUSSION AND FUTURE DIRECTIONS[6]

[6] Portions of this chapter have been published under the following references: (Fink et al., 2014a), (Fink et al., 2015a)

Through the exploration of three aspects of inflammation—nonmalignant- and tumor-associated neurolymphatic remodeling and crosstalk and cancer-associated cachexia—work presented in this dissertation has: discovered a novel role of NGF in lymphatic vessel regulation in inflammation and wound recovery; identified distinct neurolymphatic architecture signatures present in inflammatory, wound-recovered, and tumor-associated microenvironments; characterized distinct spatiotemporal tumor cell behaviors dependent on timing of establishment of tissue microenvironmental inflammatory conditions; and challenged some previous findings regarding expression of muscle atrophy and exercise-associated genes in the paraneoplastic inflammatory syndrome PDAC cancer cachexia.

NGF and Neurolymphatic Remodeling

We first studied the resolution of two cardinal signs of non-malignant inflammation—pain and swelling—by investigating molecular mechanisms that regulate neural and lymphatic vessel remodeling during the resolution of corneal inflammation. A mouse model of corneal inflammation and wound recovery was developed to study this process *in vivo*. We showed for the first time activity of NGF, the prototypical nerve survival and guidance molecule, on the lymphatic endothelium. NGF influenced the two major lymphatic vessel remodeling events that accompany shifts in microenvironmental inflammatory status—lymphangiogenesis and lymphatic vessel regression. The corneal micropocket assay revealed that NGF-laden pellets stimulated lymphangiogenesis and increased protein levels of VEGF-C. Adult human dermal lymphatic endothelial cells did not express canonical NGF receptors TrkA and $p75^{NTR}$ or activate downstream MAPK- or Akt-pathway effectors in the presence of NGF, although NGF treatment increased their migratory and tubulogenesis capacities *in vitro*. Blockade of the VEGFR-2/3 signaling pathway ablated NGF-mediated lymphangiogenesis *in vivo*. Administration of NGF also increased pain sensation and inhibited neural remodeling and lymphatic vessel regression

processes during wound recovery. These findings suggested a hierarchical relationship with NGF functioning upstream of the VEGF family members, particularly VEGF-C, to stimulate lymphangiogenesis. Taken together, these studies showed that NGF stimulates lymphangiogenesis and that NGF may act as a pathogenic factor that negatively regulates the normal neural and lymphatic vascular remodeling events that accompany wound recovery.

Microenvironment-Specific Neurolymphatic Architecture Signatures: Implications for Therapy

A major theme throughout this work has been the identification and characterization of novel neurolymphatic remodeling signatures present under distinct microenvironmental conditions. We studied neurolymphatic remodeling in two mouse organ systems with distinct nerve and lymphatic architectures in homeostasis—cornea and pinna. The cornea is one of the most densely innervated tissues in the body but is devoid of lymphatic vessels in homeostasis. Each skin leaflet of the pinna houses separate uniformly-distributed nerve and lymphatic vessel plexuses under normal physiological conditions. We used these complementary systems to study neurolymphatic remodeling in non-malignant and tumor-associated inflammation and the resolution of inflammation, or wound recovery. Suture or tumor stimuli were used to induce inflammatory conditions, and the removal of sutures stimulated wound recovery. Growing evidence suggests that the resolution of inflammation is not, however, a passive process merely allowed by loss of inflammatory mediators as they diffuse away upon stimulus removal (Serhan and Savill, 2005; Serhan et al., 2007; Serhan et al., 2008), and our neurolymphatic remodeling results supported that idea. We identified distinct neurolymphatic architecture signatures present in inflammatory, wound-recovered, and tumor-associated microenvironments. We characterized non-malignant inflammatory lymphangiogenesis and neuroremodeling both in initial and recurrent inflammation, and we discovered three novel rapid neuroremodeling

phenotypes that characterized transitions into initial inflammation, from initial inflammation to wound recovery, and from wound recovery to recurrent inflammation. We also identified novel neurolymphatic remodeling events that accompany malignancy. We found distinct differences in nerve and lymphatic penetration into the site of a suture stimulus as compared to the site of a tumor including a dramatic hyper-sprouting phenotype in nascent tumor-associated lymphatic vessels. These findings show that neurolymphatic architecture is highly responsive to microenvironmental conditions, and further organ-specific study of tumor-associated neurolymphatic signatures may identify targetable aspects of these remodeling events that are suitable for early detection imaging or treatment.

PDAC Treatments: Emphasis Lymphatics and Nerves

Due to advanced stage at diagnosis and its complex microenvironmental organization, pancreatic ductal adenocarcinoma has proven to be very difficult to treat. Surgical removal of the tumor is the most effective option, but only approximately 15% of cases are considered resectable (Yeo and Cameron, 1998; Zuckerman and Ryan, 2008). Of those cases in which resection is an option, incomplete removal of microscopic disease (R1 residual margin status) only slightly improves patient survival over those cases presenting with unresectable metastatic disease (Chang et al., 2009; Konstantinidis et al., 2013). Non-surgical options for pancreatic cancer include radiation, chemotherapy, or a combination of both. Some approved chemotherapies for the treatment of pancreatic cancer are the use of FOLFIRINOX (combination of 5-fluorouracil, leucovorin, irinotecan, and oxaliplatin), gemcitabine, albumin-bound paclitaxel, and cisplatin (as well as others) (Gresham et al., 2014; Tempero et al., 2014). However, these drugs have had limited success in prolonging patient survival. Development of targeted therapies that specialize in blocking crucial molecular pathways of the pancreatic tumor and its microenvironment is becoming an increasingly attractive therapeutic option.

Pancreatic Tumor Resection, Lymphadenectomy, and Nerve Plexus Removal

Surgical resection of pancreatic adenocarcinoma was first brought to clinical practice by Walther Kausch in Berlin in 1909 (Gerdes et al., 2005). Beginning in the mid-1930s, American surgeon Allen O. Whipple further employed and modified the pancreat(ic)oduodenectomy (PD) procedure that would bear his name; he eventually condensed the surgery into a single operation, the first of which was successfully performed in 1940 (Whipple, 1941). In a traditional PD the head of the pancreas is removed along with the duodenum, gall bladder, and end of the common bile duct (Bhatti et al., 2010; Doi et al., 2007; Duanmin et al., 2013; Henne-Bruns et al., 1998; Henne-Bruns et al., 2000; Hirono et al., 2012; Kanda et al., 2011; Kocher et al., 2007; Murakami et al., 2010; Sergeant et al., 2013; Zacharias et al., 2007). Several timely surgical advances facilitated increased success of the PD as performed by Whipple and his contemporaries including the first successful duodenectomy in a canine, the discovery that direct immediate restoration of biliary and pancreatic secretions into the gastrointestinal tract was not necessary for survival of patients, and the use of non-dissolvable silk suture rather than the more temporary catgut (Howard, 1999; Whipple, 1941). Additional scientific breakthroughs critical for decreased perioperative morbidity and mortality included the discovery and synthesis of vitamin K, the discovery of insulin, and the description of human blood types and subsequent establishment of blood banks (Howard, 1999; Whipple, 1941). Today, a broad range of similar pancreatic resection procedures are in use in modern surgical practices around the world. Differences in primary tumor placement within the pancreas—head/neck vs. body/tail—and tumor invasion into surrounding tissues and organs often necessitate customization of resection (Cui et al., 2011; Dansranjavin et al., 2006; Formentini et al., 2009; Kamisawa et al., 1995; Kurahara et al., 2004; Liu et al., 2015a; Ohta et al., 1994; Pignatelli et al., 1994; Sergeant et al., 2009; Tempia-Caliera et al., 2002; Wang et al., 2012; Yamamoto et al., 2014) beyond the

traditional PD to such procedures as distal pancreatectomy with or without splenectomy (Duanmin et al., 2013; Nagai et al., 2011), pancreaticogastrostomy (Zacharias et al., 2007), pylorus-preserving PD (Doi et al., 2007; Hirono et al., 2012; Murakami et al., 2010), pylorus-resecting PD (Hirono et al., 2012), subtotal stomach-preserving PD, pancreatojejunostomy, duodenum-preserving head resection, wedge resection of inferior vena cava, and total (Kocher et al., 2007) or regional (Tao et al., 2006) pancreatectomy (Kobayashi et al., 2010; Shimada et al., 2006).

As with surgical treatment of other malignancies, one of the most controversial aspects of modern pancreatic ductal adenocarcinoma resection has been the extent to which surrounding connective tissue, lymph nodes, and neural tissue should be removed. Evidence suggests that metastasis to lymph nodes is an early event in pancreatic cancer progression, and presence of tumor cells in lymph nodes represents one of the most negative prognostic factors with respect to patient outcomes (Benassai et al., 1999; Chen et al., 2010; Doi et al., 2007; Fujita et al., 2010; Kanda et al., 2011; Nakagohri et al., 2006; Winter et al., 2006; Yamamoto et al., 2004). Conservative surgical views support the standard PD with loco-regional lymphadenectomy (Evans et al., 2009; Farnell et al., 2005; Farnell et al., 2008; Gerdes et al., 2005; Henne-Bruns et al., 1998; Henne-Bruns et al., 2000; Hirata et al., 1997; Kanda et al., 2011; Michalski et al., 2007; Murakami et al., 2010; Nagai et al., 2011; Nimura et al., 2012; Pawlik et al., 2005; Pederzoli et al., 1997; Pissas, 1984; Samra et al., 2008; Sergeant et al., 2013; Shimada et al., 2006; Yeo et al., 2002), while others, most notably numerous Japanese groups, advocate that a more radical PD with extensive removal of retroperitoneal soft tissue and extended lymphadenectomy (Fernandez-Cruz et al., 1999; Henne-Bruns et al., 1998; Ishikawa et al., 1988; Kanda et al., 2011; Katuchova et al., 2012; Kocher et al., 2007; Manabe et al., 1989; Masui et al., 2013; Meriggi et al., 2007; Nakao et al., 1995; Ohta et al., 1993; Pedrazzoli et al., 1998; Riall et

al., 2005; Sergeant et al., 2013) results in better patient outcomes. Collected studies in Table 4 (Benassai et al., 1999; Bittner et al., 1989; Dasari et al., 2015; Doi et al., 2007; Evans et al., 2009; Farnell et al., 2005; Farnell et al., 2008; Fernandez-Cruz et al., 1999; Fujii, 2013; Gerdes et al., 2005; Henne-Bruns et al., 1998; Henne-Bruns et al., 2000; Hirata et al., 1997; Hirono et al., 2012; Imai et al., 2010; Iqbal et al., 2009; Ishikawa et al., 1988; Jang et al., 2014; Kanda et al., 2011; Ke et al., 2014; Kocher et al., 2007; Manabe et al., 1989; Masui et al., 2013; Meriggi et al., 2007; Michalski et al., 2007; Nakao et al., 1995; Nguyen et al., 2003; Nimura et al., 2012; Ohta et al., 1993; Pawlik et al., 2005; Pederzoli et al., 1997; Pedrazzoli et al., 1998; Pedrazzoli, 2015; Peparini, 2015; Pissas, 1984; Riall et al., 2005; Roche et al., 2003; Samra et al., 2008; Schoellhammer et al., 2015; Sergeant et al., 2013; Shimada et al., 2006; Svoronos et al., 2014; Tol et al., 2014; Yeo et al., 1999; Yeo et al., 2002) demonstrate the broad range of study designs and conclusions that have fueled this debate. A recent set of randomized, controlled clinical trials from several centers around the world and a mathematical model of outcomes prediction have concluded that extended lymphadenectomy does not improve survival over traditional, more conservative resection and that quality-of-life may be decreased with more radical surgery (Farnell et al., 2005; Farnell et al., 2008; Jang et al., 2014; Michalski et al., 2007; Nguyen et al., 2003; Nimura et al., 2012; Pawlik et al., 2005; Pedrazzoli et al., 1998; Riall et al., 2005; Yeo et al., 1999; Yeo et al., 2002). Leading international surgical groups have also applied their expertise to the ongoing conversation in this field. They have recently identified lymph node stations to be included in standard lymphadenectomy for head (5, 6, 8a, 12b1, 12b2, 12c, 13a, 3b, 14a, 14b, 17a, and 17b) and body/tail (10, 11, 18) pancreatic cancer resections (Tol et al., 2014) and have released recommendations suggesting discontinued use of extended lymphadenectomy for treatment of PDAC (Evans et al., 2009; Sergeant et al., 2013; Tol et al., 2014). The occasional case report continues to demonstrate the biological diversity of pancreatic malignancy and

challenge these recommendations. In 2013 a Japanese group reported that extended lymphadenectomy in a well-differentiated, chemotherapy-responsive PDAC with para-aortic lymph node metastases resulted in patient survival of over ten years (Masui et al., 2013). Peparini, *et al.*, addressed para-aortic lymph node involvement (stations 16a2 and 16b1), stating that involvement of these lymph nodes may be due to direct invasion of the primary pancreatic tumor as opposed to dissemination and seeding of migratory cancer cells in the traditional definition of metastasis and that their removal may favorably impact R margin status (Peparini, 2015). Clinical trials and expert consensus recommendations consistently recommend standard lymphadenectomy over more radical resection strategies, but, as each case of pancreatic cancer is truly a unique disease, circumstances in which extended lymph node removal is beneficial may be more clearly defined in the future.

Controversy also exists with regard to the amount of nervous tissue that should be removed as part of pancreatic tumor resection (Reviewed in (Fernandez-Cruz et al., 1999; Samra et al., 2008)). Nerve invasion by PDAC cells occurs both in intrapancreatic nerves as well as extending to peripancreatic nerve plexuses. As with lymphadenectomy, the concept of nervous tissue removal is founded on the principle that in order to prevent recurrence, all local reservoirs of tumor cells must be surgically eradicated. And as with other radical resection procedures, aggressive surgical strategy must be balanced with undesirable side effects attributable to tissue removal as peripancreatic nerve plexus removal often results in severe diarrhea.

Table 4. Standard (sLE) vs. Extended (eLE) Lymphadenectomy for Treatment of PDAC: Results and Recommendations of Collected Studies

Citation	Study Type	Results/Conclusions	Supported LE Type
Masui 2013	CR	In selected cases eLE can result in long-term patient survival: here well-differentiated, chemotherapy-responsive pancreatic cancer with PALN metastasis	Extended
Pedrazzoli 1998	P	Survival trends toward an increase in node positive patients with PD + eLE and retroperitoneal tissue removal over sLE; No increase in operative morbidity/mortality	Extended
Riall 2005	P	Survival trends toward an increase in pylorus-preserving PD with retroperitoneal LE and distal gastrectomy in PDAC patients, but this may be due to increased positive resection margins in standard resection group	Extended
Benassai 1999	R	Survival increased with eLE but may be due to patient selection; Additional prospective randomized trials are necessary	Extended
Ishikawa 1988	R	eLE and connective tissue removal is recommended for regional control of small (< 4 cm) tumors	Extended
Manabe 1989	R	Survival increased with radical pancreatectomy including soft tissue removal and eLE beyond suspected positive lymph nodes	Extended
Meriggi 2007	R	Extended peripancreatic and locoregional LE including removal of nerve and connective tissue reduces local recurrence in tumors < 4 cm in diameter	Extended
Nakao 1995	R	eLE including PALNs should be performed in patients with pancreas head cancer	Extended
Ohta 1993	R	eLE and removal of retroperitoneal connective tissue is recommended for curative resection in tumors macroscopically confined to pancreas	Extended
Fernández-Cruz 1999	Rv	Removal of primary tumor as well as eLE and removal of nerve plexus, soft tissue, and portions of nearby blood vessels are necessary to prevent tumor recurrence and spread	Extended
Samra 2008	Rv	Modified *en bloc* resection (including removal of lymphatics and neural tissue associated with superior mesenteric artery and retropancreatic tissue) may be best for PDAC of pancreas head	Modified radical/ Intermediate
Tol 2014	Exp	International Group on Pancreatic Surgery accepted Japanese Pancreas Society lymph node classification system, defined standard and extended LE procedures, and recommended standard LE for PDAC	Standard
Farnell 2005	P	Quality-of-life is decreased in patients following eLE with no survival benefit; No further trials should be performed comparing these two surgical methods	Standard
Gerdes 2005	P	Radical LE not recommended in cases of pylorus-preserving PD	Standard
Jang 2014	P	Prospective randomized clinical trial found no improvement in survival with eLE over sLE while eLE increased morbidity	Standard
Nimura 2012	P	No difference in 5-year or disease-free survival or number of involved lymph nodes; Local recurrence higher and quality-of-life lower with eLE; eLE not indicated based on trials	Standard

Pissas 1984	P	Describes pancreatic lymphatic drainage patterns and involved lymph nodes with discussion of appropriate surgical procedures to remove specific lymph node clusters; eLE may not be beneficial because of close proximity of pancreatic lymphatics and thoracic duct allowing early circulation of tumor cells	Standard
Yeo 2002	P	Extending pylorus-preserving PD with retroperitoneal LE and distal gastrectomy does not improve survival and increases morbidity in patients with periampullary carcinomas; eLE may show some benefit in PDAC with long-term follow-up	Standard
Henne-Bruns 1998	R	Retroperitoneal eLE does not improve survival over regional LE for pancreatic head tumors following R0 partial duodeno-pancreatectomy	Standard
Henne-Bruns 2000	R	Survival after partial PD does not improve with eLE and retroperitoneal tissue removal over regional LE	Standard
Hirata 1997	R	eLE does not always improve PDAC outcomes and may be responsible for increased post-operative mortality	Standard
Kanda 2011	R	A thorough but not radical degree of LE is recommended with differential dissections indicated for head vs. body/tail tumors	Standard
Pawlik 2005	R	eLE may only benefit 0.3% of patients; Too large of a population size would be necessary to sufficiently power a prospective trial making it infeasible	Standard
Shimada 2006	R	eLE does not improve outcomes in the presence of positive PALNs and is not recommended	Standard
Dasari 2015	Rv	Meta-analysis of randomized clinical trials; eLE does not improve survival over sLE but increases morbidity	Standard
Evans 2009	Rv	Survival is not improved with eLE over sLE; Recommend sLE during PDAC PD	Standard
Farnell 2008	Rv	Recommends standard PD without eLE based on survival and quality-of-life outcomes of four randomized clinical trials	Standard
Fujii 2013	Rv	Title somewhat misleading; Advocates LE with sufficient removal of LNs to provide accurate prognosis (to include lymph node ratio metric) but does not recommend extensive eLE	Standard
Iqbal 2009	Rv	Meta-analysis 1988-2005; eLE is associated with increased patient morbidity including delayed gastric emptying with no increase in survival	Standard
Ke 2014	Rv	eLE is associated with poor post-operative quality-of-life; sLE is recommended for patients with PDAC of pancreas head	Standard
Michalski 2007	Rv	Survival not improved and quality-of-life decreased with eLE; Not indicated except perhaps in the setting of additional randomized controlled trials	Standard
Pederzoli 1997	Rv	Current data does not show benefit of extensive LE; Additional prospective randomized trials are necessary	Standard
Pedrazzoli 2015	Rv	Lymph node stations 6, 8a, 8p, 12a, 12b, 12c, 13a, 13b, 14a, 14b, 14c, 14d, 16b1, 17a, and 17b should be removed as part of a sLE to accurately stage disease and decrease metastasis risk	Standard
Peparini 2015	Rv	Lymph node stations 16a2 and 16b1 (PALNs) should be included in sLE to minimize local invasion and improve resection margins	Standard

Schoellhammer 2015	Rv	eLE should not be implemented for PDAC patients due to lack of improvement in patient survival	Standard
Sergeant 2013	Rv	Sufficient evidence does not exist to indicate eLE over sLE for treatment of PDAC of pancreas head	Standard
Svoronos 2014	Rv	Five-year overal survival was not improved with eLE and eLE patients experienced a significant increase in post-operative diarrhea; sLE with PD should be used to treat PDAC of pancreas head	Standard
The studies below do not directly support one type of LE over another but provide pertinent results that should be considered in a discussion of this topic.			
Hirono 2012	P	Intraoperative physiological fluorescence imaging identified 7 lymphatic drainage pathways from pancreatic uncinate process; Removal of PALNs and skeletonization of superior mesenteric artery may both be beneficial	
Imai 2010	P	CT, MRI, and FDG-PET cannot accurately detect presence or absence of lymph node metastases; Intraoperative examination of frozen sections is recommended	
Kocher 2007	P	Sentinel pancreas lymph nodes were not identified intraoperatively; Prediction of positive lymph nodes to guide selective resection was not possible	
Nguyen 2003	P	There is no difference in quality-of-life metrics in standard vs. radical resection 2.2 years following surgery	
Roche 2003	P	Preoperative CT does not accurately predict positive lymph nodes especially in the case of micrometastasis and should not preclude curative resection or direct LE decisions	
Yeo 1999	P	Extending pylorus-preserving PD with retroperitoneal LE and distal gastrectomy does not increase morbidity and mortality over standard resection; More time and greater numbers of patients are needed to assess survival benefit	
Bittner 1989	R	Surgery for pancreatic cancer does not increase morbidity or mortality over other abdominal oncologic surgeries; Resection only benefits TNM stage I population	
Doi 2007	R	PALN metastasis correlated with increased mortality; Upon intraoperative confirmation of PALN metastasis alternative treatment strategies should be considered due to short survival duration even with eLE	

CR: Case report, Exp: Expert consensus statement, LE: Lymphadenectomy--(e) Extended, (s) Standard, P: Prospective study, PALN: Para-aortic lymph node, PD: Pancreat(ic)oduodenectomy, PDAC: Pancreatic ductal adenocarcinoma, R: Retrospective study, Rv: Review

*This table was previously published in Fink et al., 2015a.

Outcomes Prediction: Lymphatic-Specific Metrics

Outcomes prediction for pancreatic cancer patients has traditionally been based on stage classification according to the TNM (tumor, node, metastasis) system at diagnosis (Santi et al., 2011). Pancreatic cancer is rarely diagnosed in a pre-metastatic state. Unlike perineural invasion, which is nearly universally accepted to negatively impact survival, the utility of lymphatic-specific metrics in predicting patient outcomes is less well understood and appreciated. Comprehensive examination of lymph node and lymphatic vessel involvement would provide clinicians with important information about the progression characteristics of an individual patient's tumor such as its pattern and route of spread, likelihood of local/distant recurrence, and potential immunomodulatory effects. Four outcomes predictive metrics specifically address lymph node/lymphatic vessel involvement: lymph node disease (LND), lymph node burden (LNB), lymph node ratio (LNR), and lymphatic vessel invasion (LVI). Each of these measures provides distinct information regarding disease pathology and may be useful in refining prognoses. LND is defined as the confirmed presence of metastatic tumor cells in at least one lymph node. The total number of positive lymph nodes confirmed at resection constitutes LNB. LNR is the ratio of the number of positive nodes to the total number of nodes examined (John et al., 2013). LNR has been shown to be an effective tool to further stratify the TNM stage N1 patient population for outcomes prediction while decreasing likelihood of understaging and stage migration (Berger et al., 2004; Pawlik et al., 2007; Slidell et al., 2008). LVI may refer to lymphatic vessel invasion as determined by immunohistochemical staining of tissue sections or more broadly, to lymphovascular invasion, which may or may not distinguish between invaded hematogenous and lymphogenous vessels (Chen et al., 2010; Safuan et al., 2012). The relative prognostic value of each of these lymph node-/lymphatic vasculature-specific metrics is controversial. Prospective and retrospective clinical studies evaluating the

utility of these criteria are collected in Table 5 (Ausborn et al., 2013; Berger et al., 2004; Bhatti et al., 2010; Chen et al., 2010; House et al., 2007; John et al., 2013; Konstantinidis et al., 2010; La Torre et al., 2011; Murakami et al., 2010; Nakagohri et al., 2006; Pawlik et al., 2007; Riediger et al., 2009; Robinson et al., 2012; Schwarz and Smith, 2006; Sergeant et al., 2009; Sierzega et al., 2006; Slidell et al., 2008; Smith and Mezhir, 2014; Tol et al., 2015; Yamamoto et al., 2014). Contradictory conclusions from these studies highlight the remaining need for additional work before use of these metrics is informative in the general clinical setting.

Table 5. Lymphatic-Specific Outcomes Metrics: Lymph Node Disease (LND), Lymph Node Burden (LNB), Lymph Node Ratio (LNR), Lymphatic Vessel Invasion (LVI)

		Analyzed/Significant Metrics[7]			
Citation	Conclusions/Recommendations	LND	LNB	LNR	LVI
Ausborn 2013	High LNR is associated with decreased overall survival of PDAC patients only when 53BP1 expression is low				
Berger 2004	LNR > 0.15, not number of LNs examined, predicts overall survival and disease-free survival in patients with PDAC				
Bhatti 2010	LNR is a better predictor of overall survival than LNB or LND in PDAC				
Chen 2010	Lymphovascular invasion (may be blood or lymphatic vessels) predicts 5-year survival in periampullary cancer and PDAC patients				
House 2007	Presence of LND predicts survival in PDAC patients; In node positive disease, LNB and LNR are good predictors of survival				
John 2013	LNB and LNR can be used to predict cancer-specific survival in patients with PDAC of pancreas head regardless of resection margin status				
Konstantinidis 2010	Regional lymph node metastasis and direct lymph node invasion equally negatively impact survival; LNR ≥ 0.2, LNB, and LVI are useful predictors of prognosis of PDAC patients				
La Torre 2011	LND and LNR are both predictive of prognosis in PDAC patients; LNR maintains significance on multivariate analysis				
Murakami 2010	LND and LNB, not LNR, predict overall survival in PDAC patients; LNR also significant in univariate analysis				
Nakagohri 2006	LND and LVI are predictors of 3-year survival; LND is best predictor of all analyzed for PDAC patients				

[7] White: metric not analyzed; Light gray: metric analyzed but not statistically significant; Dark gray: statistically significant metric

Pawlik 2007	LNR predicts prognosis and disease-specific survival in PDAC patients				
Riediger 2009	LNR, not LND or LNB, predicts overall survival in PDAC patients				
Robinson 2012	LND and LNR are good predictors of 5-year survival of PDAC patients; LNR better when > 0.15				
Schwarz 2006	Number of lymph nodes examined and number of negative lymph nodes identified predict survival for exocrine pancreatic cancer patients				
Sergeant 2009	Extracapsular LNR predicts overall survival as does overall LNR; LNB predicts disease-free survival in PDAC patients				
Sierzega 2006	LND predicts prognosis in patients with PDAC of pancreas head; In node positive disease, LNR > 0.2 predicts survival; Specifically, Group 8 and 12 lymph nodes were prognostic				
Slidell 2008	Number of positive LNs, presence of LND, and LNR are significantly associated with survival in PDAC patients				
Smith 2014	New predictive tool available for LNR and survival that incorporates specific patient metrics and includes population characteristics				
Tol 2015	LNR above 0.18 predicts 3-year survival in PDAC patients				
Yamamoto 2014	LNB and LNR are predictors of PDAC patient prognosis, not LVI; LNR is best predictor of all metrics examined				

*This table was previously published in Fink et al., 2015a.

A major challenge in pancreatic cancer biology and treatment is the presence in lymph nodes of single or small clusters of tumor cells that are not detected by routine histopathological staining techniques (Bogoevski et al., 2004; Demeure et al., 1998; Katuchova et al., 2012; Milsmann et al., 2005; Ridwelski et al., 2001). Similar to insufficient surgical removal of primary lymph nodes (Berger et al., 2004; House et al., 2007; Meriggi et al., 2007; Pawlik et al., 2007; Schwarz and Smith, 2006; Slidell et al., 2008), failure to detect occult micrometastatic deposits in nodes may result in patient misclassification, understaging, and improperly informed outcomes prediction. Descriptions of "skip metastases" in which primary lymph nodes are negative but metastases are established in secondary nodes or distant organ sites (Farnell et al., 2005; Golse et al., 2013; Mao et al., 1995) may be attributable, at least in part, to this phenomenon. Emerging immunohistochemical and molecular techniques such as epithelial cell adhesion molecule (EpCAM/Ber-EP4) (Bogoevski et al., 2004; Milsmann et al., 2005), cytokeratin (Katuchova et al., 2012; Ridwelski et al., 2001), and carbohydrate antigen 19-9 (CA19-9; sialyl-Lewis A) staining (Ridwelski et al., 2001), and polymerase chain reaction for mutant *KRAS* (Demeure et al., 1998) have demonstrated efficacy in occult tumor cell detection in nodes, but their adaptation from the research laboratory to practical clinical application will require more extensive study.

Targeting Tumor Vasculature

Anti-angiogenic therapies were originally developed to starve tumors of important nutrients and oxygen and to reduce the number of potential routes for dissemination. However, clinical trials demonstrated that, when used alone, anti-angiogenic therapy was not sufficient to improve patient survival. Unexpectedly though, the results indicated that anti-angiogenic therapy significantly improved survival of patients with solid tumors when used in combination with conventional chemotherapies (Hurwitz et al., 2004; Saltz et al., 2008; Sandler et al., 2006).

These findings led to the evolution of the current vascular normalization theory: the use of anti-angiogenic therapy to block aberrant tumor angiogenesis and alleviate vessel dysfunction (Goel et al., 2012). By restoring the balance between pro- and anti-angiogenic factors, anti-angiogenic therapies improved vessel organization, stabilized cell-to-cell junctions, increased pericyte coverage, and, consequently, reduced fluid leakage. All these factors, in turn, relieved blood flow irregularities resulting in improved delivery of chemotherapy to all parts of the tumor (Goel et al., 2011). Unfortunately, in the setting of pancreatic cancer, anti-angiogenic therapies have had either no effect or only transient effects on improving patient survival even when used in combination with standard chemotherapies (Bergers and Hanahan, 2008; Kindler et al., 2010; Sahora et al., 2014; Sohal et al., 2013; Van Cutsem et al., 2009). PDAC tumors are unusually hypovascular and desmoplastic negating the ability of even normalized vessels to deliver therapy (Tamburrino et al., 2013). The failure of anti-angiogenic therapy in PDAC may also be the result of tumor cells circumventing the VEGF-A/VEGFR-1 blockade through autocrine or paracrine secretion of alternative angiogenic factors, such as the prototypical lymphangiogenic factors which have overlapping angiogenic functions (Bergers and Hanahan, 2008; Cao et al., 1998; Chien et al., 2009; Scavelli et al., 2004).

Targeting the tumor lymphatic vasculature as a treatment for cancer is beginning to gain interest among both basic and clinical research groups with the primary focus on anti-lymphangiogenic therapies. Lymphangiogenic growth factors are not critical for the maintenance of adult lymphatic vessels in homeostasis. This allows for extended treatment with anti-lymphangiogenic therapies in tumor settings without disruption of pre-existing vessels and with minimal drug-induced toxicities (Karpanen et al., 2006; Lin et al., 2005). Numerous pre-clinical *in vivo* studies have demonstrated that blocking pro-lymphangiogenic factors VEGF-C and VEGF-D and their receptor VEGFR-3 significantly reduces tumor lymphangiogenesis and

lymph node metastases in many tumor types including pancreatic (Koch et al., 2009), breast (He et al., 2008; Karpanen et al., 2001; Krishnan et al., 2003; Roberts et al., 2006), melanoma (Lin et al., 2005), renal (Stacker et al., 2001), lung (He et al., 2002; He et al., 2005), gastric (Chen et al., 2005; Shimizu et al., 2004), prostate (Burton et al., 2008), hepatocellular (Thelen et al., 2008), and bladder (Yang et al., 2011a). Other protein targets of lymphangiogenesis that have shown promise in inhibiting lymphatic metastasis *in vivo* include the VEGFR-3 co-receptor Nrp-2 (Caunt et al., 2008; Ou et al., 2015) and the angiopoietins Ang-1 and -2 (Holopainen et al., 2012; Neal and Wakelee, 2010). Currently, two humanized neutralizing antibodies are in clinical trials for patients with solid tumors: VGX-100, which inhibits VEGF-C (NCT01514123) and IMC-3C5, which inhibits VEGFR-3 (NCT01288989).

The blockade of a single VEGF/VEGFR pathway will likely be insufficient to inhibit tumor lymphangiogenesis and lymph node metastasis due to the multiple compensatory and overlapping roles of the VEGF ligands and receptors (Alitalo and Detmar, 2012; Bjorndahl et al., 2005b; Da et al., 2008; Scavelli et al., 2004). Other growth mechanisms outside of VEGF/VEGFR signaling may also regulate lymphangiogenesis in the tumor setting, such as PDGF-BB/PDGFR (Cao et al., 2004a) and FGF/FGFR(Cao et al., 2012). Receptor tyrosine kinase inhibitors (RTKIs) often target multiple receptors allowing them to inhibit several signaling pathways simultaneously—including the VEGFR pathways. Both pre-clinical comparative studies and clinical trials have determined the safety and efficacy of numerous anti-angiogenic/-lymphangiogenic RTKIs for the treatment of cancer including foretinib (Chen et al., 2015), cediranib (Heckman et al., 2008; Padera et al., 2008), and axitinib (Grunwald and Merseburger, 2012; Rixe et al., 2007; Spano et al., 2008). Some of these RTKIs have also been approved for clinical use. Sorafenib, which inhibits VEGFR-1 and -3, PDGFR-β, FGFR-1, and Raf proteins, has been approved for renal cell (RCC) and hepatocellular carcinomas (Procopio et al., 2012; Reataza

and Imagawa, 2014; Wilhelm et al., 2004); sunitinib, which inhibits VEGFR-1 and -3, and PDGFR-α and -β, has been approved to treat pancreatic neuroendocrine tumors, RCC, and gastrointestinal stromal tumors (Detry et al., 2013; Khagi and Saif, 2015; Kodera et al., 2011; Mankal and O'Reilly, 2013); and pazopanib, which inhibits VEGFR-1 and -3, PDGFR-α and -β, and FGFR, has been approved to treat RCC and soft tissue sarcoma (Ahn et al., 2013; Schutz et al., 2011; Verweij and Sleijfer, 2013) (RTKIs further reviewed in (Stacker et al., 2014)). Vatalanib, which inhibits VEGFR-1, -2, and -3, and PDGFR-β, is currently in clinical trials for the treatment of various solid tumors including pancreatic, ovarian, and breast cancers. This RTKI has been shown to directly inhibit angiogenesis, lymphangiogenesis, and tumor growth in pre-clinical models of pancreatic cancer as well as other cancer models (Baker et al., 2002; Drevs et al., 2000; Lin et al., 2002; Sini et al., 2008; Solorzano et al., 2001). In a recent clinical trial, vatalanib resulted in a partial or stable response for some metastatic pancreatic cancer patients who had initially failed gemcitabine treatment (Dragovich et al., 2014). Many of these lymphangiogenic receptor-targeting RTKIs hold promise for the treatment of early-diagnosed and resectable cancers (Alitalo and Detmar, 2012). Unfortunately, these are not typical characteristics of pancreatic cancer, and, consequently, many of these drugs have failed to significantly improve pancreatic cancer patient survival (Cardin et al., 2014; Goncalves et al., 2012; Kindler et al., 2011; Spano et al., 2008).

Lymphangiogenesis is not the only manner by which the lymphatic vasculature can promote tumor progression. As discussed previously, pre-existing lymphatic vessels can directly facilitate metastasis by transporting tumor cells to distant sites. Lymphatic endothelia may also contribute to immune suppression by altering DC and T cell responses. However, these functions are poorly understood and much more work needs to be done to determine if these functions can be specifically targeted in lymphatic vessels for the treatment of cancer.

Using Lymphatic Vessels to Deliver Therapies to Lymph Nodes

In pancreatic cancer, metastasis to lymph nodes and distant sites has often already occurred by the time of diagnosis. Anti-lymphangiogenic therapies may inhibit further tumor cell dissemination but will do little to reduce the growth of metastatic tumors that have already seeded at distant sites (He et al., 2005; Hoshida et al., 2006; Padera et al., 2008). Successful treatment of tumor-invaded lymph nodes has been particularly difficult to achieve. Resection of invaded lymph nodes would intuitively seem to be a promising strategy; however, as discussed above, current clinical imaging technologies cannot reliably detect single cell or microscopic lymph node metastases (Nune et al., 2011; Sevick-Muraca et al., 2014), and excision of an excessive number of lymph nodes is controversial due to conflicting evidence regarding its survival benefits and concerns about post-operative quality-of-life (Michalski et al., 2007; Witte et al., 2011). Also, conventional intravenously-administered therapies display poor access to lymphatic vessels and lymph nodes resulting in sub-optimal drug concentrations within lymph nodes (O'Hagan et al., 1992). This enables tumor cells present within lymph nodes to evade treatment and potentiate future recurrence. Using the lymphatic vasculature as a delivery system for cancer therapies to the lymph nodes has gained increasing interest. For therapies to be effectively taken up by lymphatic vessels and not blood capillaries requires specific characteristics of drug formulations such as being of a particular size and molecular weight, lipophilicity and surface charge of the drug carrier, and concentrations of the drug and carrier (reviewed in (Ali Khan et al., 2013; Singh et al., 2014)). A few anti-cancer drugs have been formulated to target the lymphatic system and have shown promise *in vivo*: a methyl poly(ethylene glycol)-distearoylphosphatidylethanolamine micelle containing doxorubicin reduced the size of lymph node metastases in a melanoma model (Li et al., 2015); addition of polyethylene glycol (PEGylation) to interferon-α2 demonstrated anti-tumor efficacy in the lymph

nodes of rats with breast cancer (Kaminskas et al., 2013); cisplatin conjugated to a copolymer block of poly(ethylene oxide)-block-poly(lysine) successfully treated lymph node metastases in a model of squamous cell carcinoma (Dunne et al., 2007); and gemcitabine loaded onto magnetic multiwalled carbon nanotubes resulted in better uptake of gemcitabine in the lymph nodes and regression of lymph node metastases in a subcutaneous model of pancreatic cancer (Yang et al., 2011a). The field of lymphatic-based drug delivery is still in its infancy and more studies are required to demonstrate efficacy and feasibility in patients.

New Murine Platforms for Real-Time Live Imaging Studies of PDAC-Associated Neurolymphatic Remodeling

Translation of the findings presented here to clinically-meaningful therapies or imaging signatures would require considerable additional development. The live imaging neurolymphatic remodeling studies presented in this dissertation were performed in mouse cornea and pinna—two accessible tissues housing neurolymphatic networks with distinct properties in homeostasis and inflammation. We used B16 melanoma cells for the majority of our experiments and in so doing created an orthotopic system in the mouse skin and a pseudo-orthotopic environment in the mouse cornea mimicking corneal melanoma. We tracked tumor cells over time through cornea and pinna lymphatic vessels by real time live imaging microscopy and showed that they entered lymphatic vessels, were cleared from sites identifiable for several days by tissue landmarks, and eventually trafficked to draining lymph nodes. Entry of tumor cells into lymphatic vessels was a relatively rare event, and properties of tumor cells trafficking through the cornea could be influenced by the inflammatory status of that tissue at the time of cell delivery. These systems have provided insight into many aspects of neurolymphatic remodeling and tumor metastasis, but extrapolation of these microenvironment-dependent principles to PDAC requires study under more appropriate organ-specific conditions. An

interesting intermediate step in the transition to the pancreas would be the use of PDAC organoids (Boj et al., 2015) in skin or corneal live imaging experiments. Organoids better represent the complexity of a tumor microenvironment and would likely be amenable to use in both of our established platforms.

Of interest for future work is the development of an intravital imaging system specifically designed to track pancreatic tumorigenesis, tumor-lymphatic/-nerve/-blood vessel interactions, and pancreatitis- and malignancy-associated neurolymphatic and blood vascular remodeling in the pancreas. Development of such a platform would first require the generation of a multi-color mouse model in which nerves, lymphatics, and blood vessels expressed distinct fluorescent reporter proteins. Pancreatitis studies could be performed in these triple-transgenic reporter animals by one or more previously established methods such as cerulein injection or Coxsackie virus challenge. Traditional orthotopic surgery protocols could be used with syngeneic fluorescent reporter cell lines to study tumor-associated neurovascular remodeling and tumor-neurovascular interactions. An alternative strategy in lieu of cell line implantation that would also enable studies of premalignant PanIN lesions would be use of the PKCY (Rhim et al., 2012) or KPCT (Stopczynski et al., 2014) modifications of the original autochthonous KPC PDAC model which include fluorescent reporter proteins in cells of the pancreas. Live imaging could be accomplished by implantation of a pancreas window as has been previously described (Ritsma et al., 2013). This platform could also be used to identify subgroups of tumor cells that preferentially migrate to/through one of the tissue networks of interest—nerves, lymphatics, or blood vessels. Live imaging data could be complemented by further studies at necropsy and of extracted tissues.

We have performed preliminary proof-of-concept experiments to demonstrate the feasibility of deep tissue imaging reconstruction of vasculature networks in fixed pancreas. tdTomato fluorescent protein was constitutively expressed in Tie-2^{+} cells using Cre recombinase technology. This enabled visualization of both blood and lymphatic endothelium by live imaging and in fixed tissue. We developed a modified CLARITY protocol in which cellular lipids were removed to facilitate 2-photon microscopy of intact organs or thick sections up to approximately 500 µm. Figure 33 shows one example of 3D blood and lymphatic vasculature reconstruction performed in $Tie2Cre^{tdT}$ mouse pancreas. Both large vessels and capillary structures can be visualized, and we are confident that inflammation- or malignancy-induced vascular architecture changes could be identified using this technology. We have also optimized immunostaining protocols for CLARITY hydrogel-perfused organs, which would enable hypothesis-driven interrogation of tissue remodeling and tumor metastasis mechanisms.

Figure 33. Tie2Cre^{tdT} pancreatic blood and lymphatic vessel network revealed by CLARITY and 2-photon microscopy. TdTomato fluorescent protein is expressed under the control of the Tie-2 promoter. Tie-2 is expressed in blood and lymphatic endothelial cells. Tie2Cre^{tdT} mice were perfused with CLARITY hydrogel monomer solution as described (Chung and Deisseroth, 2013; Chung et al., 2013b) to facilitate penetration of hydrogel deep into body organs. Pancreases were harvested and further clarified according to the CLARITY protocol. 2-photon confocal imaging was performed on approximately 500 µm thick pancreas sections. *A*. 100X maximum intensity projection. *B*. 3D projection of *A*.

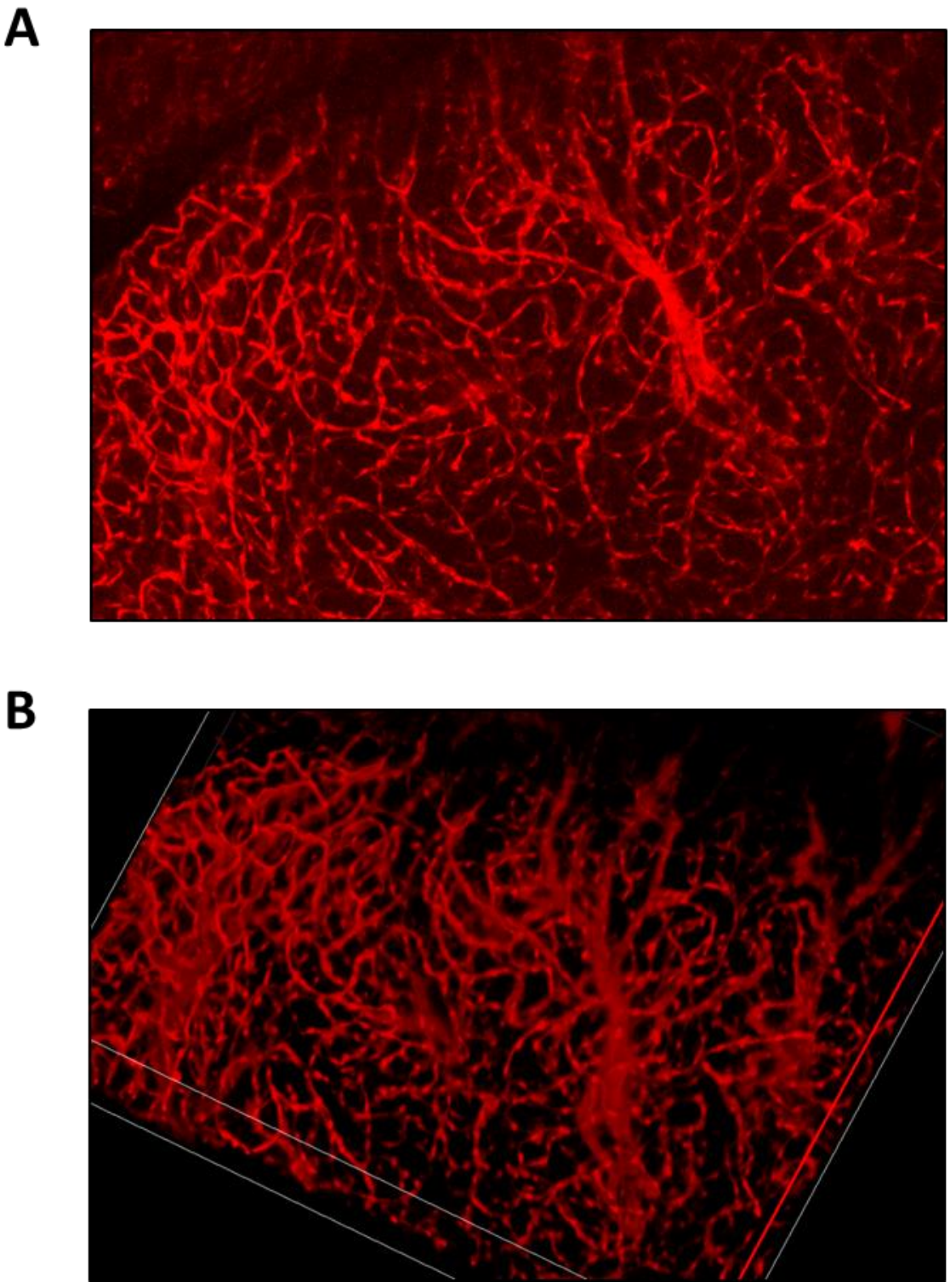

Figure 33

This multi-fluorescent imaging platform would enable at least two other lines of experimental investigation. First, live fluorescent neurovascular cells could be sorted out of pancreas (or adjacent lymph nodes or neural plexuses) with or without orthotopic/autochthonous PDAC tumor to identify tumor-dependent distinctions in biological processes and molecular characteristics of these cells, *i.e.* by *in vitro* assays such as migration, tubulogenesis, proliferation, cytokine stimulation, signaling, neurite outgrowth, etc., or by RNA-sequencing. Similarly, tumor cells found in pancreatic lymphatic vessels or nerves could be extracted by laser capture microdissection; or these experiments could be carried out in the absence of tumor cells to interrogate pancreas-specific differences in homeostatic, non-malignant inflammatory, and wound-recovered microenvironments. Second, identification of pancreas-specific neurovascular remodeling events that accompany premalignant PanIN lesions or very small tumors could be used in early detection of PDAC. We have demonstrated in this work that very small numbers of tumor cells induce local neurolymphatic remodeling signatures that are distinguishable from those caused by non-malignant inflammation and that these local remodeling events are sometimes accompanied by broader field effects outside the immediate "mini-microenvironment" of a group of tumor cells. These tenets of neurolymphatic remodeling may hold true in the pancreatic microenvironment and may be targetable for imaging.

Objective Measurement of PDAC Patient Cachexia Status and Correlation with Other Metrics

Determination of cachexia status of patients enrolled in the pancreatic cancer rapid autopsy (RAP) program remains somewhat subjective. Designation of cachexia status at autopsy is not based solely on measurable criteria but rather on the appearance of the body. Notes in pathology autopsy reports contain such phrases as "marked cachexia of the extremities," "the muscles appear somewhat atrophic," "there is grossly apparent muscle wasting that is more

prominent in the torso and upper extremities," "the body is that of a thin/cachectic elderly male," and "the extremities are thin." Differences in diagnostic criteria among pathologists performing autopsies could result in inconsistent status designations over the course of many autopsies. In the studies presented in Chapter III, we have tried to minimize this potential bias by including additional clinical criteria in our subgroup analysis. While definitions of clinically-meaningful weight loss vary and may be confounded by the rising numbers of overweight and obese patients, one of the hallmark features of cachexia is significant unintentional weight loss; thus, we included it in our modified cachexia status stratification strategy. Other clinical notes, too, provided some insight into deterioration of patient function that could be linked to cachexia with such phrases as, "presented with weight loss, extreme weakness, fatigue, decreased energy, decreased oral intake" etc., "required parenteral nutrition secondary to malnutrition," "complains of decreased body mass and weight," and the somewhat contradictory "cachectic but comfortable-appearing," documented in the records of RAP patients. Other factors linked to end-stage disease may also contribute to inconsistencies in designation of cachexia status at autopsy. In at least one RAP case cachexia status was determined to be negative, but this was qualified by the note that "if present, [cachexia] was masked by anasarca[8]." Another case notes the presence of pitting edema[9] in the extremities, which might also conceal cachexia.

A new use of an old imaging technology may help to ameliorate challenges in cachexia status designation (Martin et al., 2013a; Tan et al., 2009). Trunk CT scans are routinely used in

---

[8] Anasarca is generalized edema throughout large portions of the body due to accumulation of fluid subcutaneously or in connective tissue.

[9] Pitting edema is characterized by the persistence of an indentation when pressure is applied to an area of swelling.

PDAC diagnosis and repeated over time to track tumor progression, metastasis, and response to treatment. These scans capture a region of the lumbar spine that can be used to compute lumbar skeletal muscle index. This metric objectively quantifies muscle mass independent of BMI and is not complicated by factors that may confound visual cachexia diagnosis such as increased subcutaneous fat or generalized edema. The majority of the patients in our RAP program have the necessary scans available, and we are currently working to apply this method to obtain an unbiased skeletal muscle index to serve as an additional criterion in the final designation of cachexia status.

The broad spectrum of tissues available from our cohort of PDAC RAP patients would facilitate many additional musculature-based studies. In addition to skeletal muscle, changes to cardiac muscle have also been reported in models of cachexia. Cachectic C26 colon tumor-bearing mice had impaired cardiac function associated with structural changes in musculature and appearance of fibrosis (Tian et al., 2010). A differential gene expression signature in tumor-bearing mice compared to tumor-free controls included increased levels of the E3 ubiquitin ligases MuRF-1 and atrogin-1 as well as differential expression of B-type natriuretic peptide (BNP), c-Fos, peroxisome proliferator-activated receptor-α (PPAR- α), and carnitine palmitoyltransferase1-β (CPT1- β), and the re-emergence of fetal proteins MHC-β and Glucose transporter (GLUT)-1 (from MHC-α and GLUT-4) (Tian et al., 2011). Murine adenocarcinoma cell line 16 (MAC16) tumor-bearing nude mice developed cancer cachexia and also showed increased MuRF-1 and MAFbx gene expression; these changes were attributed to increased oxidation in cardiac muscle (Hinch et al., 2013). Another group has recently identified a "cachexokine cocktail" of seven tumor-secreted factors that are necessary and sufficient to alter cardiomyocyte metabolic pathways and cause cellular atrophy; these factors are: bridging integrator 1, syntaxin 7, multiple inositol-polyphosphate phosphatase 1, glucosidase alpha acid,

chemokine ligand 2, adamts like 4, and ataxin-10 (Schafer et al., 2015). Studies of cardiac cachexia in mouse models of PDAC or human PDAC tissue samples are lacking. Heart apex is routinely harvested as part of our rapid autopsy procedures. An examination of molecular changes in cardiac muscle in cachectic vs. non-cachectic patients would provide another level of insight into this systemic disease. Of particular interest in PDAC samples would be studies of GLUT transporter dysregulation and oxidative stress. The interplay between cardiac cachexia and chemotherapy-induced cardiac toxicity is poorly understood and could also be investigated. Similarly understudied are the effects of PDAC-associated cachexia on smooth muscle. Many patients succumb to respiratory failure in end stage PDAC; little is known about effects of cachexia on diaphragm. Studies of alterations in vasculature- and gastrointestinal tract-associated smooth muscle could also be carried out in our sample set.

The nature of systemic inflammation in PDAC-associated cachexia could also be interrogated with these samples. One of the most important aspects of our RAP program is that it is ongoing; new patients are continuously enrolled, and studies that require fresh tissue samples can be designed along with use of clinical samples taken throughout disease progression. A set of interesting questions would be how serum inflammatory cytokine profiles change as cachexia develops, how chemotherapy cycles affect these systemic markers, and how the composition of intratumoral infiltrating immune cell populations responds to or drives these changes. Fresh tumor harvest could facilitate expansion of specific inflammatory cell subpopulations and tumor cells for more detailed study of paracrine signaling and supportive vs. anti-tumor properties of immune cells in the PDAC tumor microenvironment. Similarly, relationships between glucose toxicity and perineural invasion or chemotherapy-induced peripheral neuropathy could be investigated in these well-annotated samples.

Outlook for the Future

Advances in surgical, radiation, and chemotherapeutic treatment regimens for pancreatic cancer have not greatly impacted overall survival rates for patients afflicted with this devastating disease. Early spread of tumor cells to lymph nodes, into nerves, and to distant sites often precludes curative resection, facilitates cancer chemoresistance and immune evasion, and decreases overall survival. The lymphatic and nervous systems represent two of the major understudied players in the tumor microenvironment and in the process of tumor metastasis. The intrinsic functional and structural characteristics of the lymphatic system suggest roles in immune regulation, cell trafficking, and interactions with other tissue networks and cell types, while the nearly 100% incidence of PDAC perineural invasion, mutual tumor-nerve tropism and paracrine secretions, and debilitating pain highlight the importance of nerves in the tumor microenvironment. Distortion of the physiological processes of lymphangiogenesis and neurogenesis in the tumor microenvironment and consequent effects on the biology of lymphatics, nerves, and tumor cells are complex and complicate targeting strategies. Clinical efforts to detect and use lymph node status or presence of PNI to inform treatment decisions, guide pancreatectomy, and stratify patients into prognostic cohorts have improved but remain inconsistent across groups and are not yet standardized or broadly applied. Identification, refinement, and directed studies of lymphatic- and nerve-specific metrics have highlighted the importance of these criteria as additional prognostic factors in this disease. Development of pre-clinical models of tumor-associated neurolymphatic remodeling, PNI, and lymph node metastasis and new lymphatic-directed clinical therapeutics represent two significant areas of current research. Live imaging studies in genetically engineered models that recapitulate both molecular and behavioral signatures of specific cancer types will improve our understanding of the earliest events in tumor-associated neurolymphatic remodeling, tumor-lymphatic/-nerve

interactions, and lymph node and perineural invasion. Translation of these and other preclinical findings to clinically-relevant diagnostic criteria or therapeutic interventions remains an underexplored but promising strategy to ultimately improve PDAC patient quality-of-life and outcomes.

Reference List

Abiatari, I., DeOliveira, T., Kerkadze, V., Schwager, C., Esposito, I., Giese, N.A., Huber, P., Bergman, F., Abdollahi, A., Friess, H., and Kleeff, J. (2009a). Consensus transcriptome signature of perineural invasion in pancreatic carcinoma. Mol. Cancer. Ther. *8,* 1494-1504.

Abiatari, I., Gillen, S., DeOliveira, T., Klose, T., Bo, K., Giese, N.A., Friess, H., and Kleeff, J. (2009b). The microtubule-associated protein MAPRE2 is involved in perineural invasion of pancreatic cancer cells. Int. J. Oncol. *35,* 1111-1116.

Achen, M.G., Jeltsch, M., Kukk, E., Makinen, T., Vitali, A., Wilks, A.F., Alitalo, K., and Stacker, S.A. (1998). Vascular endothelial growth factor D (VEGF-D) is a ligand for the tyrosine kinases VEGF receptor 2 (Flk1) and VEGF receptor 3 (Flt4). Proc. Natl. Acad. Sci. U. S. A. *95,* 548-553.

Adams, R.H., and Eichmann, A. (2010). Axon guidance molecules in vascular patterning. Cold Spring Harb Perspect. Biol. *2,* a001875.

Aebischer, D., Iolyeva, M., and Halin, C. (2014). The inflammatory response of lymphatic endothelium. Angiogenesis *17,* 383-393.

Ahn, H.K., Choi, J.Y., Kim, K.M., Kim, H., Choi, S.H., Park, S.H., Park, J.O., Lim, H.Y., Kang, W.K., Lee, J., and Park, Y.S. (2013). Phase II study of pazopanib monotherapy in metastatic gastroenteropancreatic neuroendocrine tumours. Br. J. Cancer *109,* 1414-1419.

Airaksinen, M.S., Titievsky, A., and Saarma, M. (1999). GDNF family neurotrophic factor signaling: four masters, one servant? Mol. Cell. Neurosci. *13,* 313-325.

Ali Khan, A., Mudassir, J., Mohtar, N., and Darwis, Y. (2013). Advanced drug delivery to the lymphatic system: lipid-based nanoformulations. Int. J. Nanomedicine *8,* 2733-2744.

Alitalo, A., and Detmar, M. (2012). Interaction of tumor cells and lymphatic vessels in cancer progression. Oncogene *31,* 4499-4508.

Angeli, V., Ginhoux, F., Llodra, J., Quemeneur, L., Frenette, P.S., Skobe, M., Jessberger, R., Merad, M., and Randolph, G.J. (2006). B cell-driven lymphangiogenesis in inflamed lymph nodes enhances dendritic cell mobilization. Immunity *24,* 203-215.

Argiles, J.M., Busquets, S., Stemmler, B., and Lopez-Soriano, F.J. (2014). Cancer cachexia: understanding the molecular basis. Nat. Rev. Cancer. *14,* 754-762.

Asp, M.L., Tian, M., Wendel, A.A., and Belury, M.A. (2010). Evidence for the contribution of insulin resistance to the development of cachexia in tumor-bearing mice. Int. J. Cancer *126,* 756-763.

Ausborn, N.L., Wang, T., Wentz, S.C., Washington, M.K., Merchant, N.B., Zhao, Z., Shyr, Y., Chakravarthy, A.B., and Xia, F. (2013). 53BP1 expression is a modifier of the prognostic value of lymph node ratio and CA 19-9 in pancreatic adenocarcinoma. BMC Cancer *13,* 155-2407-13-155.

Bailey, J.M., Swanson, B.J., Hamada, T., Eggers, J.P., Singh, P.K., Caffery, T., Ouellette, M.M., and Hollingsworth, M.A. (2008). Sonic hedgehog promotes desmoplasia in pancreatic cancer. Clin. Cancer Res. *14,* 5995-6004.

Baker, C.H., Solorzano, C.C., and Fidler, I.J. (2002). Blockade of vascular endothelial growth factor receptor and epidermal growth factor receptor signaling for therapy of metastatic human pancreatic cancer. Cancer Res. *62,* 1996-2003.

Baluk, P., Fuxe, J., Hashizume, H., Romano, T., Lashnits, E., Butz, S., Vestweber, D., Corada, M., Molendini, C., Dejana, E., and McDonald, D.M. (2007). Functionally specialized junctions between endothelial cells of lymphatic vessels. J. Exp. Med. *204,* 2349-2362.

Banerji, S., Ni, J., Wang, S.X., Clasper, S., Su, J., Tammi, R., Jones, M., and Jackson, D.G. (1999). LYVE-1, a new homologue of the CD44 glycoprotein, is a lymph-specific receptor for hyaluronan. J. Cell Biol. *144,* 789-801.

Bapat, A.A., Hostetter, G., Von Hoff, D.D., and Han, H. (2011). Perineural invasion and associated pain in pancreatic cancer. Nat. Rev. Cancer. *11,* 695-707.

Baracos, V.E. (2011). Pitfalls in defining and quantifying cachexia. J. Cachexia Sarcopenia Muscle *2,* 71-73.

Bazigou, E., Wilson, J.T., and Moore, J.E.,Jr. (2014). Primary and secondary lymphatic valve development: molecular, functional and mechanical insights. Microvasc. Res. *96,* 38-45.

Belmonte, C., Acosta, M.C., and Gallar, J. (2004). Neural basis of sensation in intact and injured corneas. Exp. Eye Res. *78,* 513-525.

Ben, Q.W., Wang, J.C., Liu, J., Zhu, Y., Yuan, F., Yao, W.Y., and Yuan, Y.Z. (2010). Positive expression of L1-CAM is associated with perineural invasion and poor outcome in pancreatic ductal adenocarcinoma. Ann. Surg. Oncol. *17,* 2213-2221.

Benassai, G., Mastrorilli, M., Mosella, F., and Mosella, G. (1999). Significance of lymph node metastases in the surgical management of pancreatic head carcinoma. J. Exp. Clin. Cancer Res. *18,* 23-28.

Berger, A.C., Watson, J.C., Ross, E.A., and Hoffman, J.P. (2004). The metastatic/examined lymph node ratio is an important prognostic factor after pancreaticoduodenectomy for pancreatic adenocarcinoma. Am. Surg. *70,* 235-40; discussion 240.

Bergers, G., and Hanahan, D. (2008). Modes of resistance to anti-angiogenic therapy. Nat. Rev. Cancer. *8,* 592-603.

Bhatti, I., Peacock, O., Awan, A.K., Semeraro, D., Larvin, M., and Hall, R.I. (2010). Lymph node ratio versus number of affected lymph nodes as predictors of survival for resected pancreatic adenocarcinoma. World J. Surg. *34,* 768-775.

Bianchi, R., Teijeira, A., Proulx, S.T., Christiansen, A.J., Seidel, C.D., Rulicke, T., Makinen, T., Hagerling, R., Halin, C., and Detmar, M. (2015). A transgenic Prox1-Cre-tdTomato reporter mouse for lymphatic vessel research. PLoS One *10,* e0122976.

Biankin, A.V., Waddell, N., Kassahn, K.S., Gingras, M.C., Muthuswamy, L.B., Johns, A.L., Miller, D.K., Wilson, P.J., Patch, A.M., Wu, J*., et al.* (2012). Pancreatic cancer genomes reveal aberrations in axon guidance pathway genes. Nature *491,* 399-405.

Bittner, R., Roscher, R., Safi, F., Dopfer, H.P., Scholzel, E., and Beger, H.G. (1989). Effect of tumor size and lymph node status on the prognosis of pancreatic cancer. Chirurg *60,* 240-245.

Bjorndahl, M., Cao, R., Nissen, L.J., Clasper, S., Johnson, L.A., Xue, Y., Zhou, Z., Jackson, D., Hansen, A.J., and Cao, Y. (2005a). Insulin-like growth factors 1 and 2 induce lymphangiogenesis in vivo. Proc. Natl. Acad. Sci. U. S. A. *102,* 15593-15598.

Bjorndahl, M.A., Cao, R., Burton, J.B., Brakenhielm, E., Religa, P., Galter, D., Wu, L., and Cao, Y. (2005b). Vascular endothelial growth factor-a promotes peritumoral lymphangiogenesis and lymphatic metastasis. Cancer Res. *65,* 9261-9268.

Blanco-Mezquita, T., Martinez-Garcia, C., Proenca, R., Zieske, J.D., Bonini, S., Lambiase, A., and Merayo-Lloves, J. (2013). Nerve growth factor promotes corneal epithelial migration by enhancing expression of matrix metalloprotease-9. Invest. Ophthalmol. Vis. Sci. *54,* 3880-3890.

Bock, F., Onderka, J., Dietrich, T., Bachmann, B., Kruse, F.E., Paschke, M., Zahn, G., and Cursiefen, C. (2007). Bevacizumab as a potent inhibitor of inflammatory corneal angiogenesis and lymphangiogenesis. Invest. Ophthalmol. Vis. Sci. *48,* 2545-2552.

Bock, F., Onderka, J., Rummelt, C., Dietrich, T., Bachmann, B., Kruse, F.E., Schlotzer-Schrehardt, U., and Cursiefen, C. (2009). Safety profile of topical VEGF neutralization at the cornea. Invest. Ophthalmol. Vis. Sci. *50,* 2095-2102.

Bockman, D.E. (2007). Nerves in the pancreas: what are they for? Am. J. Surg. *194 (Suppl to October 2007),* S61-S64.

Bockman, D.E., Buchler, M., and Beger, H.G. (1994). Interaction of pancreatic ductal carcinoma with nerves leads to nerve damage. Gastroenterology *107,* 219-230.

Bodine, S.C., Latres, E., Baumhueter, S., Lai, V.K., Nunez, L., Clarke, B.A., Poueymirou, W.T., Panaro, F.J., Na, E., Dharmarajan, K*., et al.* (2001). Identification of ubiquitin ligases required for skeletal muscle atrophy. Science *294,* 1704-1708.

Bogoevski, D., Yekebas, E.F., Schurr, P., Kaifi, J.T., Kutup, A., Erbersdobler, A., Pantel, K., and Izbicki, J.R. (2004). Mode of spread in the early phase of lymphatic metastasis in pancreatic ductal adenocarcinoma: prognostic significance of nodal microinvolvement. Ann. Surg. *240,* 993-1000; discussion 1000-1.

Boj, S.F., Hwang, C.I., Baker, L.A., Chio, I.I., Engle, D.D., Corbo, V., Jager, M., Ponz-Sarvise, M., Tiriac, H., Spector, M.S*., et al.* (2015). Organoid models of human and mouse ductal pancreatic cancer. Cell *160,* 324-338.

Bonini, S., Lambiase, A., Rama, P., Caprioglio, G., and Aloe, L. (2000). Topical treatment with nerve growth factor for neurotrophic keratitis. Ophthalmology *107,* 1347-51; discussion 1351-2.

Bouvree, K., Brunet, I., Del Toro, R., Gordon, E., Prahst, C., Cristofaro, B., Mathivet, T., Xu, Y., Soueid, J., Fortuna, V*., et al.* (2012). Semaphorin3A, Neuropilin-1, and PlexinA1 are required for lymphatic valve formation. Circ. Res. *111,* 437-445.

Breiteneder-Geleff, S., Matsui, K., Soleiman, A., Meraner, P., Poczewski, H., Kalt, R., Schaffner, G., and Kerjaschki, D. (1997). Podoplanin, novel 43-kd membrane protein of glomerular epithelial cells, is down-regulated in puromycin nephrosis. Am. J. Pathol. *151,* 1141-1152.

Buc, E., Couvelard, A., Kwiatkowski, F., Dokmak, S., Ruszniewski, P., Hammel, P., Belghiti, J., and Sauvanet, A. (2014). Adenocarcinoma of the pancreas: Does prognosis depend on mode of lymph node invasion? Eur. J. Surg. Oncol. *40,* 1578-1585.

Buchler, P., Gazdhar, A., Schubert, M., Giese, N., Reber, H.A., Hines, O.J., Giese, T., Ceyhan, G.O., Muller, M., Buchler, M.W., and Friess, H. (2005). The Notch signaling pathway is related to neurovascular progression of pancreatic cancer. Ann. Surg. *242,* 791-800, discussion 800-1.

Burton, J.B., Priceman, S.J., Sung, J.L., Brakenhielm, E., An, D.S., Pytowski, B., Alitalo, K., and Wu, L. (2008). Suppression of prostate cancer nodal and systemic metastasis by blockade of the lymphangiogenic axis. Cancer Res. *68,* 7828-7837.

Calza, L., Giardino, L., Giuliani, A., Aloe, L., and Levi-Montalcini, R. (2001). Nerve growth factor control of neuronal expression of angiogenetic and vasoactive factors. Proc. Natl. Acad. Sci. U. S. A. *98,* 4160-4165.

Cao, R., Bjorndahl, M.A., Gallego, M.I., Chen, S., Religa, P., Hansen, A.J., and Cao, Y. (2006). Hepatocyte growth factor is a lymphangiogenic factor with an indirect mechanism of action. Blood *107,* 3531-3536.

Cao, R., Bjorndahl, M.A., Religa, P., Clasper, S., Garvin, S., Galter, D., Meister, B., Ikomi, F., Tritsaris, K., Dissing, S*., et al.* (2004a). PDGF-BB induces intratumoral lymphangiogenesis and promotes lymphatic metastasis. Cancer. Cell. *6,* 333-345.

Cao, R., Eriksson, A., Kubo, H., Alitalo, K., Cao, Y., and Thyberg, J. (2004). Comparative evaluation of FGF-2-, VEGF-A-, and VEGF-C-induced angiogenesis, lymphangiogenesis, vascular fenestrations, and permeability. Circ. Res. *94,* 664-670.

Cao, R., Ji, H., Feng, N., Zhang, Y., Yang, X., Andersson, P., Sun, Y., Tritsaris, K., Hansen, A.J., Dissing, S., and Cao, Y. (2012). Collaborative interplay between FGF-2 and VEGF-C promotes lymphangiogenesis and metastasis. Proc. Natl. Acad. Sci. U. S. A. *109,* 15894-15899.

Cao, R., Lim, S., Ji, H., Zhang, Y., Yang, Y., Honek, J., Hedlund, E.M., and Cao, Y. (2011). Mouse corneal lymphangiogenesis model. Nat. Protoc. *6,* 817-826.

Cao, Y., Linden, P., Farnebo, J., Cao, R., Eriksson, A., Kumar, V., Qi, J.H., Claesson-Welsh, L., and Alitalo, K. (1998). Vascular endothelial growth factor C induces angiogenesis in vivo. Proc. Natl. Acad. Sci. U. S. A. *95,* 14389-14394.

Cardin, D.B., Goff, L., Li, C.I., Shyr, Y., Winkler, C., DeVore, R., Schlabach, L., Holloway, M., McClanahan, P., Meyer, K.*, et al.* (2014). Phase II trial of sorafenib and erlotinib in advanced pancreatic cancer. Cancer. Med. *3,* 572-579.

Cardones, A.R., Murakami, T., and Hwang, S.T. (2003). CXCR4 enhances adhesion of B16 tumor cells to endothelial cells in vitro and in vivo via beta(1) integrin. Cancer Res. *63,* 6751-6757.

Carlson, S.L., Albers, K.M., Beiting, D.J., Parish, M., Conner, J.M., and Davis, B.M. (1995). NGF modulates sympathetic innervation of lymphoid tissues. J. Neurosci. *15,* 5892-5899.

Caunt, M., Mak, J., Liang, W.C., Stawicki, S., Pan, Q., Tong, R.K., Kowalski, J., Ho, C., Reslan, H.B., Ross, J.*, et al.* (2008). Blocking neuropilin-2 function inhibits tumor cell metastasis. Cancer. Cell. *13,* 331-342.

Cellini, M., Bendo, E., Bravetti, G.O., and Campos, E.C. (2006). The use of nerve growth factor in surgical wound healing of the cornea. Ophthalmic Res. *38,* 177-181.

Cesmebasi, A., Malefant, J., Patel, S.D., Du Plessis, M., Renna, S., Tubbs, R.S., and Loukas, M. (2015). The surgical anatomy of the lymphatic system of the pancreas. Clin. Anat. *28,* 527-537.

Ceyhan, G.O., Bergmann, F., Kadihasanoglu, M., Altintas, B., Demir, I.E., Hinz, U., Muller, M.W., Giese, T., Buchler, M.W., Giese, N.A., and Friess, H. (2009a). Pancreatic neuropathy and neuropathic pain--a comprehensive pathomorphological study of 546 cases. Gastroenterology *136,* 177-186.e1.

Ceyhan, G.O., Demir, I.E., Altintas, B., Rauch, U., Thiel, G., Muller, M.W., Giese, N.A., Friess, H., and Schafer, K.H. (2008). Neural invasion in pancreatic cancer: a mutual tropism between neurons and cancer cells. Biochem. Biophys. Res. Commun. *374,* 442-447.

Ceyhan, G.O., Demir, I.E., Rauch, U., Bergmann, F., Muller, M.W., Buchler, M.W., Friess, H., and Schafer, K.H. (2009b). Pancreatic neuropathy results in "neural remodeling" and altered pancreatic innervation in chronic pancreatitis and pancreatic cancer. Am. J. Gastroenterol. *104,* 2555-2565.

Ceyhan, G.O., Deucker, S., Demir, I.E., Erkan, M., Schmelz, M., Bergmann, F., Muller, M.W., Giese, T., Buchler, M.W., Giese, N.A., and Friess, H. (2009c). Neural fractalkine expression is closely linked to pain and pancreatic neuritis in human chronic pancreatitis. Lab. Invest. *89,* 347-361.

Ceyhan, G.O., Giese, N.A., Erkan, M., Kerscher, A.G., Wente, M.N., Giese, T., Buchler, M.W., and Friess, H. (2006). The neurotrophic factor artemin promotes pancreatic cancer invasion. Ann. Surg. *244,* 274-281.

Ceyhan, G.O., Schafer, K.H., Kerscher, A.G., Rauch, U., Demir, I.E., Kadihasanoglu, M., Bohm, C., Muller, M.W., Buchler, M.W., Giese, N.A., Erkan, M., and Friess, H. (2010). Nerve growth factor and artemin are paracrine mediators of pancreatic neuropathy in pancreatic adenocarcinoma. Ann. Surg. *251,* 923-931.

Chang, D.K., Johns, A.L., Merrett, N.D., Gill, A.J., Colvin, E.K., Scarlett, C.J., Nguyen, N.Q., Leong, R.W., Cosman, P.H., Kelly, M.I*., et al.* (2009). Margin clearance and outcome in resected pancreatic cancer. J. Clin. Oncol. *27,* 2855-2862.

Chauvet, S., Burk, K., and Mann, F. (2013). Navigation rules for vessels and neurons: cooperative signaling between VEGF and neural guidance cues. Cell Mol. Life Sci. *70,* 1685-1703.

Chen, H.M., Tsai, C.H., and Hung, W.C. (2015). Foretinib inhibits angiogenesis, lymphangiogenesis and tumor growth of pancreatic cancer in vivo by decreasing VEGFR-2/3 and TIE-2 signaling. Oncotarget *6,* 14940-14952.

Chen, J.W., Bhandari, M., Astill, D.S., Wilson, T.G., Kow, L., Brooke-Smith, M., Toouli, J., and Padbury, R.T. (2010). Predicting patient survival after pancreaticoduodenectomy for malignancy: histopathological criteria based on perineural infiltration and lymphovascular invasion. HPB (Oxford) *12,* 101-108.

Chen, Z., Varney, M.L., Backora, M.W., Cowan, K., Solheim, J.C., Talmadge, J.E., and Singh, R.K. (2005). Down-regulation of vascular endothelial cell growth factor-C expression using small interfering RNA vectors in mammary tumors inhibits tumor lymphangiogenesis and spontaneous metastasis and enhances survival. Cancer Res. *65,* 9004-9011.

Cheng, P., Jin, G., Hu, X., Shi, M., Zhang, Y., Liu, R., Zhou, Y., Shao, C., Zheng, J., and Zhu, M. (2012). Analysis of tumor-induced lymphangiogenesis and lymphatic vessel invasion of pancreatic carcinoma in the peripheral nerve plexus. Cancer. Sci. *103,* 1756-1763.

Chien, M.H., Ku, C.C., Johansson, G., Chen, M.W., Hsiao, M., Su, J.L., Inoue, H., Hua, K.T., Wei, L.H., and Kuo, M.L. (2009). Vascular endothelial growth factor-C (VEGF-C) promotes angiogenesis by induction of COX-2 in leukemic cells via the VEGF-R3/JNK/AP-1 pathway. Carcinogenesis *30,* 2005-2013.

Choi, I., Chung, H.K., Ramu, S., Lee, H.N., Kim, K.E., Lee, S., Yoo, J., Choi, D., Lee, Y.S., Aguilar, B., and Hong, Y.K. (2011). Visualization of lymphatic vessels by Prox1-promoter directed GFP reporter in a bacterial artificial chromosome-based transgenic mouse. Blood *117,* 362-365.

Christians, K., and Evans, D.B. (2009). Pancreaticoduodenectomy and vascular resection: persistent controversy and current recommendations. Ann. Surg. Oncol. *16,* 789-791.

Chu, H., Zhou, H., Liu, Y., Liu, X., Hu, Y., and Zhang, J. (2007). Functional expression of CXC chemokine recepter-4 mediates the secretion of matrix metalloproteinases from mouse hepatocarcinoma cell lines with different lymphatic metastasis ability. Int. J. Biochem. Cell Biol. *39,* 197-205.

Chung, K., and Deisseroth, K. (2013). CLARITY for mapping the nervous system. Nat. Methods *10,* 508-513.

Chung, K., Wallace, J., Kim, S.Y., Kalyanasundaram, S., Andalman, A.S., Davidson, T.J., Mirzabekov, J.J., Zalocusky, K.A., Mattis, J., Denisin, A.K.*, et al.* (2013). Structural and molecular interrogation of intact biological systems. Nature *497,* 332-337.

Coma, S., Allard-Ratick, M., Akino, T., van Meeteren, L.A., Mammoto, A., and Klagsbrun, M. (2013). GATA2 and Lmo2 control angiogenesis and lymphangiogenesis via direct transcriptional regulation of neuropilin-2. Angiogenesis *16,* 939-952.

Condeelis, J., and Pollard, J.W. (2006). Macrophages: obligate partners for tumor cell migration, invasion, and metastasis. Cell *124,* 263-266.

Cong, L., Ran, F.A., Cox, D., Lin, S., Barretto, R., Habib, N., Hsu, P.D., Wu, X., Jiang, W., Marraffini, L.A., and Zhang, F. (2013). Multiplex genome engineering using CRISPR/Cas systems. Science *339,* 819-823.

Connor, A.L., Kelley, P.M., and Tempero, R.M. (2016). Lymphatic endothelial lineage assemblage during corneal lymphangiogenesis. Lab. Invest. *96,* 270-282.

Crnic, I., Strittmatter, K., Cavallaro, U., Kopfstein, L., Jussila, L., Alitalo, K., and Christofori, G. (2004). Loss of neural cell adhesion molecule induces tumor metastasis by up-regulating lymphangiogenesis. Cancer Res. *64,* 8630-8638.

Cui, K., Zhao, W., Wang, C., Wang, A., Zhang, B., Zhou, W., Yu, J., Sun, Z., and Li, S. (2011). The CXCR4-CXCL12 pathway facilitates the progression of pancreatic cancer via induction of angiogenesis and lymphangiogenesis. J. Surg. Res. *171,* 143-150.

Cui, Y., Wu, J., Zong, M., Song, G., Jia, Q., Jiang, J., and Han, J. (2009). Proteomic profiling in pancreatic cancer with and without lymph node metastasis. Int. J. Cancer *124,* 1614-1621.

Cursiefen, C., Chen, L., Borges, L.P., Jackson, D., Cao, J., Radziejewski, C., D'Amore, P.A., Dana, M.R., Wiegand, S.J., and Streilein, J.W. (2004). VEGF-A stimulates lymphangiogenesis and hemangiogenesis in inflammatory neovascularization via macrophage recruitment. J. Clin. Invest. *113,* 1040-1050.

Da, M.X., Wu, Z., and Tian, H.W. (2008). Tumor lymphangiogenesis and lymphangiogenic growth factors. Arch. Med. Res. *39,* 365-372.

Dadras, S.S. (2013). An unexpected role for EGF in lymphangiogenesis-mediated melanoma metastasis to sentinel lymph nodes. J. Invest. Dermatol. *133,* 14-16.

Dai, H., Li, R., Wheeler, T., Ozen, M., Ittmann, M., Anderson, M., Wang, Y., Rowley, D., Younes, M., and Ayala, G.E. (2007). Enhanced survival in perineural invasion of pancreatic cancer: an in vitro approach. Hum. Pathol. *38,* 299-307.

Dallas, N.A., Gray, M.J., Xia, L., Fan, F., van Buren, G.,2nd, Gaur, P., Samuel, S., Lim, S.J., Arumugam, T., Ramachandran, V., Wang, H., and Ellis, L.M. (2008). Neuropilin-2-mediated tumor growth and angiogenesis in pancreatic adenocarcinoma. Clin. Cancer Res. *14,* 8052-8060.

Dansranjavin, T., Mobius, C., Tannapfel, A., Bartels, M., Wittekind, C., Hauss, J., and Witzigmann, H. (2006). E-cadherin and DAP kinase in pancreatic adenocarcinoma and corresponding lymph node metastases. Oncol. Rep. *15,* 1125-1131.

Dasari, B.V., Pasquali, S., Vohra, R.S., Smith, A.M., Taylor, M.A., Sutcliffe, R.P., Muiesan, P., Roberts, K.J., Isaac, J., and Mirza, D.F. (2015). Extended Versus Standard Lymphadenectomy for Pancreatic Head Cancer: Meta-Analysis of Randomized Controlled Trials. J. Gastrointest. Surg. *19,* 1725-1732.

de Castro, F., Silos-Santiago, I., Lopez de Armentia, M., Barbacid, M., and Belmonte, C. (1998). Corneal innervation and sensitivity to noxious stimuli in trkA knockout mice. Eur. J. Neurosci. *10,* 146-152.

de Matos-Neto, E.M., Lima, J.D., de Pereira, W.O., Figueredo, R.G., Riccardi, D.M., Radloff, K., das Neves, R.X., Camargo, R.G., Maximiano, L.F., Tokeshi, F.*, et al.* (2015). Systemic Inflammation in Cachexia - Is Tumor Cytokine Expression Profile the Culprit? Front. Immunol. *6,* 629.

De Smedt, T., Van Mechelen, M., De Becker, G., Urbain, J., Leo, O., and Moser, M. (1997). Effect of interleukin-10 on dendritic cell maturation and function. Eur. J. Immunol. *27,* 1229-1235.

Dejana, E., Orsenigo, F., Molendini, C., Baluk, P., and McDonald, D.M. (2009). Organization and signaling of endothelial cell-to-cell junctions in various regions of the blood and lymphatic vascular trees. Cell Tissue Res. *335,* 17-25.

Delcore, R., Rodriguez, F.J., Forster, J., Hermreck, A.S., and Thomas, J.H. (1996). Significance of lymph node metastases in patients with pancreatic cancer undergoing curative resection. Am. J. Surg. *172,* 463-8; discussion 468-9.

Demeure, M.J., Doffek, K.M., Komorowski, R.A., and Wilson, S.D. (1998). Adenocarcinoma of the pancreas: detection of occult metastases in regional lymph nodes by a polymerase chain reaction-based assay. Cancer *83,* 1328-1334.

Demir, I.E., Ceyhan, G.O., Rauch, U., Altintas, B., Klotz, M., Muller, M.W., Buchler, M.W., Friess, H., and Schafer, K.H. (2010). The microenvironment in chronic pancreatitis and pancreatic cancer induces neuronal plasticity. Neurogastroenterol. Motil. *22,* 480-90, e112-3.

Detry, B., Blacher, S., Erpicum, C., Paupert, J., Maertens, L., Maillard, C., Munaut, C., Sounni, N.E., Lambert, V., Foidart, J.M.*, et al.* (2013). Sunitinib inhibits inflammatory corneal lymphangiogenesis. Invest. Ophthalmol. Vis. Sci. *54,* 3082-3093.

DiMagno, E.P., Reber, H.A., and Tempero, M.A. (1999). AGA technical review on the epidemiology, diagnosis, and treatment of pancreatic ductal adenocarcinoma. American Gastroenterological Association. Gastroenterology *117,* 1464-1484.

Ding, M., Fu, X., Tan, H., Wang, R., Chen, Z., and Ding, S. (2012). The effect of vascular endothelial growth factor C expression in tumor-associated macrophages on lymphangiogenesis and lymphatic metastasis in breast cancer. Mol. Med. Rep. *6,* 1023-1029.

Doi, R., Kami, K., Ito, D., Fujimoto, K., Kawaguchi, Y., Wada, M., Kogire, M., Hosotani, R., Imamura, M., and Uemoto, S. (2007). Prognostic implication of para-aortic lymph node metastasis in resectable pancreatic cancer. World J. Surg. *31,* 147-154.

Donaghy, M. (2003). Enlarged peripheral nerves. Practical Neurology *3,* 40-45.

D'Orlando, C., Marzetti, E., Francois, S., Lorenzi, M., Conti, V., di Stasio, E., Rosa, F., Brunelli, S., Doglietto, G.B., Pacelli, F., and Bossola, M. (2014). Gastric cancer does not affect the expression of atrophy-related genes in human skeletal muscle. Muscle Nerve *49,* 528-533.

Dragovich, T., Laheru, D., Dayyani, F., Bolejack, V., Smith, L., Seng, J., Burris, H., Rosen, P., Hidalgo, M., Ritch, P.*, et al.* (2014). Phase II trial of vatalanib in patients with advanced or metastatic pancreatic adenocarcinoma after first-line gemcitabine therapy (PCRT O4-001). Cancer Chemother. Pharmacol. *74,* 379-387.

Drevs, J., Hofmann, I., Hugenschmidt, H., Wittig, C., Madjar, H., Muller, M., Wood, J., Martiny-Baron, G., Unger, C., and Marme, D. (2000). Effects of PTK787/ZK 222584, a specific inhibitor of vascular endothelial growth factor receptor tyrosine kinases, on primary tumor, metastasis, vessel density, and blood flow in a murine renal cell carcinoma model. Cancer Res. *60,* 4819-4824.

Du, Q., Jiang, L., Wang, X., Wang, M., She, F., and Chen, Y. (2014). Tumor necrosis factor-alpha promotes the lymphangiogenesis of gallbladder carcinoma through nuclear factor-kappaB-mediated upregulation of vascular endothelial growth factor-C. Cancer. Sci. *105,* 1261-1271.

Duanmin, H., Chao, X., and Qi, Z. (2013). eEF1A2 protein expression correlates with lymph node metastasis and decreased survival in pancreatic ductal adenocarcinoma. Hepatogastroenterology *60,* 870-875.

Dunne, A.A., Boerner, H.G., Kukula, H., Schlaad, H., Wiegand, S., Werner, J.A., and Antonietti, M. (2007). Block copolymer carrier systems for translymphatic chemotherapy of lymph node metastases. Anticancer Res. *27,* 3935-3940.

Duong, T., Koopman, P., and Francois, M. (2012). Tumor lymphangiogenesis as a potential therapeutic target. J. Oncol. *2012,* 204946.

Emmett, M.S., Lanati, S., Dunn, D.B., Stone, O.A., and Bates, D.O. (2011). CCR7 mediates directed growth of melanomas towards lymphatics. Microcirculation *18,* 172-182.

Entschladen, F., Palm, D., Lang, K., Drell, T.L.,4th, and Zaenker, K.S. (2006). Neoneurogenesis: tumors may initiate their own innervation by the release of neurotrophic factors in analogy to lymphangiogenesis and neoangiogenesis. Med. Hypotheses *67,* 33-35.

Entschladen, F., Palm, D., Niggemann, B., and Zaenker, K.S. (2008). The cancer's nervous tooth: Considering the neuronal crosstalk within tumors. Semin. Cancer Biol. *18,* 171-175.

Esquenazi, S., Bazan, H.E., Bui, V., He, J., Kim, D.B., and Bazan, N.G. (2005). Topical combination of NGF and DHA increases rabbit corneal nerve regeneration after photorefractive keratectomy. Invest. Ophthalmol. Vis. Sci. *46,* 3121-3127.

Evans, D.B., Farnell, M.B., Lillemoe, K.D., Vollmer, C.,Jr, Strasberg, S.M., and Schulick, R.D. (2009). Surgical treatment of resectable and borderline resectable pancreas cancer: expert consensus statement. Ann. Surg. Oncol. *16,* 1736-1744.

Ewens, A., Mihich, E., and Ehrke, M.J. (2005). Distant metastasis from subcutaneously grown E0771 medullary breast adenocarcinoma. Anticancer Res. *25,* 3905-3915.

Fagiani, E., Lorentz, P., Kopfstein, L., and Christofori, G. (2011). Angiopoietin-1 and -2 exert antagonistic functions in tumor angiogenesis, yet both induce lymphangiogenesis. Cancer Res. *71,* 5717-5727.

Fallarino, F., Grohmann, U., You, S., McGrath, B.C., Cavener, D.R., Vacca, C., Orabona, C., Bianchi, R., Belladonna, M.L., Volpi, C.*, et al.* (2006). The combined effects of tryptophan starvation and tryptophan catabolites down-regulate T cell receptor zeta-chain and induce a regulatory phenotype in naive T cells. J. Immunol. *176,* 6752-6761.

Farnell, M.B., Aranha, G.V., Nimura, Y., and Michelassi, F. (2008). The role of extended lymphadenectomy for adenocarcinoma of the head of the pancreas: strength of the evidence. J. Gastrointest. Surg. *12,* 651-656.

Farnell, M.B., Pearson, R.K., Sarr, M.G., DiMagno, E.P., Burgart, L.J., Dahl, T.R., Foster, N., Sargent, D.J., and Pancreas Cancer Working Group. (2005). A prospective randomized trial comparing standard pancreatoduodenectomy with pancreatoduodenectomy with extended lymphadenectomy in resectable pancreatic head adenocarcinoma. Surgery *138,* 618-28; discussion 628-30.

Farrow, B., Albo, D., and Berger, D.H. (2008). The role of the tumor microenvironment in the progression of pancreatic cancer. J. Surg. Res. *149,* 319-328.

Favier, B., Alam, A., Barron, P., Bonnin, J., Laboudie, P., Fons, P., Mandron, M., Herault, J.P., Neufeld, G., Savi, P., Herbert, J.M., and Bono, F. (2006). Neuropilin-2 interacts with VEGFR-2 and VEGFR-3 and promotes human endothelial cell survival and migration. Blood *108,* 1243-1250.

Fearon, K., Strasser, F., Anker, S.D., Bosaeus, I., Bruera, E., Fainsinger, R.L., Jatoi, A., Loprinzi, C., MacDonald, N., Mantovani, G.*, et al.* (2011). Definition and classification of cancer cachexia: an international consensus. Lancet Oncol. *12,* 489-495.

Feig, C., Gopinathan, A., Neesse, A., Chan, D.S., Cook, N., and Tuveson, D.A. (2012). The pancreas cancer microenvironment. Clin. Cancer Res. *18,* 4266-4276.

Feig, C., Jones, J.O., Kraman, M., Wells, R.J., Deonarine, A., Chan, D.S., Connell, C.M., Roberts, E.W., Zhao, Q., Caballero, O.L*., et al.* (2013). Targeting CXCL12 from FAP-expressing carcinoma-associated fibroblasts synergizes with anti-PD-L1 immunotherapy in pancreatic cancer. Proc. Natl. Acad. Sci. U. S. A. *110,* 20212-20217.

Fernandez-Cruz, L., Johnson, C., and Dervenis, C. (1999). Locoregional dissemination and extended lymphadenectomy in pancreatic cancer. Dig. Surg. *16,* 313-319.

Ferrari, G., Hajrasouliha, A.R., Sadrai, Z., Ueno, H., Chauhan, S.K., and Dana, R. (2013). Nerves and neovessels inhibit each other in the cornea. Invest. Ophthalmol. Vis. Sci. *54,* 813-820.

Fink, D.M., Connor, A.L., Kelley, P.M., Steele, M.M., Hollingsworth, M.A., and Tempero, R.M. (2014a). Nerve growth factor regulates neurolymphatic remodeling during corneal inflammation and resolution. PLoS One *9,* e112737.

Fink, D.M., Connor, A.L., Kelley, P.M., Tempero, R.M., and Hollingsworth, M.A. Metastatic tumor migration in lymphatic vessels revealed by real-time intravital imaging [abstract]. In: Proceedings of the 105th Annual Meeting of the American Association for Cancer Research; 2014b Apr 5-9; San Diego, CA. Philadelphia (PA): AACR; (2014b). Abstract nr 4942.

Fink, D.M., Steele, M.M., and Hollingsworth, M.A. (2015a). The lymphatic system and pancreatic cancer. Cancer Lett. 2015 Dec 29. pii:S0304-3835(15)00745-4. doi: 10.1016/j.canlet.2015.11.048. [Epub ahead of print].

Fink, D.M., Connor, A.L., Kelley, P.M., Tempero, R.M., and Hollingsworth, M.A. Inflamed and wound recovered tumor microenvironment contributions to lymphatic-mediated metastasis [abstract]. In: Proceedings of the 106th Annual Meeting of the American Association for Cancer Research; 2015 Apr 18-22; Philadelphia, PA. Philadelphia (PA): AACR; (2015b). Abstract nr 5220.

Fischer, C., Jonckx, B., Mazzone, M., Zacchigna, S., Loges, S., Pattarini, L., Chorianopoulos, E., Liesenborghs, L., Koch, M., De Mol, M*., et al.* (2007). Anti-PlGF inhibits growth of VEGF(R)-inhibitor-resistant tumors without affecting healthy vessels. Cell *131,* 463-475.

Fogelman, D.R., Holmes, H., Mohammed, K., Katz, M.H., Prado, C.M., Lieffers, J., Garg, N., Varadhachary, G.R., Shroff, R., Overman, M.J*., et al.* (2014). Does IGFR1 inhibition result in increased muscle mass loss in patients undergoing treatment for pancreatic cancer? J. Cachexia Sarcopenia Muscle *5,* 307-313.

Formentini, A., Prokopchuk, O., Strater, J., Kleeff, J., Grochola, L.F., Leder, G., Henne-Bruns, D., Korc, M., and Kornmann, M. (2009). Interleukin-13 exerts autocrine growth-promoting effects on human pancreatic cancer, and its expression correlates with a propensity for lymph node metastases. Int. J. Colorectal Dis. *24,* 57-67.

Fujii, T. (2013). Extended lymphadenectomy in pancreatic cancer is crucial. World J. Surg. *37,* 1778-1781.

Fujita, T., Nakagohri, T., Gotohda, N., Takahashi, S., Konishi, M., Kojima, M., and Kinoshita, T. (2010). Evaluation of the prognostic factors and significance of lymph node status in invasive ductal carcinoma of the body or tail of the pancreas. Pancreas *39,* e48-54.

Fukahi, K., Fukasawa, M., Neufeld, G., Itakura, J., and Korc, M. (2004). Aberrant expression of neuropilin-1 and -2 in human pancreatic cancer cells. Clin. Cancer Res. *10,* 581-590.

Fukuda, M., Kusama, K., and Sakashita, H. (2008). Cimetidine inhibits salivary gland tumor cell adhesion to neural cells and induces apoptosis by blocking NCAM expression. BMC Cancer *8,* 376-2407-8-376.

Gallagher, I.J., Stephens, N.A., MacDonald, A.J., Skipworth, R.J., Husi, H., Greig, C.A., Ross, J.A., Timmons, J.A., and Fearon, K.C. (2012). Suppression of skeletal muscle turnover in cancer cachexia: evidence from the transcriptome in sequential human muscle biopsies. Clin. Cancer Res. *18,* 2817-2827.

Geboes, K., and Collins, S. (1998). Structural abnormalities of the nervous system in Crohn's disease and ulcerative colitis. Neurogastroenterol. Motil. *10,* 189-202.

Gelfand, M.V., Hong, S., and Gu, C. (2009). Guidance from above: common cues direct distinct signaling outcomes in vascular and neural patterning. Trends Cell Biol. *19,* 99-110.

Gerdes, B., Ramaswamy, A., Bartsch, D.K., and Rothmund, M. (2005). Peripyloric lymph node metastasis is a rare condition in carcinoma of the pancreatic head. Pancreas *31,* 88-92.

Gerli, R., Solito, R., Weber, E., and Agliano, M. (2000). Specific adhesion molecules bind anchoring filaments and endothelial cells in human skin initial lymphatics. Lymphology *33,* 148-157.

Ghiringhelli, F., Puig, P.E., Roux, S., Parcellier, A., Schmitt, E., Solary, E., Kroemer, G., Martin, F., Chauffert, B., and Zitvogel, L. (2005). Tumor cells convert immature myeloid dendritic cells into TGF-beta-secreting cells inducing CD4+CD25+ regulatory T cell proliferation. J. Exp. Med. *202,* 919-929.

Gil, Z., Cavel, O., Kelly, K., Brader, P., Rein, A., Gao, S.P., Carlson, D.L., Shah, J.P., Fong, Y., and Wong, R.J. (2010). Paracrine regulation of pancreatic cancer cell invasion by peripheral nerves. J. Natl. Cancer Inst. *102,* 107-118.

Goel, S., Duda, D.G., Xu, L., Munn, L.L., Boucher, Y., Fukumura, D., and Jain, R.K. (2011). Normalization of the vasculature for treatment of cancer and other diseases. Physiol. Rev. *91,* 1071-1121.

Goel, S., Wong, A.H., and Jain, R.K. (2012). Vascular normalization as a therapeutic strategy for malignant and nonmalignant disease. Cold Spring Harb Perspect. Med. *2,* a006486.

Gohrig, A., Detjen, K.M., Hilfenhaus, G., Korner, J.L., Welzel, M., Arsenic, R., Schmuck, R., Bahra, M., Wu, J.Y., Wiedenmann, B., and Fischer, C. (2014). Axon guidance factor SLIT2 inhibits neural invasion and metastasis in pancreatic cancer. Cancer Res. *74,* 1529-1540.

Golse, N., Lebeau, R., Lombard-Bohas, C., Hervieu, V., Ponchon, T., and Adham, M. (2013). Lymph node involvement beyond peripancreatic region in pancreatic head cancers: when results belie expectations. Pancreas *42,* 239-248.

Goncalves, A., Gilabert, M., Francois, E., Dahan, L., Perrier, H., Lamy, R., Re, D., Largillier, R., Gasmi, M., Tchiknavorian, X*., et al.* (2012). BAYPAN study: a double-blind phase III randomized trial comparing gemcitabine plus sorafenib and gemcitabine plus placebo in patients with advanced pancreatic cancer. Ann. Oncol. *23,* 2799-2805.

Gresham, G.K., Wells, G.A., Gill, S., Cameron, C., and Jonker, D.J. (2014). Chemotherapy regimens for advanced pancreatic cancer: a systematic review and network meta-analysis. BMC Cancer *14,* 471-2407-14-471.

Grunwald, V., and Merseburger, A.S. (2012). Axitinib for the treatment of patients with advanced metastatic renal cell carcinoma (mRCC) after failure of prior systemic treatment. Onco Targets Ther. *5,* 111-117.

Guerra, C., Collado, M., Navas, C., Schuhmacher, A.J., Hernandez-Porras, I., Canamero, M., Rodriguez-Justo, M., Serrano, M., and Barbacid, M. (2011). Pancreatitis-induced inflammation contributes to pancreatic cancer by inhibiting oncogene-induced senescence. Cancer. Cell. *19,* 728-739.

Guerra, C., Schuhmacher, A.J., Canamero, M., Grippo, P.J., Verdaguer, L., Perez-Gallego, L., Dubus, P., Sandgren, E.P., and Barbacid, M. (2007). Chronic pancreatitis is essential for induction of pancreatic ductal adenocarcinoma by K-Ras oncogenes in adult mice. Cancer. Cell. *11,* 291-302.

Gunther, K., Leier, J., Henning, G., Dimmler, A., Weissbach, R., Hohenberger, W., and Forster, R. (2005). Prediction of lymph node metastasis in colorectal carcinoma by expressionof chemokine receptor CCR7. Int. J. Cancer *116,* 726-733.

Guo, J., Lou, W., Ji, Y., and Zhang, S. (2013). Effect of CCR7, CXCR4 and VEGF-C on the lymph node metastasis of human pancreatic ductal adenocarcinoma. Oncol. Lett. *5,* 1572-1578.

Hagerling, R., Pollmann, C., Kremer, L., Andresen, V., and Kiefer, F. (2011). Intravital two-photon microscopy of lymphatic vessel development and function using a transgenic Prox1 promoter-directed mOrange2 reporter mouse. Biochem. Soc. Trans. *39,* 1674-1681.

Hall, K.L., Volk-Draper, L.D., Flister, M.J., and Ran, S. (2012). New model of macrophage acquisition of the lymphatic endothelial phenotype. PLoS One *7,* e31794.

Hanahan, D., and Coussens, L.M. (2012). Accessories to the crime: functions of cells recruited to the tumor microenvironment. Cancer. Cell. *21,* 309-322.

Harrell, M.I., Iritani, B.M., and Ruddell, A. (2007). Tumor-induced sentinel lymph node lymphangiogenesis and increased lymph flow precede melanoma metastasis. Am. J. Pathol. *170,* 774-786.

Hartveit, E. (1990). Attenuated cells in breast stroma: the missing lymphatic system of the breast. Histopathology *16,* 533-543.

He, H., Di, Y., Liang, M., Yang, F., Yao, L., Hao, S., Li, J., Jiang, Y., Jin, C., and Fu, D. (2013a). The microRNA-218 and ROBO-1 signaling axis correlates with the lymphatic metastasis of pancreatic cancer. Oncol. Rep. *30,* 651-658.

He, W.A., Berardi, E., Cardillo, V.M., Acharyya, S., Aulino, P., Thomas-Ahner, J., Wang, J., Bloomston, M., Muscarella, P., Nau, P.*, et al.* (2013b). NF-kappaB-mediated Pax7 dysregulation in the muscle microenvironment promotes cancer cachexia. J. Clin. Invest. *123,* 4821-4835.

He, X.W., Liu, T., Chen, Y.X., Cheng, D.J., Li, X.R., Xiao, Y., and Feng, Y.L. (2008). Calcium carbonate nanoparticle delivering vascular endothelial growth factor-C siRNA effectively inhibits lymphangiogenesis and growth of gastric cancer in vivo. Cancer Gene Ther. *15,* 193-202.

He, Y., Kozaki, K., Karpanen, T., Koshikawa, K., Yla-Herttuala, S., Takahashi, T., and Alitalo, K. (2002). Suppression of tumor lymphangiogenesis and lymph node metastasis by blocking vascular endothelial growth factor receptor 3 signaling. J. Natl. Cancer Inst. *94,* 819-825.

He, Y., Rajantie, I., Pajusola, K., Jeltsch, M., Holopainen, T., Yla-Herttuala, S., Harding, T., Jooss, K., Takahashi, T., and Alitalo, K. (2005). Vascular endothelial cell growth factor receptor 3-mediated activation of lymphatic endothelium is crucial for tumor cell entry and spread via lymphatic vessels. Cancer Res. *65,* 4739-4746.

Heckman, C.A., Holopainen, T., Wirzenius, M., Keskitalo, S., Jeltsch, M., Yla-Herttuala, S., Wedge, S.R., Jurgensmeier, J.M., and Alitalo, K. (2008). The tyrosine kinase inhibitor cediranib blocks ligand-induced vascular endothelial growth factor receptor-3 activity and lymphangiogenesis. Cancer Res. *68,* 4754-4762.

Henne-Bruns, D., Vogel, I., Luttges, J., Kloppel, G., and Kremer, B. (2000). Surgery for ductal adenocarcinoma of the pancreatic head: staging, complications, and survival after regional versus extended lymphadenectomy. World J. Surg. *24,* 595-601; discussion 601-2.

Henne-Bruns, D., Vogel, I., Luttges, J., Kloppel, G., and Kremer, B. (1998). Ductal adenocarcinoma of the pancreas head: survival after regional versus extended lymphadenectomy. Hepatogastroenterology *45,* 855-866.

Hezel, A.F., Kimmelman, A.C., Stanger, B.Z., Bardeesy, N., and Depinho, R.A. (2006). Genetics and biology of pancreatic ductal adenocarcinoma. Genes Dev. *20,* 1218-1249.

Hinch, E.C., Sullivan-Gunn, M.J., Vaughan, V.C., McGlynn, M.A., and Lewandowski, P.A. (2013). Disruption of pro-oxidant and antioxidant systems with elevated expression of the ubiquitin

proteosome system in the cachectic heart muscle of nude mice. J. Cachexia Sarcopenia Muscle *4,* 287-293.

Hingorani, S.R., Wang, L., Multani, A.S., Combs, C., Deramaudt, T.B., Hruban, R.H., Rustgi, A.K., Chang, S., and Tuveson, D.A. (2005). Trp53R172H and KrasG12D cooperate to promote chromosomal instability and widely metastatic pancreatic ductal adenocarcinoma in mice. Cancer. Cell. *7,* 469-483.

Hirakawa, S., Detmar, M., Kerjaschki, D., Nagamatsu, S., Matsuo, K., Tanemura, A., Kamata, N., Higashikawa, K., Okazaki, H., Kameda, K.*, et al.* (2009). Nodal lymphangiogenesis and metastasis: Role of tumor-induced lymphatic vessel activation in extramammary Paget's disease. Am. J. Pathol. *175,* 2235-2248.

Hirata, K., Sato, T., Mukaiya, M., Yamashiro, K., Kimura, M., Sasaki, K., and Denno, R. (1997). Results of 1001 pancreatic resections for invasive ductal adenocarcinoma of the pancreas. Arch. Surg. *132,* 771-6; discussion 777.

Hirono, S., Tani, M., Kawai, M., Okada, K., Miyazawa, M., Shimizu, A., Uchiyama, K., and Yamaue, H. (2012). Identification of the lymphatic drainage pathways from the pancreatic head guided by indocyanine green fluorescence imaging during pancreaticoduodenectomy. Dig. Surg. *29,* 132-139.

Hirosue, S., Vokali, E., Raghavan, V.R., Rincon-Restrepo, M., Lund, A.W., Corthesy-Henrioud, P., Capotosti, F., Halin Winter, C., Hugues, S., and Swartz, M.A. (2014). Steady-state antigen scavenging, cross-presentation, and CD8+ T cell priming: a new role for lymphatic endothelial cells. J. Immunol. *192,* 5002-5011.

Holopainen, T., Saharinen, P., D'Amico, G., Lampinen, A., Eklund, L., Sormunen, R., Anisimov, A., Zarkada, G., Lohela, M., Helotera, H.*, et al.* (2012). Effects of angiopoietin-2-blocking antibody on endothelial cell-cell junctions and lung metastasis. J. Natl. Cancer Inst. *104,* 461-475.

Honors, M.A., and Kinzig, K.P. (2012). The role of insulin resistance in the development of muscle wasting during cancer cachexia. J. Cachexia Sarcopenia Muscle *3,* 5-11.

Hoshida, T., Isaka, N., Hagendoorn, J., di Tomaso, E., Chen, Y.L., Pytowski, B., Fukumura, D., Padera, T.P., and Jain, R.K. (2006). Imaging steps of lymphatic metastasis reveals that vascular endothelial growth factor-C increases metastasis by increasing delivery of cancer cells to lymph nodes: therapeutic implications. Cancer Res. *66,* 8065-8075.

Hosono, K., Suzuki, T., Tamaki, H., Sakagami, H., Hayashi, I., Narumiya, S., Alitalo, K., and Majima, M. (2011). Roles of prostaglandin E2-EP3/EP4 receptor signaling in the enhancement of lymphangiogenesis during fibroblast growth factor-2-induced granulation formation. Arterioscler. Thromb. Vasc. Biol. *31,* 1049-1058.

House, M.G., Gonen, M., Jarnagin, W.R., D'Angelica, M., DeMatteo, R.P., Fong, Y., Brennan, M.F., and Allen, P.J. (2007). Prognostic significance of pathologic nodal status in patients with resected pancreatic cancer. J. Gastrointest. Surg. *11,* 1549-1555.

Howard, J.M. (1999). Development and progress in resective surgery for pancreatic cancer. World J. Surg. *23,* 901-906.

Hruban, R.H., and Adsay, N.V. (2009). Molecular classification of neoplasms of the pancreas. Hum. Pathol. *40,* 612-623.

Huang, D., Swanson, E.A., Lin, C.P., Schuman, J.S., Stinson, W.G., Chang, W., Hee, M.R., Flotte, T., Gregory, K., and Puliafito, C.A. (1991). Optical coherence tomography. Science *254,* 1178-1181.

Huang, W.C., Nagahashi, M., Terracina, K.P., and Takabe, K. (2013). Emerging Role of Sphingosine-1-phosphate in Inflammation, Cancer, and Lymphangiogenesis. Biomolecules *3,* 10.3390/biom3030408.

Hunter, K.E., Palermo, C., Kester, J.C., Simpson, K., Li, J.P., Tang, L.H., Klimstra, D.S., Vlodavsky, I., and Joyce, J.A. (2014). Heparanase promotes lymphangiogenesis and tumor invasion in pancreatic neuroendocrine tumors. Oncogene *33,* 1799-1808.

Hurwitz, H., Fehrenbacher, L., Novotny, W., Cartwright, T., Hainsworth, J., Heim, W., Berlin, J., Baron, A., Griffing, S., Holmgren, E.*, et al.* (2004). Bevacizumab plus irinotecan, fluorouracil, and leucovorin for metastatic colorectal cancer. N. Engl. J. Med. *350,* 2335-2342.

Hwang, T.L., Lee, L.Y., Wang, C.C., Liang, Y., Huang, S.F., and Wu, C.M. (2012). CCL7 and CCL21 overexpression in gastric cancer is associated with lymph node metastasis and poor prognosis. World J. Gastroenterol. *18,* 1249-1256.

Ichise, T., Yoshida, N., and Ichise, H. (2010). H-, N- and Kras cooperatively regulate lymphatic vessel growth by modulating VEGFR3 expression in lymphatic endothelial cells in mice. Development *137,* 1003-1013.

Imai, H., Doi, R., Kanazawa, H., Kamo, N., Koizumi, M., Masui, T., Iwanaga, Y., Kawaguchi, Y., Takada, Y., Isoda, H., and Uemoto, S. (2010). Preoperative assessment of para-aortic lymph node metastasis in patients with pancreatic cancer. Int. J. Clin. Oncol. *15,* 294-300.

Imoto, A., Mitsunaga, S., Inagaki, M., Aoyagi, K., Sasaki, H., Ikeda, M., Nakachi, K., Higuchi, K., and Ochiai, A. (2012). Neural invasion induces cachexia via astrocytic activation of neural route in pancreatic cancer. Int. J. Cancer *131,* 2795-2807.

Inman, K.S., Francis, A.A., and Murray, N.R. (2014). Complex role for the immune system in initiation and progression of pancreatic cancer. World J. Gastroenterol. *20,* 11160-11181.

Inturrisi, C.E. (2003). Pharmacology of analgesia: basic principles. In Cancer Pain: Assessment and Management, Bruera, E. D., and Portenoy, R. K. eds., (Cambridge, UK: Cambridge University Press) pp. 111-123.

Iqbal, N., Lovegrove, R.E., Tilney, H.S., Abraham, A.T., Bhattacharya, S., Tekkis, P.P., and Kocher, H.M. (2009). A comparison of pancreaticoduodenectomy with extended pancreaticoduodenectomy: a meta-analysis of 1909 patients. Eur. J. Surg. Oncol. *35,* 79-86.

Irino, T., Takeuchi, H., Matsuda, S., Saikawa, Y., Kawakubo, H., Wada, N., Takahashi, T., Nakamura, R., Fukuda, K., Omori, T., and Kitagawa, Y. (2014). CC-Chemokine receptor CCR7: a key molecule for lymph node metastasis in esophageal squamous cell carcinoma. BMC Cancer *14,* 291-2407-14-291.

Isaji, S., Kawarada, Y., and Uemoto, S. (2004). Classification of pancreatic cancer: comparison of Japanese and UICC classifications. Pancreas *28,* 231-234.

Ishikawa, O., Ohhigashi, H., Sasaki, Y., Kabuto, T., Fukuda, I., Furukawa, H., Imaoka, S., and Iwanaga, T. (1988). Practical usefulness of lymphatic and connective tissue clearance for the carcinoma of the pancreas head. Ann. Surg. *208,* 215-220.

Issa, A., Le, T.X., Shoushtari, A.N., Shields, J.D., and Swartz, M.A. (2009). Vascular endothelial growth factor-C and C-C chemokine receptor 7 in tumor cell-lymphatic cross-talk promote invasive phenotype. Cancer Res. *69,* 349-357.

Jang, J.Y., Kang, M.J., Heo, J.S., Choi, S.H., Choi, D.W., Park, S.J., Han, S.S., Yoon, D.S., Yu, H.C., Kang, K.J., Kim, S.G., and Kim, S.W. (2014). A prospective randomized controlled study comparing outcomes of standard resection and extended resection, including dissection of the nerve plexus and various lymph nodes, in patients with pancreatic head cancer. Ann. Surg. *259,* 656-664.

Jee, D., and Lee, W.K. (2012). Inhibitory effect of intravitreal injection of bevacizumab on nerve growth factor. Curr. Eye Res. *37,* 408-415.

Jeltsch, M., Kaipainen, A., Joukov, V., Meng, X., Lakso, M., Rauvala, H., Swartz, M., Fukumura, D., Jain, R.K., and Alitalo, K. (1997). Hyperplasia of lymphatic vessels in VEGF-C transgenic mice. Science *276,* 1423-1425.

Jeong, H.S., Jones, D., Liao, S., Wattson, D.A., Cui, C.H., Duda, D.G., Willett, C.G., Jain, R.K., and Padera, T.P. (2015). Investigation of the Lack of Angiogenesis in the Formation of Lymph Node Metastases. J. Natl. Cancer Inst. *107,* 10.1093/jnci/djv155. Print 2015 Sep.

Jimenez-Andrade, J.M., Herrera, M.B., Ghilardi, J.R., Vardanyan, M., Melemedjian, O.K., and Mantyh, P.W. (2008). Vascularization of the dorsal root ganglia and peripheral nerve of the mouse: implications for chemical-induced peripheral sensory neuropathies. Mol. Pain *4,* 10-8069-4-10.

John, B.J., Naik, P., Ironside, A., Davidson, B.R., Fusai, G., Gillmore, R., Watkins, J., and Rahman, S.H. (2013). Redefining the R1 resection for pancreatic ductal adenocarcinoma: tumour lymph nodal burden and lymph node ratio are the only prognostic factors associated with survival. HPB (Oxford) *15,* 674-680.

Johns, N., Hatakeyama, S., Stephens, N.A., Degen, M., Degen, S., Frieauff, W., Lambert, C., Ross, J.A., Roubenoff, R., Glass, D.J., Jacobi, C., and Fearon, K.C. (2014). Clinical classification of cancer cachexia: phenotypic correlates in human skeletal muscle. PLoS One *9,* e83618.

Johnson, L.A., Clasper, S., Holt, A.P., Lalor, P.F., Baban, D., and Jackson, D.G. (2006). An inflammation-induced mechanism for leukocyte transmigration across lymphatic vessel endothelium. J. Exp. Med. *203,* 2763-2777.

Johnson, L.A., and Jackson, D.G. (2013). The chemokine CX3CL1 promotes trafficking of dendritic cells through inflamed lymphatics. J. Cell. Sci. *126,* 5259-5270.

Jones, D., Li, Y., He, Y., Xu, Z., Chen, H., and Min, W. (2012). Mirtron microRNA-1236 inhibits VEGFR-3 signaling during inflammatory lymphangiogenesis. Arterioscler. Thromb. Vasc. Biol. *32,* 633-642.

Jones, D., Xu, Z., Zhang, H., He, Y., Kluger, M.S., Chen, H., and Min, W. (2010). Functional analyses of the bone marrow kinase in the X chromosome in vascular endothelial growth factor-induced lymphangiogenesis. Arterioscler. Thromb. Vasc. Biol. *30,* 2553-2561.

Joo, M.J., Yuhan, K.R., Hyon, J.Y., Lai, H., Hose, S., Sinha, D., and O'Brien, T.P. (2004). The effect of nerve growth factor on corneal sensitivity after laser in situ keratomileusis. Arch. Ophthalmol. *122,* 1338-1341.

Joukov, V., Pajusola, K., Kaipainen, A., Chilov, D., Lahtinen, I., Kukk, E., Saksela, O., Kalkkinen, N., and Alitalo, K. (1996). A novel vascular endothelial growth factor, VEGF-C, is a ligand for the Flt4 (VEGFR-3) and KDR (VEGFR-2) receptor tyrosine kinases. EMBO J. *15,* 290-298.

Jung, K.Y., Cho, S.W., Kim, Y.A., Kim, D., Oh, B.C., Park do, J., and Park, Y.J. (2015). Cancers with Higher Density of Tumor-Associated Macrophages Were Associated with Poor Survival Rates. J. Pathol. Transl. Med. *49,* 318-324.

Kaifi, J.T., Yekebas, E.F., Schurr, P., Obonyo, D., Wachowiak, R., Busch, P., Heinecke, A., Pantel, K., and Izbicki, J.R. (2005). Tumor-cell homing to lymph nodes and bone marrow and CXCR4 expression in esophageal cancer. J. Natl. Cancer Inst. *97,* 1840-1847.

Kaipainen, A., Korhonen, J., Mustonen, T., van Hinsbergh, V.W., Fang, G.H., Dumont, D., Breitman, M., and Alitalo, K. (1995). Expression of the fms-like tyrosine kinase 4 gene becomes restricted to lymphatic endothelium during development. Proc. Natl. Acad. Sci. U. S. A. *92,* 3566-3570.

Kameda, K., Shimada, H., Ishikawa, T., Takimoto, A., Momiyama, N., Hasegawa, S., Misuta, K., Nakano, A., Nagashima, Y., and Ichikawa, Y. (1999). Expression of highly polysialylated neural cell adhesion molecule in pancreatic cancer neural invasive lesion. Cancer Lett. *137,* 201-207.

Kaminskas, L.M., Ascher, D.B., McLeod, V.M., Herold, M.J., Le, C.P., Sloan, E.K., and Porter, C.J. (2013). PEGylation of interferon alpha2 improves lymphatic exposure after subcutaneous and intravenous administration and improves antitumour efficacy against lymphatic breast cancer metastases. J. Control. Release *168,* 200-208.

Kamisawa, T., Isawa, T., Koike, M., Tsuruta, K., and Okamoto, A. (1995). Hematogenous metastases of pancreatic ductal carcinoma. Pancreas *11,* 345-349.

Kanda, M., Fujii, T., Nagai, S., Kodera, Y., Kanzaki, A., Sahin, T.T., Hayashi, M., Yamada, S., Sugimoto, H., Nomoto, S.*, et al.* (2011). Pattern of lymph node metastasis spread in pancreatic cancer. Pancreas *40,* 951-955.

Kankaanpaa, P., Paavolainen, L., Tiitta, S., Karjalainen, M., Paivarinne, J., Nieminen, J., Marjomaki, V., Heino, J., and White, D.J. (2012). BioImageXD: an open, general-purpose and high-throughput image-processing platform. Nat. Methods *9,* 683-689.

Karaman, S., and Detmar, M. (2014). Mechanisms of lymphatic metastasis. J. Clin. Invest. *124,* 922-928.

Karpanen, T., Egeblad, M., Karkkainen, M.J., Kubo, H., Yla-Herttuala, S., Jaattela, M., and Alitalo, K. (2001). Vascular endothelial growth factor C promotes tumor lymphangiogenesis and intralymphatic tumor growth. Cancer Res. *61,* 1786-1790.

Karpanen, T., Wirzenius, M., Makinen, T., Veikkola, T., Haisma, H.J., Achen, M.G., Stacker, S.A., Pytowski, B., Yla-Herttuala, S., and Alitalo, K. (2006). Lymphangiogenic growth factor responsiveness is modulated by postnatal lymphatic vessel maturation. Am. J. Pathol. *169,* 708-718.

Katuchova, J., Bober, J., Katuch, V., and Radonak, J. (2012). Significance of lymph node micrometastasis in pancreatic cancer patients. Eur. Surg. Res. *48,* 10-15.

Katz, M.H., Hwang, R., Fleming, J.B., and Evans, D.B. (2008). Tumor-node-metastasis staging of pancreatic adenocarcinoma. CA Cancer. J. Clin. *58,* 111-125.

Kawada, K., and Taketo, M.M. (2011). Significance and mechanism of lymph node metastasis in cancer progression. Cancer Res. *71,* 1214-1218.

Kawai, Y., Kaidoh, M., and Ohhashi, T. (2008). MDA-MB-231 produces ATP-mediated ICAM-1-dependent facilitation of the attachment of carcinoma cells to human lymphatic endothelial cells. Am. J. Physiol. Cell. Physiol. *295,* C1123-32.

Kawai, Y., Kaidoh, M., Yokoyama, Y., Sano, K., and Ohhashi, T. (2009). Chemokine CCL2 facilitates ICAM-1-mediated interactions of cancer cells and lymphatic endothelial cells in sentinel lymph nodes. Cancer. Sci. *100,* 419-428.

Kayahara, M., Nagakawa, T., Konishi, I., Ueno, K., Ohta, T., and Miyazaki, I. (1991). Clinicopathological study of pancreatic carcinoma with particular reference to the invasion of the extrapancreatic neural plexus. Int. J. Pancreatol. *10,* 105-111.

Kayahara, M., Nagakawa, T., Ueno, K., Ohta, T., Takeda, T., and Miyazaki, I. (1993). An evaluation of radical resection for pancreatic cancer based on the mode of recurrence as determined by autopsy and diagnostic imaging. Cancer *72,* 2118-2123.

Kayahara, M., Nakagawara, H., Kitagawa, H., and Ohta, T. (2007). The nature of neural invasion by pancreatic cancer. Pancreas *35,* 218-223.

Ke, K., Chen, W., and Chen, Y. (2014). Standard and extended lymphadenectomy for adenocarcinoma of the pancreatic head: a meta-analysis and systematic review. J. Gastroenterol. Hepatol. *29,* 453-462.

Kedra, B., Popiela, T., Sierzega, M., and Precht, A. (2001). Prognostic factors of long-term survival after resective procedures for pancreatic cancer. Hepatogastroenterology *48,* 1762-1766.

Keklikoglou, I., Hosaka, K., Bender, C., Bott, A., Koerner, C., Mitra, D., Will, R., Woerner, A., Muenstermann, E., Wilhelm, H., Cao, Y., and Wiemann, S. (2014). MicroRNA-206 functions as a pleiotropic modulator of cell proliferation, invasion and lymphangiogenesis in pancreatic adenocarcinoma by targeting ANXA2 and KRAS genes. Oncogene

Kelley, P.M., Connor, A.L., and Tempero, R.M. (2013). Lymphatic vessel memory stimulated by recurrent inflammation. Am. J. Pathol. *182,* 2418-2428.

Kelley, P.M., Steele, M.M., and Tempero, R.M. (2011). Regressed lymphatic vessels develop during corneal repair. Lab. Invest. *91,* 1643-1651.

Kenyon, B.M., Voest, E.E., Chen, C.C., Flynn, E., Folkman, J., and D'Amato, R.J. (1996). A model of angiogenesis in the mouse cornea. Invest. Ophthalmol. Vis. Sci. *37,* 1625-1632.

Kerjaschki, D., Bago-Horvath, Z., Rudas, M., Sexl, V., Schneckenleithner, C., Wolbank, S., Bartel, G., Krieger, S., Kalt, R., Hantusch, B*., et al.* (2011). Lipoxygenase mediates invasion of intrametastatic lymphatic vessels and propagates lymph node metastasis of human mammary carcinoma xenografts in mouse. J. Clin. Invest. *121,* 2000-2012.

Kessenbrock, K., Plaks, V., and Werb, Z. (2010). Matrix metalloproteinases: regulators of the tumor microenvironment. Cell *141,* 52-67.

Khagi, S., and Saif, M.W. (2015). Pancreatic neuroendocrine tumors: targeting the molecular basis of disease. Curr. Opin. Oncol. *27,* 38-43.

Kilarski, W.W., Guc, E., Teo, J.C., Oliver, S.R., Lund, A.W., and Swartz, M.A. (2013). Intravital immunofluorescence for visualizing the microcirculatory and immune microenvironments in the mouse ear dermis. PLoS One *8,* e57135.

Kim, E.C., Lee, W.S., and Kim, M.S. (2010a). The inhibitory effects of bevacizumab eye drops on NGF expression and corneal wound healing in rats. Invest. Ophthalmol. Vis. Sci. *51,* 4569-4573.

Kim, M., Koh, Y.J., Kim, K.E., Koh, B.I., Nam, D.H., Alitalo, K., Kim, I., and Koh, G.Y. (2010b). CXCR4 signaling regulates metastasis of chemoresistant melanoma cells by a lymphatic metastatic niche. Cancer Res. *70,* 10411-10421.

Kim, R., Emi, M., Tanabe, K., and Arihiro, K. (2006). Tumor-driven evolution of immunosuppressive networks during malignant progression. Cancer Res. *66,* 5527-5536.

Kimura, W., Morikane, K., Esaki, Y., Chan, W.C., and Pour, P.M. (1998). Histologic and biologic patterns of microscopic pancreatic ductal adenocarcinomas detected incidentally at autopsy. Cancer *82,* 1839-1849.

Kindler, H.L., Ioka, T., Richel, D.J., Bennouna, J., Letourneau, R., Okusaka, T., Funakoshi, A., Furuse, J., Park, Y.S., Ohkawa, S*., et al.* (2011). Axitinib plus gemcitabine versus placebo plus gemcitabine in patients with advanced pancreatic adenocarcinoma: a double-blind randomised phase 3 study. Lancet Oncol. *12,* 256-262.

Kindler, H.L., Niedzwiecki, D., Hollis, D., Sutherland, S., Schrag, D., Hurwitz, H., Innocenti, F., Mulcahy, M.F., O'Reilly, E., Wozniak, T.F*., et al.* (2010). Gemcitabine plus bevacizumab compared with gemcitabine plus placebo in patients with advanced pancreatic cancer: phase III trial of the Cancer and Leukemia Group B (CALGB 80303). J. Clin. Oncol. *28,* 3617-3622.

Kirchgessner, A.L., and Gershon, M.D. (1990). Innervation of the pancreas by neurons in the gut. J. Neurosci. *10,* 1626-1642.

Kobayashi, K., Sadakari, Y., Ohtsuka, T., Takahata, S., Nakamura, M., Mizumoto, K., and Tanaka, M. (2010). Factors in intraductal papillary mucinous neoplasms of the pancreas predictive of lymph node metastasis. Pancreatology *10,* 720-725.

Koch, M., Dettori, D., Van Nuffelen, A., Souffreau, J., Marconcini, L., Wallays, G., Moons, L., Bruyere, F., Oliviero, S., Noel, A*., et al.* (2009). VEGF-D deficiency in mice does not affect embryonic or postnatal lymphangiogenesis but reduces lymphatic metastasis. J. Pathol. *219,* 356-364.

Kocher, H.M., Sohail, M., Benjamin, I.S., and Patel, A.G. (2007). Technical limitations of lymph node mapping in pancreatic cancer. Eur. J. Surg. Oncol. *33,* 887-891.

Kodera, Y., Katanasaka, Y., Kitamura, Y., Tsuda, H., Nishio, K., Tamura, T., and Koizumi, F. (2011). Sunitinib inhibits lymphatic endothelial cell functions and lymph node metastasis in a breast cancer model through inhibition of vascular endothelial growth factor receptor 3. Breast Cancer Res. *13,* R66.

Koide, N., Yamada, T., Shibata, R., Mori, T., Fukuma, M., Yamazaki, K., Aiura, K., Shimazu, M., Hirohashi, S., Nimura, Y., and Sakamoto, M. (2006). Establishment of perineural invasion models and analysis of gene expression revealed an invariant chain (CD74) as a possible molecule involved in perineural invasion in pancreatic cancer. Clin. Cancer Res. *12,* 2419-2426.

Konstantinidis, I.T., Deshpande, V., Zheng, H., Wargo, J.A., Fernandez-del Castillo, C., Thayer, S.P., Androutsopoulos, V., Lauwers, G.Y., Warshaw, A.L., and Ferrone, C.R. (2010). Does the mechanism of lymph node invasion affect survival in patients with pancreatic ductal adenocarcinoma? J. Gastrointest. Surg. *14,* 261-267.

Konstantinidis, I.T., Warshaw, A.L., Allen, J.N., Blaszkowsky, L.S., Castillo, C.F., Deshpande, V., Hong, T.S., Kwak, E.L., Lauwers, G.Y., Ryan, D.P*., et al.* (2013). Pancreatic ductal

adenocarcinoma: is there a survival difference for R1 resections versus locally advanced unresectable tumors? What is a "true" R0 resection? Ann. Surg. *257,* 731-736.

Kopfstein, L., Veikkola, T., Djonov, V.G., Baeriswyl, V., Schomber, T., Strittmatter, K., Stacker, S.A., Achen, M.G., Alitalo, K., and Christofori, G. (2007). Distinct roles of vascular endothelial growth factor-D in lymphangiogenesis and metastasis. Am. J. Pathol. *170,* 1348-1361.

Koyama, H., Kobayashi, N., Harada, M., Takeoka, M., Kawai, Y., Sano, K., Fujimori, M., Amano, J., Ohhashi, T., Kannagi, R*., et al.* (2008). Significance of tumor-associated stroma in promotion of intratumoral lymphangiogenesis: pivotal role of a hyaluronan-rich tumor microenvironment. Am. J. Pathol. *172,* 179-193.

Krafft, C., and Popp, J. (2015). The many facets of Raman spectroscopy for biomedical analysis. Anal. Bioanal Chem. *407,* 699-717.

Krishnan, J., Kirkin, V., Steffen, A., Hegen, M., Weih, D., Tomarev, S., Wilting, J., and Sleeman, J.P. (2003). Differential in vivo and in vitro expression of vascular endothelial growth factor (VEGF)-C and VEGF-D in tumors and its relationship to lymphatic metastasis in immunocompetent rats. Cancer Res. *63,* 713-722.

Kubo, H., Cao, R., Brakenhielm, E., Makinen, T., Cao, Y., and Alitalo, K. (2002). Blockade of vascular endothelial growth factor receptor-3 signaling inhibits fibroblast growth factor-2-induced lymphangiogenesis in mouse cornea. Proc. Natl. Acad. Sci. U. S. A. *99,* 8868-8873.

Kumon, R.E., Pollack, M.J., Faulx, A.L., Olowe, K., Farooq, F.T., Chen, V.K., Zhou, Y., Wong, R.C., Isenberg, G.A., Sivak, M.V., Chak, A., and Deng, C.X. (2010). In vivo characterization of pancreatic and lymph node tissue by using EUS spectrum analysis: a validation study. Gastrointest. Endosc. *71,* 53-63.

Kurahara, H., Shinchi, H., Mataki, Y., Maemura, K., Noma, H., Kubo, F., Sakoda, M., Ueno, S., Natsugoe, S., and Takao, S. (2011). Significance of M2-polarized tumor-associated macrophage in pancreatic cancer. J. Surg. Res. *167,* e211-9.

Kurahara, H., Takao, S., Maemura, K., Mataki, Y., Kuwahata, T., Maeda, K., Sakoda, M., Iino, S., Ishigami, S., Ueno, S., Shinchi, H., and Natsugoe, S. (2013). M2-polarized tumor-associated macrophage infiltration of regional lymph nodes is associated with nodal lymphangiogenesis and occult nodal involvement in pN0 pancreatic cancer. Pancreas *42,* 155-159.

Kurahara, H., Takao, S., Maemura, K., Shinchi, H., Natsugoe, S., and Aikou, T. (2004). Impact of vascular endothelial growth factor-C and -D expression in human pancreatic cancer: its relationship to lymph node metastasis. Clin. Cancer Res. *10,* 8413-8420.

Kurahara, H., Takao, S., Shinchi, H., Maemura, K., Mataki, Y., Sakoda, M., Hayashi, T., Kuwahata, T., Minami, K., Ueno, S., and Natsugoe, S. (2010). Significance of lymphangiogenesis in primary tumor and draining lymph nodes during lymphatic metastasis of pancreatic head cancer. J. Surg. Oncol. *102,* 809-815.

La Torre, M., Cavallini, M., Ramacciato, G., Cosenza, G., Rossi Del Monte, S., Nigri, G., Ferri, M., Mercantini, P., and Ziparo, V. (2011). Role of the lymph node ratio in pancreatic ductal adenocarcinoma. Impact on patient stratification and prognosis. J. Surg. Oncol. *104,* 629-633.

Lambiase, A., Aloe, L., Mantelli, F., Sacchetti, M., Perrella, E., Bianchi, P., Rocco, M.L., and Bonini, S. (2012). Capsaicin-induced corneal sensory denervation and healing impairment are reversed by NGF treatment. Invest. Ophthalmol. Vis. Sci. *53,* 8280-8287.

Lambiase, A., Bonini, S., Aloe, L., Rama, P., and Bonini, S. (2000a). Anti-inflammatory and healing properties of nerve growth factor in immune corneal ulcers with stromal melting. Arch. Ophthalmol. *118,* 1446-1449.

Lambiase, A., Bonini, S., Micera, A., Rama, P., Bonini, S., and Aloe, L. (1998a). Expression of nerve growth factor receptors on the ocular surface in healthy subjects and during manifestation of inflammatory diseases. Invest. Ophthalmol. Vis. Sci. *39,* 1272-1275.

Lambiase, A., Manni, L., Bonini, S., Rama, P., Micera, A., and Aloe, L. (2000b). Nerve growth factor promotes corneal healing: structural, biochemical, and molecular analyses of rat and human corneas. Invest. Ophthalmol. Vis. Sci. *41,* 1063-1069.

Lambiase, A., Manni, L., Rama, P., and Bonini, S. (2003). Clinical application of nerve growth factor on human corneal ulcer. Arch. Ital. Biol. *141,* 141-148.

Lambiase, A., Mantelli, F., Sacchetti, M., Rossi, S., Aloe, L., and Bonini, S. (2011). Clinical applications of NGF in ocular diseases. Arch. Ital. Biol. *149,* 283-292.

Lambiase, A., Rama, P., Bonini, S., Caprioglio, G., and Aloe, L. (1998b). Topical treatment with nerve growth factor for corneal neurotrophic ulcers. N. Engl. J. Med. *338,* 1174-1180.

Larrivee, B., Freitas, C., Suchting, S., Brunet, I., and Eichmann, A. (2009). Guidance of vascular development: lessons from the nervous system. Circ. Res. *104,* 428-441.

Leak, L.V. (1976). The structure of lymphatic capillaries in lymph formation. Fed. Proc. *35,* 1863-1871.

Leak, L.V., and Burke, J.F. (1966). Fine structure of the lymphatic capillary and the adjoining connective tissue area. Am. J. Anat. *118,* 785-809.

Lee, J.Y., Park, C., Cho, Y.P., Lee, E., Kim, H., Kim, P., Yun, S.H., and Yoon, Y.S. (2010). Podoplanin-expressing cells derived from bone marrow play a crucial role in postnatal lymphatic neovascularization. Circulation *122,* 1413-1425.

Leek, R.D., and Harris, A.L. (2002). Tumor-associated macrophages in breast cancer. J. Mammary Gland Biol. Neoplasia *7,* 177-189.

Li, J., Ma, Q., Liu, H., Guo, K., Li, F., Li, W., Han, L., Wang, F., and Wu, E. (2011a). Relationship between neural alteration and perineural invasion in pancreatic cancer patients with hyperglycemia. PLoS One *6,* e17385.

Li, J.L., Goh, C.C., Keeble, J.L., Qin, J.S., Roediger, B., Jain, R., Wang, Y., Chew, W.K., Weninger, W., and Ng, L.G. (2012). Intravital multiphoton imaging of immune responses in the mouse ear skin. Nat. Protoc. *7,* 221-234.

Li, M., Zhao, J., Qiao, J., Song, C., and Zhao, Z. (2014). EphB4 regulates the growth and migration of pancreatic cancer cells. Tumour Biol. *35,* 6855-6859.

Li, M., and Zhao, Z. (2013). Clinical implications of EphB4 receptor expression in pancreatic cancer. Mol. Biol. Rep. *40,* 1735-1741.

Li, R., Wheeler, T., Dai, H., and Ayala, G. (2003). Neural cell adhesion molecule is upregulated in nerves with prostate cancer invasion. Hum. Pathol. *34,* 457-461.

Li, W., Kohara, H., Uchida, Y., James, J.M., Soneji, K., Cronshaw, D.G., Zou, Y.R., Nagasawa, T., and Mukouyama, Y.S. (2013). Peripheral nerve-derived CXCL12 and VEGF-A regulate the patterning of arterial vessel branching in developing limb skin. Dev. Cell. *24,* 359-371.

Li, X., Dong, Q., Yan, Z., Lu, W., Feng, L., Xie, C., Xie, Z., Su, B., and Liu, M. (2015). MPEG-DSPE polymeric micelle for translymphatic chemotherapy of lymph node metastasis. Int. J. Pharm. *487,* 8-16.

Li, Z., Burns, A.R., Han, L., Rumbaut, R.E., and Smith, C.W. (2011b). IL-17 and VEGF are necessary for efficient corneal nerve regeneration. Am. J. Pathol. *178,* 1106-1116.

Liao, D., Luo, Y., Markowitz, D., Xiang, R., and Reisfeld, R.A. (2009). Cancer associated fibroblasts promote tumor growth and metastasis by modulating the tumor immune microenvironment in a 4T1 murine breast cancer model. PLoS One *4,* e7965.

Liao, S., and von der Weid, P.Y. (2015). Lymphatic system: an active pathway for immune protection. Semin. Cell Dev. Biol. *38,* 83-89.

Lin, B., Podar, K., Gupta, D., Tai, Y.T., Li, S., Weller, E., Hideshima, T., Lentzsch, S., Davies, F., Li, C.*, et al.* (2002). The vascular endothelial growth factor receptor tyrosine kinase inhibitor PTK787/ZK222584 inhibits growth and migration of multiple myeloma cells in the bone marrow microenvironment. Cancer Res. *62,* 5019-5026.

Lin, F.J., Chen, X., Qin, J., Hong, Y.K., Tsai, M.J., and Tsai, S.Y. (2010). Direct transcriptional regulation of neuropilin-2 by COUP-TFII modulates multiple steps in murine lymphatic vessel development. J. Clin. Invest. *120,* 1694-1707.

Lin, J., Lalani, A.S., Harding, T.C., Gonzalez, M., Wu, W.W., Luan, B., Tu, G.H., Koprivnikar, K., VanRoey, M.J., He, Y., Alitalo, K., and Jooss, K. (2005). Inhibition of lymphogenous metastasis

using adeno-associated virus-mediated gene transfer of a soluble VEGFR-3 decoy receptor. Cancer Res. *65,* 6901-6909.

Liu, Q.H., Shi, M.L., Bai, J., and Zheng, J.N. (2015a). Identification of ANXA1 as a lymphatic metastasis and poor prognostic factor in pancreatic ductal adenocarcinoma. Asian Pac. J. Cancer. Prev. *16,* 2719-2724.

Liu, X., Guo, X.Z., Li, H.Y., Chen, J., Ren, L.N., and Wu, C.Y. (2014a). KAI1 inhibits lymphangiogenesis and lymphatic metastasis of pancreatic cancer in vivo. Hepatobiliary. Pancreat. Dis. Int. *13,* 87-92.

Liu, X., Xiao, Q., Bai, X., Yu, Z., Sun, M., Zhao, H., Mi, X., Wang, E., Yao, W., Jin, F*., et al.* (2014b). Activation of STAT3 is involved in malignancy mediated by CXCL12-CXCR4 signaling in human breast cancer. Oncol. Rep. *32,* 2760-2768.

Liu, Z., Luo, G., Guo, M., Jin, K., Xiao, Z., Liu, L., Liu, C., Xu, J., Ni, Q., Long, J., and Yu, X. (2015b). Lymph node status predicts the benefit of adjuvant chemoradiotherapy for patients with resected pancreatic cancer. Pancreatology *15,* 253-258.

Lund, A.W., Duraes, F.V., Hirosue, S., Raghavan, V.R., Nembrini, C., Thomas, S.N., Issa, A., Hugues, S., and Swartz, M.A. (2012). VEGF-C promotes immune tolerance in B16 melanomas and cross-presentation of tumor antigen by lymph node lymphatics. Cell. Rep. *1,* 191-199.

Ma, J., Jiang, Y., Jiang, Y., Sun, Y., and Zhao, X. (2008). Expression of nerve growth factor and tyrosine kinase receptor A and correlation with perineural invasion in pancreatic cancer. J. Gastroenterol. Hepatol. *23,* 1852-1859.

Maby-El Hajjami, H., and Petrova, T.V. (2008). Developmental and pathological lymphangiogenesis: from models to human disease. Histochem. Cell Biol. *130,* 1063-1078.

Mace, T.A., Ameen, Z., Collins, A., Wojcik, S., Mair, M., Young, G.S., Fuchs, J.R., Eubank, T.D., Frankel, W.L., Bekaii-Saab, T., Bloomston, M., and Lesinski, G.B. (2013). Pancreatic cancer-associated stellate cells promote differentiation of myeloid-derived suppressor cells in a STAT3-dependent manner. Cancer Res. *73,* 3007-3018.

Maitra, A., Fukushima, N., Takaori, K., and Hruban, R.H. (2005). Precursors to invasive pancreatic cancer. Adv. Anat. Pathol. *12,* 81-91.

Makino, I., Kitagawa, H., Ohta, T., Nakagawara, H., Tajima, H., Ohnishi, I., Takamura, H., Tani, T., and Kayahara, M. (2008). Nerve plexus invasion in pancreatic cancer: spread patterns on histopathologic and embryological analyses. Pancreas *37,* 358-365.

Manabe, T., Ohshio, G., Baba, N., Miyashita, T., Asano, N., Tamura, K., Yamaki, K., Nonaka, A., and Tobe, T. (1989). Radical pancreatectomy for ductal cell carcinoma of the head of the pancreas. Cancer *64,* 1132-1137.

Mancino, M., Ametller, E., Gascon, P., and Almendro, V. (2011). The neuronal influence on tumor progression. Biochim. Biophys. Acta *1816,* 105-118.

Mandriota, S.J., Jussila, L., Jeltsch, M., Compagni, A., Baetens, D., Prevo, R., Banerji, S., Huarte, J., Montesano, R., Jackson, D.G.*, et al.* (2001). Vascular endothelial growth factor-C-mediated lymphangiogenesis promotes tumour metastasis. EMBO J. *20,* 672-682.

Mankal, P., and O'Reilly, E. (2013). Sunitinib malate for the treatment of pancreas malignancies--where does it fit? Expert Opin. Pharmacother. *14,* 783-792.

Mao, C., Domenico, D.R., Kim, K., Hanson, D.J., and Howard, J.M. (1995). Observations on the developmental patterns and the consequences of pancreatic exocrine adenocarcinoma. Findings of 154 autopsies. Arch. Surg. *130,* 125-134.

Marchesi, F., Locatelli, M., Solinas, G., Erreni, M., Allavena, P., and Mantovani, A. (2010). Role of CX3CR1/CX3CL1 axis in primary and secondary involvement of the nervous system by cancer. J. Neuroimmunol. *224,* 39-44.

Marchesi, F., Piemonti, L., Fedele, G., Destro, A., Roncalli, M., Albarello, L., Doglioni, C., Anselmo, A., Doni, A., Bianchi, P.*, et al.* (2008). The chemokine receptor CX3CR1 is involved in the neural tropism and malignant behavior of pancreatic ductal adenocarcinoma. Cancer Res. *68,* 9060-9069.

Marconi, C., Bianchini, F., Mannini, A., Mugnai, G., Ruggieri, S., and Calorini, L. (2008). Tumoral and macrophage uPAR and MMP-9 contribute to the invasiveness of B16 murine melanoma cells. Clin. Exp. Metastasis *25,* 225-231.

Marfurt, C.F., Jones, M.A., and Thrasher, K. (1998). Parasympathetic innervation of the rat cornea. Exp. Eye Res. *66,* 437-448.

Marfurt, C.F., Kingsley, R.E., and Echtenkamp, S.E. (1989). Sensory and sympathetic innervation of the mammalian cornea. A retrograde tracing study. Invest. Ophthalmol. Vis. Sci. *30,* 461-472.

Martin, L., Birdsell, L., Macdonald, N., Reiman, T., Clandinin, M.T., McCargar, L.J., Murphy, R., Ghosh, S., Sawyer, M.B., and Baracos, V.E. (2013). Cancer cachexia in the age of obesity: skeletal muscle depletion is a powerful prognostic factor, independent of body mass index. J. Clin. Oncol. *31,* 1539-1547.

Martin, L., Senesse, P., Gioulbasanis, I., Antoun, S., Bozzetti, F., Deans, C., Strasser, F., Thoresen, L., Jagoe, R.T., Chasen, M.*, et al.* (2015). Diagnostic criteria for the classification of cancer-associated weight loss. J. Clin. Oncol. *33,* 90-99.

Martinez-Corral, I., Olmeda, D., Dieguez-Hurtado, R., Tammela, T., Alitalo, K., and Ortega, S. (2012). In vivo imaging of lymphatic vessels in development, wound healing, inflammation, and tumor metastasis. Proc. Natl. Acad. Sci. U. S. A. *109,* 6223-6228.

Maruyama, K., Ii, M., Cursiefen, C., Jackson, D.G., Keino, H., Tomita, M., Van Rooijen, N., Takenaka, H., D'Amore, P.A., Stein-Streilein, J., Losordo, D.W., and Streilein, J.W. (2005). Inflammation-induced lymphangiogenesis in the cornea arises from CD11b-positive macrophages. J. Clin. Invest. *115,* 2363-2372.

Masui, T., Kubota, T., Aoki, K., Nakanishi, Y., Miyamoto, T., Nagata, J., Morino, K., Fukugaki, A., Takamura, M., Sugimoto, S., Onuma, H., and Tokuka, A. (2013). Long-term survival after resection of pancreatic ductal adenocarcinoma with para-aortic lymph node metastasis: case report. World J. Surg. Oncol. *11,* 195-7819-11-195.

Mauro, C., Pietro, L., and Emilio, C.C. (2007). The use of nerve growth factor in herpetic keratitis: a case report. J. Med. Case Rep. *1,* 124.

McColl, B.K., Baldwin, M.E., Roufail, S., Freeman, C., Moritz, R.L., Simpson, R.J., Alitalo, K., Stacker, S.A., and Achen, M.G. (2003). Plasmin activates the lymphangiogenic growth factors VEGF-C and VEGF-D. J. Exp. Med. *198,* 863-868.

McKenna, C.C., and Lwigale, P.Y. (2011). Innervation of the mouse cornea during development. Invest. Ophthalmol. Vis. Sci. *52,* 30-35.

Melani, M., and Weinstein, B.M. (2010). Common factors regulating patterning of the nervous and vascular systems. Annu. Rev. Cell Dev. Biol. *26,* 639-665.

Meriggi, F., Gramigna, P., and Forni, E. (2007). Extended lymphadenectomy in cephalic pancreatoduodenectomy. Personal observations. Hepatogastroenterology *54,* 549-555.

Michalski, C.W., Kleeff, J., Wente, M.N., Diener, M.K., Buchler, M.W., and Friess, H. (2007). Systematic review and meta-analysis of standard and extended lymphadenectomy in pancreaticoduodenectomy for pancreatic cancer. Br. J. Surg. *94,* 265-273.

Mignini, F., Sabbatini, M., Coppola, L., and Cavallotti, C. (2012). Analysis of nerve supply pattern in human lymphatic vessels of young and old men. Lymphat Res. Biol. *10,* 189-197.

Milsmann, C., Fuzesi, L., Werner, C., Becker, H., and Horstmann, O. (2005). Significance of occult lymphatic tumor spread in pancreatic cancer. Chirurg *76,* 1064-1072.

Miteva, D.O., Rutkowski, J.M., Dixon, J.B., Kilarski, W., Shields, J.D., and Swartz, M.A. (2010). Transmural flow modulates cell and fluid transport functions of lymphatic endothelium. Circ. Res. *106,* 920-931.

Miyazaki, H., Yoshimatsu, Y., Akatsu, Y., Mishima, K., Fukayama, M., Watabe, T., and Miyazono, K. (2014). Expression of platelet-derived growth factor receptor beta is maintained by Prox1 in lymphatic endothelial cells and is required for tumor lymphangiogenesis. Cancer. Sci. *105,* 1116-1123.

Morisada, T., Oike, Y., Yamada, Y., Urano, T., Akao, M., Kubota, Y., Maekawa, H., Kimura, Y., Ohmura, M., Miyamoto, T.*, et al.* (2005). Angiopoietin-1 promotes LYVE-1-positive lymphatic vessel formation. Blood *105,* 4649-4656.

Mukouyama, Y.S., Gerber, H.P., Ferrara, N., Gu, C., and Anderson, D.J. (2005). Peripheral nerve-derived VEGF promotes arterial differentiation via neuropilin 1-mediated positive feedback. Development *132,* 941-952.

Mukouyama, Y.S., Shin, D., Britsch, S., Taniguchi, M., and Anderson, D.J. (2002). Sensory nerves determine the pattern of arterial differentiation and blood vessel branching in the skin. Cell *109,* 693-705.

Muller, A., Homey, B., Soto, H., Ge, N., Catron, D., Buchanan, M.E., McClanahan, T., Murphy, E., Yuan, W., Wagner, S.N.*, et al.* (2001). Involvement of chemokine receptors in breast cancer metastasis. Nature *410,* 50-56.

Muller, L.J., Marfurt, C.F., Kruse, F., and Tervo, T.M. (2003). Corneal nerves: structure, contents and function. Exp. Eye Res. *76,* 521-542.

Muller, M.W., Giese, N.A., Swiercz, J.M., Ceyhan, G.O., Esposito, I., Hinz, U., Buchler, P., Giese, T., Buchler, M.W., Offermanns, S., and Friess, H. (2007). Association of axon guidance factor semaphorin 3A with poor outcome in pancreatic cancer. Int. J. Cancer *121,* 2421-2433.

Munn, D.H., and Mellor, A.L. (2007). Indoleamine 2,3-dioxygenase and tumor-induced tolerance. J. Clin. Invest. *117,* 1147-1154.

Munn, D.H., and Mellor, A.L. (2006). The tumor-draining lymph node as an immune-privileged site. Immunol. Rev. *213,* 146-158.

Munn, D.H., Sharma, M.D., Baban, B., Harding, H.P., Zhang, Y., Ron, D., and Mellor, A.L. (2005). GCN2 kinase in T cells mediates proliferative arrest and anergy induction in response to indoleamine 2,3-dioxygenase. Immunity *22,* 633-642.

Murakami, M., Zheng, Y., Hirashima, M., Suda, T., Morita, Y., Ooehara, J., Ema, H., Fong, G.H., and Shibuya, M. (2008). VEGFR1 tyrosine kinase signaling promotes lymphangiogenesis as well as angiogenesis indirectly via macrophage recruitment. Arterioscler. Thromb. Vasc. Biol. *28,* 658-664.

Murakami, Y., Uemura, K., Sudo, T., Hayashidani, Y., Hashimoto, Y., Nakashima, A., Yuasa, Y., Kondo, N., Ohge, H., and Sueda, T. (2010). Number of metastatic lymph nodes, but not lymph node ratio, is an independent prognostic factor after resection of pancreatic carcinoma. J. Am. Coll. Surg. *211,* 196-204.

Muscaritoli, M., Molfino, A., Lucia, S., and Rossi Fanelli, F. (2015). Cachexia: a preventable comorbidity of cancer. A T.A.R.G.E.T. approach. Crit. Rev. Oncol. Hematol. *94,* 251-259.

Nagai, K., Doi, R., Koizumi, M., Masui, T., Kawaguchi, Y., Yoshizawa, A., and Uemoto, S. (2011). Noninvasive intraductal papillary mucinous neoplasm with para-aortic lymph node metastasis: report of a case. Surg. Today *41,* 147-152.

Nagakawa, T., Kobayashi, H., Ueno, K., Ohta, T., Kayahara, M., and Miyazaki, I. (1994). Clinical study of lymphatic flow to the paraaortic lymph nodes in carcinoma of the head of the pancreas. Cancer *73,* 1155-1162.

Naidoo, K., Jones, R., Dmitrovic, B., Wijesuriya, N., Kocher, H., Hart, I.R., and Crnogorac-Jurcevic, T. (2012). Proteome of formalin-fixed paraffin-embedded pancreatic ductal adenocarcinoma and lymph node metastases. J. Pathol. *226,* 756-763.

Nakagohri, T., Kinoshita, T., Konishi, M., Takahashi, S., and Gotohda, N. (2006). Nodal involvement is strongest predictor of poor survival in patients with invasive adenocarcinoma of the head of the pancreas. Hepatogastroenterology *53,* 447-451.

Nakamura, K., Tan, F., Li, Z., and Thiele, C.J. (2011). NGF activation of TrkA induces vascular endothelial growth factor expression via induction of hypoxia-inducible factor-1alpha. Mol. Cell. Neurosci. *46,* 498-506.

Nakao, A., Harada, A., Nonami, T., Kaneko, T., Murakami, H., Inoue, S., Takeuchi, Y., and Takagi, H. (1995). Lymph node metastases in carcinoma of the head of the pancreas region. Br. J. Surg. *82,* 399-402.

Nathanson, S.D., Shah, R., and Rosso, K. (2015). Sentinel lymph node metastases in cancer: causes, detection and their role in disease progression. Semin. Cell Dev. Biol. *38,* 106-116.

Neal, J., and Wakelee, H. (2010). AMG-386, a selective angiopoietin-1/-2-neutralizing peptibody for the potential treatment of cancer. Curr. Opin. Mol. Ther. *12,* 487-495.

Nguyen, T.C., Sohn, T.A., Cameron, J.L., Lillemoe, K.D., Campbell, K.A., Coleman, J., Sauter, P.K., Abrams, R.A., Hruban, R.H., and Yeo, C.J. (2003). Standard vs. radical pancreaticoduodenectomy for periampullary adenocarcinoma: a prospective, randomized trial evaluating quality of life in pancreaticoduodenectomy survivors. J. Gastrointest. Surg. *7,* 1-9; discussion 9-11.

Nimura, Y., Nagino, M., Takao, S., Takada, T., Miyazaki, K., Kawarada, Y., Miyagawa, S., Yamaguchi, A., Ishiyama, S., Takeda, Y.*, et al.* (2012). Standard versus extended lymphadenectomy in radical pancreatoduodenectomy for ductal adenocarcinoma of the head of the pancreas: long-term results of a Japanese multicenter randomized controlled trial. J. Hepatobiliary. Pancreat. Sci. *19,* 230-241.

Nobis, M., McGhee, E.J., Morton, J.P., Schwarz, J.P., Karim, S.A., Quinn, J., Edward, M., Campbell, A.D., McGarry, L.C., Evans, T.R.*, et al.* (2013). Intravital FLIM-FRET imaging reveals dasatinib-induced spatial control of src in pancreatic cancer. Cancer Res. *73,* 4674-4686.

Nune, S.K., Gunda, P., Majeti, B.K., Thallapally, P.K., and Forrest, M.L. (2011). Advances in lymphatic imaging and drug delivery. Adv. Drug Deliv. Rev. *63,* 876-885.

Ochi, N., Matsuo, Y., Sawai, H., Yasuda, A., Takahashi, H., Sato, M., Funahashi, H., Okada, Y., and Manabe, T. (2007). Vascular endothelial growth factor-C secreted by pancreatic cancer cell line promotes lymphatic endothelial cell migration in an in vitro model of tumor lymphangiogenesis. Pancreas *34,* 444-451.

Oh, S.J., Jeltsch, M.M., Birkenhager, R., McCarthy, J.E., Weich, H.A., Christ, B., Alitalo, K., and Wilting, J. (1997). VEGF and VEGF-C: specific induction of angiogenesis and lymphangiogenesis in the differentiated avian chorioallantoic membrane. Dev. Biol. *188,* 96-109.

O'Hagan, D., Christy, N., and Davis, S. (1992). Particulates and lymphatic drug delivery. In Lymphatic transport of drugs, Charman, W., and Stella, V. eds., (Boca Raton, FL, USA: CRC Press Inc.) pp. 279-280-315.

Ohta, T., Nagakawa, T., Ueno, K., Kayahara, M., Mori, K., Kobayashi, H., Takeda, T., and Miyazaki, I. (1993). The mode of lymphatic and local spread of pancreatic carcinomas less than 4.0 cm in size. Int. Surg. *78,* 208-212.

Ohta, T., Terada, T., Nagakawa, T., Tajima, H., Itoh, H., Fonseca, L., and Miyazaki, I. (1994). Pancreatic trypsinogen and cathepsin B in human pancreatic carcinomas and associated metastatic lesions. Br. J. Cancer *69,* 152-156.

Olszewski, W.L., Stanczyk, M., Gewartowska, M., Domaszewska-Szostek, A., and Durlik, M. (2012). Lack of functioning intratumoral lymphatics in colon and pancreas cancer tissue. Lymphat Res. Biol. *10,* 112-117.

O'Morchoe, C.C. (1997). Lymphatic system of the pancreas. Microsc. Res. Tech. *37,* 456-477.

Oommen, S., Gupta, S.K., and Vlahakis, N.E. (2011). Vascular endothelial growth factor A (VEGF-A) induces endothelial and cancer cell migration through direct binding to integrin {alpha}9{beta}1: identification of a specific {alpha}9{beta}1 binding site. J. Biol. Chem. *286,* 1083-1092.

Ou, J.J., Wei, X., Peng, Y., Zha, L., Zhou, R.B., Shi, H., Zhou, Q., and Liang, H.J. (2015). Neuropilin-2 mediates lymphangiogenesis of colorectal carcinoma via a VEGFC/VEGFR3 independent signaling. Cancer Lett. *358,* 200-209.

Padera, T.P., Kadambi, A., di Tomaso, E., Carreira, C.M., Brown, E.B., Boucher, Y., Choi, N.C., Mathisen, D., Wain, J., Mark, E.J., Munn, L.L., and Jain, R.K. (2002). Lymphatic metastasis in the absence of functional intratumor lymphatics. Science *296,* 1883-1886.

Padera, T.P., Kuo, A.H., Hoshida, T., Liao, S., Lobo, J., Kozak, K.R., Fukumura, D., and Jain, R.K. (2008). Differential response of primary tumor versus lymphatic metastasis to VEGFR-2 and VEGFR-3 kinase inhibitors cediranib and vandetanib. Mol. Cancer. Ther. *7,* 2272-2279.

Pai, R.K., Beck, A.H., Mitchem, J., Linehan, D.C., Chang, D.T., Norton, J.A., and Pai, R.K. (2011). Pattern of lymph node involvement and prognosis in pancreatic adenocarcinoma: direct lymph node invasion has similar survival to node-negative disease. Am. J. Surg. Pathol. *35,* 228-234.

Pang, M.F., Georgoudaki, A.M., Lambut, L., Johansson, J., Tabor, V., Hagikura, K., Jin, Y., Jansson, M., Alexander, J.S., Nelson, C.M.*, et al.* (2015). TGF-beta1-induced EMT promotes targeted migration of breast cancer cells through the lymphatic system by the activation of CCR7/CCL21-mediated chemotaxis. Oncogene

Pannala, R., Leibson, C.L., Rabe, K.G., Timmons, L.J., Ransom, J., de Andrade, M., Petersen, G.M., and Chari, S.T. (2009). Temporal association of changes in fasting blood glucose and body mass index with diagnosis of pancreatic cancer. Am. J. Gastroenterol. *104,* 2318-2325.

Pawlik, T.M., Abdalla, E.K., Barnett, C.C., Ahmad, S.A., Cleary, K.R., Vauthey, J.N., Lee, J.E., Evans, D.B., and Pisters, P.W. (2005). Feasibility of a randomized trial of extended lymphadenectomy for pancreatic cancer. Arch. Surg. *140,* 584-9; discussion 589-91.

Pawlik, T.M., Gleisner, A.L., Cameron, J.L., Winter, J.M., Assumpcao, L., Lillemoe, K.D., Wolfgang, C., Hruban, R.H., Schulick, R.D., Yeo, C.J., and Choti, M.A. (2007). Prognostic relevance of lymph node ratio following pancreaticoduodenectomy for pancreatic cancer. Surgery *141,* 610-618.

Pederzoli, P., Bassi, C., Falconi, M., and Pedrazzoli, S. (1997). Does the extent of lymphatic resection affect the outcome in pancreatic cancer? Digestion *58,* 536-541.

Pedrazzoli, S. (2015). Extent of lymphadenectomy to associate with pancreaticoduodenectomy in patients with pancreatic head cancer for better tumor staging. Cancer Treat. Rev. *41,* 577-587.

Pedrazzoli, S., DiCarlo, V., Dionigi, R., Mosca, F., Pederzoli, P., Pasquali, C., Kloppel, G., Dhaene, K., and Michelassi, F. (1998). Standard versus extended lymphadenectomy associated with pancreatoduodenectomy in the surgical treatment of adenocarcinoma of the head of the pancreas: a multicenter, prospective, randomized study. Lymphadenectomy Study Group. Ann. Surg. *228,* 508-517.

Penet, M.F., Gadiya, M.M., Krishnamachary, B., Nimmagadda, S., Pomper, M.G., Artemov, D., and Bhujwalla, Z.M. (2011). Metabolic signatures imaged in cancer-induced cachexia. Cancer Res. *71,* 6948-6956.

Peparini, N. (2015). Mesopancreas: A boundless structure, namely the rationale for dissection of the paraaortic area in pancreaticoduodenectomy for pancreatic head carcinoma. World J. Gastroenterol. *21,* 2865-2870.

Peppicelli, S., Bianchini, F., and Calorini, L. (2014). Inflammatory cytokines induce vascular endothelial growth factor-C expression in melanoma-associated macrophages and stimulate melanoma lymph node metastasis. Oncol. Lett. *8,* 1133-1138.

Pflicke, H., and Sixt, M. (2009). Preformed portals facilitate dendritic cell entry into afferent lymphatic vessels. J. Exp. Med. *206,* 2925-2935.

Pignatelli, M., Ansari, T.W., Gunter, P., Liu, D., Hirano, S., Takeichi, M., Kloppel, G., and Lemoine, N.R. (1994). Loss of membranous E-cadherin expression in pancreatic cancer: correlation with lymph node metastasis, high grade, and advanced stage. J. Pathol. *174,* 243-248.

Pisano, M., Triacca, V., Barbee, K.A., and Swartz, M.A. (2015). An in vitro model of the tumor-lymphatic microenvironment with simultaneous transendothelial and luminal flows reveals mechanisms of flow enhanced invasion. Integr. Biol. (Camb) *7,* 525-533.

Pissas, A. (1984). Anatomoclinical and anatomosurgical essay on the lymphatic circulation of the pancreas. Anat. Clin. *6,* 255-280.

Podgrabinska, S., Kamalu, O., Mayer, L., Shimaoka, M., Snoeck, H., Randolph, G.J., and Skobe, M. (2009). Inflamed lymphatic endothelium suppresses dendritic cell maturation and function via Mac-1/ICAM-1-dependent mechanism. J. Immunol. *183,* 1767-1779.

Pour, P.M., Bell, R.H., and Batra, S.K. (2003). Neural invasion in the staging of pancreatic cancer. Pancreas *26,* 322-325.

Preynat-Seauve, O., Contassot, E., Schuler, P., Piguet, V., French, L.E., and Huard, B. (2007). Extralymphatic tumors prepare draining lymph nodes to invasion via a T-cell cross-tolerance process. Cancer Res. *67,* 5009-5016.

Procopio, G., Verzoni, E., Testa, I., Nicolai, N., Salvioni, R., and Debraud, F. (2012). Experience with sorafenib in the treatment of advanced renal cell carcinoma. Ther. Adv. Urol. *4,* 303-313.

Quaegebeur, A., Lange, C., and Carmeliet, P. (2011). The neurovascular link in health and disease: molecular mechanisms and therapeutic implications. Neuron *71,* 406-424.

Ran, S., and Montgomery, K.E. (2012). Macrophage-mediated lymphangiogenesis: the emerging role of macrophages as lymphatic endothelial progenitors. Cancers (Basel) *4,* 618-657.

Rasanen, K., and Vaheri, A. (2010). Activation of fibroblasts in cancer stroma. Exp. Cell Res. *316,* 2713-2722.

Reataza, M., and Imagawa, D.K. (2014). Advances in managing hepatocellular carcinoma. Front. Med. *8,* 175-189.

Rhim, A.D., Mirek, E.T., Aiello, N.M., Maitra, A., Bailey, J.M., McAllister, F., Reichert, M., Beatty, G.L., Rustgi, A.K., Vonderheide, R.H., Leach, S.D., and Stanger, B.Z. (2012). EMT and dissemination precede pancreatic tumor formation. Cell *148,* 349-361.

Riall, T.S., Cameron, J.L., Lillemoe, K.D., Campbell, K.A., Sauter, P.K., Coleman, J., Abrams, R.A., Laheru, D., Hruban, R.H., and Yeo, C.J. (2005). Pancreaticoduodenectomy with or without distal gastrectomy and extended retroperitoneal lymphadenectomy for periampullary adenocarcinoma--part 3: update on 5-year survival. J. Gastrointest. Surg. *9,* 1191-204; discussion 1204-6.

Ridwelski, K., Meyer, F., Fahlke, J., Kasper, U., Roessner, A., and Lippert, H. (2001). Value of cytokeratin and Ca 19-9 antigen in immunohistological detection of disseminated tumor cells in lymph nodes in pancreas carcinoma. Chirurg *72,* 920-926.

Riediger, H., Keck, T., Wellner, U., zur Hausen, A., Adam, U., Hopt, U.T., and Makowiec, F. (2009). The lymph node ratio is the strongest prognostic factor after resection of pancreatic cancer. J. Gastrointest. Surg. *13,* 1337-1344.

Ristimaki, A., Narko, K., Enholm, B., Joukov, V., and Alitalo, K. (1998). Proinflammatory cytokines regulate expression of the lymphatic endothelial mitogen vascular endothelial growth factor-C. J. Biol. Chem. *273,* 8413-8418.

Ritsma, L., Steller, E.J., Ellenbroek, S.I., Kranenburg, O., Borel Rinkes, I.H., and van Rheenen, J. (2013). Surgical implantation of an abdominal imaging window for intravital microscopy. Nat. Protoc. *8,* 583-594.

Rixe, O., Bukowski, R.M., Michaelson, M.D., Wilding, G., Hudes, G.R., Bolte, O., Motzer, R.J., Bycott, P., Liau, K.F., Freddo, J.*, et al.* (2007). Axitinib treatment in patients with cytokine-refractory metastatic renal-cell cancer: a phase II study. Lancet Oncol. *8,* 975-984.

Roberts, E.W., Deonarine, A., Jones, J.O., Denton, A.E., Feig, C., Lyons, S.K., Espeli, M., Kraman, M., McKenna, B., Wells, R.J.*, et al.* (2013). Depletion of stromal cells expressing fibroblast activation protein-alpha from skeletal muscle and bone marrow results in cachexia and anemia. J. Exp. Med. *210,* 1137-1151.

Roberts, N., Kloos, B., Cassella, M., Podgrabinska, S., Persaud, K., Wu, Y., Pytowski, B., and Skobe, M. (2006). Inhibition of VEGFR-3 activation with the antagonistic antibody more potently suppresses lymph node and distant metastases than inactivation of VEGFR-2. Cancer Res. *66,* 2650-2657.

Robinson, S.M., Rahman, A., Haugk, B., French, J.J., Manas, D.M., Jaques, B.C., Charnley, R.M., and White, S.A. (2012). Metastatic lymph node ratio as an important prognostic factor in pancreatic ductal adenocarcinoma. Eur. J. Surg. Oncol. *38,* 333-339.

Roche, C.J., Hughes, M.L., Garvey, C.J., Campbell, F., White, D.A., Jones, L., and Neoptolemos, J.P. (2003). CT and pathologic assessment of prospective nodal staging in patients with ductal adenocarcinoma of the head of the pancreas. AJR Am. J. Roentgenol. *180,* 475-480.

Rodriguez-Diaz, R., Abdulreda, M.H., Formoso, A.L., Gans, I., Ricordi, C., Berggren, P.O., and Caicedo, A. (2011). Innervation patterns of autonomic axons in the human endocrine pancreas. Cell. Metab. *14,* 45-54.

Rossi, S., Mantelli, F., Lambiase, A., and Aloe, L. (2012). Bevacizumab eye drop treatment stimulates tear secretion in rats through changes in VEGF and NGF lacrimal gland levels. Arch. Ital. Biol. *150,* 15-21.

Rouhani, S.J., Eccles, J.D., Riccardi, P., Peske, J.D., Tewalt, E.F., Cohen, J.N., Liblau, R., Makinen, T., and Engelhard, V.H. (2015). Roles of lymphatic endothelial cells expressing peripheral tissue antigens in CD4 T-cell tolerance induction. Nat. Commun. *6,* 6771.

Rubbia-Brandt, L., Terris, B., Giostra, E., Dousset, B., Morel, P., and Pepper, M.S. (2004). Lymphatic vessel density and vascular endothelial growth factor-C expression correlate with malignant behavior in human pancreatic endocrine tumors. Clin. Cancer Res. *10,* 6919-6928.

Safuan, S., Storr, S.J., Patel, P.M., and Martin, S.G. (2012). A comparative study of adhesion of melanoma and breast cancer cells to blood and lymphatic endothelium. Lymphat Res. Biol. *10,* 173-181.

Sahora, K., Schindl, M., Kuehrer, I., Eisenhut, A., Werba, G., Brostjan, C., Telek, B., Ba'ssalamah, A., Stift, J., Schoppmann, S.F., and Gnant, M. (2014). A phase II trial of two durations of Bevacizumab added to neoadjuvant gemcitabine for borderline and locally advanced pancreatic cancer. Anticancer Res. *34,* 2377-2384.

Saltz, L.B., Clarke, S., Diaz-Rubio, E., Scheithauer, W., Figer, A., Wong, R., Koski, S., Lichinitser, M., Yang, T.S., Rivera, F.*, et al.* (2008). Bevacizumab in combination with oxaliplatin-based chemotherapy as first-line therapy in metastatic colorectal cancer: a randomized phase III study. J. Clin. Oncol. *26,* 2013-2019.

Samii, A., Unger, J., and Lange, W. (1999). Vascular endothelial growth factor expression in peripheral nerves and dorsal root ganglia in diabetic neuropathy in rats. Neurosci. Lett. *262,* 159-162.

Samra, J.S., Gananadha, S., and Hugh, T.J. (2008). Surgical management of carcinoma of the head of pancreas: extended lymphadenectomy or modified en bloc resection? ANZ J. Surg. *78,* 228-236.

Sandler, A., Gray, R., Perry, M.C., Brahmer, J., Schiller, J.H., Dowlati, A., Lilenbaum, R., and Johnson, D.H. (2006). Paclitaxel-carboplatin alone or with bevacizumab for non-small-cell lung cancer. N. Engl. J. Med. *355,* 2542-2550.

Santi, I., Brandt, A., and Hemminki, K. (2011). What is the major prognostic factor in tumor-node-metastasis staging of pancreatic adenocarcinoma? Ann. Surg. Oncol. *18,* 300-301.

Sawa, Y., Sugimoto, Y., Ueki, T., Ishikawa, H., Sato, A., Nagato, T., and Yoshida, S. (2007). Effects of TNF-alpha on leukocyte adhesion molecule expressions in cultured human lymphatic endothelium. J. Histochem. Cytochem. *55,* 721-733.

Saygili, E., Pekassa, M., Saygili, E., Rackauskas, G., Hommes, D., Noor-Ebad, F., Gemein, C., Zink, M.D., Schwinger, R.H., Weis, J.*, et al.* (2011). Mechanical stretch of sympathetic neurons induces VEGF expression via a NGF and CNTF signaling pathway. Biochem. Biophys. Res. Commun. *410,* 62-67.

Scavelli, C., Vacca, A., Di Pietro, G., Dammacco, F., and Ribatti, D. (2004). Crosstalk between angiogenesis and lymphangiogenesis in tumor progression. Leukemia *18,* 1054-1058.

Schacht, V., Ramirez, M.I., Hong, Y.K., Hirakawa, S., Feng, D., Harvey, N., Williams, M., Dvorak, A.M., Dvorak, H.F., Oliver, G., and Detmar, M. (2003). T1alpha/podoplanin deficiency disrupts normal lymphatic vasculature formation and causes lymphedema. EMBO J. *22,* 3546-3556.

Schafer, M., Oeing, C.U., Rohm, M., Baysal-Temel, E., Lehmann, L.H., Bauer, R., Volz, H.C., Boutros, M., Sohn, D., Sticht, C*., et al.* (2015). Ataxin-10 is part of a cachexokine cocktail triggering cardiac metabolic dysfunction in cancer cachexia. Mol. Metab. *5,* 67-78.

Schledzewski, K., Falkowski, M., Moldenhauer, G., Metharom, P., Kzhyshkowska, J., Ganss, R., Demory, A., Falkowska-Hansen, B., Kurzen, H., Ugurel, S*., et al.* (2006). Lymphatic endothelium-specific hyaluronan receptor LYVE-1 is expressed by stabilin-1+, F4/80+, CD11b+ macrophages in malignant tumours and wound healing tissue in vivo and in bone marrow cultures in vitro: implications for the assessment of lymphangiogenesis. J. Pathol. *209,* 67-77.

Schneider, C.A., Rasband, W.S., and Eliceiri, K.W. (2012). NIH Image to ImageJ: 25 years of image analysis. Nat. Methods *9,* 671-675.

Schneider, M., Buchler, P., Giese, N., Giese, T., Wilting, J., Buchler, M.W., and Friess, H. (2006). Role of lymphangiogenesis and lymphangiogenic factors during pancreatic cancer progression and lymphatic spread. Int. J. Oncol. *28,* 883-890.

Schoellhammer, H.F., Goldner, B.S., Kim, J., and Singh, G. (2015). Beyond the whipple operation: radical resections for cancers of the head of the pancreas. Indian. J. Surg. Oncol. *6,* 41-46.

Schoppmann, S.F., Birner, P., Stockl, J., Kalt, R., Ullrich, R., Caucig, C., Kriehuber, E., Nagy, K., Alitalo, K., and Kerjaschki, D. (2002). Tumor-associated macrophages express lymphatic endothelial growth factors and are related to peritumoral lymphangiogenesis. Am. J. Pathol. *161,* 947-956.

Schoppmann, S.F., Fenzl, A., Nagy, K., Unger, S., Bayer, G., Geleff, S., Gnant, M., Horvat, R., Jakesz, R., and Birner, P. (2006). VEGF-C expressing tumor-associated macrophages in lymph node positive breast cancer: impact on lymphangiogenesis and survival. Surgery *139,* 839-846.

Schulz, P., Fischer, C., Detjen, K.M., Rieke, S., Hilfenhaus, G., von Marschall, Z., Bohmig, M., Koch, I., Kehrberger, J., Hauff, P*., et al.* (2011). Angiopoietin-2 drives lymphatic metastasis of pancreatic cancer. FASEB J. *25,* 3325-3335.

Schulz, P., Scholz, A., Rexin, A., Hauff, P., Schirner, M., Wiedenmann, B., and Detjen, K. (2008). Inducible re-expression of p16 in an orthotopic mouse model of pancreatic cancer inhibits lymphangiogenesis and lymphatic metastasis. Br. J. Cancer *99,* 110-117.

Schutz, F.A., Choueiri, T.K., and Sternberg, C.N. (2011). Pazopanib: Clinical development of a potent anti-angiogenic drug. Crit. Rev. Oncol. Hematol. *77,* 163-171.

Schwarz, R.E., and Smith, D.D. (2006). Extent of lymph node retrieval and pancreatic cancer survival: information from a large US population database. Ann. Surg. Oncol. *13,* 1189-1200.

Seo, K., Choi, J., Park, M., and Rhee, C. (2001a). Angiogenesis effects of nerve growth factor (NGF) on rat corneas. J. Vet. Sci. *2,* 125-130.

Seo, N., Hayakawa, S., Takigawa, M., and Tokura, Y. (2001b). Interleukin-10 expressed at early tumour sites induces subsequent generation of CD4(+) T-regulatory cells and systemic collapse of antitumour immunity. Immunology *103,* 449-457.

Sergeant, G., Ectors, N., Fieuws, S., Aerts, R., and Topal, B. (2009). Prognostic relevance of extracapsular lymph node involvement in pancreatic ductal adenocarcinoma. Ann. Surg. Oncol. *16,* 3070-3079.

Sergeant, G., Melloul, E., Lesurtel, M., Deoliveira, M.L., and Clavien, P.A. (2013). Extended lymphadenectomy in patients with pancreatic cancer is debatable. World J. Surg. *37,* 1782-1788.

Serhan, C.N., Brain, S.D., Buckley, C.D., Gilroy, D.W., Haslett, C., O'Neill, L.A., Perretti, M., Rossi, A.G., and Wallace, J.L. (2007). Resolution of inflammation: state of the art, definitions and terms. FASEB J. *21,* 325-332.

Serhan, C.N., Chiang, N., and Van Dyke, T.E. (2008). Resolving inflammation: dual anti-inflammatory and pro-resolution lipid mediators. Nat. Rev. Immunol. *8,* 349-361.

Serhan, C.N., and Savill, J. (2005). Resolution of inflammation: the beginning programs the end. Nat. Immunol. *6,* 1191-1197.

Sevick-Muraca, E.M., Kwon, S., and Rasmussen, J.C. (2014). Emerging lymphatic imaging technologies for mouse and man. J. Clin. Invest. *124,* 905-914.

Shi, K., Queiroz, K.C., Roelofs, J.J., van Noesel, C.J., Richel, D.J., and Spek, C.A. (2014). Protease-activated receptor 2 suppresses lymphangiogenesis and subsequent lymph node metastasis in a murine pancreatic cancer model. J. Pathol. *234,* 398-409.

Shi, Y., Tong, M., Wu, Y., Yang, Z., Hoffman, R.M., Zhang, Y., Tian, Y., Qi, M., Lin, Y., Liu, Y.*, et al.* (2013). VEGF-C ShRNA inhibits pancreatic cancer growth and lymphangiogenesis in an orthotopic fluorescent nude mouse model. Anticancer Res. *33,* 409-417.

Shields, J.D., Emmett, M.S., Dunn, D.B., Joory, K.D., Sage, L.M., Rigby, H., Mortimer, P.S., Orlando, A., Levick, J.R., and Bates, D.O. (2007). Chemokine-mediated migration of melanoma cells towards lymphatics--a mechanism contributing to metastasis. Oncogene *26,* 2997-3005.

Shields, J.D., Kourtis, I.C., Tomei, A.A., Roberts, J.M., and Swartz, M.A. (2010). Induction of lymphoidlike stroma and immune escape by tumors that express the chemokine CCL21. Science *328,* 749-752.

Shimada, K., Nara, S., Esaki, M., Sakamoto, Y., Kosuge, T., and Hiraoka, N. (2011). Intrapancreatic nerve invasion as a predictor for recurrence after pancreaticoduodenectomy in patients with invasive ductal carcinoma of the pancreas. Pancreas *40,* 464-468.

Shimada, K., Sakamoto, Y., Sano, T., and Kosuge, T. (2006). The role of paraaortic lymph node involvement on early recurrence and survival after macroscopic curative resection with extended lymphadenectomy for pancreatic carcinoma. J. Am. Coll. Surg. *203,* 345-352.

Shimizu, K., Kubo, H., Yamaguchi, K., Kawashima, K., Ueda, Y., Matsuo, K., Awane, M., Shimahara, Y., Takabayashi, A., Yamaoka, Y., and Satoh, S. (2004). Suppression of VEGFR-3 signaling inhibits lymph node metastasis in gastric cancer. Cancer. Sci. *95,* 328-333.

Siegel, R.L., Miller, K.D., and Jemal, A. (2016). Cancer statistics, 2016. CA Cancer. J. Clin. *66,* 7-30.

Siegel, R.L., Miller, K.D., and Jemal, A. (2015). Cancer statistics, 2015. CA Cancer. J. Clin. *65,* 5-29.

Sierzega, M., Popiela, T., Kulig, J., and Nowak, K. (2006). The ratio of metastatic/resected lymph nodes is an independent prognostic factor in patients with node-positive pancreatic head cancer. Pancreas *33,* 240-245.

Singh, I., Swami, R., Khan, W., and Sistla, R. (2014). Lymphatic system: a prospective area for advanced targeting of particulate drug carriers. Expert Opin. Drug Deliv. *11,* 211-229.

Sini, P., Samarzija, I., Baffert, F., Littlewood-Evans, A., Schnell, C., Theuer, A., Christian, S., Boos, A., Hess-Stumpp, H., Foekens, J.A*., et al.* (2008). Inhibition of multiple vascular endothelial growth factor receptors (VEGFR) blocks lymph node metastases but inhibition of VEGFR-2 is sufficient to sensitize tumor cells to platinum-based chemotherapeutics. Cancer Res. *68,* 1581-1592.

Sipos, B., Kojima, M., Tiemann, K., Klapper, W., Kruse, M.L., Kalthoff, H., Schniewind, B., Tepel, J., Weich, H., Kerjaschki, D., and Kloppel, G. (2005). Lymphatic spread of ductal pancreatic adenocarcinoma is independent of lymphangiogenesis. J. Pathol. *207,* 301-312.

Slidell, M.B., Chang, D.C., Cameron, J.L., Wolfgang, C., Herman, J.M., Schulick, R.D., Choti, M.A., and Pawlik, T.M. (2008). Impact of total lymph node count and lymph node ratio on staging and survival after pancreatectomy for pancreatic adenocarcinoma: a large, population-based analysis. Ann. Surg. Oncol. *15,* 165-174.

Smith, B.J., and Mezhir, J.J. (2014). An interactive Bayesian model for prediction of lymph node ratio and survival in pancreatic cancer patients. J. Am. Med. Inform. Assoc. *21,* e203-11.

Sohal, D.P., Metz, J.M., Sun, W., Giantonio, B.J., Plastaras, J.P., Ginsberg, G., Kochman, M.L., Teitelbaum, U.R., Harlacker, K., Heitjan, D.F*., et al.* (2013). Toxicity study of gemcitabine, oxaliplatin, and bevacizumab, followed by 5-fluorouracil, oxaliplatin, bevacizumab, and radiotherapy, in patients with locally advanced pancreatic cancer. Cancer Chemother. Pharmacol. *71,* 1485-1491.

Solares, C.A., Brown, I., Boyle, G.M., Parsons, P.G., and Panizza, B. (2009). Neural cell adhesion molecule expression: no correlation with perineural invasion in cutaneous squamous cell carcinoma of the head and neck. Head Neck *31,* 802-806.

Solito, R., Alessandrini, C., Fruschelli, M., Pucci, A.M., and Gerli, R. (1997). An immunological correlation between the anchoring filaments of initial lymph vessels and the neighboring elastic fibers: a unified morphofunctional concept. Lymphology *30,* 194-202.

Solorzano, C.C., Baker, C.H., Bruns, C.J., Killion, J.J., Ellis, L.M., Wood, J., and Fidler, I.J. (2001). Inhibition of growth and metastasis of human pancreatic cancer growing in nude mice by PTK 787/ZK222584, an inhibitor of the vascular endothelial growth factor receptor tyrosine kinases. Cancer Biother. Radiopharm. *16,* 359-370.

Sornelli, F., Lambiase, A., Mantelli, F., and Aloe, L. (2010). NGF and NGF-receptor expression of cultured immortalized human corneal endothelial cells. Mol. Vis. *16,* 1439-1447.

Spano, J.P., Chodkiewicz, C., Maurel, J., Wong, R., Wasan, H., Barone, C., Letourneau, R., Bajetta, E., Pithavala, Y., Bycott, P*., et al.* (2008). Efficacy of gemcitabine plus axitinib compared with gemcitabine alone in patients with advanced pancreatic cancer: an open-label randomised phase II study. Lancet *371,* 2101-2108.

Sperveslage, J., Frank, S., Heneweer, C., Egberts, J., Schniewind, B., Buchholz, M., Bergmann, F., Giese, N., Munding, J., Hahn, S.A*., et al.* (2012). Lack of CCR7 expression is rate limiting for lymphatic spread of pancreatic ductal adenocarcinoma. Int. J. Cancer *131,* E371-81.

Stacker, S.A., Caesar, C., Baldwin, M.E., Thornton, G.E., Williams, R.A., Prevo, R., Jackson, D.G., Nishikawa, S., Kubo, H., and Achen, M.G. (2001). VEGF-D promotes the metastatic spread of tumor cells via the lymphatics. Nat. Med. *7,* 186-191.

Stacker, S.A., Williams, S.P., Karnezis, T., Shayan, R., Fox, S.B., and Achen, M.G. (2014). Lymphangiogenesis and lymphatic vessel remodelling in cancer. Nat. Rev. Cancer. *14,* 159-172.

Stephens, N.A., Gallagher, I.J., Rooyackers, O., Skipworth, R.J., Tan, B.H., Marstrand, T., Ross, J.A., Guttridge, D.C., Lundell, L., Fearon, K.C., and Timmons, J.A. (2010). Using transcriptomics to identify and validate novel biomarkers of human skeletal muscle cancer cachexia. Genome Med. *2,* 1.

Steven, P., Bock, F., Huttmann, G., and Cursiefen, C. (2011). Intravital two-photon microscopy of immune cell dynamics in corneal lymphatic vessels. PLoS One *6,* e26253.

Stopczynski, R.E., Normolle, D.P., Hartman, D.J., Ying, H., DeBerry, J.J., Bielefeldt, K., Rhim, A.D., DePinho, R.A., Albers, K.M., and Davis, B.M. (2014). Neuroplastic changes occur early in the development of pancreatic ductal adenocarcinoma. Cancer Res. *74,* 1718-1727.

Storr, S.J., Safuan, S., Mitra, A., Elliott, F., Walker, C., Vasko, M.J., Ho, B., Cook, M., Mohammed, R.A., Patel, P.M*., et al.* (2012). Objective assessment of blood and lymphatic vessel invasion and association with macrophage infiltration in cutaneous melanoma. Mod. Pathol. *25,* 493-504.

Sugimura, K., Miyata, H., Tanaka, K., Takahashi, T., Kurokawa, Y., Yamasaki, M., Nakajima, K., Takiguchi, S., Mori, M., and Doki, Y. (2015). High infiltration of tumor-associated macrophages is

associated with a poor response to chemotherapy and poor prognosis of patients undergoing neoadjuvant chemotherapy for esophageal cancer. J. Surg. Oncol. *111,* 752-759.

Sun, W., Leong, C.N., Zhang, Z., and Lu, J.J. (2010). Proposing the lymphatic target volume for elective radiation therapy for pancreatic cancer: a pooled analysis of clinical evidence. Radiat. Oncol. *5,* 28-717X-5-28.

Suzuki, M., Takahashi, T., Ouchi, K., and Matsuno, S. (1994). Perineural tumor invasion and its relation with the lymphogenous spread in human and experimental carcinoma of bile duct. A computer-aided 3-D reconstruction study. Tohoku J. Exp. Med. *172,* 17-28.

Svoronos, C., Tsoulfas, G., Katsourakis, A., Noussios, G., Chatzitheoklitos, E., and Marakis, N.G. (2014). Role of extended lymphadenectomy in the treatment of pancreatic head adenocarcinoma: review and meta-analysis. ANZ J. Surg. *84,* 706-711.

Swanson, B.J., McDermott, K.M., Singh, P.K., Eggers, J.P., Crocker, P.R., and Hollingsworth, M.A. (2007). MUC1 is a counter-receptor for myelin-associated glycoprotein (Siglec-4a) and their interaction contributes to adhesion in pancreatic cancer perineural invasion. Cancer Res. *67,* 10222-10229.

Swartz, M.A. (2014). Immunomodulatory roles of lymphatic vessels in cancer progression. Cancer. Immunol. Res. *2,* 701-707.

Sweat, R.S., Sloas, D.C., and Murfee, W.L. (2014). VEGF-C Induces Lymphangiogenesis and Angiogenesis in the Rat Mesentery Culture Model. Microcirculation

Tacconi, C., Correale, C., Gandelli, A., Spinelli, A., Dejana, E., D'Alessio, S., and Danese, S. (2015). Vascular endothelial growth factor C disrupts the endothelial lymphatic barrier to promote colorectal cancer invasion. Gastroenterology *148,* 1438-51.e8.

Takahashi, H., Ohigashi, H., Ishikawa, O., Gotoh, K., Yamada, T., Nagata, S., Tomita, Y., Eguchi, H., Doki, Y., and Yano, M. (2012). Perineural invasion and lymph node involvement as indicators of surgical outcome and pattern of recurrence in the setting of preoperative gemcitabine-based chemoradiation therapy for resectable pancreatic cancer. Ann. Surg. *255,* 95-102.

Tal, O., Lim, H.Y., Gurevich, I., Milo, I., Shipony, Z., Ng, L.G., Angeli, V., and Shakhar, G. (2011). DC mobilization from the skin requires docking to immobilized CCL21 on lymphatic endothelium and intralymphatic crawling. J. Exp. Med. *208,* 2141-2153.

Tamburrino, A., Piro, G., Carbone, C., Tortora, G., and Melisi, D. (2013). Mechanisms of resistance to chemotherapeutic and anti-angiogenic drugs as novel targets for pancreatic cancer therapy. Front. Pharmacol. *4,* 56.

Tammela, T., and Alitalo, K. (2010). Lymphangiogenesis: Molecular mechanisms and future promise. Cell *140,* 460-476.

Tan, B.H., Birdsell, L.A., Martin, L., Baracos, V.E., and Fearon, K.C. (2009). Sarcopenia in an overweight or obese patient is an adverse prognostic factor in pancreatic cancer. Clin. Cancer Res. *15,* 6973-6979.

Tan, M.H., Bryars, J., and Moore, J. (2006). Use of nerve growth factor to treat congenital neurotrophic corneal ulceration. Cornea *25,* 352-355.

Tang, R.F., Itakura, J., Aikawa, T., Matsuda, K., Fujii, H., Korc, M., and Matsumoto, Y. (2001). Overexpression of lymphangiogenic growth factor VEGF-C in human pancreatic cancer. Pancreas *22,* 285-292.

Tao, J., Li, T., Li, K., Xiong, J., Yang, Z., Wu, H., and Wang, C. (2006). Effect of HIF-1alpha on VEGF-C induced lymphangiogenesis and lymph nodes metastases of pancreatic cancer. J. Huazhong Univ. Sci. Technolog Med. Sci. *26,* 562-564.

Tempero, M.A., Malafa, M.P., Behrman, S.W., Benson, A.B.,3rd, Casper, E.S., Chiorean, E.G., Chung, V., Cohen, S.J., Czito, B., Engebretson, A*., et al.* (2014). Pancreatic adenocarcinoma, version 2.2014: featured updates to the NCCN guidelines. J. Natl. Compr. Canc Netw. *12,* 1083-1093.

Tempia-Caliera, A.A., Horvath, L.Z., Zimmermann, A., Tihanyi, T.T., Korc, M., Friess, H., and Buchler, M.W. (2002). Adhesion molecules in human pancreatic cancer. J. Surg. Oncol. *79,* 93-100.

Tewalt, E.F., Cohen, J.N., Rouhani, S.J., Guidi, C.J., Qiao, H., Fahl, S.P., Conaway, M.R., Bender, T.P., Tung, K.S., Vella, A.T*., et al.* (2012). Lymphatic endothelial cells induce tolerance via PD-L1 and lack of costimulation leading to high-level PD-1 expression on CD8 T cells. Blood *120,* 4772-4782.

Tezel, E., Kawase, Y., Takeda, S., Oshima, K., and Nakao, A. (2001). Expression of neural cell adhesion molecule in pancreatic cancer. Pancreas *22,* 122-125.

Thelen, A., Scholz, A., Benckert, C., von Marschall, Z., Schroder, M., Wiedenmann, B., Neuhaus, P., Rosewicz, S., and Jonas, S. (2008). VEGF-D promotes tumor growth and lymphatic spread in a mouse model of hepatocellular carcinoma. Int. J. Cancer *122,* 2471-2481.

Tian, H., Callahan, C.A., DuPree, K.J., Darbonne, W.C., Ahn, C.P., Scales, S.J., and de Sauvage, F.J. (2009). Hedgehog signaling is restricted to the stromal compartment during pancreatic carcinogenesis. Proc. Natl. Acad. Sci. U. S. A. *106,* 4254-4259.

Tian, M., Asp, M.L., Nishijima, Y., and Belury, M.A. (2011). Evidence for cardiac atrophic remodeling in cancer-induced cachexia in mice. Int. J. Oncol. *39,* 1321-1326.

Tian, M., Nishijima, Y., Asp, M.L., Stout, M.B., Reiser, P.J., and Belury, M.A. (2010). Cardiac alterations in cancer-induced cachexia in mice. Int. J. Oncol. *37,* 347-353.

Tol, J.A., Brosens, L.A., van Dieren, S., van Gulik, T.M., Busch, O.R., Besselink, M.G., and Gouma, D.J. (2015). Impact of lymph node ratio on survival in patients with pancreatic and periampullary cancer. Br. J. Surg. *102,* 237-245.

Tol, J.A., Gouma, D.J., Bassi, C., Dervenis, C., Montorsi, M., Adham, M., Andren-Sandberg, A., Asbun, H.J., Bockhorn, M., Buchler, M.W*., et al.* (2014). Definition of a standard lymphadenectomy in surgery for pancreatic ductal adenocarcinoma: a consensus statement by the International Study Group on Pancreatic Surgery (ISGPS). Surgery *156,* 591-600.

Tomlinson, D.R., and Gardiner, N.J. (2008). Glucose neurotoxicity. Nat. Rev. Neurosci. *9,* 36-45.

Torer, N., Kayaselcuk, F., Nursal, T.Z., Yildirim, S., Tarim, A., Noyan, T., and Karakayali, H. (2007). Adhesion molecules as prognostic markers in pancreatic adenocarcinoma. J. Surg. Oncol. *96,* 419-423.

Torre, L.A., Bray, F., Siegel, R.L., Ferlay, J., Lortet-Tieulent, J., and Jemal, A. (2015). Global cancer statistics, 2012. CA Cancer. J. Clin. *65,* 87-108.

Tran Cao, H.S., McElroy, M., Kaushal, S., Hoffman, R.M., and Bouvet, M. (2011). Imaging of the interaction of cancer cells and the lymphatic system. Adv. Drug Deliv. Rev. *63,* 886-889.

Tran, E., Chinnasamy, D., Yu, Z., Morgan, R.A., Lee, C.C., Restifo, N.P., and Rosenberg, S.A. (2013). Immune targeting of fibroblast activation protein triggers recognition of multipotent bone marrow stromal cells and cachexia. J. Exp. Med. *210,* 1125-1135.

Truman, L.A., Bentley, K.L., Smith, E.C., Massaro, S.A., Gonzalez, D.G., Haberman, A.M., Hill, M., Jones, D., Min, W., Krause, D.S., and Ruddle, N.H. (2012). ProxTom lymphatic vessel reporter mice reveal Prox1 expression in the adrenal medulla, megakaryocytes, and platelets. Am. J. Pathol. *180,* 1715-1725.

Uchida, D., Onoue, T., Kuribayashi, N., Tomizuka, Y., Tamatani, T., Nagai, H., and Miyamoto, Y. (2011). Blockade of CXCR4 in oral squamous cell carcinoma inhibits lymph node metastases. Eur. J. Cancer *47,* 452-459.

Vakoc, B.J., Lanning, R.M., Tyrrell, J.A., Padera, T.P., Bartlett, L.A., Stylianopoulos, T., Munn, L.L., Tearney, G.J., Fukumura, D., Jain, R.K., and Bouma, B.E. (2009). Three-dimensional microscopy of the tumor microenvironment in vivo using optical frequency domain imaging. Nat. Med. *15,* 1219-1223.

Van Cutsem, E., Vervenne, W.L., Bennouna, J., Humblet, Y., Gill, S., Van Laethem, J.L., Verslype, C., Scheithauer, W., Shang, A., Cosaert, J., and Moore, M.J. (2009). Phase III trial of bevacizumab in combination with gemcitabine and erlotinib in patients with metastatic pancreatic cancer. J. Clin. Oncol. *27,* 2231-2237.

Veikkola, T., Jussila, L., Makinen, T., Karpanen, T., Jeltsch, M., Petrova, T.V., Kubo, H., Thurston, G., McDonald, D.M., Achen, M.G., Stacker, S.A., and Alitalo, K. (2001). Signalling via vascular

endothelial growth factor receptor-3 is sufficient for lymphangiogenesis in transgenic mice. EMBO J. *20,* 1223-1231.

Verweij, J., and Sleijfer, S. (2013). Pazopanib, a new therapy for metastatic soft tissue sarcoma. Expert Opin. Pharmacother. *14,* 929-935.

Vigl, B., Aebischer, D., Nitschke, M., Iolyeva, M., Rothlin, T., Antsiferova, O., and Halin, C. (2011). Tissue inflammation modulates gene expression of lymphatic endothelial cells and dendritic cell migration in a stimulus-dependent manner. Blood *118,* 205-215.

Viola, K., Kopf, S., Huttary, N., Vonach, C., Kretschy, N., Teichmann, M., Giessrigl, B., Raab, I., Stary, S., Krieger, S.*, et al.* (2013). Bay11-7082 inhibits the disintegration of the lymphendothelial barrier triggered by MCF-7 breast cancer spheroids; the role of ICAM-1 and adhesion. Br. J. Cancer *108,* 564-569.

Vlahakis, N.E., Young, B.A., Atakilit, A., and Sheppard, D. (2005). The lymphangiogenic vascular endothelial growth factors VEGF-C and -D are ligands for the integrin alpha9beta1. J. Biol. Chem. *280,* 4544-4552.

von der Weid, P.Y., and Zawieja, D.C. (2004). Lymphatic smooth muscle: the motor unit of lymph drainage. Int. J. Biochem. Cell Biol. *36,* 1147-1153.

von Haehling, S., and Anker, S.D. (2014). Prevalence, incidence and clinical impact of cachexia: facts and numbers-update 2014. J. Cachexia Sarcopenia Muscle *5,* 261-263.

Von Marschall, Z., Scholz, A., Stacker, S.A., Achen, M.G., Jackson, D.G., Alves, F., Schirner, M., Haberey, M., Thierauch, K.H., Wiedenmann, B., and Rosewicz, S. (2005). Vascular endothelial growth factor-D induces lymphangiogenesis and lymphatic metastasis in models of ductal pancreatic cancer. Int. J. Oncol. *27,* 669-679.

Wang, X., Pang, Y., Ku, G., Xie, X., Stoica, G., and Wang, L.V. (2003). Noninvasive laser-induced photoacoustic tomography for structural and functional in vivo imaging of the brain. Nat. Biotechnol. *21,* 803-806.

Wang, Z., Wu, J., Li, G., Zhang, X., Tong, M., Wu, Z., and Liu, Z. (2012). Lymphangiogenesis and biological behavior in pancreatic carcinoma and other pancreatic tumors. Mol. Med. Rep. *5,* 959-963.

Wehler, T., Wolfert, F., Schimanski, C.C., Gockel, I., Herr, W., Biesterfeld, S., Seifert, J.K., Adwan, H., Berger, M.R., Junginger, T., Galle, P.R., and Moehler, M. (2006). Strong expression of chemokine receptor CXCR4 by pancreatic cancer correlates with advanced disease. Oncol. Rep. *16,* 1159-1164.

Wetterwald, A., Hoffstetter, W., Cecchini, M.G., Lanske, B., Wagner, C., Fleisch, H., and Atkinson, M. (1996). Characterization and cloning of the E11 antigen, a marker expressed by rat osteoblasts and osteocytes. Bone *18,* 125-132.

Whipple, A.O. (1941). The Rationale of Radical Surgery for Cancer of the Pancreas and Ampullary Region. Ann. Surg. *114,* 612-615.

Wigle, J.T., and Oliver, G. (1999). Prox1 function is required for the development of the murine lymphatic system. Cell *98,* 769-778.

Wilentz, R.E., Iacobuzio-Donahue, C.A., Argani, P., McCarthy, D.M., Parsons, J.L., Yeo, C.J., Kern, S.E., and Hruban, R.H. (2000). Loss of expression of Dpc4 in pancreatic intraepithelial neoplasia: evidence that DPC4 inactivation occurs late in neoplastic progression. Cancer Res. *60,* 2002-2006.

Wiley, H.E., Gonzalez, E.B., Maki, W., Wu, M.T., and Hwang, S.T. (2001). Expression of CC chemokine receptor-7 and regional lymph node metastasis of B16 murine melanoma. J. Natl. Cancer Inst. *93,* 1638-1643.

Wilhelm, S.M., Carter, C., Tang, L., Wilkie, D., McNabola, A., Rong, H., Chen, C., Zhang, X., Vincent, P., McHugh, M.*, et al.* (2004). BAY 43-9006 exhibits broad spectrum oral antitumor activity and targets the RAF/MEK/ERK pathway and receptor tyrosine kinases involved in tumor progression and angiogenesis. Cancer Res. *64,* 7099-7109.

Winter, J.M., Cameron, J.L., Campbell, K.A., Arnold, M.A., Chang, D.C., Coleman, J., Hodgin, M.B., Sauter, P.K., Hruban, R.H., Riall, T.S.*, et al.* (2006). 1423 pancreaticoduodenectomies for pancreatic cancer: A single-institution experience. J. Gastrointest. Surg. *10,* 1199-210; discussion 1210-1.

Witte, M.H., Dellinger, M.T., McDonald, D.M., Nathanson, S.D., Boccardo, F.M., Campisi, C.C., Sleeman, J.P., and Gershenwald, J.E. (2011). Lymphangiogenesis and hemangiogenesis: potential targets for therapy. J. Surg. Oncol. *103,* 489-500.

Woo, H.M., Bentley, E., Campbell, S.F., Marfurt, C.F., and Murphy, C.J. (2005). Nerve growth factor and corneal wound healing in dogs. Exp. Eye Res. *80,* 633-642.

Wu, H., Xu, J.B., He, Y.L., Peng, J.J., Zhang, X.H., Chen, C.Q., Li, W., and Cai, S.R. (2012). Tumor-associated macrophages promote angiogenesis and lymphangiogenesis of gastric cancer. J. Surg. Oncol. *106,* 462-468.

Wu, P.C., Hsieh, T.Y., Tsai, Z.U., and Liu, T.M. (2015). In vivo quantification of the structural changes of collagens in a melanoma microenvironment with second and third harmonic generation microscopy. Sci. Rep. *5,* 8879.

Xiong, L., Shuhendler, A.J., and Rao, J. (2012). Self-luminescing BRET-FRET near-infrared dots for in vivo lymph-node mapping and tumour imaging. Nat. Commun. *3,* 1193.

Xu, Y., Yuan, L., Mak, J., Pardanaud, L., Caunt, M., Kasman, I., Larrivee, B., Del Toro, R., Suchting, S., Medvinsky, A.*, et al.* (2010). Neuropilin-2 mediates VEGF-C-induced lymphatic sprouting together with VEGFR3. J. Cell Biol. *188,* 115-130.

Yagi, H., Tan, W., Dillenburg-Pilla, P., Armando, S., Amornphimoltham, P., Simaan, M., Weigert, R., Molinolo, A.A., Bouvier, M., and Gutkind, J.S. (2011). A synthetic biology approach reveals a CXCR4-G13-Rho signaling axis driving transendothelial migration of metastatic breast cancer cells. Sci. Signal. *4,* ra60.

Yamamoto, S., Tomita, Y., Hoshida, Y., Nagano, H., Dono, K., Umeshita, K., Sakon, M., Ishikawa, O., Ohigashi, H., Nakamori, S., Monden, M., and Aozasa, K. (2004). Increased expression of valosin-containing protein (p97) is associated with lymph node metastasis and prognosis of pancreatic ductal adenocarcinoma. Ann. Surg. Oncol. *11,* 165-172.

Yamamoto, Y., Ikoma, H., Morimura, R., Konishi, H., Murayama, Y., Komatsu, S., Shiozaki, A., Kuriu, Y., Kubota, T., Nakanishi, M.*, et al.* (2014). The clinical impact of the lymph node ratio as a prognostic factor after resection of pancreatic cancer. Anticancer Res. *34,* 2389-2394.

Yan, J., Jiang, Y., Ye, M., Liu, W., and Feng, L. (2014). The clinical value of lymphatic vessel density, intercellular adhesion molecule 1 and vascular cell adhesion molecule 1 expression in patients with oral tongue squamous cell carcinoma. J. Cancer. Res. Ther. *10 Suppl,* C125-30.

Yan, Z.X., Jiang, Z.H., and Liu, N.F. (2012). Angiopoietin-2 promotes inflammatory lymphangiogenesis and its effect can be blocked by the specific inhibitor L1-10. Am. J. Physiol. Heart Circ. Physiol. *302,* H215-23.

Yang, F., Jin, C., Yang, D., Jiang, Y., Li, J., Di, Y., Hu, J., Wang, C., Ni, Q., and Fu, D. (2011a). Magnetic functionalised carbon nanotubes as drug vehicles for cancer lymph node metastasis treatment. Eur. J. Cancer *47,* 1873-1882.

Yang, H., Kim, C., Kim, M.J., Schwendener, R.A., Alitalo, K., Heston, W., Kim, I., Kim, W.J., and Koh, G.Y. (2011b). Soluble vascular endothelial growth factor receptor-3 suppresses lymphangiogenesis and lymphatic metastasis in bladder cancer. Mol. Cancer. *10,* 36-4598-10-36.

Yang, X.M., Han, H.X., Sui, F., Dai, Y.M., Chen, M., and Geng, J.G. (2010). Slit-Robo signaling mediates lymphangiogenesis and promotes tumor lymphatic metastasis. Biochem. Biophys. Res. Commun. *396,* 571-577.

Ye, Y., Dang, D., Zhang, J., Viet, C.T., Lam, D.K., Dolan, J.C., Gibbs, J.L., and Schmidt, B.L. (2011). Nerve growth factor links oral cancer progression, pain, and cachexia. Mol. Cancer. Ther. *10,* 1667-1676.

Yeo, C.J., and Cameron, J.L. (1998). Prognostic factors in ductal pancreatic cancer. Langenbecks Arch. Surg. *383,* 129-133.

Yeo, C.J., Cameron, J.L., Lillemoe, K.D., Sohn, T.A., Campbell, K.A., Sauter, P.K., Coleman, J., Abrams, R.A., and Hruban, R.H. (2002). Pancreaticoduodenectomy with or without distal gastrectomy and extended retroperitoneal lymphadenectomy for periampullary adenocarcinoma, part 2: randomized controlled trial evaluating survival, morbidity, and mortality. Ann. Surg. *236,* 355-66; discussion 366-8.

Yeo, C.J., Cameron, J.L., Sohn, T.A., Coleman, J., Sauter, P.K., Hruban, R.H., Pitt, H.A., and Lillemoe, K.D. (1999). Pancreaticoduodenectomy with or without extended retroperitoneal lymphadenectomy for periampullary adenocarcinoma: comparison of morbidity and mortality and short-term outcome. Ann. Surg. *229,* 613-22; discussion 622-4.

Yi, S.Q., Miwa, K., Ohta, T., Kayahara, M., Kitagawa, H., Tanaka, A., Shimokawa, T., Akita, K., and Tanaka, S. (2003). Innervation of the pancreas from the perspective of perineural invasion of pancreatic cancer. Pancreas *27,* 225-229.

Yoshitomi, H., Kobayashi, S., Ohtsuka, M., Kimura, F., Shimizu, H., Yoshidome, H., and Miyazaki, M. (2008). Specific expression of endoglin (CD105) in endothelial cells of intratumoral blood and lymphatic vessels in pancreatic cancer. Pancreas *37,* 275-281.

You, L., Kruse, F.E., and Volcker, H.E. (2000). Neurotrophic factors in the human cornea. Invest. Ophthalmol. Vis. Sci. *41,* 692-702.

Yu, C.Q., Zhang, M., Matis, K.I., Kim, C., and Rosenblatt, M.I. (2008a). Vascular endothelial growth factor mediates corneal nerve repair. Invest. Ophthalmol. Vis. Sci. *49,* 3870-3878.

Yu, J., Zhang, X., Kuzontkoski, P.M., Jiang, S., Zhu, W., Li, D.Y., and Groopman, J.E. (2014). Slit2N and Robo4 regulate lymphangiogenesis through the VEGF-C/VEGFR-3 pathway. Cell. Commun. Signal. *12,* 25-811X-12-25.

Yu, S., Duan, J., Zhou, Z., Pang, Q., Wuyang, J., Liu, T., He, X., Xinfa, L., and Chen, Y. (2008b). A critical role of CCR7 in invasiveness and metastasis of SW620 colon cancer cell in vitro and in vivo. Cancer. Biol. Ther. *7,* 1037-1043.

Yuan, Z.Y., Luo, R.Z., Peng, R.J., Wang, S.S., and Xue, C. (2014). High infiltration of tumor-associated macrophages in triple-negative breast cancer is associated with a higher risk of distant metastasis. Onco Targets Ther. *7,* 1475-1480.

Zacharias, T., Jaeck, D., Oussoultzoglou, E., Neuville, A., and Bachellier, P. (2007). Impact of lymph node involvement on long-term survival after R0 pancreaticoduodenectomy for ductal adenocarcinoma of the pancreas. J. Gastrointest. Surg. *11,* 350-356.

Zamder, E., and Weddell, G. (1951). Observations on the innervation of the cornea. J. Anat. *85,* 68-99.

Zeng, Q., Cheng, Y., Zhu, Q., Yu, Z., Wu, X., Huang, K., Zhou, M., Han, S., and Zhang, Q. (2008). The relationship between overexpression of glial cell-derived neurotrophic factor and its RET receptor with progression and prognosis of human pancreatic cancer. J. Int. Med. Res. *36,* 656-664.

Zhang, B., Zhao, W.H., Zhou, W.Y., Yu, W.S., Yu, J.M., and Li, S. (2007). Expression of vascular endothelial growth factors-C and -D correlate with evidence of lymphangiogenesis and angiogenesis in pancreatic adenocarcinoma. Cancer Detect. Prev. *31,* 436-442.

Zhang, B.C., Gao, J., Wang, J., Rao, Z.G., Wang, B.C., and Gao, J.F. (2011). Tumor-associated macrophages infiltration is associated with peritumoral lymphangiogenesis and poor prognosis in lung adenocarcinoma. Med. Oncol. *28,* 1447-1452.

Zhang, G., Brady, J., Liang, W.C., Wu, Y., Henkemeyer, M., and Yan, M. (2015). EphB4 forward signalling regulates lymphatic valve development. Nat. Commun. *6,* 6625.

Zhang, Z., Procissi, D., Li, W., Kim, D.H., Li, K., Han, G., Huan, Y., and Larson, A.C. (2013). High resolution MRI for non-invasive mouse lymph node mapping. J. Immunol. Methods *400-401,* 23-29.

Zhao, B., Cui, K., Wang, C.L., Wang, A.L., Zhang, B., Zhou, W.Y., Zhao, W.H., and Li, S. (2011). The chemotactic interaction between CCL21 and its receptor, CCR7, facilitates the progression of pancreatic cancer via induction of angiogenesis and lymphangiogenesis. J. Hepatobiliary. Pancreat. Sci. *18,* 821-828.

Zheng, W., Nurmi, H., Appak, S., Sabine, A., Bovay, E., Korhonen, E.A., Orsenigo, F., Lohela, M., D'Amico, G., Holopainen, T.*, et al.* (2014). Angiopoietin 2 regulates the transformation and integrity of lymphatic endothelial cell junctions. Genes Dev. *28,* 1592-1603.

Zhou, H.J., Chen, X., Huang, Q., Liu, R., Zhang, H., Wang, Y., Jin, Y., Liang, X., Lu, L., Xu, Z., and Min, W. (2014). AIP1 mediates vascular endothelial cell growth factor receptor-3-dependent angiogenic and lymphangiogenic responses. Arterioscler. Thromb. Vasc. Biol. *34,* 603-615.

Zhu, Z., Friess, H., diMola, F.F., Zimmermann, A., Graber, H.U., Korc, M., and Buchler, M.W. (1999). Nerve growth factor expression correlates with perineural invasion and pain in human pancreatic cancer. J. Clin. Oncol. *17,* 2419-2428.

Zorgetto, V.A., Silveira, G.G., Oliveira-Costa, J.P., Soave, D.F., Soares, F.A., and Ribeiro-Silva, A. (2013). The relationship between lymphatic vascular density and vascular endothelial growth factor A (VEGF-A) expression with clinical-pathological features and survival in pancreatic adenocarcinomas. Diagn. Pathol. *8,* 170-1596-8-170.

Zuckerman, D.S., and Ryan, D.P. (2008). Adjuvant therapy for pancreatic cancer: a review. Cancer *112,* 243-249.

Zumsteg, A., Baeriswyl, V., Imaizumi, N., Schwendener, R., Ruegg, C., and Christofori, G. (2009). Myeloid cells contribute to tumor lymphangiogenesis. PLoS One *4,* e7067.

Zuo, H.D., Tang, W., Zhang, X.M., Zhao, Q.H., and Xiao, B. (2012a). CT and MR imaging patterns for pancreatic carcinoma invading the extrapancreatic neural plexus (Part II): Imaging of pancreatic carcinoma nerve invasion. World J. Radiol. *4,* 13-20.

Zuo, H.D., Zhang, X.M., Li, C.J., Cai, C.P., Zhao, Q.H., Xie, X.G., Xiao, B., and Tang, W. (2012b). CT and MR imaging patterns for pancreatic carcinoma invading the extrapancreatic neural plexus (Part I): Anatomy, imaging of the extrapancreatic nerve. World J. Radiol. *4,* 36-43.

Appendix A: Skeletal Muscle Total RNA Extraction Protocol

DAY 1:

Homogenization

1. Spray with RNase*Zap*, rinse, and wipe dry work surface, pipettor, spatulas, tweezers and gloves. Get liquid nitrogen, dry ice, and wet ice. May also need mortar and pestle to break up tissue pieces.
2. Place spatulas, tweezers, and polycons containing tissue on dry ice.
3. Work in fume hood with double gloves and lab coat. Lay down paper towels to work over.
4. Add 3 mL TRIzol to one 15 mL conical per sample.
5. Clean VirTishear homogenizer with 1 N NaOH and rinse with several L of purified water.
6. Use tweezers to place piece of tissue in conical.
7. Homogenize tissue using VirTishear homogenizer until in suspension. Three to four cycles at speed 5 for about 10 - 15 seconds each works well.
8. Add another 7 mL TRIzol to each sample.
9. Vortex vigorously; incubate 5 minutes at room temperature.
10. Add 0.2 mL chloroform per 1 mL of TRIzol (2 mL) and shake vigorously by hand for 30 seconds. Incubate 5 minutes at room temperature.
11. Centrifuge 45 minutes at 3200 rpm at 4°C.

RNA Isolation

1. Remove the top aqueous phase and transfer to a new tube without disturbing the interphase or lower organic phase. Organic phase can be stored overnight at 4°C.
2. Add 0.5 mL isopropanol per 1 mL TRIzol (5 mL) and incubate overnight at -20°C.

DAY 2:

3. Centrifuge 45 minutes at 3200 rpm at 4°C; decant supernatant.
4. Wash in 1 mL 75% EtOH per 1 mL TRIzol (10 mL). Vortex and centrifuge 45 minutes at 3200 rpm at 4°C; decant supernatant.
5. Resuspend pellet in small volume (<500 µL) 75% EtOH. Transfer to microfuge tube. Rinse conical with 500 µL 75% EtOH and add to microfuge tube. Mix well. RNA can be stored in 75% EtOH at -20°C if necessary.
6. Centrifuge 5 minutes at 16,100 rcf at 4°C. Remove supernatant. Repeat.
7. Allow pellet to air dry in hood for 10 minutes.
8. Resuspend pellet in 50 µL RNase-free water.
9. Analyze RNA concentration and quality by NanoDrop spectroscopy and BioAnalyzer/Fragment Analyzer RNA Integrity Number/RNA Quality Number.
10. Store RNA at -80°C.